1979

Live load distribution in skewed prestressed concrete i-beam and spread box-beam bridges, August 1979 22'P

E. S. deCastro

D. R. Mertz

C. N. Kostem

D. A. VanHorn

Technical Report Documentation Page

1. Report No.	2. Government Accession No.	3. Recipient's Catalog No.
FHWA-PA-RD-72-4-3		

4. Title and Subtitle	5. Report Date
LIVE LOAD DISTRIBUTION IN SKEWED PRESTRESSED CONCRETE I-BEAM AND SPREAD BOX-BEAM BRIDGES	August 1979
	6. Performing Organization Code

7. Author(s)	8. Performing Organization Report No.
Ernesto S. deCastro, Celal N. Kostem, Dennis R. Mertz, David A. VanHorn	No. 387.3

9. Performing Organization Name and Address	10. Work Unit No. (TRAIS)
Department of Civil Engineering Fritz Engineering Laboratory #13 Lehigh University Bethlehem, Pennsylvania 18015	11. Contract or Grant No. Project 72-4
12. Sponsoring Agency Name and Address	13. Type of Report and Period Covered
Pennsylvania Department of Transportation P. O. Box 2926 Harrisburg, Pennsylvania 17120	Interim Report
	14. Sponsoring Agency Code

15. Supplementary Notes

Prepared in cooperation with the U. S. Department of Transportation, Federal Highway Administration

16. Abstract

This is the fourth report on the research investigation entitled "Development and Refinement of Load Distribution Provisions for Prestressed Concrete Beam-Slab Bridges" (Pennsylvania Department of Transportation 72-4). The effects of skew on the design moments and on the lateral distributions of statically applied vehicular loads are examined for prestressed concrete I-beam and prestressed concrete spread box-beam bridge superstructures. The finite element method is utilized to analyze 120 I-beam superstructures and 72 box-beam superstructures ranging in length from 34 ft. to 128 ft. and in roadway width from 24 ft. to 72 ft. Skew effects are correlated for bridges of different widths, span lengths, number of beams, and number of design lanes, and empirical expressions are developed to facilitate computation of lateral load distribution factors for interior and exterior beams. The proposed skew distribution factors are actually based upon appropriate modifications to the distribution factors for right bridges. In general, the skew correction factor reduces the distribution factor for interior beams and increases the distribution factor for exterior beams. The magnitude of the skew effect is primarily a function of skew angle and of bridge span and beam spacing.

17. Key Words	18. Distribution Statement
Prestressed Concrete I-Beam Bridge Design, Live-Load Distribution for Highway Bridges, Skewed Prestressed Concrete Bridges	

19. Security Classif. (of this report)	20. Security Classif. (of this page)	21. No. of Pages	22. Price
Unclassified	Unclassified	221	

Form DOT F 1700.7 (8-72) Reproduction of completed page authorized

COMMONWEALTH OF PENNSYLVANIA

Department of Transportation

Office of Research and Special Studies

Wade L. Gramling, P.E. - Chief

Istvan Janauschek, P.E. - Research Coordinator

Project 72-4: Development and Refinement of
Load Distribution Provisions for
Prestressed Concrete Beam-Slab Bridges

LIVE LOAD DISTRIBUTION

IN

SKEWED PRESTRESSED CONCRETE

I-BEAM AND SPREAD BOX-BEAM BRIDGES

by

Ernesto S. deCastro
Celal N. Kostem
Dennis R. Mertz
David A. VanHorn

Prepared in cooperation with the Pennsylvania Department of Transportation and the U. S. Department of Transportation, Federal Highway Administration.

LEHIGH UNIVERSITY

Office of Research

Bethlehem, Pennsylvania

August 1979

Fritz Engineering Laboratory Report No. 387.3

ABSTRACT

This is the fourth report on the research investigation entitled "Development and Refinement of Load Distribution Provisions for Prestressed Concrete Beam-Slab Bridges: (PennDOT 72-4). The effects of skew on the design moments and on the lateral distributions of statically applied vehicular loads are examined for prestressed concrete I-beam and prestressed concrete spread box-beam bridge superstructures. The finite element method is utilized to analyze 120 I-beam superstructures and 72 box-beam superstructures ranging in length from 34 ft. to 128 ft. and in roadway width from 24 ft. to 72 ft. Skew effects are correlated for bridges of different widths, span lengths, number of beams, and number of design lanes, and empirical expressions are developed to facilitate computation of lateral load distribution factors for interior and exterior beams. The proposed skew distribution factors are actually based upon appropriate modifications to the distribution factors for right bridges. In general, the skew correction factor reduces the distribution factor for interior beams and increases the distribution factor for exterior beams. The magnitude of the skew effect is primarily a function of skew angle and of bridge span and beam spacing.

TABLE OF CONTENTS

TABLE OF CONTENTS (continued)

TABLE OF CONTENTS (continued)

TABLE OF CONTENTS (continued)

1. INTRODUCTION

1.1 General

The structural behavior of prestressed concrete beam-slab highway bridge superstructures subjected to design vehicle loading conditions has been the subject of extensive research conducted at Lehigh University and sponsored by the Pennsylvania Department of Transportation. The bridge superstructures, which were considered during this investigation, consisted basically of equally spaced, longitudinal, precast, prestressed concrete beams with cast-in-place composite reinforced concrete deck slabs. Field tests of in-service bridges of this type indicated the need for refinement of the specification provisions governing live load distribution for right bridges (Refs. 7,8,16,21,22,31,57), and for development of similar specification provisions for skew bridges (Ref. 51).

The overall research program was initially directed towards the study of prestressed concrete spread box-beam superstructures and resulted in the development of new specification provisions governing the lateral distribution of live loads for right bridges of this type (Refs. 2,38). A similar study was then undertaken to develop load distribution criteria for right bridges with prestressed concrete I-beams (Ref. 62).

Despite the fact that skewed beam-slab bridges are quite common in modern highway bridge construction, specific provisions for live load distribution for such bridges are not included in current

design specifications (Ref. 2,3). Prior to the study discussed in this report very little work had been done on skewed bridges, and virtually no work had been done on skewed beam-slab bridges with prestressed concrete I-beams or with prestressed concrete box-beams (Ref. 63).

1.2 Objectives and Scope

The research discussed in this report expands the live load distribution concepts previously developed for right prestressed concrete I-beam or box-beam bridges to include the effects of skew. Design recommendations are proposed for both types of superstructures based upon the analysis of numerous bridges with varying width, spacing, span, number of beams, and angle of skew. The design recommendations are based upon empirical expressions which were formulated utilizing the results of analytical experiments, and which cover interior and exterior beams for both I-beam and box-beam superstructures.

The two basic beam-slab bridge sections utilized in this study are shown in Fig. 1. Figure 1a shows a typical cross-section of a bridge with prestressed concrete I-beams. Figure 1b shows a typical section with prestressed concrete box-beams. As shown in Fig. 2, the beams are equally spaced, and are parallel to the direction of traffic. The design loading on the bridge is the HS20-44 standard truck shown in Fig. 3 and described in Ref. 2. The vehicle used in the field testing of bridges is also shown in Fig. 3. This test vehicle simulates the HS20-44 design vehicle, and is employed in the correlation of field test results with analytical formulations.

The angle of skew (skew angle) referred to in this study is defined as the acute angle between the support line and the longitudinal axis of the beams (Fig. 2b). A skew angle of 90 degrees indicates that the structure is a right bridge (Fig. 2a). It is important, however, to distinguish between the skewness and the angle of skew of a bridge. For example, a bridge with a relatively large skew angle (say 60 degrees) has comparatively less skewness than a 30 degree skew bridge, which exhibits significant skewness but has a relatively small skew angle.

This is the fourth report in a series of five reports included within PennDOT Research Project No. 72-4, entitled "Development and Refinement of Load Distribution for Prestressed Concrete Beam-Slab Bridges". The final report will discuss: (1) the effects of curbs and parapets on the load distribution behavior of right I-beam bridges, (2) the effects of midspan or multiple diaphragms and (3) the extension of the overall study to include continuous bridges.

1.3 Previous Studies

Lateral load distribution in bridges has been the subject of numerous previous investigations. A summary of completed research with bibliography is reported in Ref. 63. A detailed description of studies related to beam-slab bridges, including various methods of analysis, is given by Sanders and Elleby in Ref. 49, by Motarjemi and VanHorn in Ref. 38, and by Wegmuller and Kostem in Ref. 58.

Sanders and Elleby discussed various methods of load distribution analysis employed by previous investigators, and their corresponding results (Ref. 49). Using the theoretical methods and test results of these investigators, Sanders and Elleby proposed load distribution criteria for highway bridges. The resulting proposals for distribution of live load in highway bridges were complicated and were not practical for design applications. The study did not include skew bridges.

Motarjemi and VanHorn developed a method of analysis suitable for spread box-beam slab type bridges (Ref. 38). In this method, the bridge superstructure is reduced to an articulated structure by introducing a series of beam and plate elements. Using the flexibility approach, the bridge superstructure is solved for stresses and displacement. This method of analysis was used to develop the newly accepted specification provision on load distribution for spread box-beam bridges (Ref. 2).

Wegmuller and Kostem used the finite element method to analyze prestressed concrete I-beam bridges (Ref. 58). In this method, the bridge superstructure is discretized into plate and eccentrically attached stiffener elements. The method was applied to field tested beam-slab type highway bridges constructed with prestressed concrete I-beams. A study was made of several variables which affect load distribution. The authors showed that a stiffened plate superstructure could be adequately idealized by the given model and analyzed using the finite element method. The analytical modeling technique for the above approach is given by Kostem (Ref. 29).

The finite element approach, utilizing plate and eccentrically attached stiffener elements as applied to highway bridges, was reported by deCastro and Kostem (Ref. 13). Zellin, Kostem and VanHorn used this method of analysis to determine live load distribution factors for prestressed concrete I-beam bridges (Ref. 62). Distribution factors were determined for several bridge configurations with varying width, spacing, number of beams and span length under the critical HS20-44 vehicular loadings. Based on the results, simplified distribution factor equations were obtained for the interior beams and exterior beams of right bridges.

Very little experimental data is available on skewed beam-slab bridges (Ref. 63). A field test of a 45^{o} skew spread box-beam bridge was compared with a field test of a right bridge of nearly identical dimensions and is reported by Schaffer and VanHorn in Ref. 51. A laboratory test of a 60^{o} skew composite bridge with steel I-beams is reported by Hondros and Marsh in Ref. 25.

The field test results for the 45^{o} skew spread box-beam bridge indicated that the experimental distribution factor for interior girders was considerably less than the design distribution factor (Refs. 42,51); whereas, for exterior girders, the experimental values were greater than the design values. In the same study, the authors indicated the desirability of including the influence curbs and parapets in future design considerations. The test results from the 60^{o} skew composite bridge with steel I-beams indicated that the skew caused a general reduction in the beam strains of about 17 percent (Ref. 25).

The work by Chen, Newmark and Siess (Ref. 9) and the work by Gustafson and Wright (Ref. 23) contributed significantly to the analytical study of skewed beam-slab structures.

Chen, Newmark and Siess used the finite difference method to analyze skewed bridges. Finite difference operators in skewed coordinates were generated and the system of difference equations was solved by computer. The major assumptions employed, in addition to those usually made for plates, were (Ref. 9):

1. There is no composite action between the beam and the slab;
2. Diaphragms and their effects are negligible;
3. The beam acts on the slab along a line and is not distributed over a finite width;
4. There is no overhang at the edge of the bridge; the edge beams are located at the sides of the bridge; and
5. The value of Poisson's ratio is assumed to be zero.

Influence values for moments and deflections were computed for various ratios of spacing and length, for various relative stiffnesses of the beam to the slab, and for different angles of skew. Influence surfaces for moments and deflections were then derived for some of the structures studied. Moment coefficients for skew bridges subjected to standard truck loadings were determined and some general relationships pertaining to design were derived.

Because of the assumptions, the analytical procedure and the subsequent results are applicable only to noncomposite steel I-beam

bridges. The procedure could be adapted to composite bridges by using the composite section in the beam stiffness computation. However, the accuracy of the results with this approach cannot be assessed. Moreover, because of the third assumption, the width of the beam which affects the load distribution in prestressed concrete I-beam bridges as reported in Ref. 62, cannot be taken into account. Finally this analytical procedure was carried out only for five-beam bridges.

Gustafson and Wright (Ref. 23) presented a finite element method of analysis employing parallelogram plate elements and eccentric beam elements. Two typical composite skew bridges with steel I-beams were analyzed and the behavior due to the skew as well as the effects of midspan diaphragms, were illustrated. The parallelogram plate elements which were used did not satisfy slope compatibility requirements at element boundaries, and, therefore, relative accuracy could not be ascertained. The work was not expanded to include load distribution analysis of general skewed beam-slab structures.

Additional research on skew bridges is summarized in Ref. 63. These reports deal primarily with skew slab bridges, skew cellular bridges, and skew bridges with only edge beams, and are not directly applicable to this particular study.

1.4 Analytical Approach

The finite element method was chosen as the analytical basis for this research to facilitate realistic modeling of skew bridge

structures. Using the finite element method, design vehicular loads can easily be applied anywhere on the bridge structure, and beam and slab moments can be readily computed at critical sections.

There are two basic approaches to the finite element method of analysis: (1) the stiffness approach, and (2) the flexibility approach. It has been found that for complex structures of arbitrary form, the displacement method provides a more systematic formulation (Ref. 65). Consequently the computer programming can be simplified and an efficient solution of large and complex structural systems can be obtained. The displacement approach was therefore adopted in this study.

The basic concepts and steps necessary for a finite element analysis are discussed in general terms in this section, and in more specific terms in Refs. 5,17,18,33,58,64,65. The extension of this analytical procedure to the elements used in beam-slab bridge superstructures is discussed in subsequent chapters of this report.

1.4.1 The Finite Element Method of Analysis

The basic concept of the finite element method is that the structure may be idealized into an assemblage of individual structural components, or elements. The structure consists of a finite number of joints, or nodal points (Ref. 65).

The finite element method of analysis may be divided into the following basic steps: (1) structural idealization, (2) evaluation of element properties, (3) assembly of the force displacement equations, and (4) structural analysis.

Structural idealization is the subdivision of the original structure into an assemblage of discrete elements. These elements are generally simple structural components of sizes and shape that retain the material and physical properties of the original structure. The proper structure idealization is obtained by using element shapes that follow the shape and boundaries of the original structure.

Typical structural idealizations for the beam-slab bridge structures considered in this research are shown in Figs. 4 and 5. Figure 4 illustrates the discretization of a prestressed concrete I-beam-slab bridge utilizing plate elements and eccentric beam elements. The plates are general in shape and follow the beam delineation and structural boundaries. The beams are eccentrically attached to the plate elements along the element boundaries.

Figure 5 illustrates the structural idealization of a spread box-beam bridge. Plate finite elements model the deck and the top and bottom plate of the box-beams. Web elements model the web of the box-beams and interconnect the top and bottom plate elements.

The finite element idealization requires that each element deform similarly to the deformations developed in the corresponding region of the original continuum. This is accomplished by prescribing deformation patterns which provide internal compatibility within the elements and at the same time achieve full compatibility of displacements along the boundary (Ref. 65).

Since the elements are interconnected only at the nodes, the elastic characteristics of the element must be adequately represented

by the relationship between forces applied to a limited number of nodal points and deflections resulting therefrom. The force deflection relationship is expressed conveniently by the stiffness properties of the finite element.

Once the element properties have been defined, the analysis of stresses and deflections becomes a standard structural problem. As in any structural analysis, the requirements of equilibrium, compatibility and the force displacement relationship must be satisfied by the solution. In the finite element model, internal element forces must equilibrate externally applied forces at the nodes, and element deformations must be such that they are compatible at the nodes and boundaries before and after the loads are applied. It should be noted that this analysis procedure does not insure equilibrium of stresses along element boundaries. In general stresses in adjacent elements are not similar. Intuitively, however, finite elements that satisfy compatibility along the boundaries should give better results.

1.4.2 Development of Bridge Design Criteria

The 1969 AASHO Bridge Specification (Ref. 1) provides the live load distribution factor equation for which the interior and exterior beams of beam-slab bridges must be designed. The expressions are different for different types of bridges, and are functions of the center-to-center spacing of the beams only. In 1973 AASHTO adopted a new specification provision which included the width, length, number of lanes, and number of beams among the parameters governing the load distribution in spread box-beam bridges (Ref. 2).

A similar refinement to the specification provisions for prestressed concrete I-beams is given in Ref. 62.

The research discussed in this report was directed towards developing specification provisions which will reflect the influence of skew in load distribution criteria. Three major steps were involved: (1) the theoretical development of an analysis procedure suitable for general skew beam-slab structures subjected to vehicular loadings, (2) the application of the method of analysis to highway bridges that represent general beam-slab bridge configurations; and (3) the development of simple expressions for the determination of the design load for interior and exterior beams.

The basic theoretical developments for a finite element analysis of skewed bridges is presented in Chapter 2. The application of these developments to highway bridges with prestressed concrete I-beam bridges is presented in Chapter 3 along with the development of simplified design equations. Additional theoretical development required for the analysis of box-beam bridges, the analysis of highway bridges with spread box-beams, and the development of generalized design equations for such structures are presented in Chapter 4.

2. ELASTIC ANALYSIS OF SKEW STIFFENED PLATES AND BRIDGES

2.1 Introduction

The finite element procedures necessary for the analysis of a generalized stiffened structure are discussed in this chapter. As was done for rectangular stiffened plate problems by Wegmuller and Kostem (Ref. 58), the structure is discretized into deck plates and stiffener elements (Fig. 4). General skewed elastic plate finite elements with in-plane and out-of-plane plate behavior are used to model the deck slab. An eccentric beam finite element with shear deformation properties is introduced to represent the beam and the spacers or diaphragms.

The finite element method is used to analyze skew and right bridges. Comparisons are made with available solutions and field tests. The applicability of the method of analysis to beam-slab highway bridge superstructures is demonstrated.

2.2 Analysis of Skewed Elastic Plates

Plate problems with arbitrary geometrical boundaries are invariably complex and difficult to analyze. Their solution, however, is of considerable importance to the safe and efficient construction of skewed slabs, floor systems, or bridges. The classical theory of elasticity solutions for these problems are limited and are, in general, restricted to only the very simple cases. However, the finite element method is a powerful analytical tool which can easily handle

arbitrary geometry, boundary conditions, and loading configurations. The finite element approach to these types of problems has been previously demonstrated on numerous occasions (Refs. 10,11,18,35, 56,64).

A finite element analysis technique for skewed plates is presented in Appendix A. The formulation has been kept general enough to facilitate its extension to skew, eccentrically stiffened structures such as beam-slab bridge superstructures. Because of the eccentricity of the beams to the plate in such structures, the plate develops in-plane and plate bending response, and both behaviors are considered in the analysis. The elements developed in Appendix A, which represent the in-plane and out-of-plane behavior of elastic thin plates, will be utilized to model and analyze general stiffened plates, skew bridges with prestressed concrete I-beams, and skew bridges with prestressed concrete spread box-beams.

2.3 Analysis of Stiffened Structures

A brief survey of the methods of analyzing plates with stiffeners is given by Wegmuller and Kostem in Ref. 58. In general, the methods of analysis may be classified according to the following structural idealizations: (1) orthotropic plate model, (2) equivalent grid model, (3) plate and stiffeners model, and (4) folded plate model. Each method has limitations imposed on it because of the associated modeling scheme (Refs. 58,59).

The equivalent plate model idealizes the behavior of stiffened plates by plate bending action. In this method the properties of the stiffeners are "smeared" throughout the plate, and the resulting structure is analyzed as a plate problem.

In the equivalent grid model the structure is idealized as a grillage of beam elements. In cases where the slab is the only connection between longitudinal stiffeners, the slab is modeled by transverse beam elements at sufficient intervals. The analysis follows standard structural analysis procedures.

Two major difficulties are associated with the equivalent plate or equivalent grid mode. First, plate and beam properties must be adequately determined so as to accurately represent the actual structure. Second, the actual stresses in the beams and the slab must be computed from the analyzed equivalent structure.

The plate with stiffeners model and the folded plate model have gained full acceptance in the analysis of stiffened plates (Refs. 23,58,60). The actual properties of the plate and the stiffeners are used, and the actual stresses are derived directly from the analysis. In this investigation, the plate and stiffeners model is used for I-beam bridges and the folded plate model is used for box-beam bridges.

The analysis of stiffened plate structures can be formulated by combining the classical plate and beam theories (Ref. 58). The standard assumptions for plate analysis are listed in Appendix A. For the beam, the assumption is made that all deformations can be

described in terms of the vertical displacement of the longitudinal axis and the rotation of the beam cross-section. This assumption neglects the deformation of the cross-section of the beam, and hence strains normal to the longitudinal axis of the beam are not considered. The classical approach, however, results in a system of equations which is not easily solved except for very simple loads and boundary conditions. The problem becomes even more complex for skewed structures.

The overall objectives of this study dictate that the method of analysis must be sufficiently general so that design details may be considered separately without using "smearing" techniques. The method should also be readily adaptable to a variety of structural configurations and loading considerations. Since the finite element method of analysis meets these requirements, it was chosen for this investigation. A detailed development of the finite element analytical technique as applied to skewed stiffened plates is included in Appendix B.

2.4 Numerical Examples and Comparisons

The combined beam and plate elements previously described were used to analyze various structures and the results of such analyses were compared with available solutions and with field test data. Generalized structural behavior of various bridges was investigated to validate the analytical technique, and to provide insight which would facilitate load distribution studies. The procedure discussed in this section is the analytical basis for the lateral load distribution analysis of prestressed concrete I-beam bridges which will be presented in Chapter 3.

2.4.1 Beam Moments in Skewed Non-Composite Bridges

One of the beam-slab bridge configurations analyzed in Ref. 9 was investigated utilizing the finite element method of analysis and results were compared. The bridge is assumed to be non-composite as discussed in the reported solution (section 1.3). The structure is a five-beam bridge with spacing to span ratio of 0.1. The plate-to-beam stiffness ratio H, defined as the ratio of beam rigidity to the plate rigidity, is equal to 5. Poisson's ratio and the beam eccentricity are taken as zero.

The beam slab structure, as a right bridge (90^{o} skew), and as a 30^{o} skew bridge, is shown in Fig. 6. The same bridge with 60^{o} and 45^{o} skew is shown in Fig. 7. The right bridge and the 30^{o} skew bridge are shown in the same figure to illustrate the change in geometry due to the skew. A single concentrated load P is placed at midspan on Beam C. The discretization, as shown in Figs. 6 and 7 includes two plate elements between the beams and eight plate elements along the span. The figures also show the location of maximum moment as determined by the finite element analysis.

The moment coefficients for each beam as determined by the analysis, the reported results from Ref. 9, and another finite element solution (Ref. 23) are shown in Fig. 8.

The finite difference analysis underestimates the two finite element solutions. The following observations can be made from the finite element results:

1. There is a decrease in the moment coefficients of the interior beams as the skew angle changes from 90^{o} to 30^{o}. A slight increase in the exterior beam moment can be noted.
2. The rate of decrease is gradual from 90^{o} to 45^{o} skew but abrupt beyond 45^{o}. The rate of change is relatively constant for the exterior beam.
3. The location of maximum moment response is towards the obtuse angle corner of the structure. The section of maximum response is not the skew centerline but varies for different angles of skew.

The decrease in the total beam moments in a bridge superstructure, as the skew angle is changed, is reflected in the above results. For the same width and span, the skew bridge transfers the load more efficiently to the supports. The interior beam moment is further reduced by the increase in the participation of the exterior beams.

2.4.2. Beam Moments in Composite Skew Bridges

The beams in composite bridge structures are eccentrically attached to the slab, and it is necessary to include such eccentricity to achieve a realistic analysis. In the following example, the effect of considering eccentricity is demonstrated through comparison with the analysis discussed in the previous example.

The five-beam structure in the previous comparison was analyzed as a composite bridge. An eccentricity of 28 inches corresponding

to a beam moment of inertia of 126584.0 in.^{4} and area of 576.0 in.^{2} was introduced. A torsional ratio $GK_T/EI = 0.035$ was also included to achieve a more representative bridge analysis. The principal ratios and the beam slab dimensions were comparable to those of the Bartonsville Bridge (Ref. 7).

The difference between composite and non-composite analysis is shown in Fig. 9. The following observations can be deduced from the figure:

1. The beam directly under the load carries a major portion of the total load in a composite structure. The increase in moment coefficients of beams B and C is balanced by the decrease in the moment coefficient of beam A.

2. The reduction and the rate of reduction in moment coefficients for the interior beam seems to be almost the same for both composite and non-composite analyses.

The above example demonstrates the necessity of considering beam eccentricity when the beams are integrally and eccentrically connected to the slab.

The effect of constraining the supports to rotate about the line of support can be seen in Table 1 for the case of a 95^o skew bridge. For this problem, it can be seen that the effect of such constraint is quire negligible.

2.4.3 Load Distribution in a Reinforced Concrete Skew Bridge

An actual reinforced concrete skew bridge has been tested under static loads (Ref. 6). The bridge has a 60° skew, simple span, and is supported by four reinforced concrete beams which are monolithic with the deck slab. The field tests were done by the team of Burdette and Goodpasture of the University of Tennessee (Ref. 6). The bridge is located on U. S. 41A over Elk River, and has a span of 50 ft. and beam spacing of 6 ft. 10 in. center-to-center.

The loads are applied as shown in Fig. 10 and the distribution of load is shown in Table 2. Good agreement between field test and analytical results can be observed.

2.4.4 Composite Versus Non-Composite Behavior

For the purpose of comparison, the bridges tested by AASHO in the AASHO road test series (Ref. 24) can be analyzed using the method previously discussed. The composite bridges, designated 2B and 3B in the report, are shown in Fig. 11. The bridges have three beams, 15 ft. width and 50 ft. span length. Bridges 2B and 3B have different beam section properties as indicated in Fig. 11. The steel I-beams are connected to the slab by shear connectors designed for full composite action. The structure is loaded by a test vehicle with a front axle load of 6.8 kips and a rear axle load of 14.3 kips. The vehicle is initially positioned with the drive wheel at midspan in the longitudinal direction and at the center of the width in the transverse direction. The structure is then analyzed as a composite bridge and as a non-composite bridge. The percent of the total moment carried by the beams

as indicated by the field test data and the finite element analyses are listed in the second column of Table 3. The following observations can be made:

1. The finite element results predicted that a higher percentage of the load would be carried by the beams in the composite structure. The values are comparable with field test results.
2. As expected, a higher percentage of the total moment is carried by the beams when acting compositely with the slab.
3. The load carried by the beams is higher for the stiffer beam sections.
4. For this type of loading, there is very little difference in the percent of load carried by each beam as shown in Table 3.

The design moments for each beam can also be computed and compared to the 1953 AASHO provisions. The drive wheels are placed at midspan and the truck is positioned across the width so as to produce the critical loading condition. The structure is then analyzed as a composite and non-composite bridge. The distribution factors computed for each case are compared in Fig. 12. The comparison shows that the distribution factor for the center beams is overestimated by the AASHO specification provision, and that the distribution factor for the exterior beams is substantially underestimated.

3. LATERAL LOAD DISTRIBUTION IN SKEWED I-BEAM BRIDGES

3.1 Introduction

In the design of beam-slab highway bridges, the live load bending moments are determined with the use of load distribution factors. The distribution factor determines the fraction of the wheel loads that is applied to a longitudinal beam. The applicable distribution factor is given by AASHTO in the Standard Specifications for highway bridges for right bridges (Section 1.4.2 and Ref. 3). However, as discussed in Section 1.1, load distribution factors are not given for skew bridges.

This chapter presents the lateral load distribution analysis of skewed beam-slab bridges with prestressed concrete I-beams. Skew bridges of various widths, spacing, span length and number of beams are analyzed using the finite element method of analysis presented in Chapter 2. Live load distribution factors are computed for interior and exterior beams for design vehicle loading. Distribution factors resulting from the critical combination of vehicular loadings are selected and correlated with bridge parameters to arrive at a simplified design equation for computing distribution factors.

3.2 Beam Moments in Skewed I-Beam Bridges

The HS20-44 design vehicle as defined in Section 1.2 is used in the following lateral load distribution study (Ref. 2). The moment

in a particular beam produced by one design vehicle placed anywhere on the bridge is expressed in terms of the moment coefficient. This coefficient is defined as the ratio of the composite beam moment to the total right bridge moment, which is numerically equal to the moment produced by the given load on a simple beam of equal span. For convenience, the coefficient is expressed as a percent. A plot of moment coefficients against the lateral position of the load represents the moment influence line of the beam under consideration.

3.2.1 Computation of Load Distribution Factors

The load distribution factor is applied to the wheel loads in the design of the beams in beam-slab bridges (Ref. 3). This factor can be determined from the plot of the moment coefficients, i.e., influence lines, following the requirements of the AASHTO Specifications (Ref. 3). According to the specification provisions governing live load distribution, the design traffic lane must be 12 ft. wide (Fig. 13). The design truck, which occupies 6 ft. of the lane, should be positioned in the lane, and the lane should be positioned on the bridge, such that the loading will produce the maximum moment response for the beam being considered. The same definition of loading applies to bridges with two or more lanes, except that the lanes should not overlap (Ref. 3 and Fig. 13). A minimum distance of 2 ft. is specified between the edges of the lane and the wheel of the design vehicle. The sum of the moment coefficients for the beam at the specified positions of the trucks gives the distribution factor for the particular beam. Thus,

$$D.F. = \frac{\Sigma \text{ moment coefficients } (\%)}{100\%} \tag{3.1}$$

for axle loading, and

$$D.F. = \frac{2\ \Sigma \text{ moment coefficients } (\%)}{100\%} \tag{3.2}$$

for wheel loading.

Truck loads must be positioned so as to arrive at the maximum distribution factor. To ensure appropriate positioning, a 12 ft. lane is placed on the structure at x = 0, where x is the distance of the leftmost boundary of the lane from the leftmost curb (Fig. 13a). A truck load is then positioned within the lane so as to obtain the highest moment coefficient from the moment influence line of the beam. The position of the truck in the lane is determined by the distance x_1, which is greater than or equal to 2 ft., but is less than or equal to 4 ft. so as to maintain a 2 ft. clearance between the line of wheels and the boundaries of the lane. Finally, the lane is moved to a new value of x, e.g. x =1, and the truck is repositioned again within the lane so as to obtain the highest moment coefficient for this new lane position. The procedure is repeated until the lane has covered the entire width of the bridge. The maximum moment coefficient value obtained in the above process is used in the distribution factor calculation in Eq. 3.2. For two or more design lanes, the corresponding number of lanes are placed on the bridge (Fig. 13b). The second step is repeated for all lanes until all trucks are positioned in each lane in such a manner that the sum of the moment coefficients is a maximum. The lanes are then moved to a new position on the bridge and the

procedure of positioning the trucks in each lane is repeated. The largest sum of the moment coefficients obtained in the above process is used in the distribution factor calculation in Eq. 3.2.

3.2.2 Maximum Beam Moments

The maximum moment caused by the HS20-44 truck on a simple span right bridge occurs under the drive wheels, when the center of gravity of the wheel loads and the drive wheels are equiddistant from the center of the span (Ref. 19). Consequently, in the lateral load distribution analysis of right bridges, the design truck load is placed on the bridge so that the drive wheels are at d/2 distance from midspan where d is the distance from the centroid of the wheel loads to the drive wheels (Ref. 62). The beam moments in the distribution factor calculations are also computed at the section under the drive wheels.

For skew bridges, however, the position of the load that produces the maximum response in a beam, and the location of the beam section where the maximum moment occurs are not known. Moreover, for the same beam, the location of the maximum moment section can differ for different lane positions of the truck. The position of the load which produces the maximum moment response, and the location of the maximum moment section in a beam of a skew bridge, are different from those of a right bridge. This point can be illustrated by the following example.

The structure is a five-beam bridge, 24 ft. wide and 60 ft. long, with a relative beam-to-slab stiffness ratio of 5. The beams

are equally spaced at 6 ft., and the slab is 7-1/2 in. throughout. The HS20-44 truck loads are placed one at a time at five positions across the width of the bridge, so that the distance of the centroid of each truck from its consecutive position is 4.5 ft. In each of the lane positions, the longitudinal position of the truck is varied until the maximum moment is obtained for each beam. The distance of the centroid of the truck between longitudinal positions is d/2 = 2.33 ft. This distance is selected primarily for convenience, and because the change in the computed moments near the midspan between two consecutive longitudinal positions is less than 1%. The above loading procedure is carried out for each beam of the bridge at skew angles of 90° (right bridge), 45°, and 30° (Figs. 14 through 18). The direction of the truck is always with the front wheels towards the right (Fig. 3). The computed moments are based on the averaged nodal moments.

The positions of the truck centroid and the location of maximum moment in beam A are shown in Fig. 14 for the bridge with skews of 90°, 45°, and 30°. While the maximum moment section occurs at d/2 from midspan for all angles of skew, the positions of the truck differ for each case. Similar observations can be made for beams B and C (Figs. 15 and 16). For beams D and E, the positions of the truck centroid and the location of the maximum beam moment section are shown in Figs. 17 and 18. In these cases the maximum moment section and the positions of the load are different for different angles of skew. Based on these results, one would expect the critical load position and the location of the maximum beam moment section, to be different for another skew bridge with a different number of beams, spacing or span length.

Obviously, significant difficulty would be encountered in carrying out the above procedure for all of the beams of bridges which must be minimized if the maximum moment can be approximated by the moment produced in the beam with the load centroids at midspan.

3.2.3 Beam Moments with Load Centroid at Midspan

In this section, the beam moments in the skew bridge of Section 3.2.2 caused by the HS20-44 truck loads are determined for load centroids located at midspan. These moments are computed at the beam section d/2 from midspan and in the direction of the obtuse angle corner at the supports. The object of this procedure is to determine if there is a significant difference between these moments and the maximum moments as determined in the previous section.

The moments for beam C with the load centroid at midspan, and the moments from the procedure in Section 3.2.2, are shown in Fig. 19. Moments are shown for the five lane positions across the width at skew angles of 45^{o} and 30^{o}. The figure shows that there is a small difference in the moments between the two load positions. The larger difference occurs at larger skews and at lane loads away from beam C. It is also of interest to compare the moments in beam C resulting from loads on lanes 1 and 5. It can be seen that the larger moment is produced with the truck going in the direction of the acute angle corner of the support, i.e., lane 5 (Figs. 16 and 19).

The above investigation indicates that placing the load centroid at midspan will aproximately produce the maximum moment response in a beam without significant loss in accuracy. Also, the desired

moment for the lateral load distribution study can be computed at the beam section at d/2 from midspan and in the direction of the obtuse angle corner.

It should be noted, however, that in general the distance from the midspan of the beam to the section of maximum moment will not be d/2 for other bridges. A study of the beam moments in the skew bridges analyzed in Section 3.4 shows that the moment at d/2, if different from the maximum moment, can be in error by 2% for the shorter bridges and by less than 1% for the longer bridges. However, such error is within practical design limits and is acceptable.

3.3 Effect of Skew on Load Distribution

In order to gain an initial insight into the behavior of skew bridges and to determine the important parameters that must be considered in load distribution studies, an analytical investigation was carried out for two basic bridge widths. This section presents findings based on the analyses of thirty bridges with curb-to-curb widths of 24 ft. and 42 ft.

3.3.1 Effect of Skew on Beam Moments

The effect of skew on the individual beam moments is shown in Fig. 20. The bridge analyzed was a five-beam bridge, 60 ft. long and 24 ft. wide with beam spacing of 6 ft. The truck was placed on the skew bridge similar to the manner in which it would be placed on a right bridge to produce the maximum moment. The skew angle was then varied and the moment percentages were computed for each case.

The two load positions indicated in Fig. 20 illustrate the shift in distribution of the load as the skew angle changes. The results indicate a more uniform distribution of load with decreasing angle of skew. The angle of skew did not have a significant effect on the exterior beam directly under the load. The load distribution in a 60° skew bridge was also not significantly different from that in a right bridge.

3.3.2 Effect of Skew and Number of Beams

A 24 ft. wide bridge with a span of 60 ft. was analyzed with two design lanes. The truck loads were placed near the center of the bridge section as close as possible to each other in accordance with the 1973 AASHTO Specification (Ref. 3). Beginning with four beams, the number of beams was increased to five and then to six to establish two new sets of bridges with constant span lengths. Consequently, the beam spacing changed from 8 ft. to 6 ft. and 4.75 ft., respectively. For each set the skew angles investigated were 90° (right bridge), 60°, 45°, and 30°. Thus a total of twelve bridges was analyzed.

Figure 21 shows the distribution factors resulting from the analysis. Also shown for comparison is the current AASHTO distribution factor of S/5.5 (Ref. 3). The distribution factor decreased as the angle of skew decreased. The decrease in the distribution factor was gradual from 90° to 45°. The number of beams and spacing did not seem to affect the rate of reduction.

3.3.3 Effect of Skew with Span Length

The five-beam bridge, 24 ft. wide with 6 ft. beam spacing, was analyzed with a span of 30 ft. and 120 ft. The appropriate beam sizes in accordance with the standards for Bridge Design BD-201 (Ref. 43) were used. For each length the skew angles considered were 90°, 45°, and 30°. Distribution factors for the beams were computed based on the critical location of one or two HS20-44 design vehicle(s) positioned across the width of the bridge. For this initial study the vehicle was positioned in the longitudinal direction, similar to the manner in which it would be placed on the right bridge to produce the maximum moment.

The distribution factors for the beams are shown in Fig. 22. Beams B and C of the 30 ft. series with skews are not shown. For these configurations, one rear wheel and one front wheel were off of the bridge so that load distribution comparison with longer bridges was not practical.

In beam C, the amount of reduction in the distribution factor was marginal from 90° to 45° skew for the lengths considered. However, a considerable change in the rate of reduction was observed for skew angles less than 45°. Also, for the long span bridges, the rate of reduction decreased as the skew angle decreased.

Exterior beam A had practically no reduction in the distribution factor as the angle of skew decreased, except for the 30 ft. case. It should be noted that for the 30 ft. span with small skew angles some of the wheels of the vehicle were off of the bridge.

3.3.4 Effect of Skew on Distribution Factor versus S/L

The plots of the distribution factors versus S/L for the 24 ft. wide bridges with five beams and at skew angles of 90^{o}, 45^{o}, and 30^{o} are shown in Fig. 23. Similar plots for the 42 ft. wide bridges with six beams are shown in Fig. 24. The span lengths investigated were 30 ft., 60 ft., and 120 ft. for the 24 ft. wide bridges; and 42 ft., 59 ft., and 101 ft. for the 42 ft. wide bridges. These dimensions correspond to W_c/L ratio of 0.80, 0.40, and 0.20 for the 24 ft. wide bridges and 1.0, 0.70, and 0.42 for the 42 ft. wide bridges.

The two figures indicate that at a high S/L ratio there is a larger decrease in the distribution factor as the skew angle decreases. Furthermore, the decrease in the distribution factor is larger at smaller skew angles for the wider bridge. The above results imply that the aspect ratio of the bridge is an important parameter governing the skew reduction of load distribution factors.

3.4 Load Distribution Factors for Skewed I-Beam Bridges

In the development of the distribution factor formula for right bridges about 300 bridges were investigated (Ref. 62). These bridges varied in width, number of beams, and span length to cover the bridge configurations encountered in practive. In this section, thirty of these representative right bridges were selected and each one was analyzed for skew angles of 90^{o} (right bridge), 60^{o}, 45^{o}, and 30^{o}. Thus, in effect, a total of 120 bridges were analyzed.

3.4.1 Design of the Experiment

The bridges analyzed with different skew angles are listed in Table 4. The basic widths considered were 24, 48, and 72 ft., curb-to-curb. The number of beams were varied from 4 to 16, and consequently, the beam spacings varied from 4'-10" to 9'-6". Different lengths ranging from 30 ft. to 120 ft. inclusive were used. Detailed descriptions of the bridges employed in this investigation are presented in Refs. 12 and 66. Reference 12 also contains the graphic presentation of the influence lines developed for the bridges considered herein. Reference 43 was used in the determination of beam properties.

3.4.2. Distribution Factors in Skew Bridges

With the use of the procedure outlined in Section 3.2.1, distribution factors were computed for all interior and exterior beams. In determining distribution factors, consideration was given to the maximum number of design lanes that could be placed on a given bridge width. The maximum interior and exterior beam distribution factors for each bridge were selected and are listed in Tables 5 and 6 respectively. The full list of distribution factors for different design lanes can be found in Ref. 12.

The interior beam distribution factors for the 24 ft. wide bridges with four, five, and six beams are plotted against S/L in Fig. 25. Similar plots are presented for the 48 ft. wide bridges with six, nine, and eleven beams in Fig. 26, and for the 72 ft. wide bridges with nine, twelve, and sixteen beams in Fig. 27. In addition to the observations made in Section 3.3, the following can be observed from the figures:

1. The rate of reduction is usually larger for larger spacing, for wider bridges, and at smaller angles of skew.
2. There is, however, a limit to the increase in the rate of reduction.

The second observation may be interpreted as follows. At large spacing and short spans the lateral distribution of the load is small and hence the distribution factor is small. At narrow beam spacing, the distribution factor is also small. Consequently, the amount of reduction because of the skew is found to be relatively smaller for these cases. The influence line plots for moments in the individual beams in this study are given in Ref. 12.

The plots of the maximum distribution factors for the exterior beams against the S/L ratio are shown in Figs. 28, 29, and 30 for the three bridge widths. Compared to the interior beams, a similar but smaller reduction in the distribution factor was observed for the shorter bridges. However, an increase in the distribution factor was observed for longer bridge spans. The increase in the distribution factor may be attributed to the greater participation of the exterior beams when the bridge has a skew.

3.4.3 Development of the Distribution Factor Equations

Determination of factors for prestressed concrete I-beam bridges with no skew is the subject of a comprehensive study in Ref. 62. It is therefore the aim of this section to provide only the reduction factor for such bridges with a given angle of skew.

The reduction factor for interior beams in a given skewed bridge is computed utilizing the beam distribution factor for a right bridge (90^{o} skew) with the same width, number of beams and span length as the base. These reduction factors are expressed as percent reductions, and are always zero for right bridges. With the use of the Lehigh University Amalgamated Package for Statistics, LEAPS (Ref. 30), the percent reduction in distribution factor was correlated with combinations of such varieales as skew angle, span length, number of beams, number of loaded lanes, and bridge width. The variables found to have good correlation with the percent reduction were the spacing-to-length ratio S/L and the bridge width-to-span ratio W_c/L in combination with the square of the cotangent of the skew angle. A regression analysis of the percent reduction against these variables resulted in the following equation:

$$PCTR = \left(45 \frac{S}{L} + 2 \frac{W_c}{L}\right) \cot^2 \phi \qquad (3.3)$$

where PCTR = reduction factor in percent which is to be applied to the distribution factor for an interior beam of a right bridge with given S, W_c, and L.

S = beam spacing

W_c = curb-to-curb width

L = span length

ϕ = skew angle

For the exterior beams, a simplified equation was determined by trial and error and is proposed as follows:

$$PCTR_{(EXT)} = 50\left(\frac{S}{L} - 0.12\right)\cot\phi \qquad (3.4)$$

where $PCTR_{(EXT)}$ = reduction (positive) or amplification (negative) which is to be applied to the distribution factor for an exterior beam of a right bridge with given S, W_c, and L.

The above equations are limited to the following bridge dimensions:

$$4'\text{-}6'' \leq S \leq 9'\text{-}0''$$

$$48'\text{-}0'' \leq L \leq 120'\text{-}0''$$

$$30^{\circ} \leq \phi \leq 90^{\circ}$$

The computed distribution factors, the percent reductions based on the above equations, and the analytical results for the bridges investigated are listed in Ref. 12. The equations are found to be conservative in most cases except in the case of the large spacing, 30° skew, and very short span. The plots of the proposed equation for interior beams are shown in Figs. 31, 32, and 33 for the bridges investigated.

3.5 Design Recommendations

From the results of this study, the following simplified procedures are recommended for the determination of the live load distribution factors in prestressed concrete I-beam bridges with skew:

1. The load distribution factor for interior beams may be determined by applying to the distribution factor, for interior beams of the bridge without the skew, a reduction specified by the following formula:

$$DF = DF_{90}\left(1.0 - \frac{PCTR}{100}\right) \tag{3.5}$$

where DF = distribution factor for the interior beam of the bridge with skew angle

DF_{90} = distribution factor for the interior beam of the bridge without skew, and

PCTR = reduction in percent as specified by Eq. 3.3.

2. The load distribution factor for exterior beams may be determined by applying to the distribution factor, for exterior beams of the bridge without the skew, a factor specified by the following formula:

$$DF_{(EXT)} = DF_{90(EXT)}\left(1.0 - \frac{PCTR_{(EXT)}}{100}\right) \tag{3.6}$$

where $DF_{(EXT)}$ = distribution factor in the exterior beam of the bridge with skew angle

$DF_{90(EXT)}$ = distribution factor in the exterior beam of the bridge without skew, and

PCTR = amplification or reduction factor as specified by Eq. 3.4.

A plot of the smallest and the largest percent reduction in the distribution factors for interior beams using the proposed equation and the bridge dimensions investigated in this study is shown in Fig. 34. A similar plot for exterior beams is shown in Fig. 35.

3.6 Summary

The load distribution behavior of skewed I-beam bridges under design vehicular loads has been discussed. Load distribution factors were computed for the interior and exterior beams of bridges constructed with prestressed concrete I-beams. The skew angles investigated were 90°, 60°, 45°, and 30°. The following observations were made:

1. The load distribution factor decreases with decreasing angle of skew.
2. The rate of reduction in the distribution factor is gradual from 90° to 45° but is abrupt from 45° to 30°.
3. The rate of reduction in the distribution factor decreases with increasing span length.
4. The bridge width-to-span ratio and beam spacing-to-span ratio, and the skew angle significantly affect the amount of reduction.

Based on a statistical correlation of bridge parameters with numerical results, simplified distribution factor equations were obtained for interior and exterior beams.

4. LATERAL LOAD DISTRIBUTION IN SKEWED SPREAD BOX-BEAM BRIDGES

4.1 Introduction

The design and construction of spread box-beam bridges (Fig. 1(b) is a relatively recent development, and the load distribution characteristics for this type of bridge have been the subject of several investigations (Section 1.1.2 of Ref. 63). Extensive field investigations of spread box-beam bridges have been carried out at Lehigh University (Refs. 16,21,22,31,51,57), however, with the exception of Ref. 51, all of these investigations have been for right bridges.

The field investigations confirmed the need for a realistic procedure for determining live load distribution for spread box-beam bridges with and without skew. The theoretical analysis developed by Motarjemi and VanHorn (Ref. 38) provided a new specification provision for lateral load distribution for right bridges with prestressed concrete spread box-beams (Ref. 2). The analysis of right and skewed box-beam bridges is discussed in this chapter and design equations are developed for use in determining the lateral load distribution in skewed spread box-beam bridges. The design equations are similar in form to the previous expressions for lateral load distribution in skewed I-beam bridges and are actually the product of two terms. The first term is the distribution factor for an identical right (no skew)

bridge. The second term is a modification factor which accounts for the effect of the skew.

A total of 72 bridges of various widths, spans, number of beams and skew angle were analyzed and a computerized process was developed to calculate distribution factors for each particular bridge. A combination of three computer programs (PRESAP, SAPIV, and POSTSAP) was used for overall bridge analysis. PRESAP produced input required by SAPIV utilizing simple bridge dimensions. Program SAPIV (Ref. 4) was used to analyze the discretized bridge structure by means of the finite element method. Program POSTSAP utilized the stresses computed by SAPIV to calculate the required lateral distribution factors. Finally, a regression analysis was carried out on the distribution factors which were calculated by POSTSAP. Utilizing program LEAPS (Ref. 30), design equations, which delineate the required skew modifications, were developed.

4.2 Method of Analysis

4.2.1 General

The analysis of spread box-beam bridges is a complex problem where relative solution accuracy can often be constrained by available computer storage. Because of the large differences in the node numbers of the assembled elements, the size of the bandwidth, which determines the amount of computer storage required, can become excessively large. The total number of elements and the resulting system of equations are also larger than for a corresponding I-beam

bridge with an equal number of beams. Consequently, the computational effort required for a given analysis is substantial, and it is therefore necessary to use a minimum number of elements while at the same time obtaining results with a reasonable degree of accuracy.

4.2.2 Assumptions

The beam-slab bridge configuration utilized in this investigation consisted of a concrete deck of constant thickness, supported on equally spaced prismatic box-beams (Fig. 1b). The deck acts compositely with the simply supported beams. Although the Pennsylvania Department of Transportation (PennDOT) specifications would require diaphragms for the majority of the bridges analyzed, diaphragms were not considered. Previous work involving the Philadelphia Bridge (Ref. 31) indicated that diaphragms have only limited effect on distribution factors, thus supporting this simplifying assumption. The concrete in both the slab and the beams was assumed to respond to service loads as a linear elastic, homogeneous, isotropic material.

Boundary conditions for the finite element model were specified in the global coordinate system, and consequently support nodes were not constrained to rotate about the skewed line of support. The effect of such an assumption on maximum beam moments was discussed in Section 2.4.2 and was found to be of negligible concern.

4.2.3 Modeling Procedure

The pre-processor PRESAP Modeling Procedure which creates the input required by program SAPIV, was used to model the bridge

structures. A general discretization, identical for all bridge configurations, was chosen for the parametric study. Consequently, a coarser discretization was utilized for longer bridges than for shorter bridges; however, such an approach greatly simplified the parametric study and did not adversely effect the accuracy of the analysis of overall bridge behavior. The actual discretization was optimized for a bridge of average span, and an attempt was made to achieve a favorable aspect ratio (approximately equal to 1.0) for the elements at the skew midspan of each bridge. The elements extending from the ends of the bridges toward midspan were long and narrow with relatively poor aspect ratios (up to 18.0). Since the intent of this investigation was to determine the stresses at the skew midspan only, a poor aspect ratio was acceptable for elements which were not in close proximity to the midspan.

The typical discretization utilized for the analysis of skewed, spread box-beam bridges is shown in Fig. 36 for a 3-beam bridge. The longitudinal discretization consisted of eight elements, including two elements at midspan with an aspect ratio of one, and six additional elements with aspect ratios which varied with bridge span. Laterally, the overhangs and beam flanges were modeled with single elements, while two elements were used to model the deck between each beam. The deck and top flange of the beam were modeled with plate bending elements, which exhibit plane stress and flexural response (Ref. 4). The webs and bottom flange of the beams were modeled with plane stress elements since any out-of-plane behavior of these members has negligible effect on overall bridge behavior.

In effect, the St. Venant torsional stiffness of the box-beams was modeled by the in-plane behavior of their components, whereas the minor effects of warping torsion, resulting from out-of-plane distortion of the web or bottom flange, were neglected (Ref. 58).

4.2.4 Calculation of Distribution Factors

The post-processor POSTSAP used the output from SAPIV to calculate lateral load distribution factors. Values of stresses were obtained from the SAP IV output through direct reading, or through interpolation, for the points along the bridge cross-section as shown in Fig. 37. Straight line distributions were assumed between these stress points, and the resulting stress distributions were integrated to compute the forces acting on the cross-section. The neutral axis for each beam was obtained by locating the point of zero stress for each stress distribution. Assuming that the effective width of the slab for each beam was the center-to-center beam spacing, the bending moment for each beam was computed about its neutral axis. The lateral load distribution factor was then obtained by dividing the resulting moment in each beam by the maximum simple-span moment which would be produced in a similar beam by one line of wheel loads.

4.3 Validation of the Analytical Method

4.3.1 Comparison with Field Test Results

The Brookville Bridge (Fig. 38) which has a skew of 45^{o} was modeled using the procedure previously discussed. All reported moments were presented as the product of a number multiplied by the

modulus of elasticity (Ref. 51), and no information was available which would permit determination of the actual modulus of elasticity of the bridge. Consequently, all comparisons were based upon the percentage of total moment in the bridge which was resisted by each girder. Table 7 compares the field test data with the results obtained from the finite element model. The largest difference between the two values is only 3% and is quite acceptable for the purposes of this investigation.

4.3.2 Comparison with an Alternate Analytical Method

Further model validation was carried out by comparing results obtained from a SAP IV finite element analysis with results computed for right bridges utilizing a finite strip analysis, as reported by Motarjami (Ref. 38). The comparisons were made on bridges having a typical 7-beam cross-section with a curb-to-curb width of 54 ft. Five different bridge lengths were used, with S/L ratios varying from 1/4 to 1/10. The distribution factors obtained from the SAP IV analyses were approximately 8% greater than the results reported by Motarjemi (Table 8). This difference was due to the fact that a different lane definition was used for each analysis. In the Motarjemi analysis, the 54 ft. roadway was divided into four traffic lanes, each 13 ft.-6 in. in width. The vehicles, considered to be 10 feet in width, were then shifted within each of the lanes to produce the maximum distribution factor. This method was consistent with AASHTO provisions in effect at that time. However, the SAP IV analysis, included in this study, was based on the current AASHTO

provisions, which specify load lane widths of 12 ft. The current provisions allow the positioning of load lanes across the roadway width, as well as the positioning of load vehicles within the load lanes. The movement of vehicles within the lanes gives use to more critical loading conditions.

4.4 Load Distribution Factors for Skewed Box-Beam Bridges

4.4.1 Design of the Experiment

To effectively develop a design equation which will accurately predict the lateral load distribution in spread box-beam bridges, the analytical experiment must include a representative sampling of bridge configurations, and must seek to determine the specific parameters which significantly influence overall bridge behavior. The general behavior of skewed, spread box-beam bridges was modeled in this investigation by 72 bridges of different widths, number of beams, span length, and skew angle.

The box-beam bridges selected for this study are listed in Table 9. Each of the 18 bridges listed in Table 9 was investigated at skew angles of 90^{o}, 60^{o}, 45^{o}, and 30^{o}. As a result of the new lane width definition included in the current AASHTO specifications (Ref. 3), the bridge widths, which were considered, are different from those used in Ref. 38 for the study of right bridges. The widths considered are 24 ft., 48 ft., and 72 ft. corresponding to 12 foot lane widths for 2, 4, and 6 design lanes respectively (Ref. 3). These bridge widths are from curb-to-curb and do not include the overhang of 2 ft. on each side of the bridge.

A uniform thickness of 7-1/2 inches was used for the deck slab. Curbs, parapets and diaphragms were not considered. A 48/48 prestressed concrete box-beam (Ref. 43) (48" wide and 48" high) was used for all beams in all bridges. The selection of this particular beam size was made in order to have the stiffest possible beams. Thus, the beams under the load carried a large percentage of the vehicular loading. This has resulted in high distribution factors; consequently the reported results are consistently on the conservative side. Young's modulus was held constant for all bridge configurations and for all elements of each bridge.

Two general loading schemes were utilized to determine distribution factors for both interior and exterior box-beams. Five load conditions, using HS20-44 standard trucks, were applied whenever possible (when the bridge was wide enough); however, the positioning of the design lanes, and of the vehicles within the lanes, was varied depending upon whether interior or exterior beams were being analyzed. For the case of interior beams, lanes and vehicles were crowded as closely as possible to the interior beam. For analysis of exterior beams, the 12 ft. wide traffic lanes and design vehicles were laterally crowded towards an exterior beam. Longitudinally, the design vehicles were positioned in each lane in such a manner that all drive axles fell on the bridge's skew midspan. The rear axles of the design vehicle were placed towards the obtuse angle at the supports. This longitudinal placement produced a very close approximation of the absolute maximum moment in each beam.

4.4.2 Distribution Factors

The maximum distribution factors for the 18 bridges listed in Table 9 with skews of 90°, 60°, 45°, and 30° are listed in Table 10

for interior beams and in Table 11 for exterior beams. Distribution factors were calculated using the procedure previously discussed and indicate that a decrease in the angle of skew results in a significant reduction in the distribution factor for both interior and exterior beams. This reduction can be attributed to the fact that the principal bending of the bridge is in the direction of the skew and is not in the direction of the span. Additionally the cross-sectional geometry of a skewed, spread box-beam bridge provides a better lateral distribution of the loads and consequently results in better participation of all beams in the overall response of the structure.

The larger reduction in the distribution factors at shorter span lengths for the interior beams can be attributed to the fact that, at large skews, some of the design vehicle's wheels were either off of the bridge or very close to the supports. The observed reduction in the distribution factors was, however, considerably larger than that experienced by similar prestressed concrete I-beam bridges. It was further observed that as the length of the bridge span increased, the distribution factor for exterior box-beams also increased.

In the case of interior box-beams, the maximum distribution factor was generally achieved when the bridge was fully loaded. For exterior box-beams, the maximum distribution factors occurred under different load configurations for each of the various bridges. In two-lane bridges maximum moments were achieved when the bridge was fully loaded with two design vehicles. For a four-lane bridge the

governing load condition was found to occur when either three or four vehicles were on the span. The three vehicle load condition created a maximum moment for shorter, less skewed bridges, whereas the four vehicle condition governed for longer, more skewed bridges. The critical load pattern for a six-lane bridge followed the same trend as that of a four-lane bridge with the exception that either four or five design vehicles resulted in maximum moments in exterior box-beams.

4.4.3 Development of the Distribution Factor Equations

The line load bending moments in the interior or exterior beams of skewed, spread box-beam bridges may be determined by applying to the beams the fraction of the wheel load specified by the following formula:

$$DF_{\phi} = DF_{90} \left(1 - \frac{PR}{100}\right) \qquad (4.1)$$

where PR = the percentage reduction appropriate for either interior or exterior box-beams in a skewed bridge

DF_{90} = the distribution factor for an interior or exterior beam of a similar right bridge (i.e., same span, width, and beam spacing)

DF_{ϕ} = the distribution factor for the interior or exterior beam of a bridge with skew angle ϕ

Maximum percentage reductions for interior and exterior box-beams are listed in Tables 12 and 13 for the various bridges analyzed in this study. A regression analysis was carried out on these values, utilizing the Lehigh Amalgamated Package for Statistics (LEAPS)

computer program (Ref. 30), to determine appropriate design equations for the percentage reduction (PR) factor included in Eq. 4.1.

The following forms of equations were regressed:

$$PR = K\left(\frac{S}{L}\right)^{x}\left(\frac{W_c}{L}\right)^{y}(\cot\phi)^{z} \tag{4.2}$$

$$PR = K\left(\frac{S}{L}\right)^{x}(\cot\phi)^{y} \tag{4.3}$$

$$PR = K\left(\frac{W}{L}\right)^{x}(\cot\phi)^{y} \tag{4.4}$$

These equations consider various combinations of the critical parameters of span length (L), beam spacing (S), and curb-to-curb width (W_c). Specific results are discussed in the following section; however, it was generally found that an expression in the form of Eq. 4.2 most accurately represented the data obtained from the analytical experiment. This observation emphasizes the influence of bridge aspect ratio (W_c/L) on overall structural behavior. However, it was also observed that Eq. 4.3, which has a simpler form, adequately approximated the experimental data. This observation indicated that the influence of bridge aspect ratio was less significant than that of spacing to length (S/L) ratio or skew angle.

4.5 Design Recommendations

Distribution factors for skewed, spread box-beam bridges may be determined from Eq. 4.1 utilizing the following expressions for the percentage reduction (PR) factor for interior or exterior box-beams.

Interior Box-Beams

$$PR = 29.0\left(\frac{W_c}{L}\right)^{1/10}\left(\frac{S}{L}\right)^{1/2}\left(\cot\ \phi\right)^{3/2} \qquad (4.5)$$

or

$$PR = 33.0\left(\frac{S}{L}\right)^{1/2}\left(\cot\ \phi\right) \qquad (4.6)$$

Exterior Box-Beams

$$PR = 19.5\left(\frac{W_c}{L}\right)^{1/3}\left(\frac{S}{L}\right)^{1/5}\left(\cot\ \phi\right)^{4/3} \qquad (4.7)$$

or

$$PR = 30.0\left(\frac{S}{L}\right)^{1/2}\left(\cot\ \phi\right) \qquad (4.8)$$

Figures 39 through 50 present comparisons between the results of the analytical experiment and the proposed empirical expression for skew distribution factors (Eq. 4.1). As previously discussed, Eqs. 4.5 and 4.7 more accurately represent the experimental data; however, Eqs. 4.6 and 4.8 have a much simpler form, can be readily adopted for design application, and provide an adequate approximation of overall bridge behavior. Although the more sophisticated expressions are preferred on the basis of their improved accuracy, the simpler expressions are adequate for routine bridge design.

All of the above expressions are limited by the following bridge dimensions:

$$24' \leq W_c \leq 72'$$

$$42' \leq L \leq 128'$$

$$30^\circ \leq \phi \leq 90^\circ$$

4.6 Summary

The load distribution behavior of skewed, spread box-beam bridges under design vehicular loads has been discussed. Load distribution factors were computed for the interior and exterior beams of bridges constructed with prestressed concrete box-beams. The skew angles investigated were 90°, 60°, 45°, and 30°. The following observations were made:

1. The load distribution factor decreases with decreasing angle of skew.
2. The reduction factor is largest at shorter span lengths for interior beams and at longer span lengths for exterior beams. This behavior is primarily the result of increased participation of the exterior beams in longer spans.
3. The bridge width-to-span ratio, the beam spacing-to-span ratio, and the skew angle sufficiently affect the magnitude of the percentage reduction factor.

Based upon a statistical correlation of bridge parameters with numerical results, simplified equations for computing distribution factors for interior and exterior box-beams were developed.

5. SUMMARY AND RECOMMENDATION

This report describes the development of skew-effect correction factors which are to be applied to the live-load distribution factors in beam-slab highway bridge superstructures supported by prestressed concrete I-beams or box-beams.

Initially, an analytical procedure utilizing the finite element method was developed to evaluate the response of skewed-bridge superstructures to design-vehicle loading. The analytical technique was validated through comparisons with previous field test results of in-service bridges and by comparisons with alternate analytical solutions. An analytical experiment was then designed for each type of bridge to study the effects of various parameters on live-load distribution. A total of 120 I-beam and 72 box-beam superstructures were analyzed under numerous loading conditions. The results of these analyses provided a data base which was utilized to develop appropriate design equations for both interior and exterior beams. The design equations were based upon formulating appropriate corrections to the distribution factors for similar right bridges to account for skew, and yielded the live-load distribution factors required for the design of skewed bridge superstructures.

Based upon the results of this study, it is recommended that the expressions governing live-load distribution in skewed beam-slab bridges, as presented in Sections 3.5 and 4.5 of this report, be

adopted as modifications to the specification provisions currently governing live-load distribution in right beam-slab bridges. The proposed expressions are relatively simple in form and clearly yield values which accurately represent the behavior of skewed beam-slab bridges.

6. ACKNOWLEDGMENTS

This study was conducted in the Department of Civil Engineering and Fritz Engineering Laboratory, under the auspices of the Lehigh University Office of Research, as a part of the research investigation entitled "Development and Refinement of Load Distribution Provisions for Prestressed Concrete Beam-Slab Bridges" sponsored by the Pennsylvania Department of Transportation; the U. S. Department of Transportation, Federal Highway Administration; and the Reinforced Concrete Research Council.

The basic research planning and administrative coordination in this investigation were in cooperation with the following individuals representing the Pennsylvania Department of Transportation: B. F. Kotalik, Chief Bridge Engineer; H. P. Koretzky, and Hans Streibel, all from the Bridge Division; and Istvan Januaschek, Research Coordinator; from the Office of Research and Special Studies.

The following members of the staff at Lehigh University made significant contributions: Bert Hoffman in the programming and execution of some of the computer analysis, and Charles R. Kubic in the assembly of material and the writing of this report.

TABLE 1

MOMENT COEFFICIENTS AND REACTIONS IN A 45° SKEW BRIDGE WITH CHANGE IN BOUNDARY CONDITIONS

Beam	Moment Coefficients x L x P		Reactions at Left Support x P	
	S.S.[1]	Skew S.S.[2]	S.S.[1]	Skew S.S.[2]
A	0.00232	0.0233	0.0614	0.0600
B	0.0437	0.0439	0.0371	0.0412
C	0.0922	0.0918	0.1085	0. .028
D	0.0437	0.0439	0.2545	0.2254
E	0.00232	0.0233	0.0385	0.0706

[1]Simply supported.

[2]Simply supported and constrained to rotate about skew line of support, $\beta = 45^{\circ}$.

TABLE 2

LOAD DISTRIBUTION COEFFICIENTS - BRIDGE 3[1]

	Ratio of Bending Moments (%)	
	Interior Girders	Exterior Girders
Field Test	60	40
Analytical Results	59	41

[1]Ref. 6

TABLE 3

MOMENT PERCENTAGES

Bridge		Σ Beam Moment	Beam Moment/Σ Beam Moment		
		Truck Moment	Interior	Center	Exterior
2B	Field Test (Ref. 24)	89.30	34.0	32.0	34.0
	Finite Element (composite)	93.57	32.6	34.0	33.2
	Finite Element (non-composite)	92.13	33.2	33.8	33.0
3B	Field Test (Ref. 24)	92.10	33.8	33.4	29.2
	Finite Element (composite)	94.50	32.7	34.3	33.0
	Finite Element (non-composite)	83.95	33.2	33.8	33.0

TABLE 4

LIST OF BRIDGES ANALYZED

Bridge No.	Width (ft.)	Number of Beams	Spacing (in.)	Length (ft.)	Beam Size	S/L
1	24.00	6	57.60	120.00	AASHO-VI	.0400
2	24.00	6	57.60	72.00	24/42	.0667
3	24.00	6	57.60	38.40	20/30	.1250
4	24.00	5	72.00	120.00	AASHO-VI	.0500
5	24.00	5	72.00	60.00	20/39	.1000
6	24.00	5	72.00	42.00	20/30	.1429
7	24.00	4	96.00	120.00	AASHO-VI	.0667
8	24.00	4	96.00	64.00	24/45	.1250
9	24.00	4	96.00	40.00	20/30	.2000
10	48.00	11	57.60	120.00	AASHO-VI	.0400
11	48.00	11	57.60	84.00	24/48	.0571
12	48.00	11	57.60	48.00	20/30	.1000
13	48.00	9	72.00	105.00	28/63	.0571
14	48.00	9	72.00	60.00	20/39	.1000
15	48.00	9	72.00	42.00	20/30	.1429
16	48.00	6	115.20	96.00	AASHO-VI	.1000
17	48.00	6	115.20	57.60	24/45	.1667
18	48.00	6	115.20	48.00	20/33	.2000
19	72.00	16	57.60	120.00	ASSHO-VI	.0400
20	72.00	16	57.60	57.60	20/36	.0833
21	72.00	16	57.60	38.40	AASHO-I	.1250
22	72.00	14	66.50	110.80	AASHO-VI	.0500
23	72.00	14	66.50	66.50	24/42	.0833
24	72.00	14	66.50	38.80	AASHO-I	.1429
25	72.00	12	78.50	114.50	AASHO-VI	.0571
26	72.00	12	78.50	65.50	24/42	.1000
27	72.00	12	78.50	39.30	20/30	.1667
28	72.00	9	108.00	108.00	AASHO-VI	.0833
29	72.00	9	108.00	54.00	24/42	.1667
30	72.00	9	108.00	45.00	24/36	.2000

TABLE 5

MAXIMUM DISTRIBUTION FACTORS - INTERIOR BEAMS

Bridge No.	NUMBER OF LOADED LANES AND SKEW ANGLE								
	*NL	**NLL	90°	NLL	60°	NLL	45°	NLL	30°
1	2	2	.81	2	.79	2	.77	2	.71
2	2	2	.84	2	.81	2	.77	2	.66
3	2	2	.96	2	.94	2	.93	2	.86
4	2	2	.96	2	.92	2	.88	2	.82
5	2	2	1.05	2	.99	2	.92	2	.78
6	2	2	1.17	2	1.07	2	.95	2	.76
7	2	2	1.23	2	1.20	2	1.18	2	1.08
8	2	2	1.30	2	1.24	2	1.17	2	.99
9	2	2	1.32	2	1.23	2	1.14	2	.88
10	4	4	.94	4	.91	4	.87	4	.79
11	4	4	.94	4	.90	4	.87	4	.75
12	4	2	1.03	3	.98	3	.94	3	.87
13	4	4	1.17	4	1.13	4	1.09	4	.97
14	4	4	1.20	4	1.14	4	1.08	4	.89
15	4	4	1.24	3	1.13	3	1.07	3	.83
16	4	4	1.84	4	1.79	4	1.74	4	1.59
17	4	4	1.83	4	1.77	4	1.70	4	1.45
18	4	4	1.86	4	1.72	4	1.58	3	1.24
19	6	5	.94	5	.92	5	.90	5	.84
20	6	4	.95	4	.91	4	.87	5	.75
21	6	4	.97	4	.91	4	.96	5	.72
22	6	5	1.07	5	1.05	5	1.04	5	.98
23	6	4	1.07	4	1.04	4	1.01	5	.89
24	6	4	1.09	4	1.02	5	.96	5	.77
25	6	5	1.23	5	1.21	5	1.19	5	1.11
26	6	4	1.24	5	1.20	5	1.16	5	1.03
27	6	4	1.30	4	1.21	5	1.12	5	.89
28	6	5	1.72	5	1.68	5	1.65	6	1.51
29	6	4	1.74	5	1.68	5	1.61	5	1.33
30	6	4	1.77	5	1.68	5	1.60	5	1.23

*Number of Lanes
**Number of Loaded Lanes

TABLE 6

MAXIMUM DISTRIBUTION FACTORS - EXTERIOR BEAMS

Bridge No.	NUMBER OF LOADED LANES AND SKEW ANGLE								
	*NL	**NLL	90°	NLL	60°	NLL	45°	NLL	30°
1	2	2	.69	2	.70	2	.70	2	.72
2	3	2	.67	2	.67	2	.67	2	.64
3	2	2	.56	1	.57	1	.57	2	.58
4	2	2	.80	2	.81	2	.82	2	.83
5	2	2	.75	2	.77	2	.78	2	.73
6	2	2	.73	2	.73	2	.72	2	.62
7	2	2	1.01	2	1.02	2	1.02	2	1.01
8	2	2	.95	2	.95	2	.94	2	.88
9	2	2	.87	2	.87	2	.86	2	.74
10	4	2	.71	2	.72	2	.73	3	.73
11	4	4	.68	2	.68	2	.68	4	.65
12	4	1	.62	1	.61	1	.61	2	.59
13	4	2	.83	2	.83	2	.84	4	.83
14	4	2	.78	2	.76	2	.76	4	.70
15	4	2	.72	2	.74	4	.71	4	.62
16	4	2	1.10	2	1.10	2	1.11	4	1.09
17	4	2	1.02	2	1.01	2	1.00	4	.92
18	4	2	1.08	2	1.03	4	.99	4	.85
19	6	2	.70	2	.71	2	.72	3	.72
20	6	6	.65	2	.64	2	.63	2	.58
21	6	1	.61	1	.60	2	.60	2	.53
22	6	2	.78	2	.78	2	.79	2	.78
23	6	2	.74	2	.72	2	.73	2	.67
24	6	1	.68	2	.66	2	.67	6	.58
25	6	2	.88	2	.89	2	.91	3	.91
26	6	2	.83	2	.85	2	.86	6	.80
27	6	1	.74	2	.75	2	.75	2	.63
28	6	2	1.09	2	1.10	2	1.11	3	1.09
29	6	2	.97	2	.96	2	.95	6	.86
30	6	2	.95	2	.93	2	.91	6	.80

*Number of Lanes
**Number of Loaded Lanes

TABLE 7

BROOKVILLE BRIDGE COMPARISON

Percentage of Total Moment Taken by Each Girder (Fig. 38)

Method \ Girder	A	B	C	D
Field Test	44%	31%	15%	10%
Model	47%	32%	14%	7%

TABLE 8

MOTARJEMI COMPARISON

Load Distribution Factors as Reported by Motarjemi and by Model Analysis

S/L	Motarjemi	Model
1/4	1.08	1.16
1/5	1.12	1.20
1/6	1.13	1.21
1/8	1.15	1.23
1/10	1.15	1.24

TABLE 9

LIST OF SPREAD BOX-BEAM BRIDGES

Bridge No.	Width (ft.)	Number of Beams	Spacing (in.)	Length (ft.)	Beam Size	S/L
1	24.00	3	122.50	40.83	3-48/48	.2500
2	24.00	3	122.50	71.46	3-48/48	.1430
3	24.00	3	122.50	122.50	3-48/48	.0830
4	24.00	4	81.67	34.03	4-48/48	.2000
5	24.00	4	81.67	47.64	4-48/48	.1430
6	24.00	4	81.67	102.08	4-48/48	.0670
7	48.00	5	133.25	44.42	5-48/48	.2500
8	48.00	5	133.25	88.83	5-48/48	.1250
9	48.00	5	133.25	11.04	5-48/48	.1000
10	48.00	7	88.83	37.01	7-48/48	.2000
11	48.00	7	88.83	59.22	7-48/48	.1250
12	48.00	7	88.83	111.03	7-48/48	.0670
13	72.00	8	117.29	39.10	8-48/48	.2500
14	72.00	8	117.29	78.19	8-48/48	.1250
15	72.00	8	117.29	97.74	8-48/48	.1000
16	72.00	9	102.62	42.75	9-48/48	.2000
17	72.00	9	102.62	68.42	9-48/48	.1250
18	72.00	9	102.62	128.25	9-48/48	.0670

TABLE 10

MAXIMUM DISTRIBUTION FACTOR - INTERIOR BEAMS

Bridge Number	90°	60°	45°	30°
1	1.73	1.62	1.45	1.12
2	1.63	1.56	1.46	1.22
3	1.51	1.47	1.40	1.23
4	1.17	1.07	0.96	0.79
5	1.13	1.07	0.98	0.80
6	1.07	1.04	0.99	0.86
7	1.92	1.82	1.66	1.32
8	1.87	1.80	1.69	1.42
9	1.85	1.79	1.69	1.43
10	1.39	1.27	1.12	0.86
11	1.32	1.25	1.16	0.95
12	1.27	1.22	1.16	0.98
13	1.72	1.61	1.46	1.18
14	1.67	1.60	1.51	1.25
15	1.66	1.61	1.52	1.27
16	1.55	1.46	1.33	1.04
17	1.51	1.44	1.35	1.12
18	1.47	1.42	1.35	1.14

TABLE 11

MAXIMUM DISTRIBUTION FACTOR - EXTERIOR BEAMS

Bridge Number	NL	90°		60°		45°		30°	
		NLL	DF	NLL	DF	NLL	DF	NLL	DF
1	2	2	1.30	2	1.21	2	1.12	2	0.93
2	2	2	1.34	2	1.28	2	1.22	2	1.08
3	2	2	1.36	2	1.32	2	1.27	2	1.16
4	2	2	1.01	2	0.94	2	0.87	2	0.72
5	2	2	1.03	2	0.98	2	0.91	2	0.79
6	2	2	1.05	2	1.02	2	0.99	2	0.90
7	4	3	1.45	3	1.34	3	1.22	4	1.01
8	4	3	1.48	4	1.40	4	1.34	4	1.17
9	4	3	1.50	4	1.43	4	1.37	4	1.21
10	4	3	1.09	3	1.01	3	0.91	4	0.75
11	4	3	1.13	3	1.05	4	0.98	4	0.85
12	4	3	1.15	4	1.09	4	1.05	4	0.93
13	6	4	1.32	4	1.22	4	1.11	4	0.92
14	6	4	1.39	4	1.31	5	1.22	5	1.05
15	6	5	1.40	5	1.32	5	1.24	5	1.08
16	6	4	1.22	4	1.13	4	1.03	4	0.86
17	6	4	1.26	4	1.19	5	1.10	5	0.95
18	6	5	1.29	5	1.22	5	1.15	5	1.00

TABLE 12

MAXIMUM PERCENTAGE REDUCTION - INTERIOR BEAMS

Bridge Number	90°	60°	45°	30°
1	0.00	6.36	16.18	35.26
2		4.29	10.43	25.15
3		2.65	7.28	18.54
4		8.55	17.95	32.48
5		5.31	13.27	29.20
6		2.80	7.48	19.63
7		5.21	13.54	31.25
8		3.74	9.63	24.06
9		3.24	8.65	22.70
10		8.63	19.42	38.13
11		5.30	12.12	28.03
12		3.94	8.66	22.83
13		6.40	15.12	31.40
14		4.19	9.58	25.15
15		3.01	8.43	23.49
16		5.81	14.20	32.90
17		4.64	10.60	25.83
18	0.00	3.40	8.16	22.45

TABLE 13

MAXIMUM PERCENTAGE REDUCTION - EXTERIOR BEAMS

Bridge Number	90°	60°	45°	30°
1	0.00	6.92	13.85	28.46
2		4.48	8.96	19.40
3		2.94	6.62	14.71
4		6.93	13.86	28.71
5		4.85	11.65	23.30
6		2.86	5.71	14.29
7		7.59	15.86	30.34
8		5.41	9.46	20.95
9		4.67	8.67	19.33
10		7.34	16.51	31.19
11		7.08	13.27	24.78
12		5.22	8.70	19.13
13		7.58	15.91	30.30
14		5.76	12.23	24.46
15		5.71	11.43	22.86
16		7.38	15.57	29.51
17		5.56	12.70	24.60
18	0.00	5.43	10.85	22.48

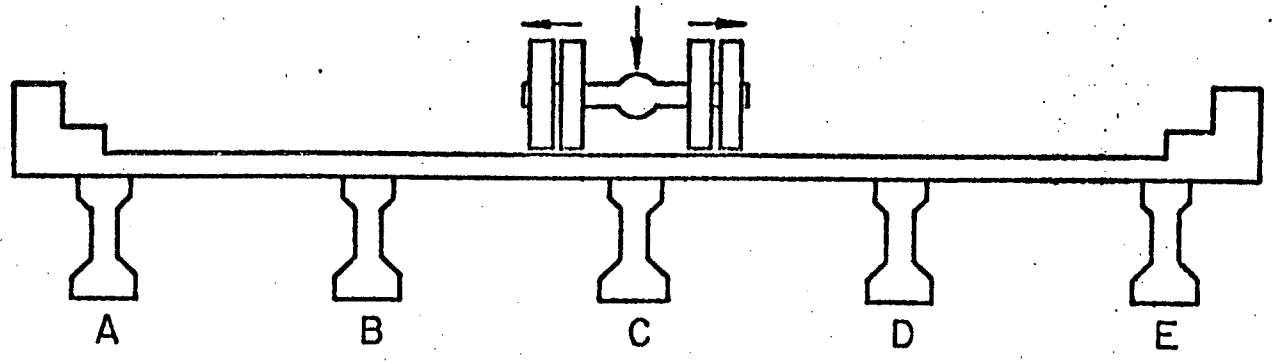

(a) Prestressed Concrete I-beam Bridge

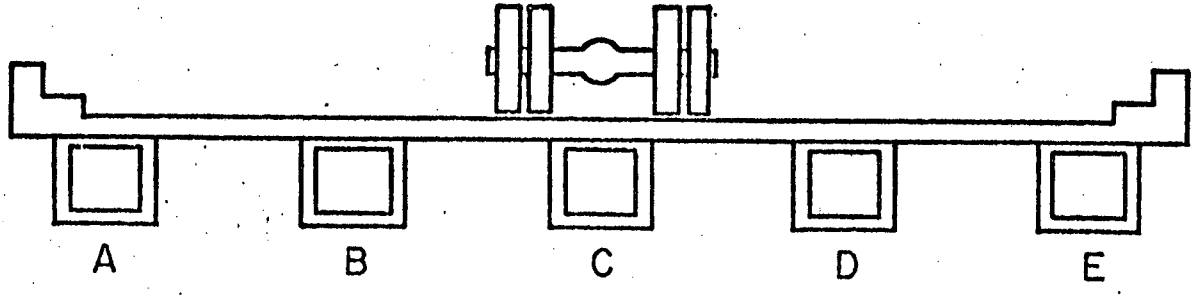

(b) Prestressed Concrete Spread Box-Beam Bridge

Fig. 1 Beam-Slab Bridge Cross Section

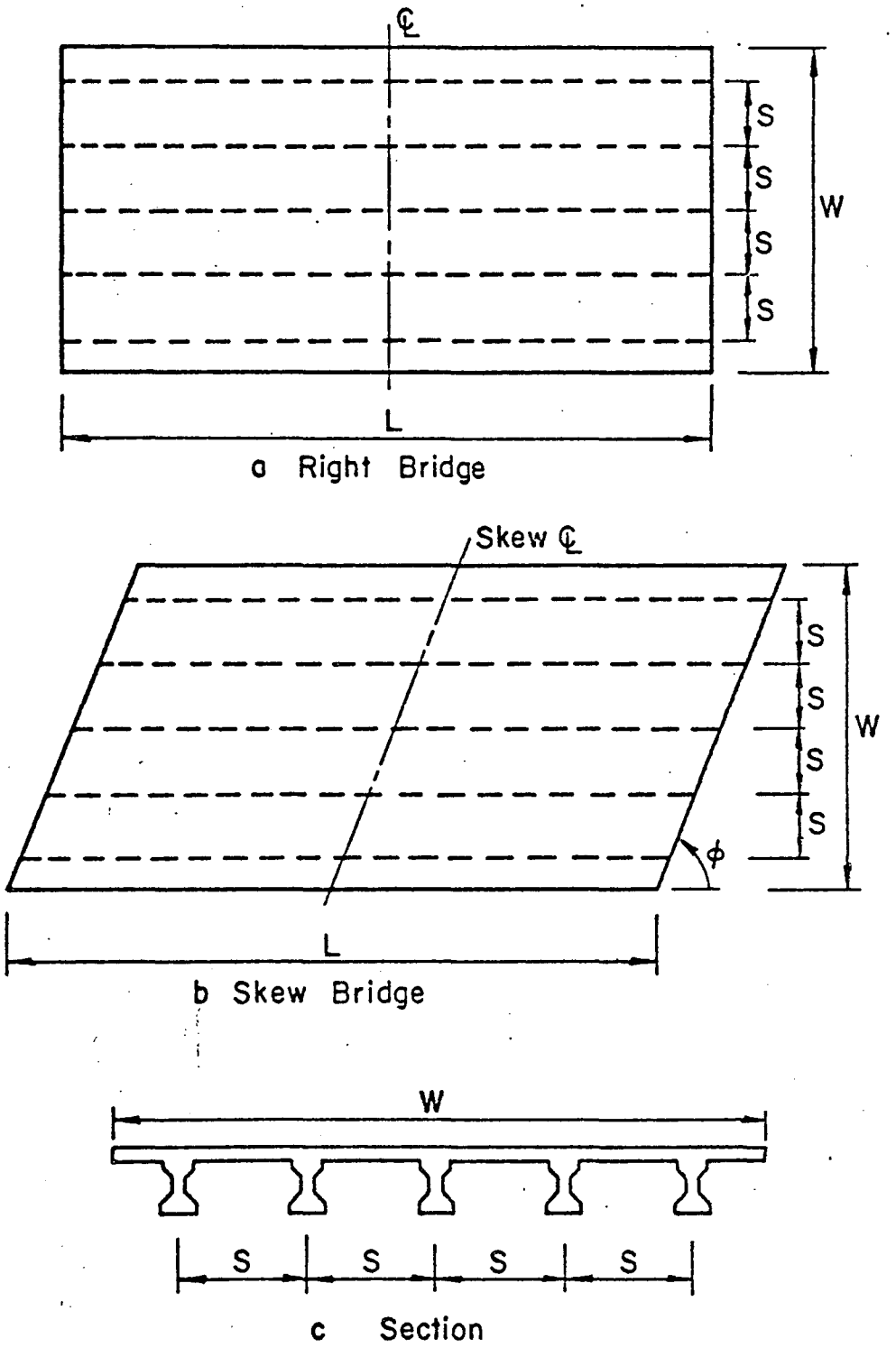

Fig. 2 Plan and Cross Section of a Beam-Slab Bridge

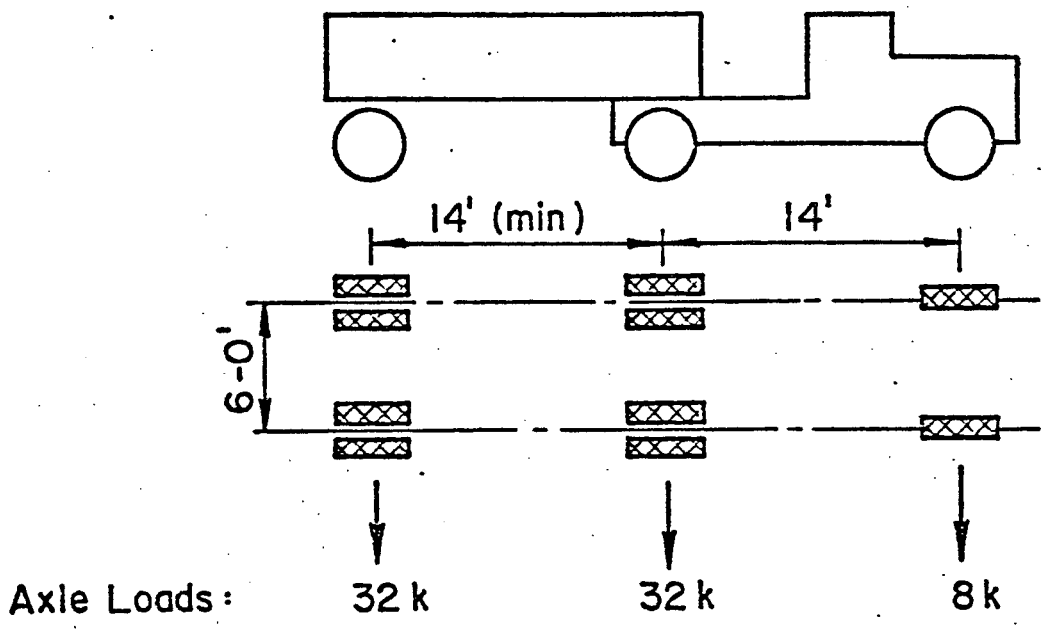

HS 20-44 Design Load Vehicle

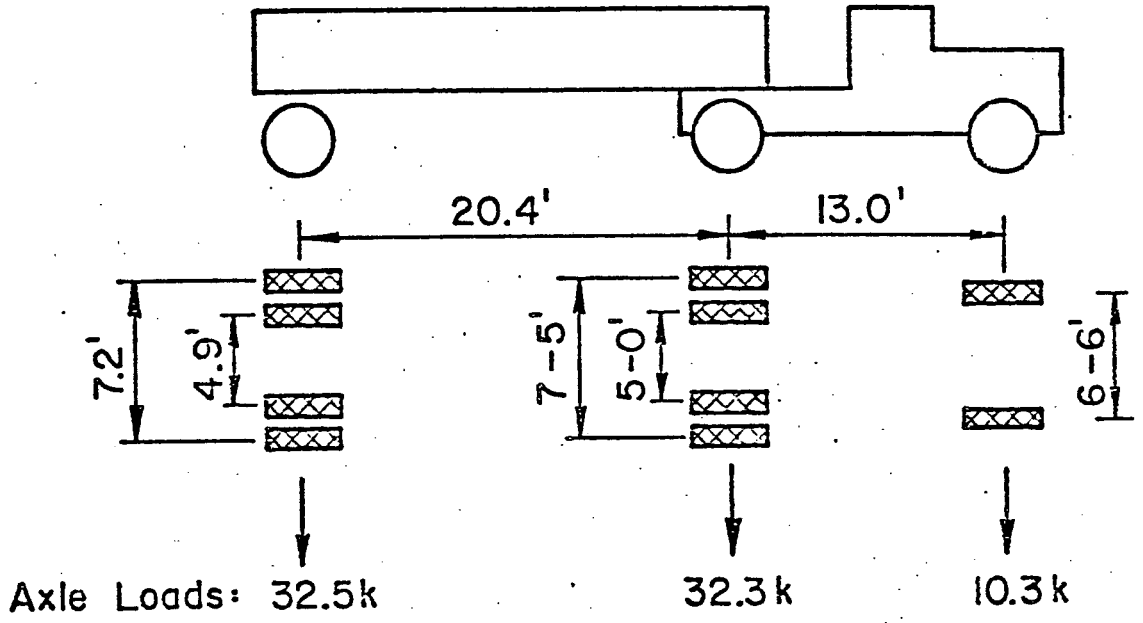

Test Vehicle

Fig. 3 Vehicular Loadings

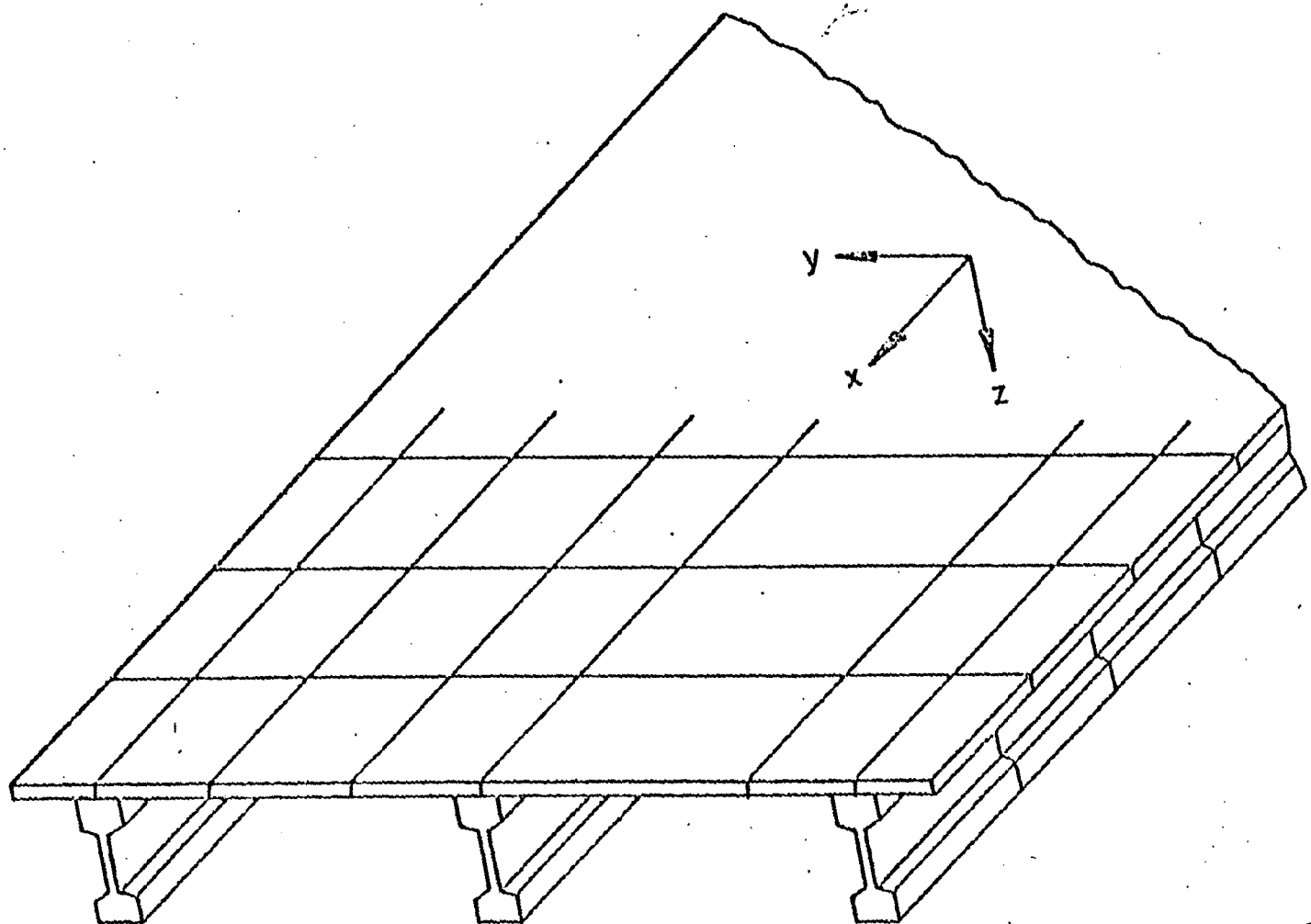

Fig. 4 Finite Element Discretization of a Prestressed Concrete I-Beam Bridge

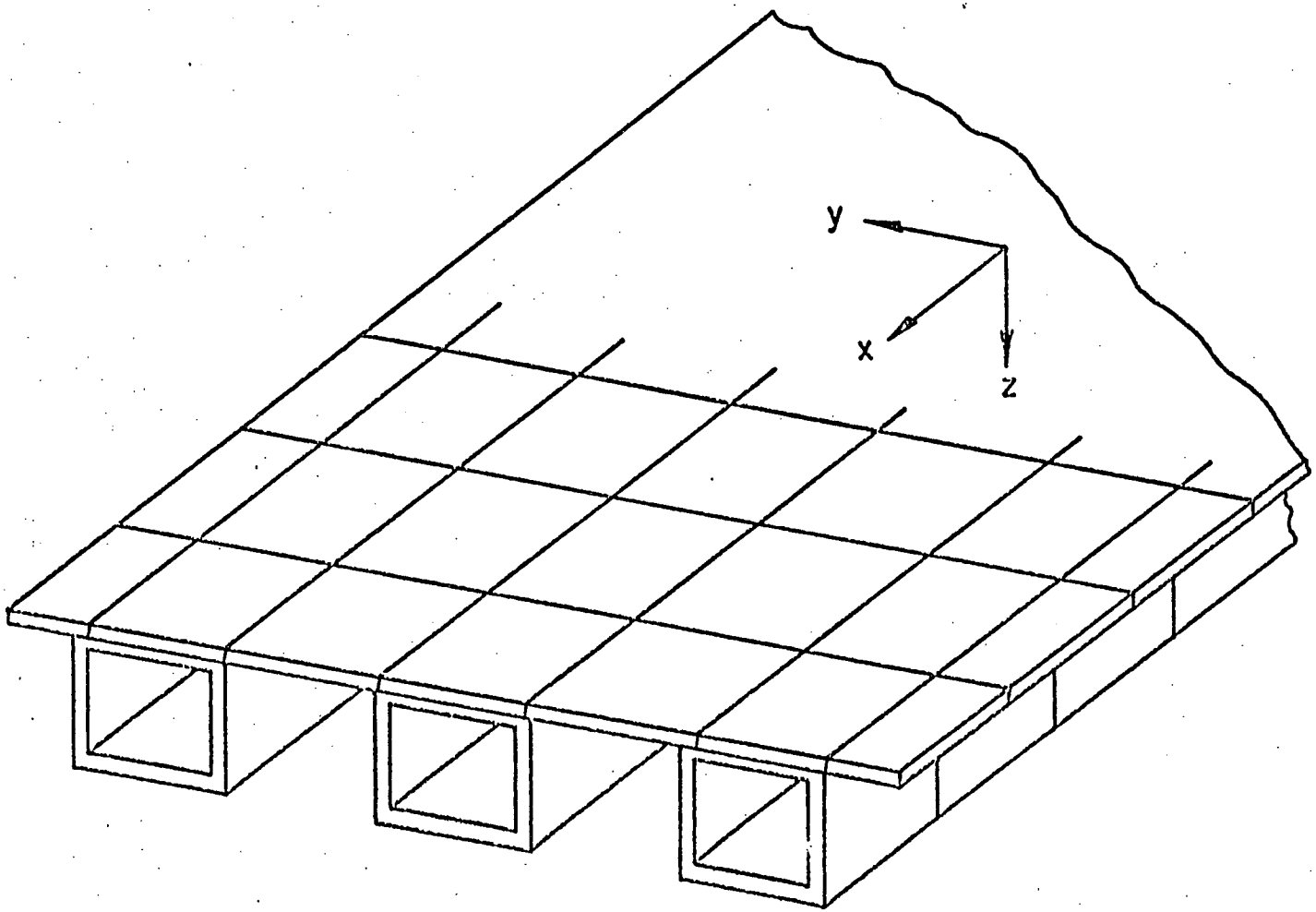

Fig. 5 Finite Element Discretization of a Prestressed Concrete Spread Box-Beam Bridge

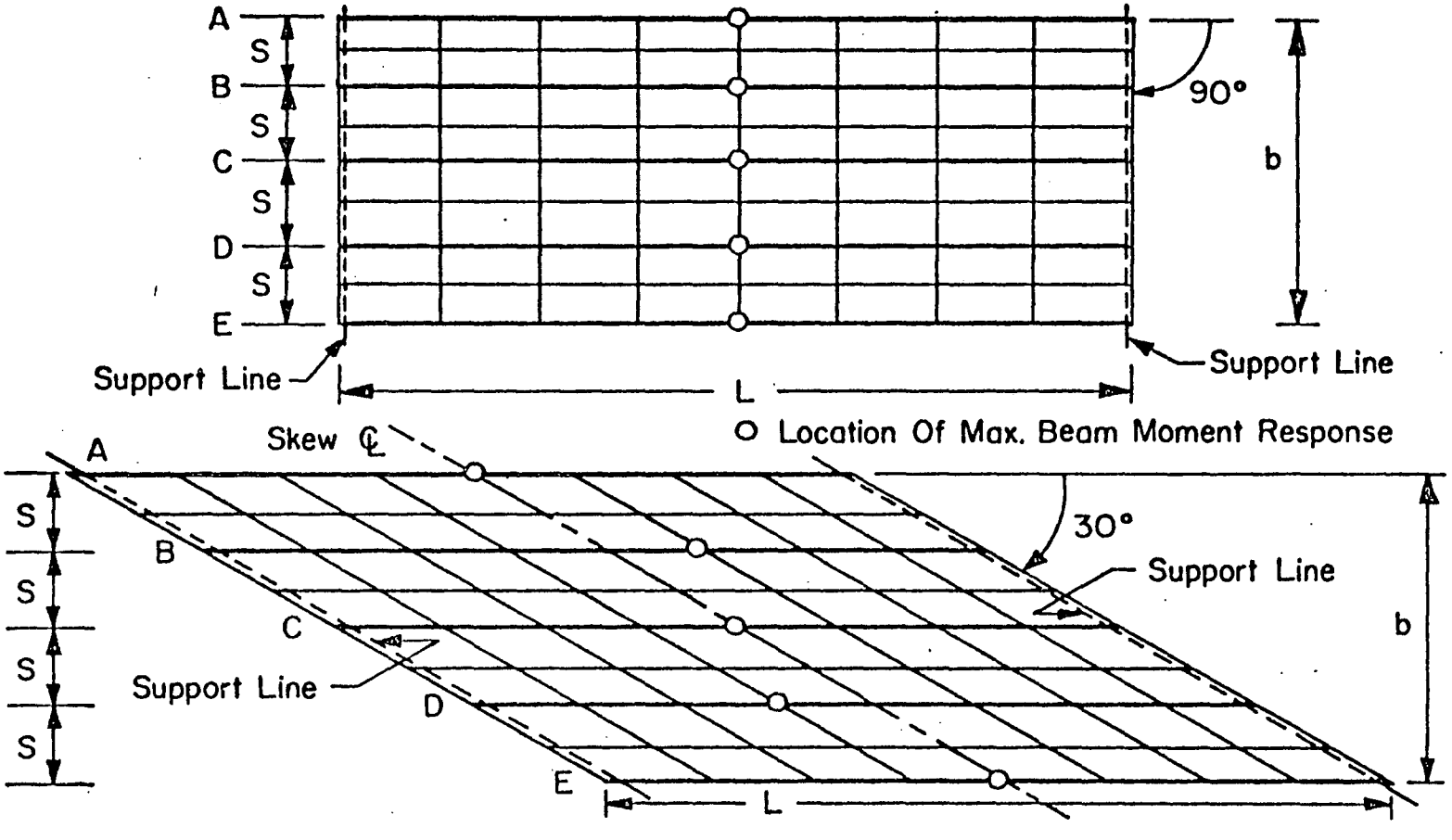

Fig. 6 Location of the Maximum Beam Moment Response in a 90° Skew Bridge (Right Bridge) and a 30° Skew Bridge - Concentrated Load at Midspan of Beam C

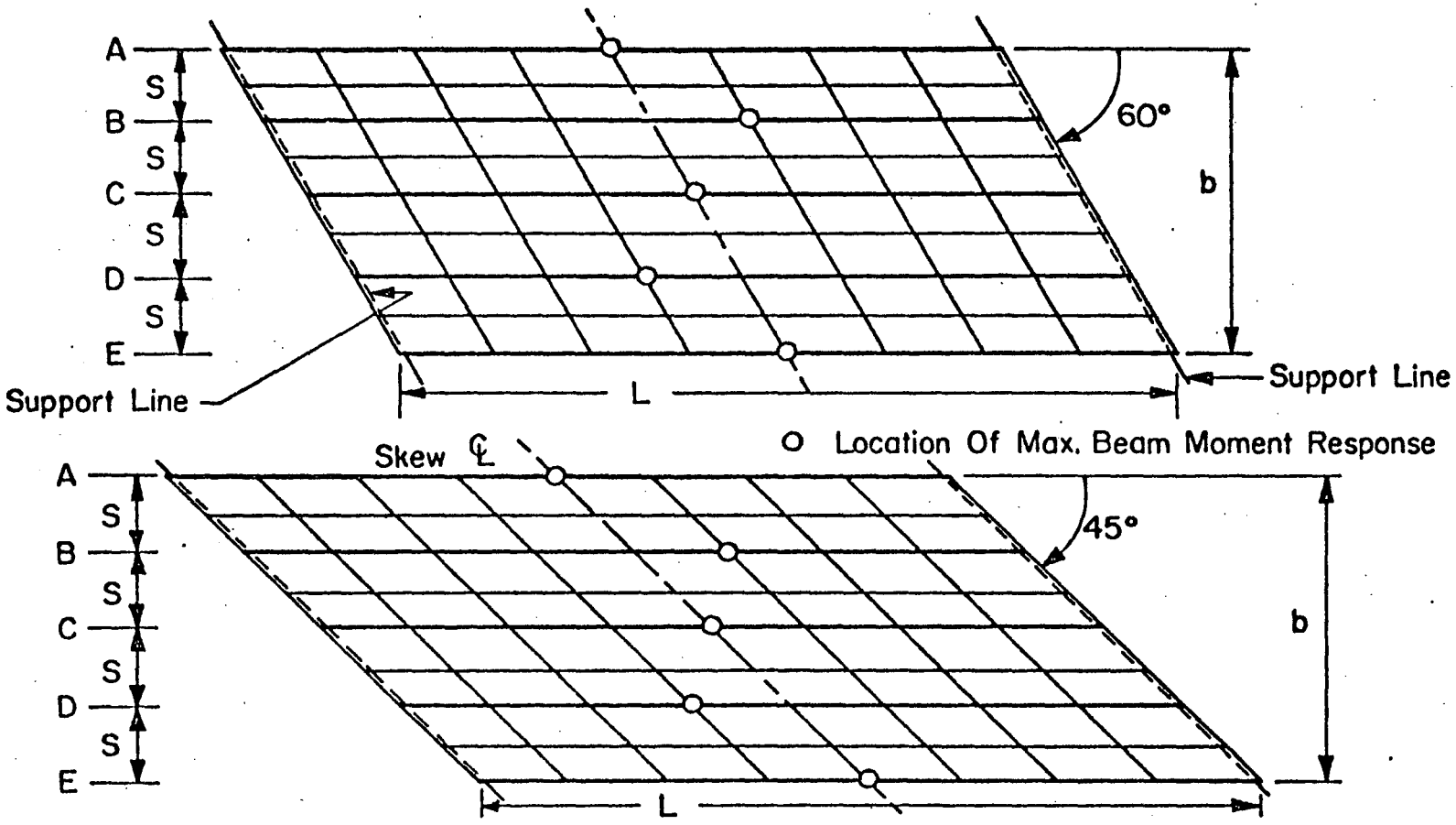

Fig. 7 Location of the Maximum Beam Moment Response in a 60° Skew Bridge and a 45° Skew Bridge - Concentrated Load at Midspan of Beam C

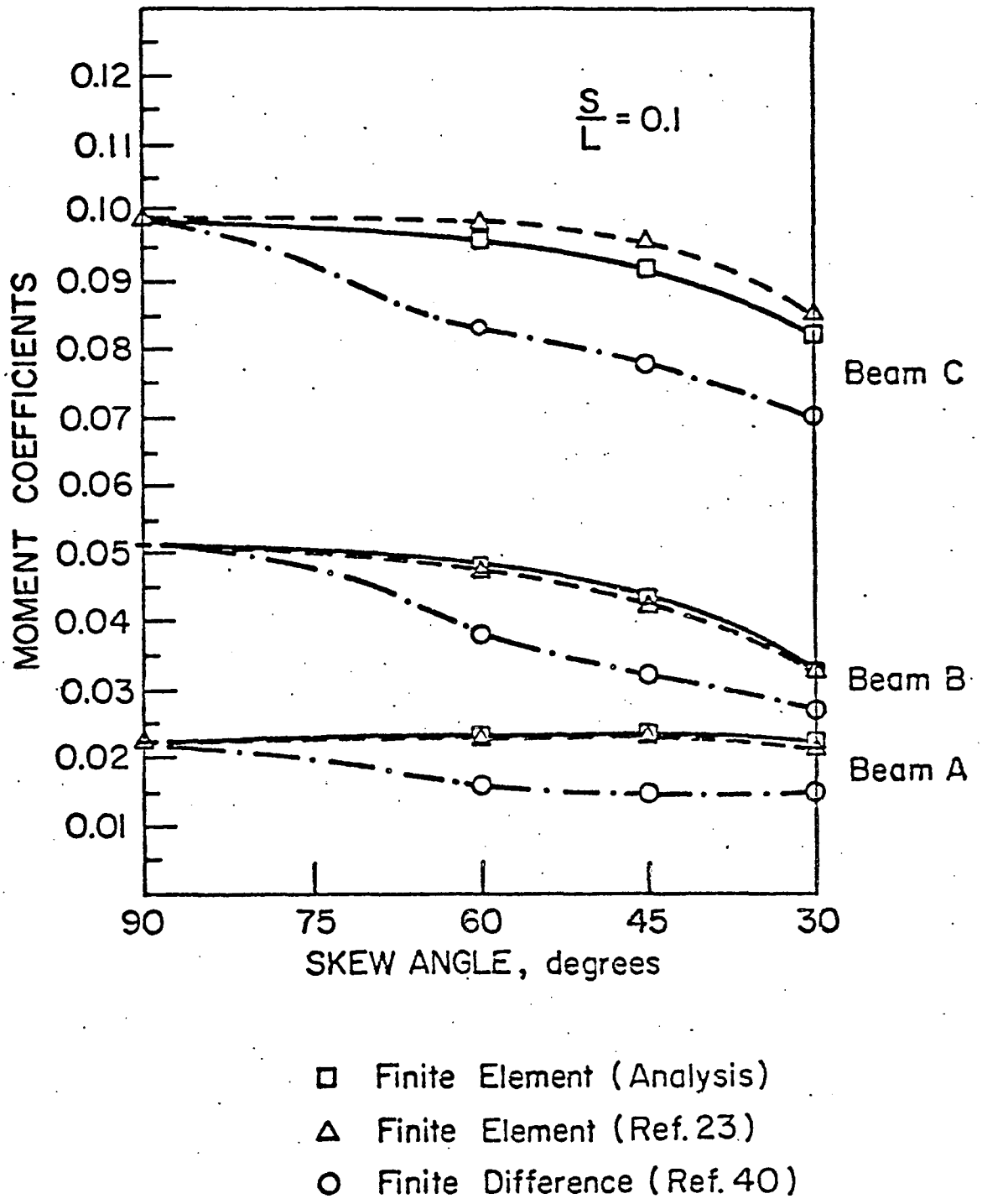

Fig. 8 Moment Coefficients in a 5-Beam Bridge Neglecting the Eccentricity of the Beams to the Slab

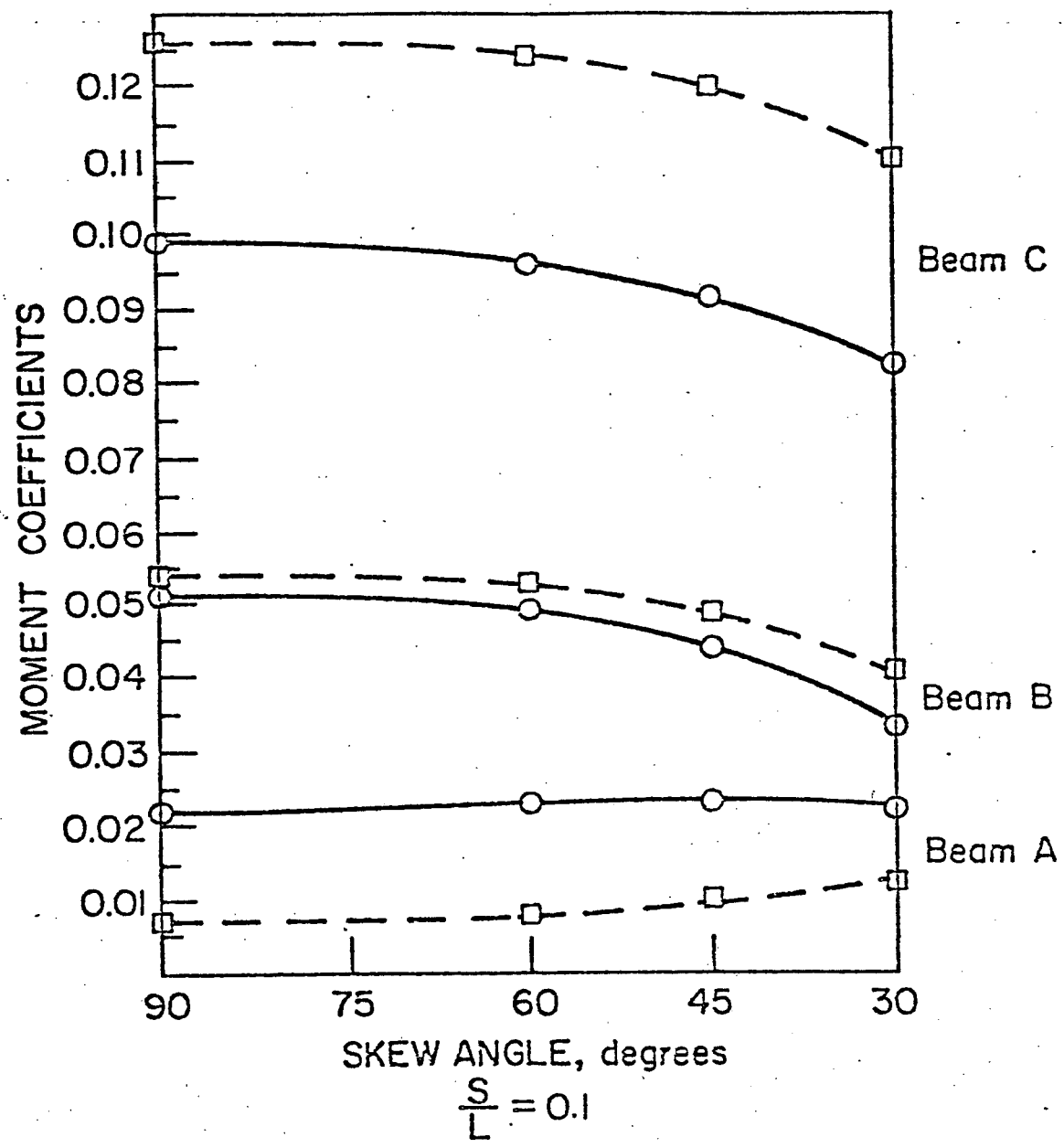

Fig. 9 Moment Coefficients in a 5-Beam Bridge Including the Beam Eccentricity and Torsional Rigidity

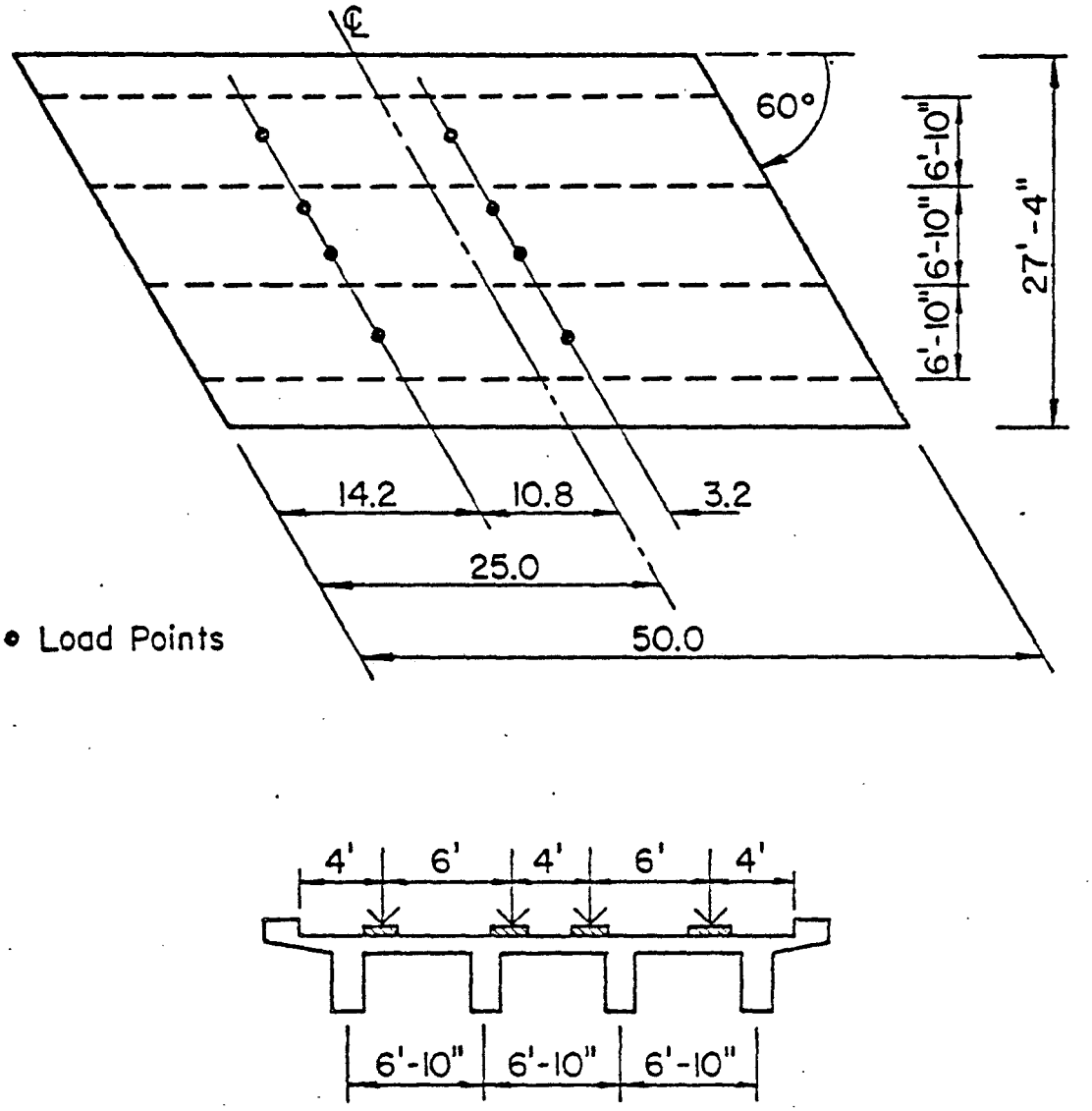

Fig. 10 Static Load Test of Bridge 3 (Ref. 6)

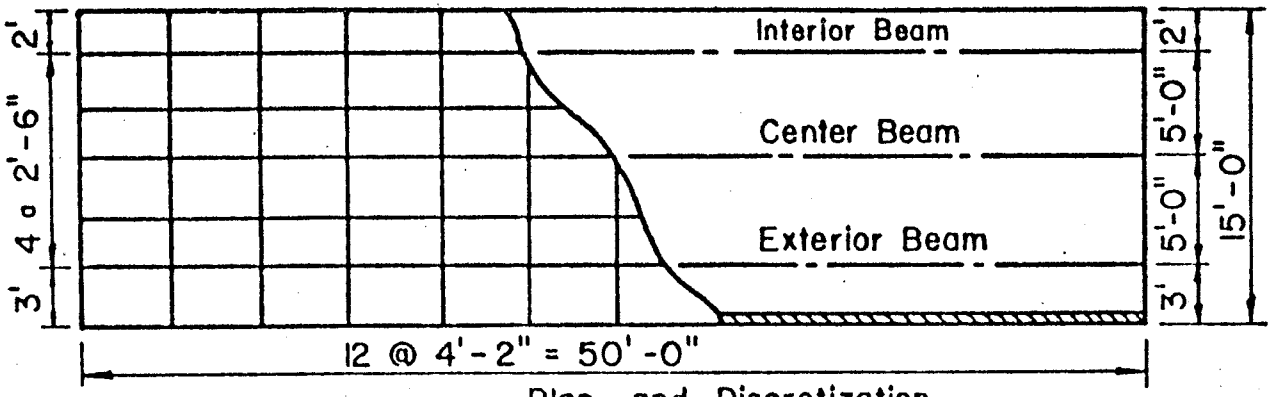

Plan and Discretization

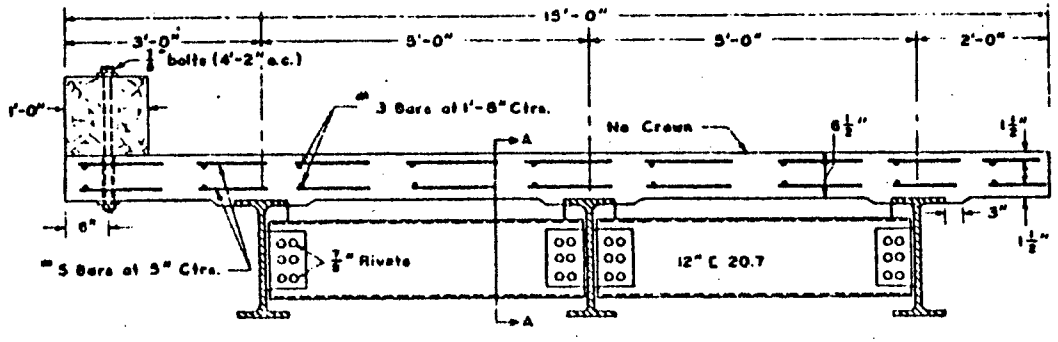

Beam Properties

Bridge	Beam Size	I_x (in^4) w/Coverplate
2B	w18 x 50	1040
3B	w18 x 60	1176

Fig. 11 AASHO Test Bridge (Ref. 24)

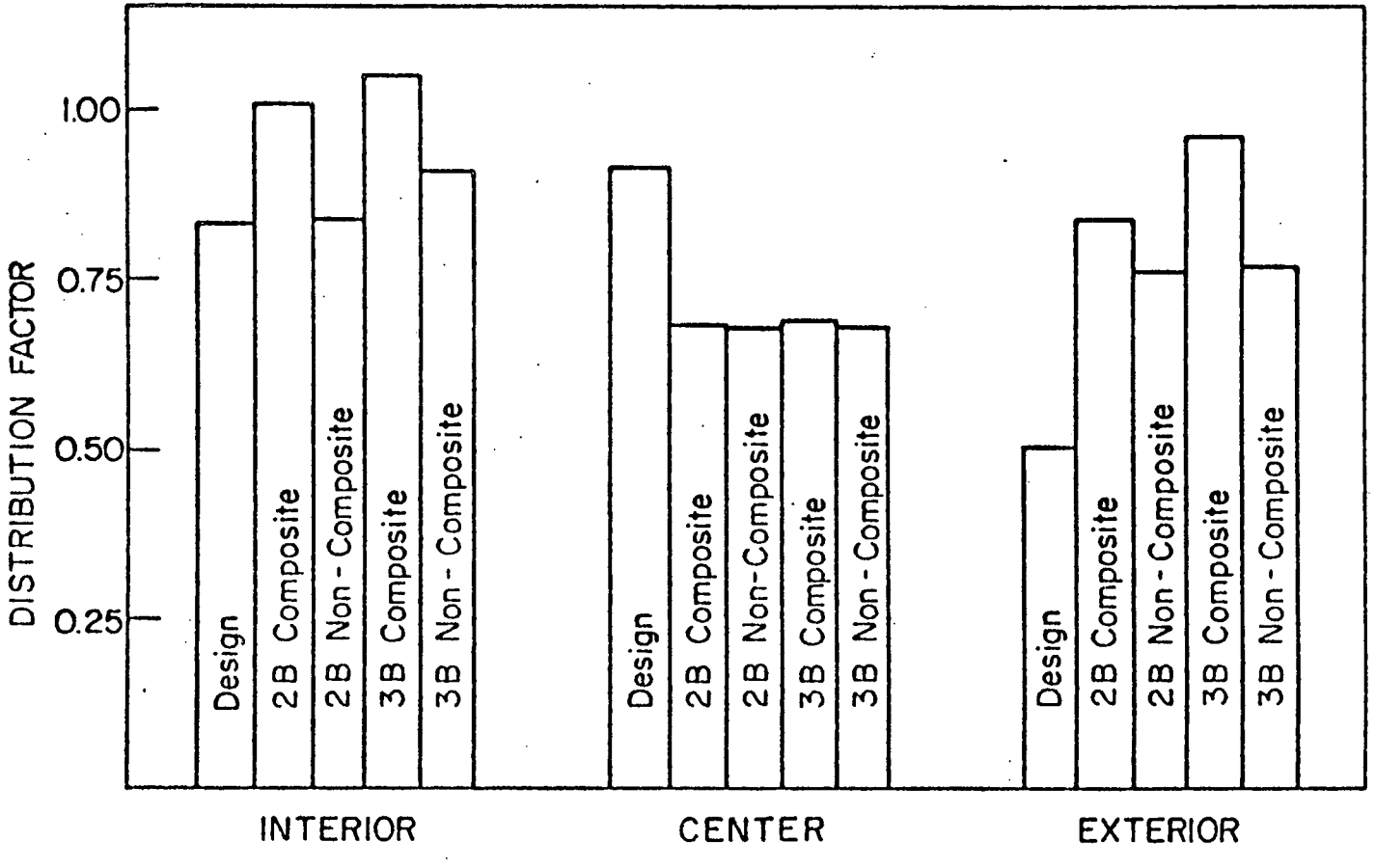

Fig. 12 Distribution Factors for Interior, Center and Exterior Bridge Beams - AASHO Test Bridge

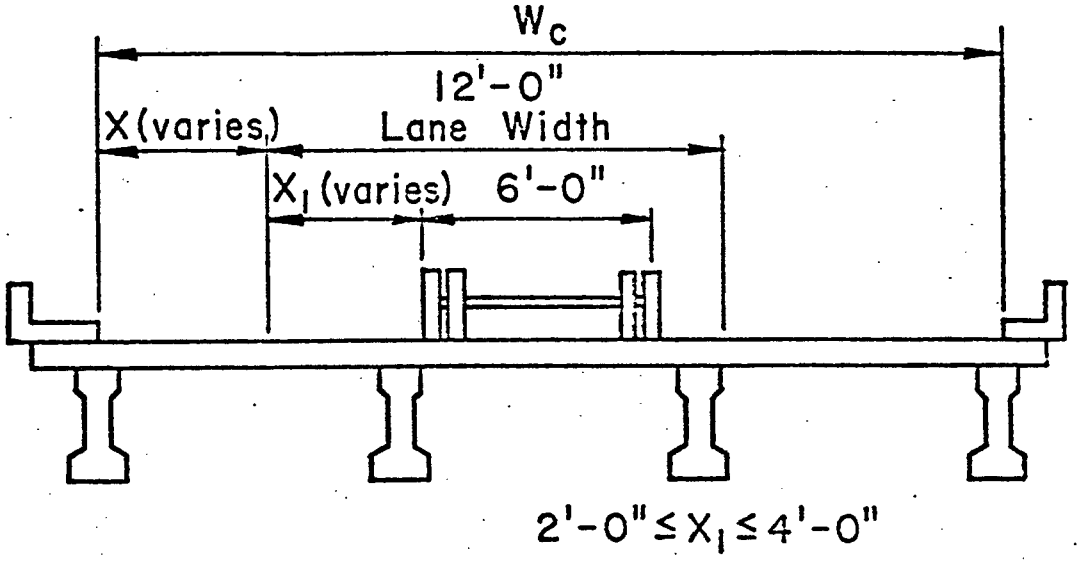

(a) One Lane

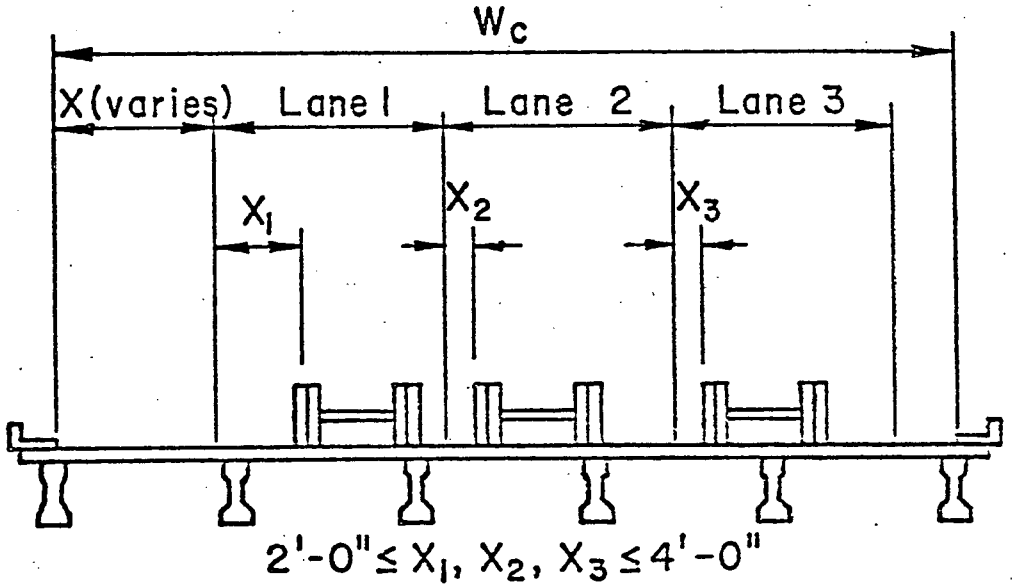

(b) Two Lanes

Fig. 13 Design Traffic Lanes

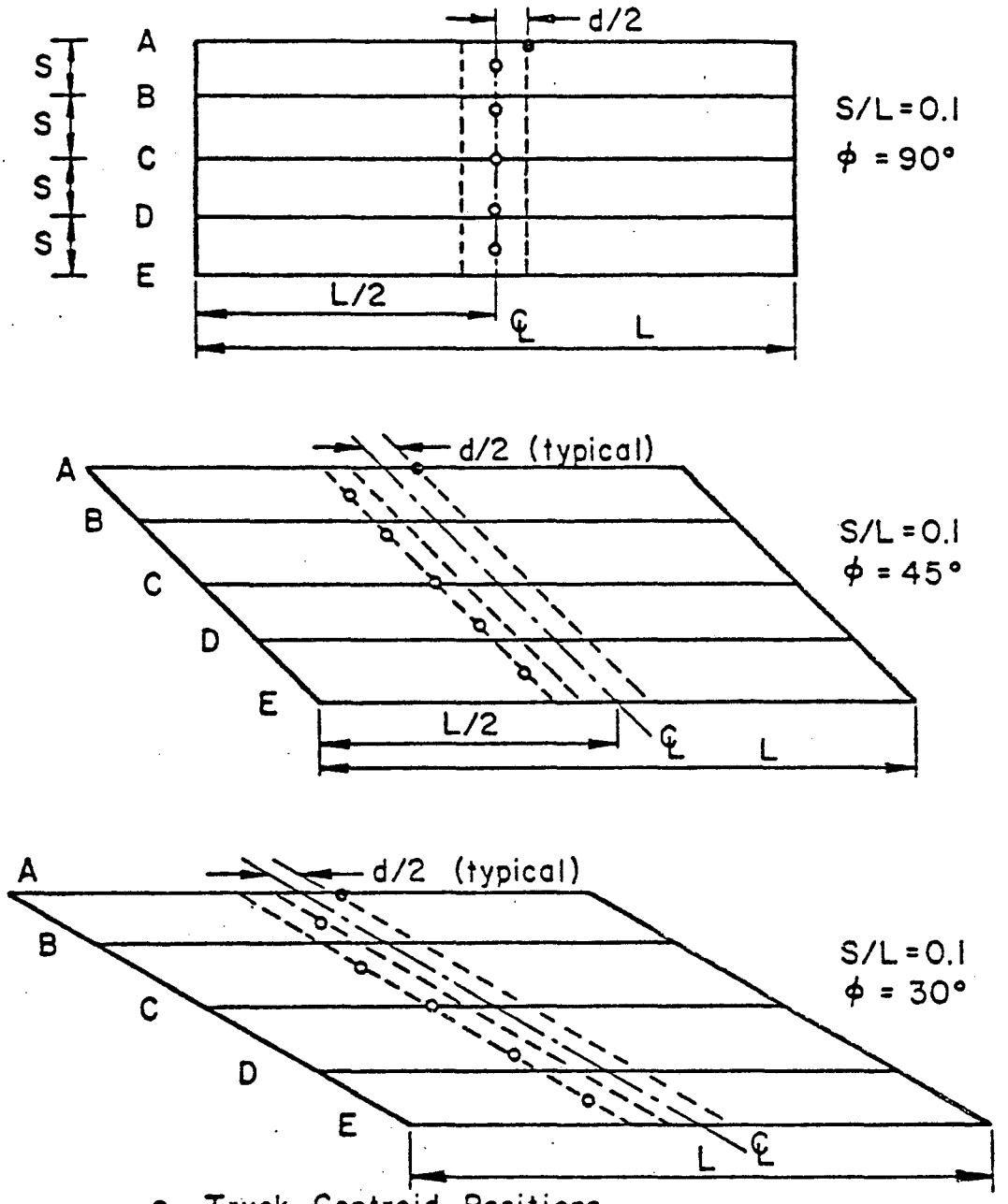

Fig. 14 Load Positions and Locations of Maximum Moment REsponse - Beam A

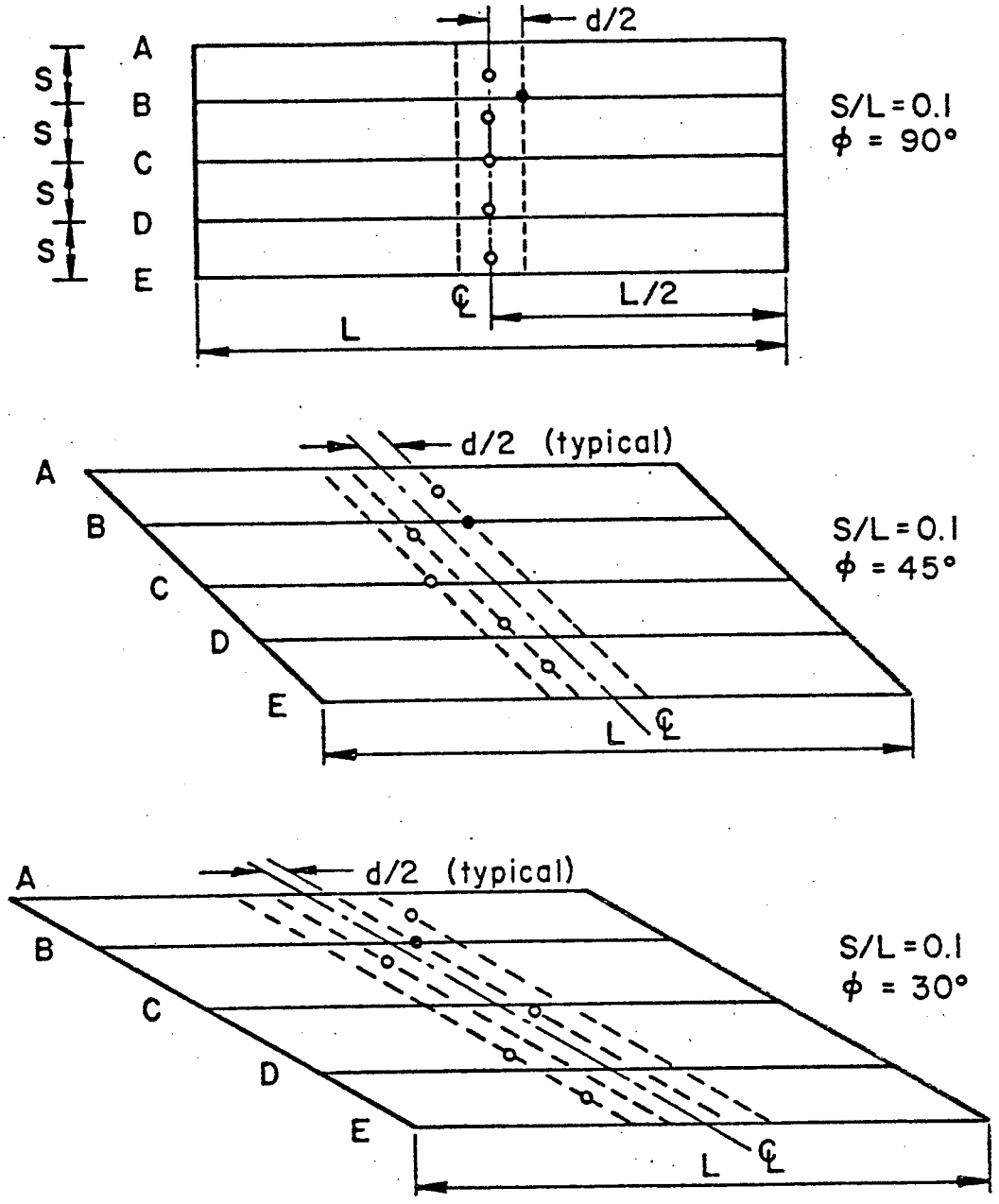

Fig. 15 Load Positions and Location of Maximum Moment Response - Beam B

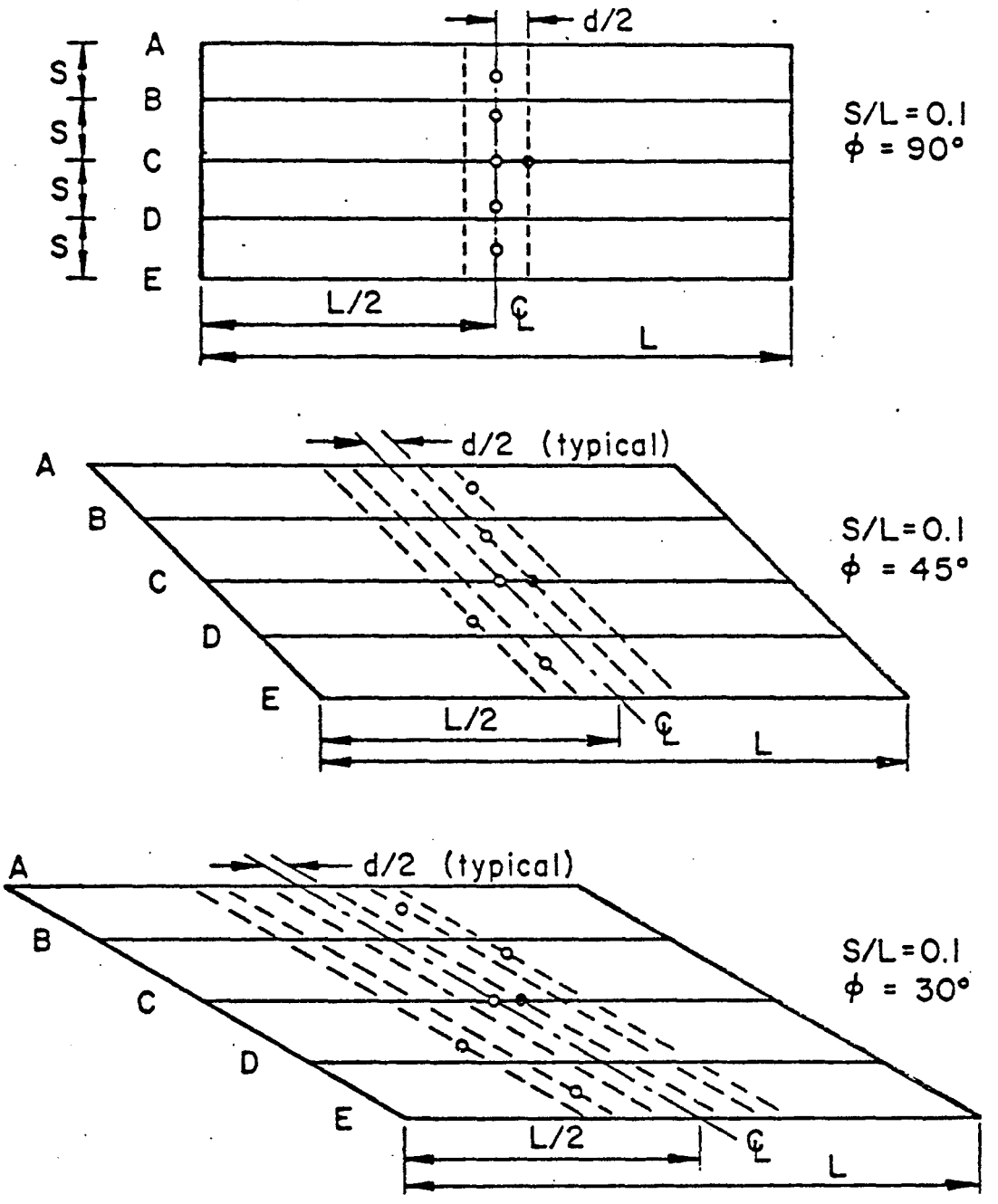

Fig. 16 Load Positions and Location of Maximum Moment Response - Beam C

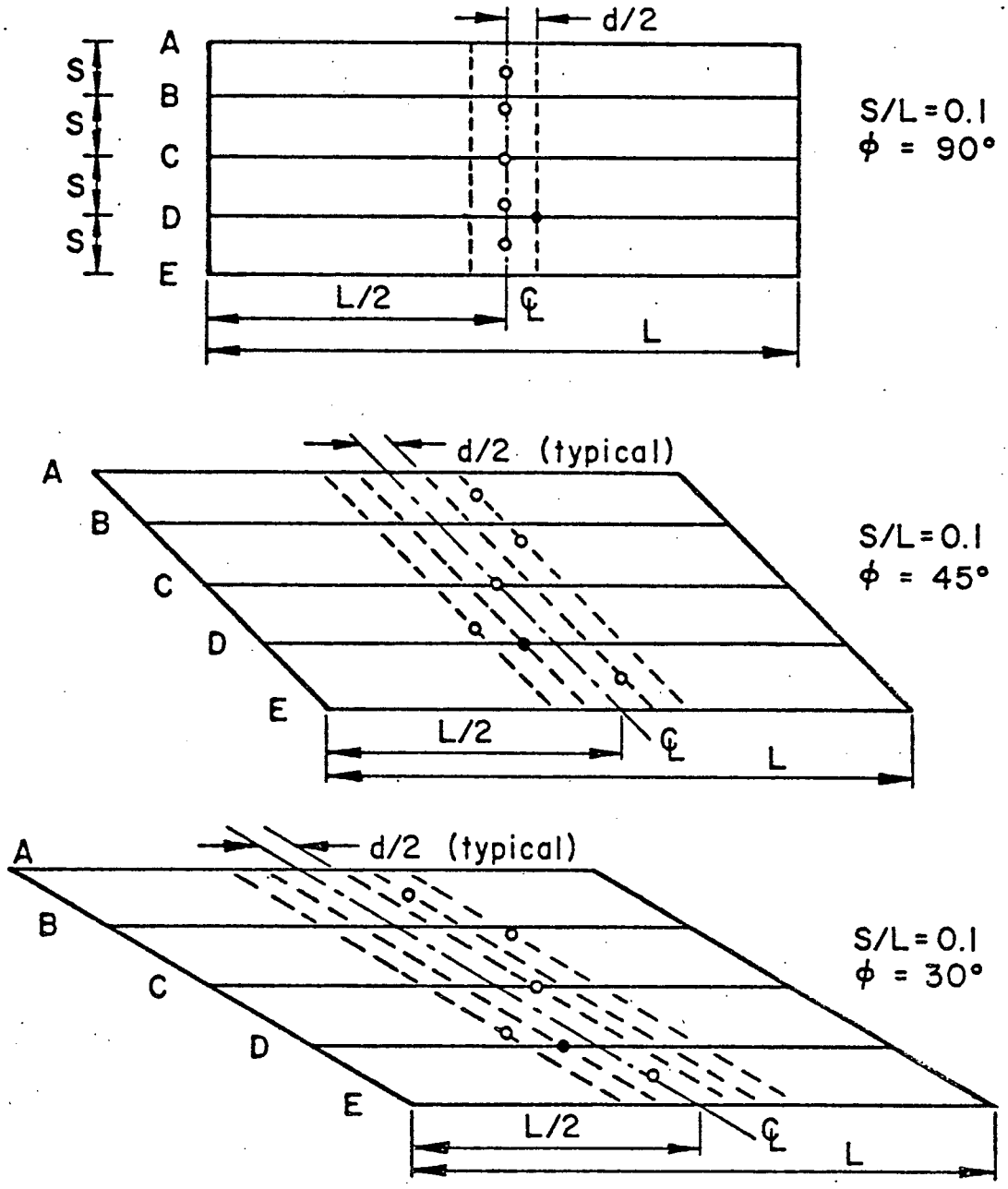

Fig. 17 Load Positions and Location of Maximum Moment Response - Beam D

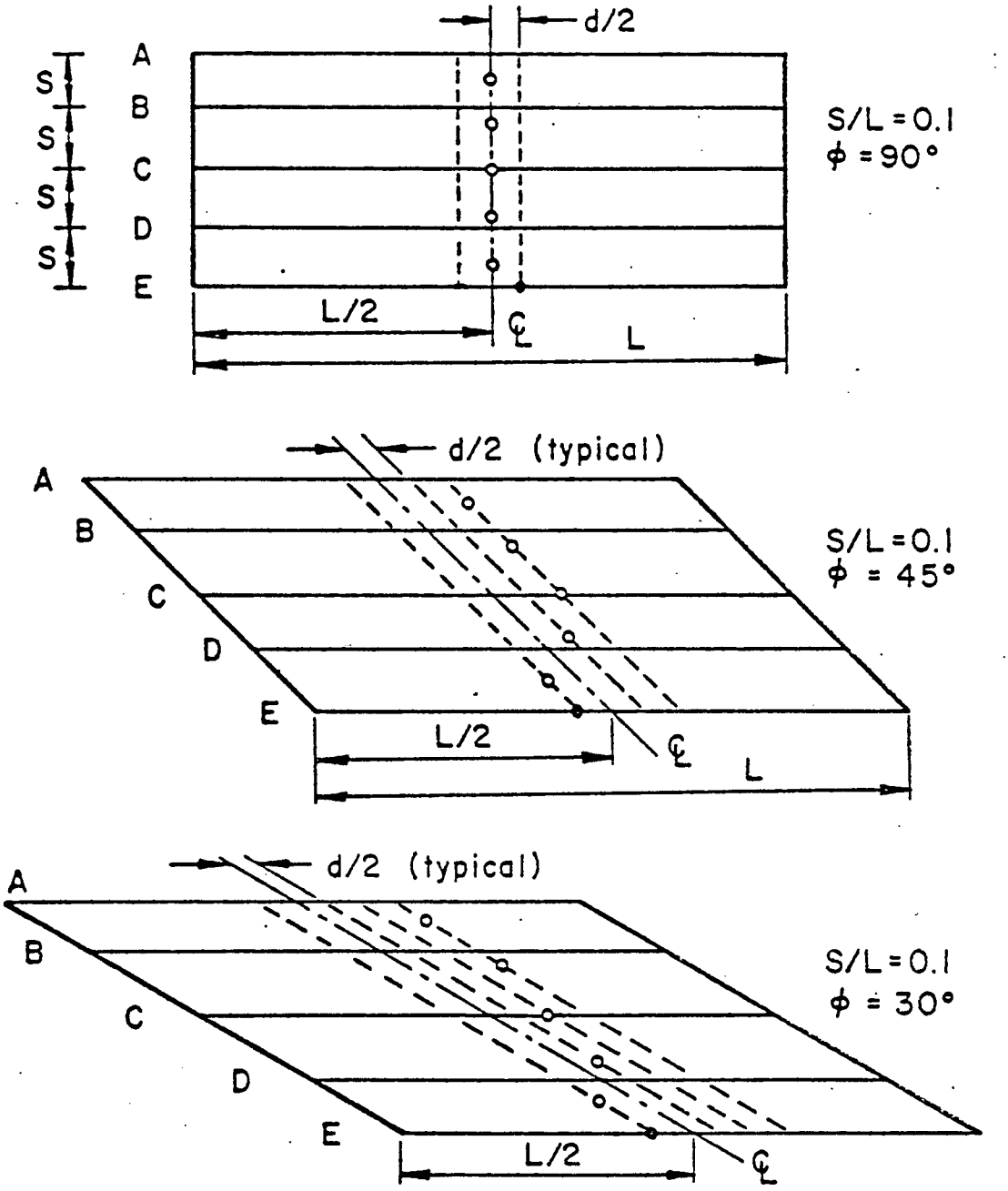

Fig. 18 Load Positions and Location of Maximum Moment Response - Beam E

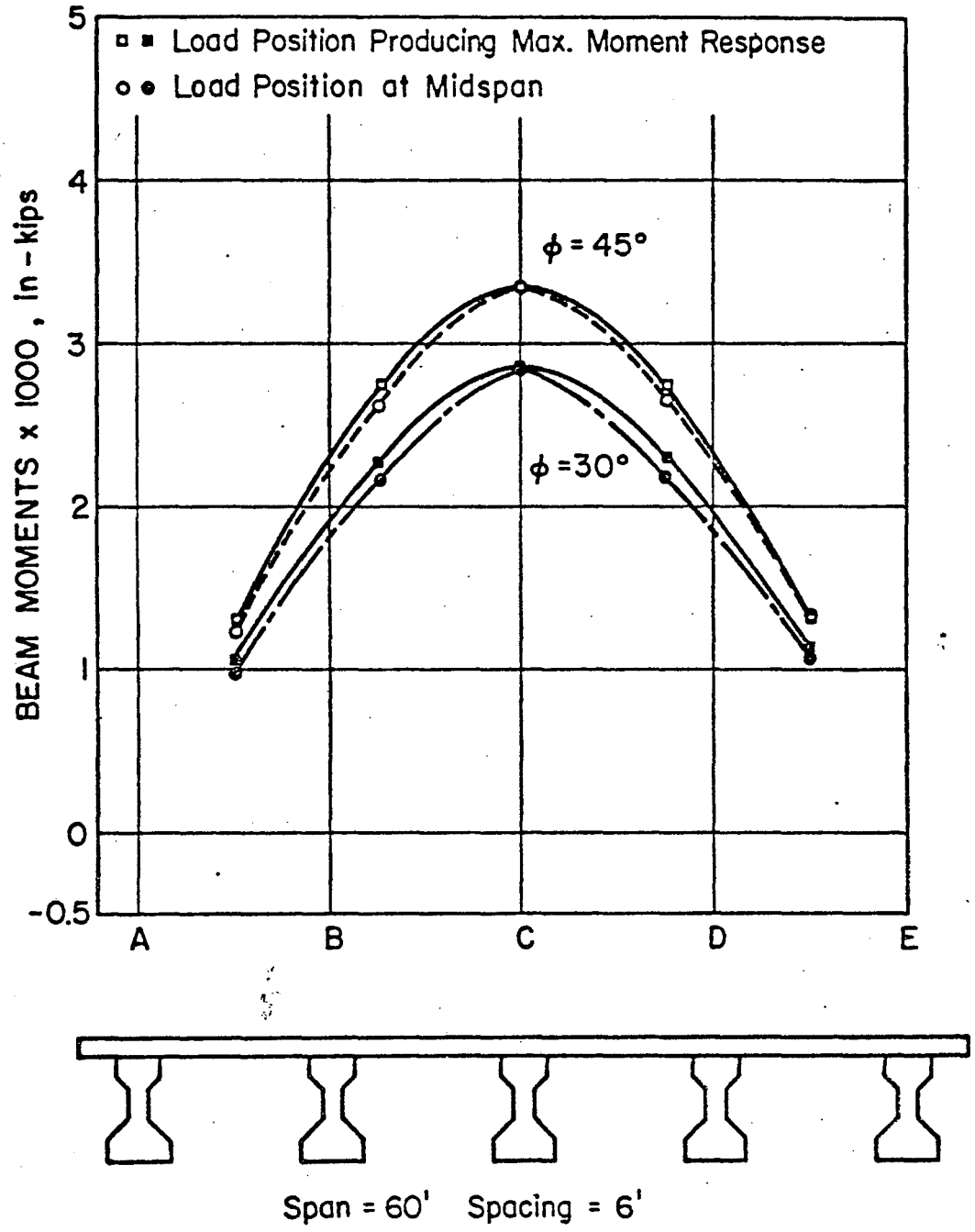

Fig. 19 Influence Lines for Moment, 45° and 30° Skew Bridges - Beam C

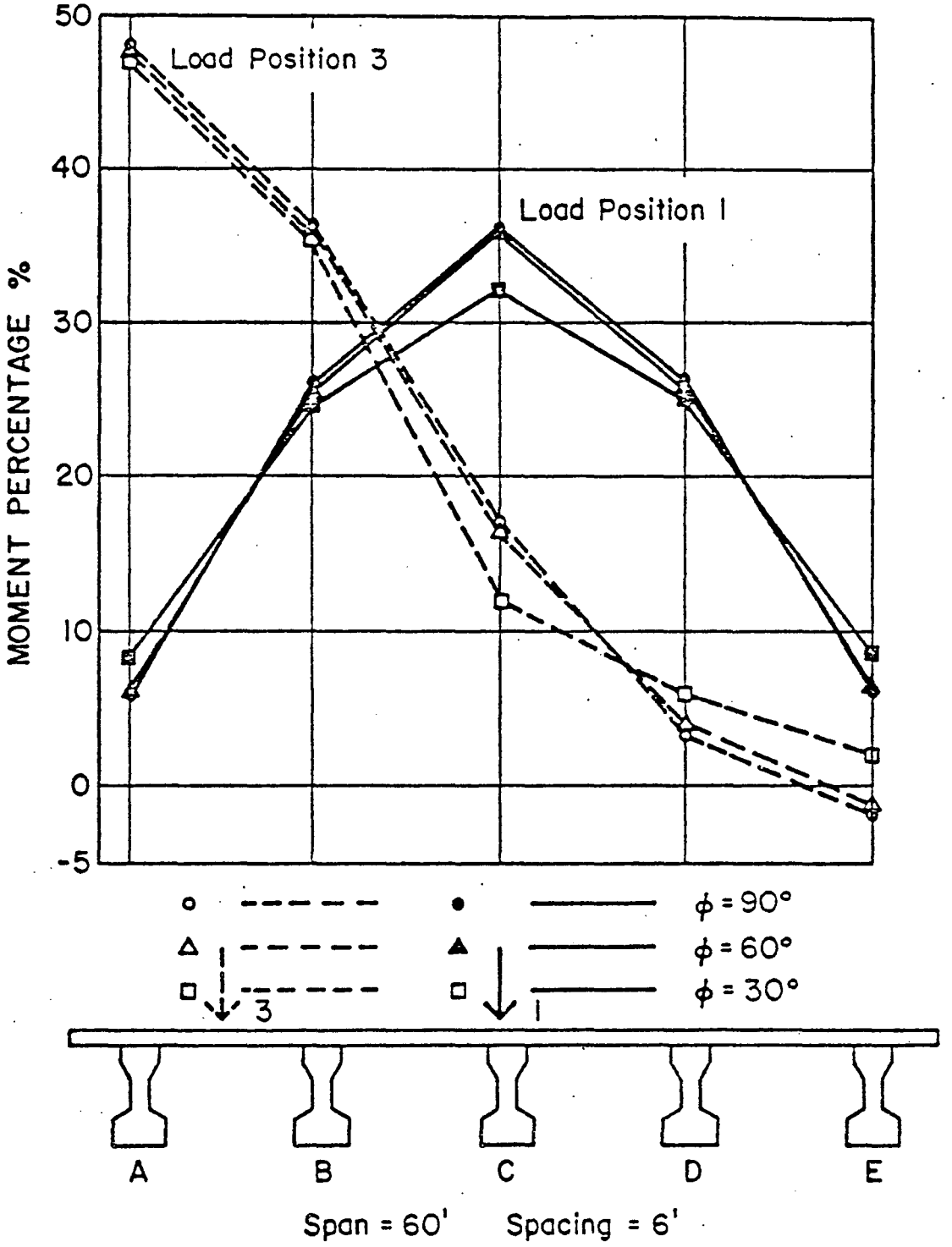

Fig. 20 Lateral Distribution of a Truck Load: Truck Centroid on Beam C and Between Beams A and B

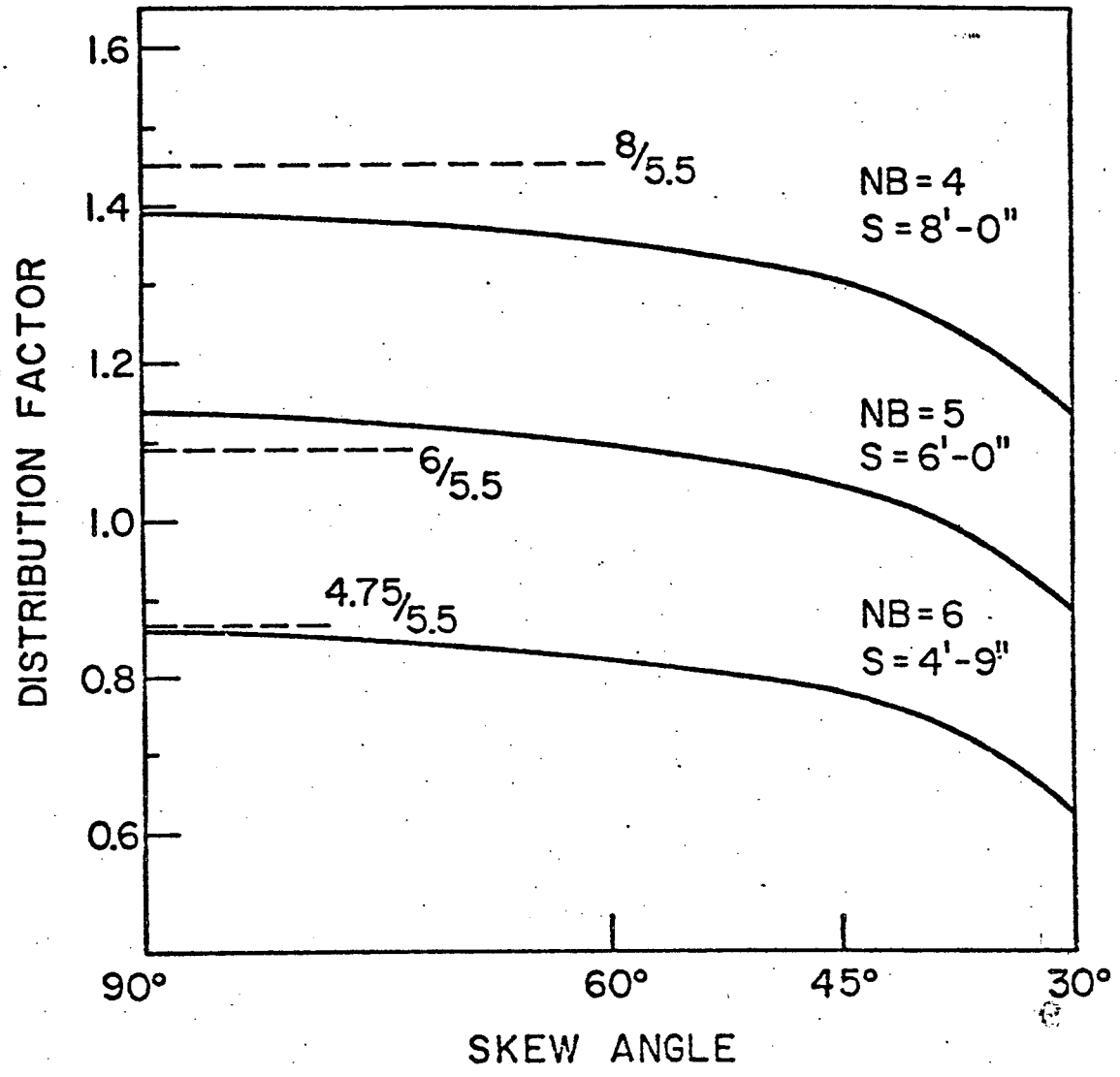

Fig. 21 Live Load Distribution Factors in the 24 ft. Wide 60 ft. Span Skew Bridges with Varying Number of Beams

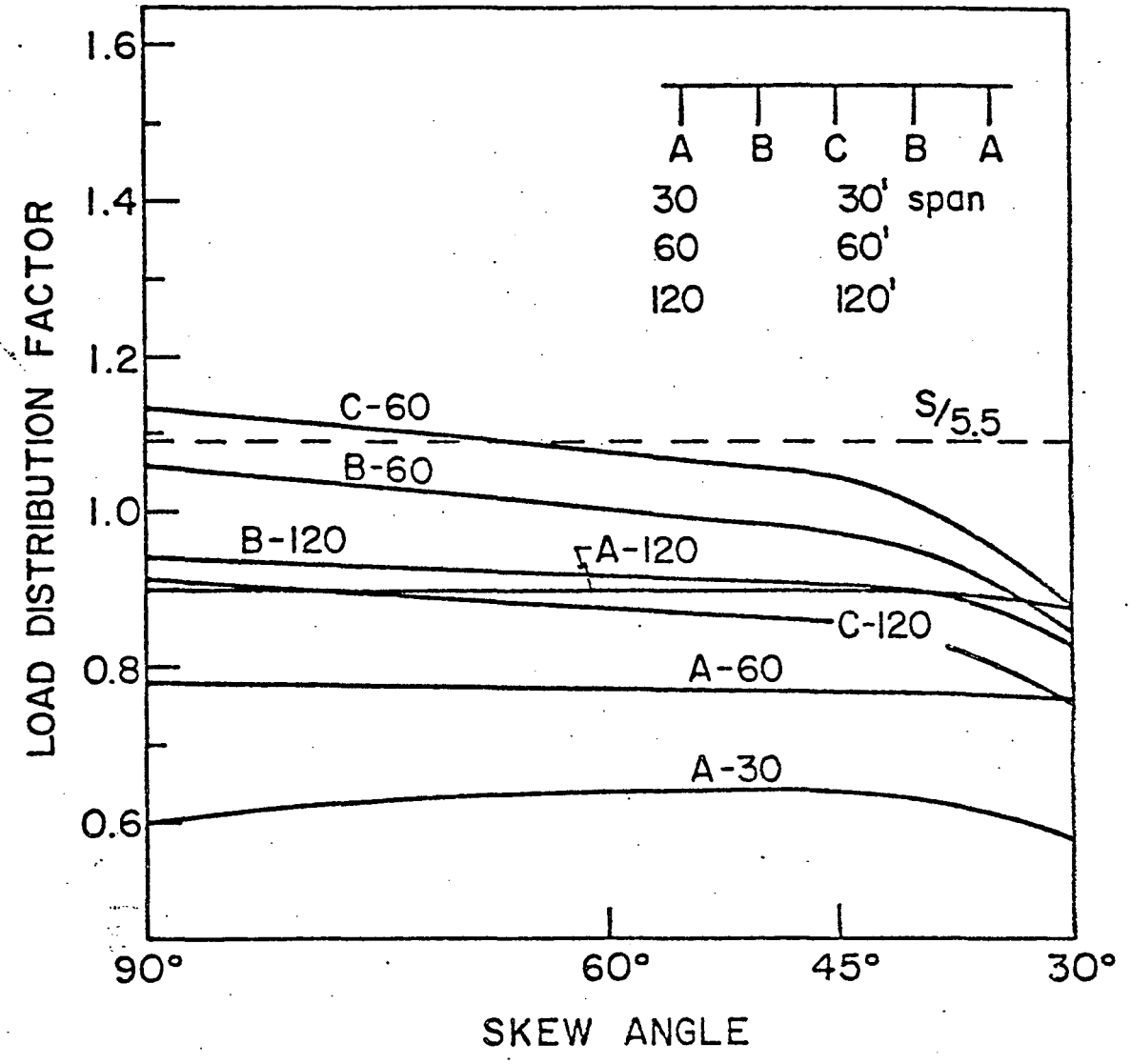

Fig. 22 Live Load Distribution Factors in the 24 ft. Wide Skew Bridges, 5 Beams with Varying Span Length

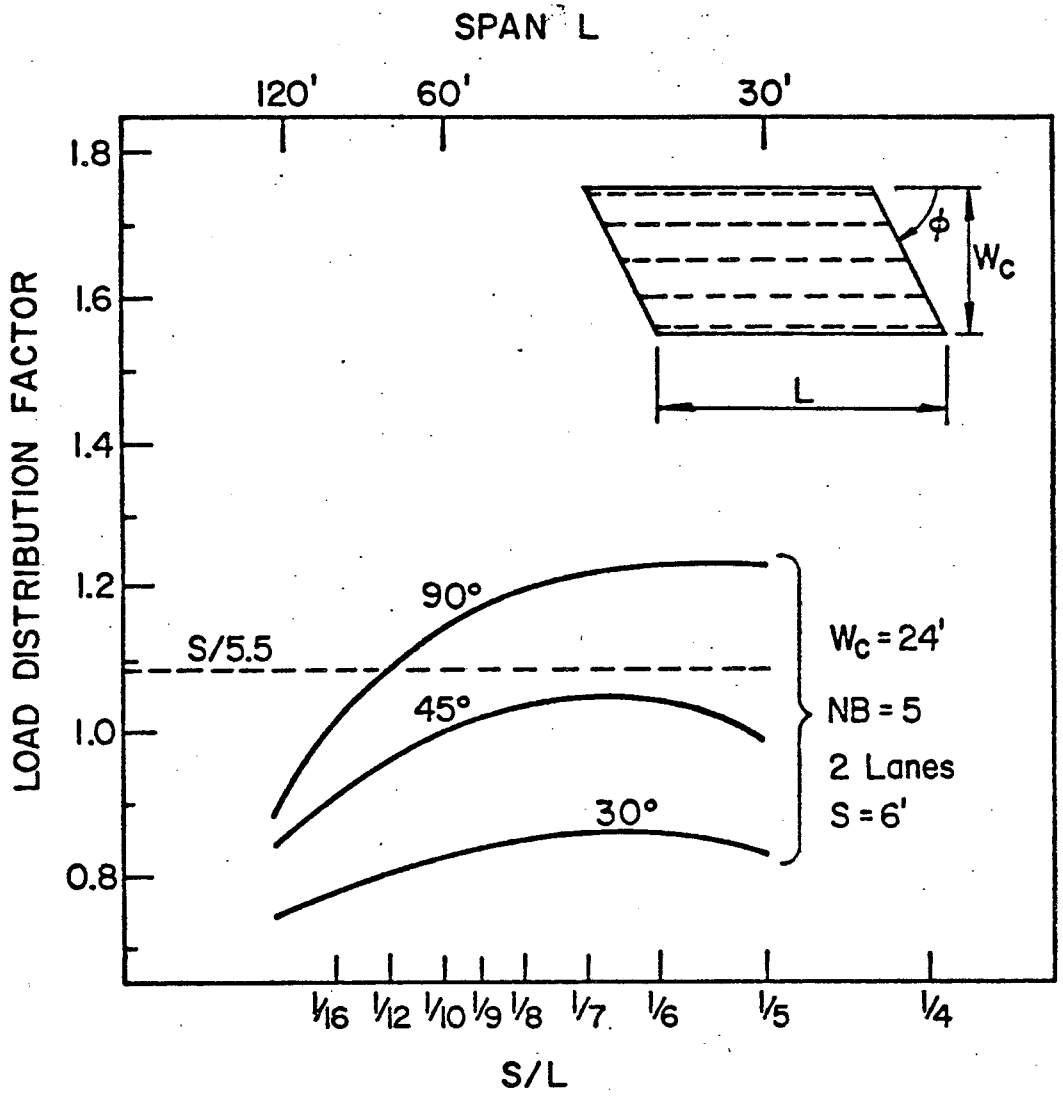

Fig. 23 Live Load Distribution Factors in the 24 ft. Wide Skew Bridge with 5 Beams

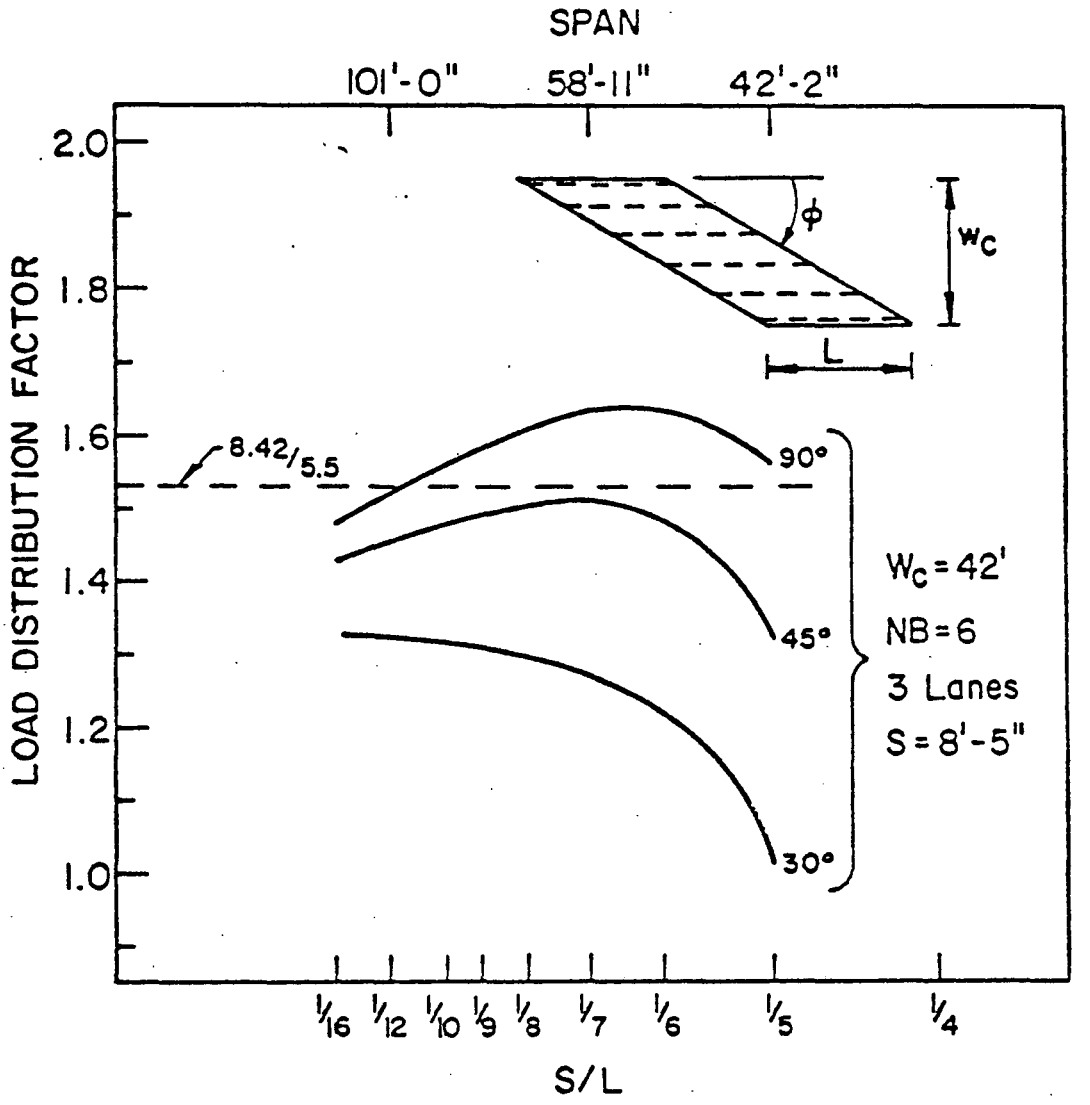

Fig. 24 Live Load Distribution Factors in the 42 ft. Wide Skew Bridges with 6 Beams

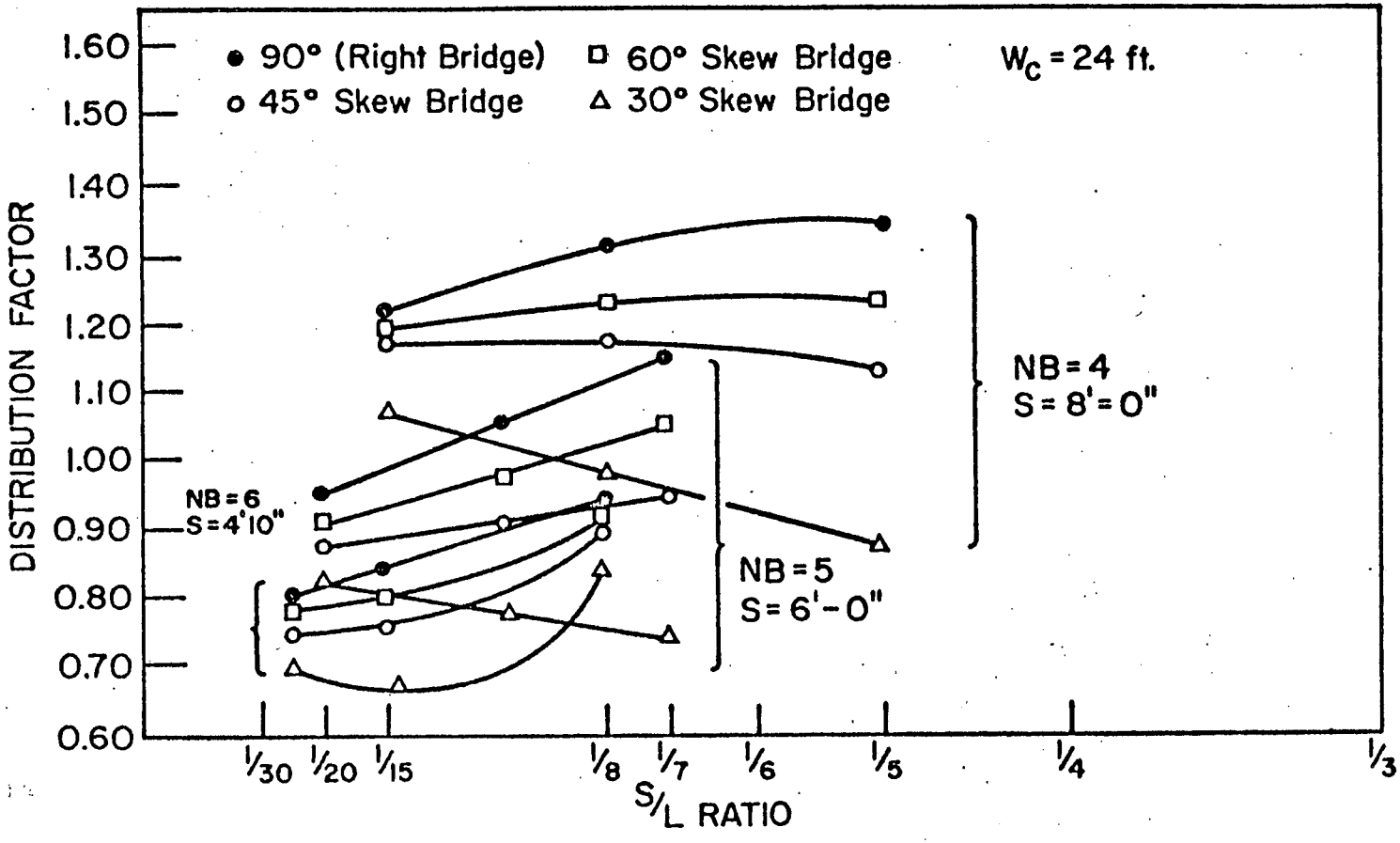

Fig. 25 Distribution Factors for Interior Beams - 24 ft. Wide Bridges

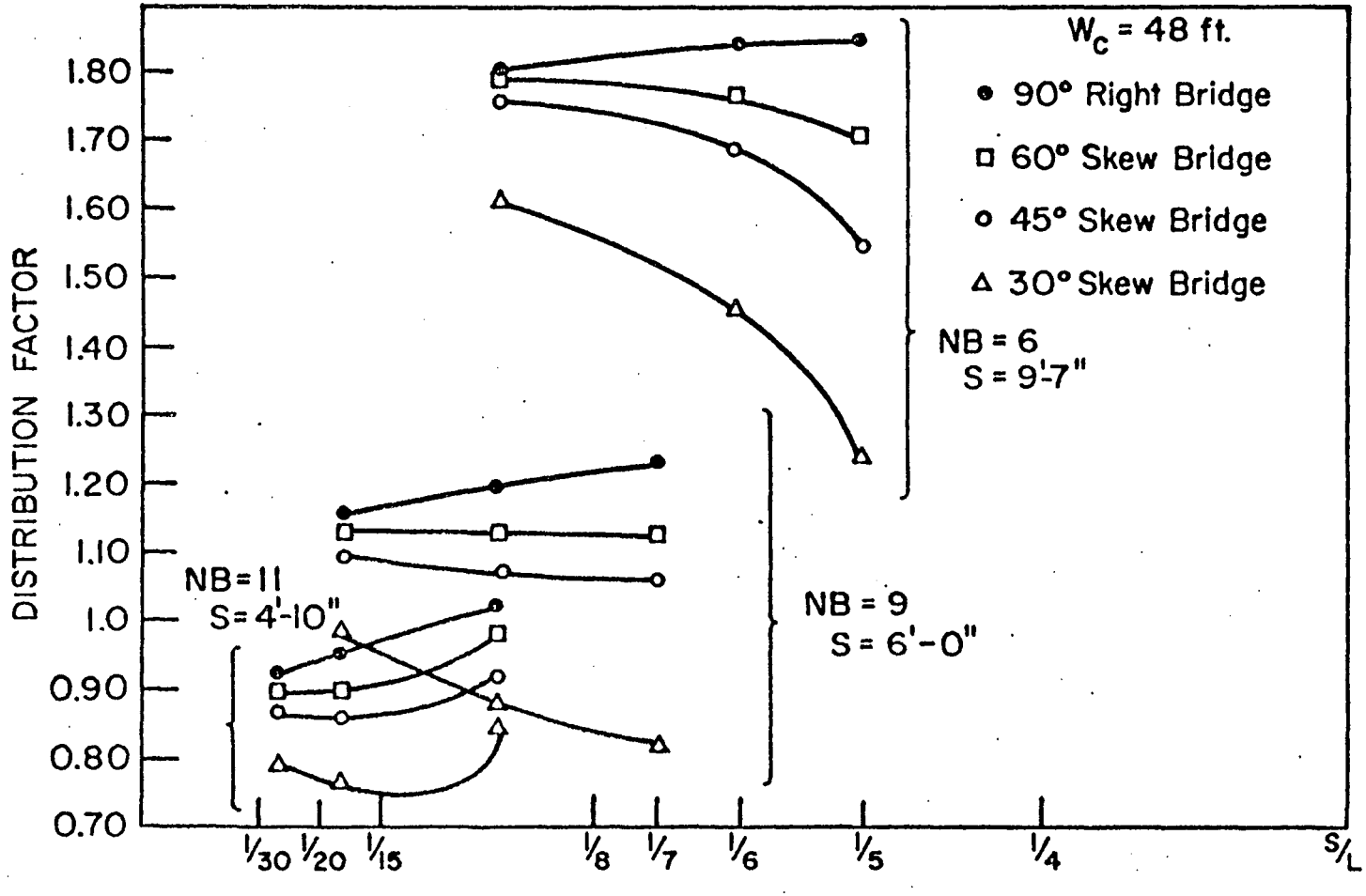

Fig. 26 Distribution Factors for Interior Beams - 48 ft. Wide Bridges

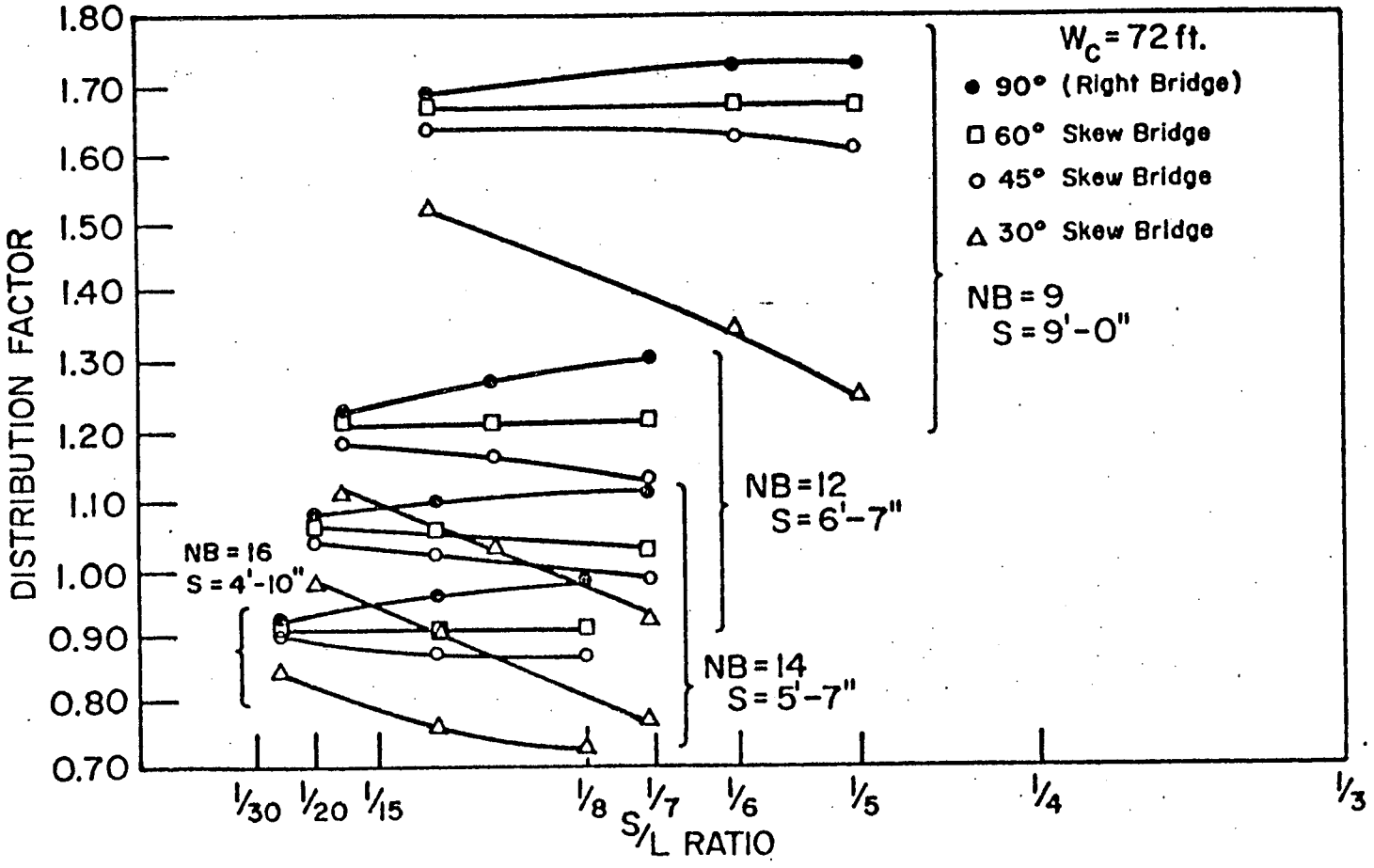

Fig. 27 Distribution Factors for Interior Beams 72 ft. Wide Bridges

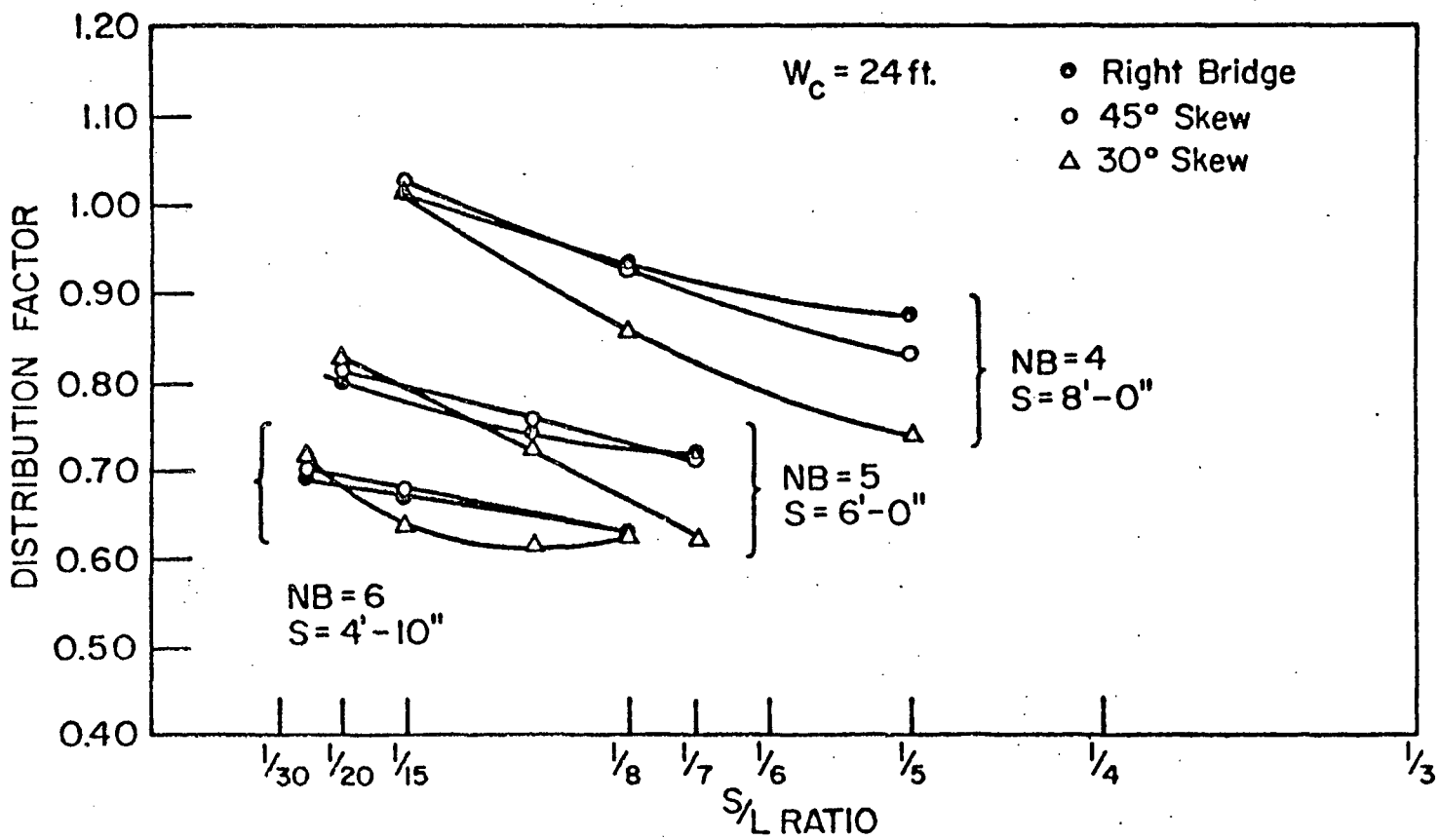

Fig. 28 Distribution Factors for Exterior Beams - 24 ft. Wide Bridges

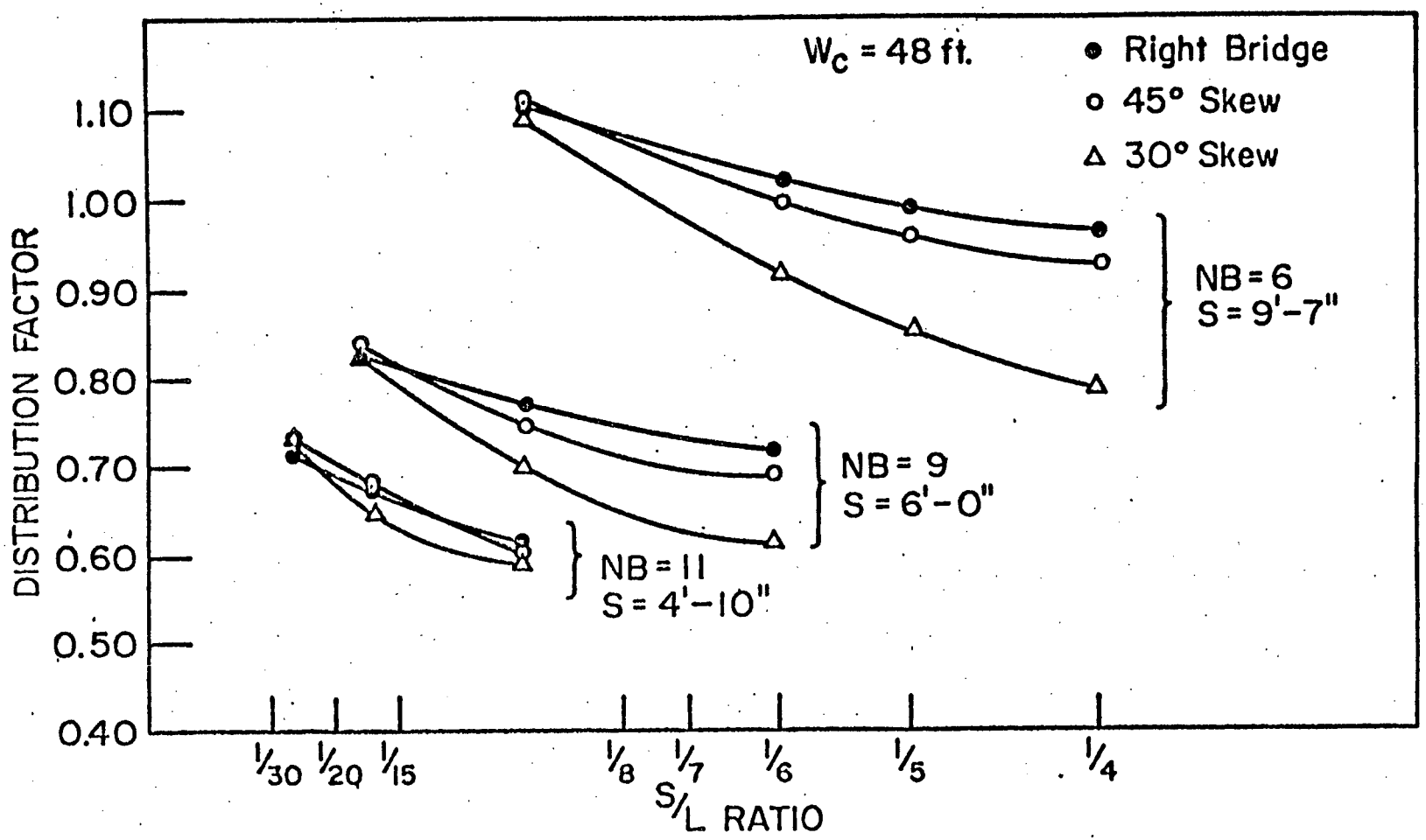

Fig. 29 Distribution Factors for Exterior Beams - 48 ft. Wide Bridges

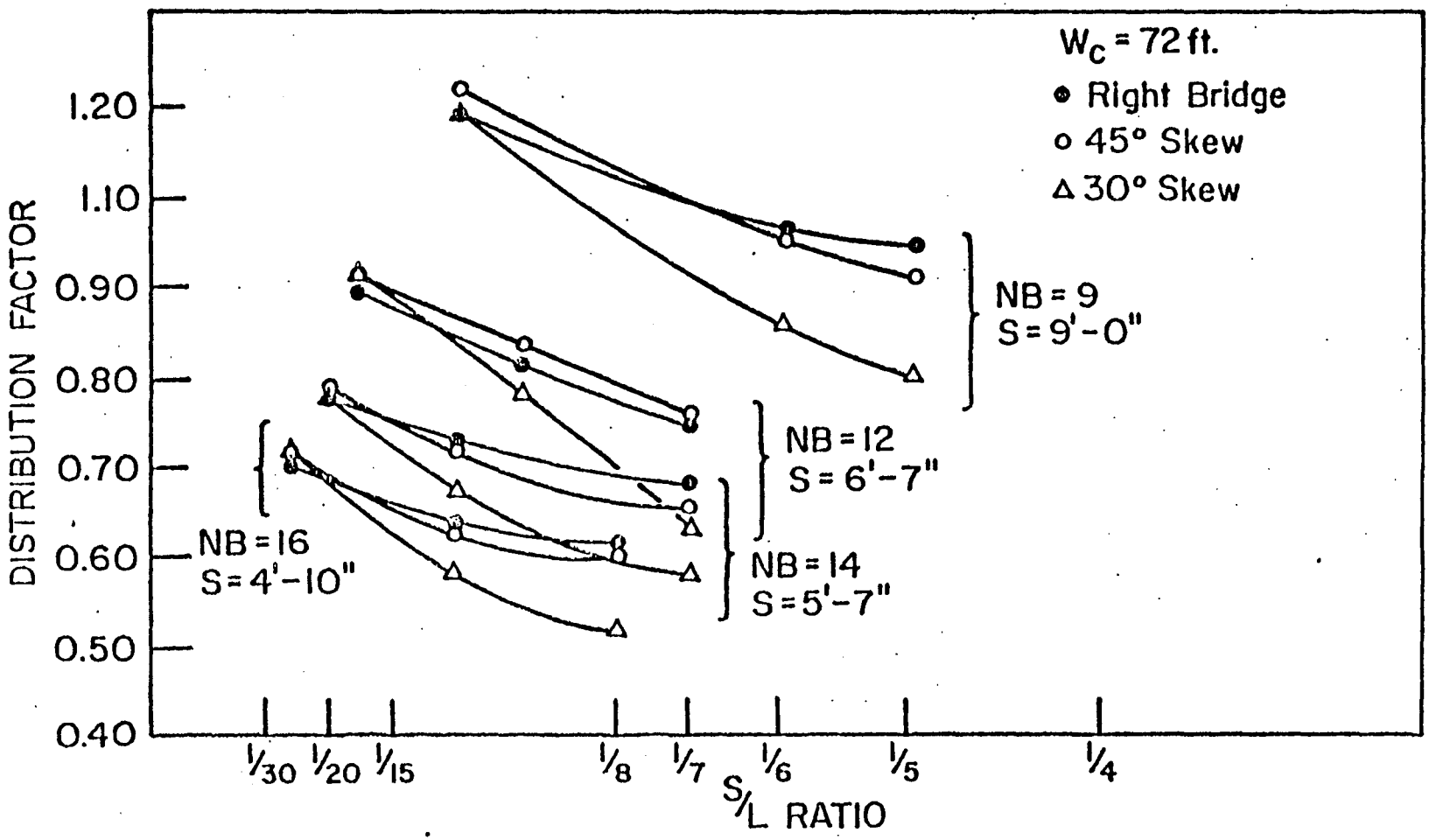

Fig. 30 Distribution Factors for Exterior Beams - 72 ft. Wide Bridges

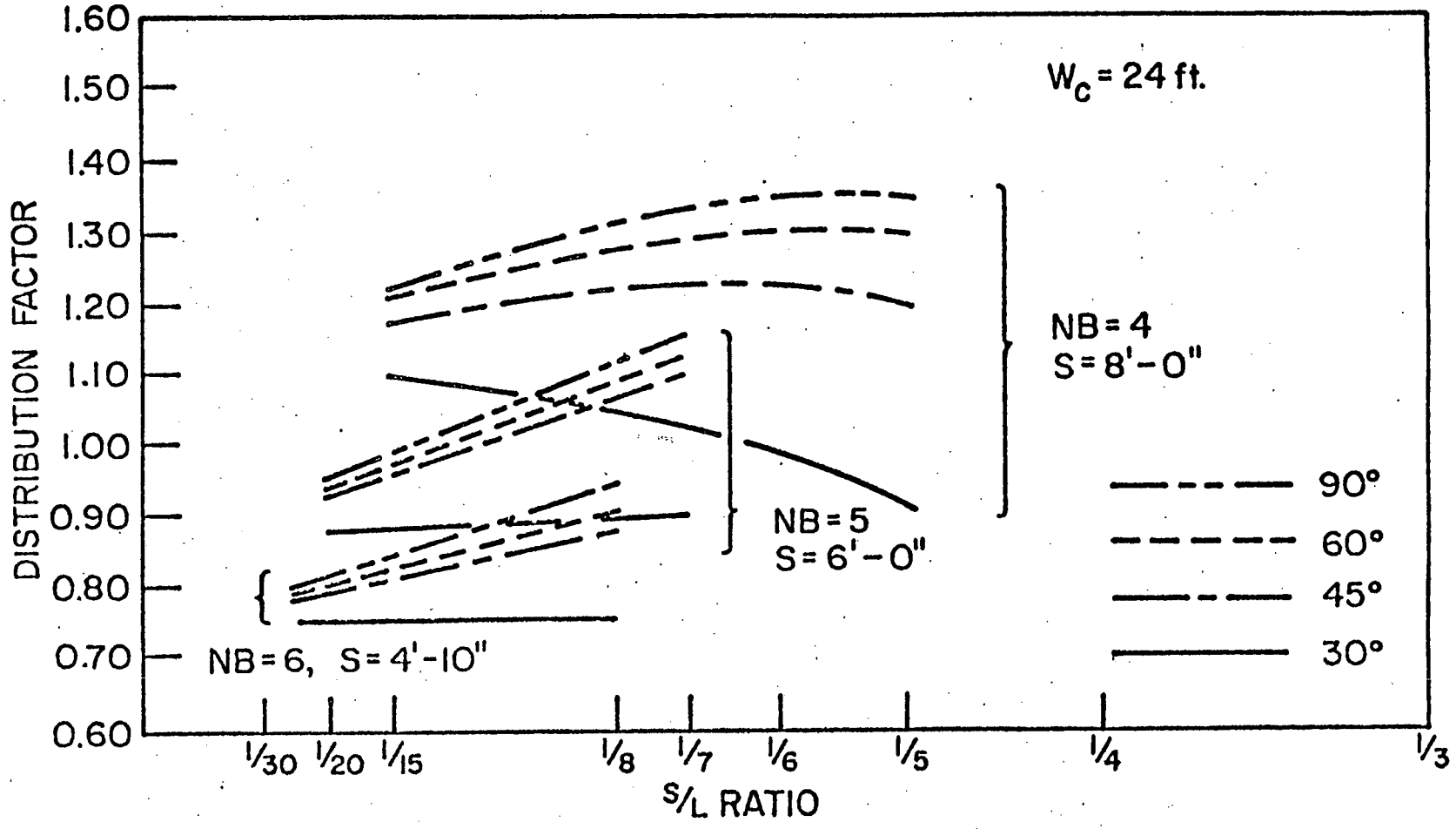

Fig. 31 Analytically Developed Distribution Factors for Interior Beams - 24 ft. Wide Bridges

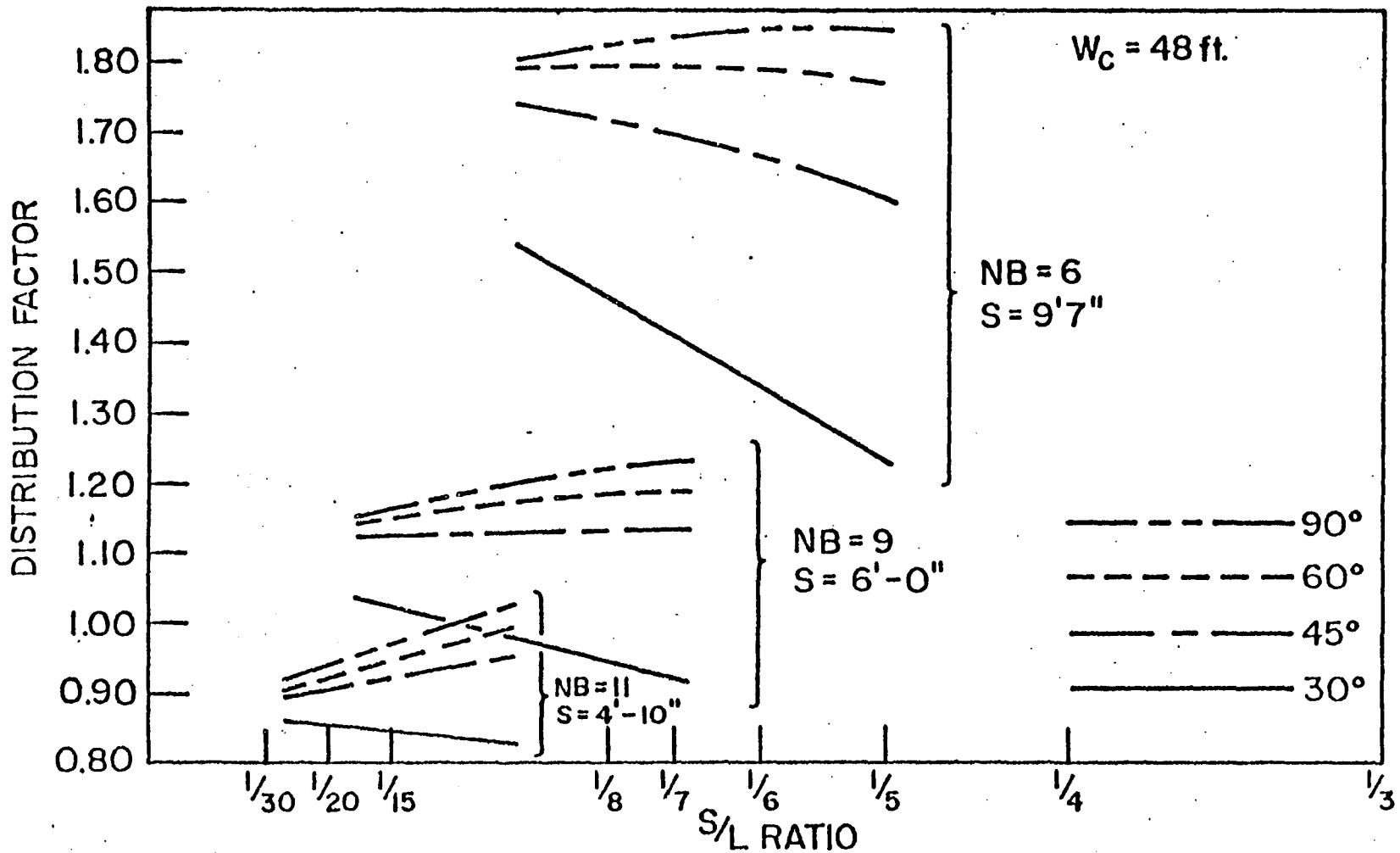

Fig. 32 Analytically Developed Distribution Factors - 48 ft. Wide Bridges

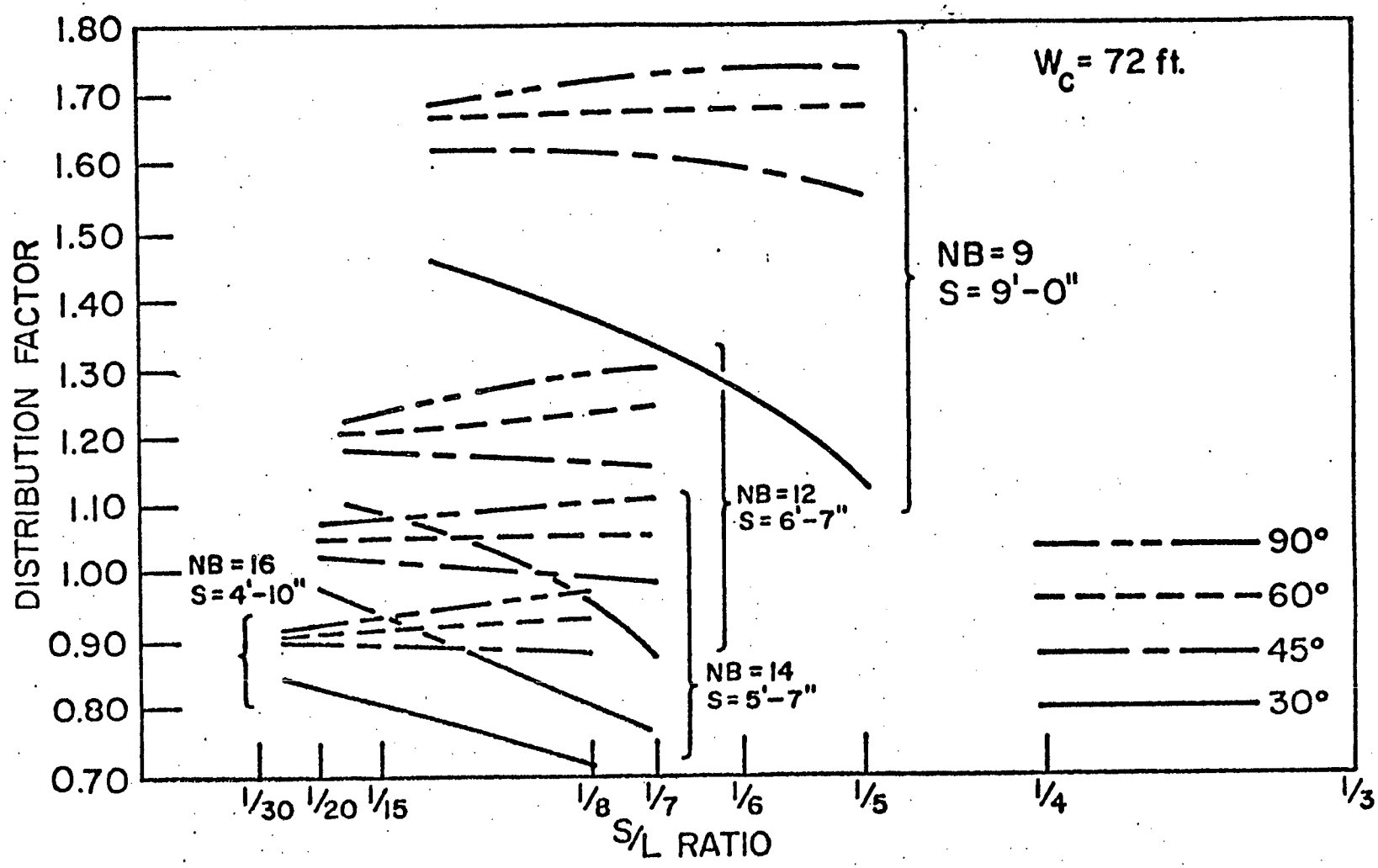

Fig. 33 Analytically Developed Distribution Factors - 72 ft. Wide Bridges

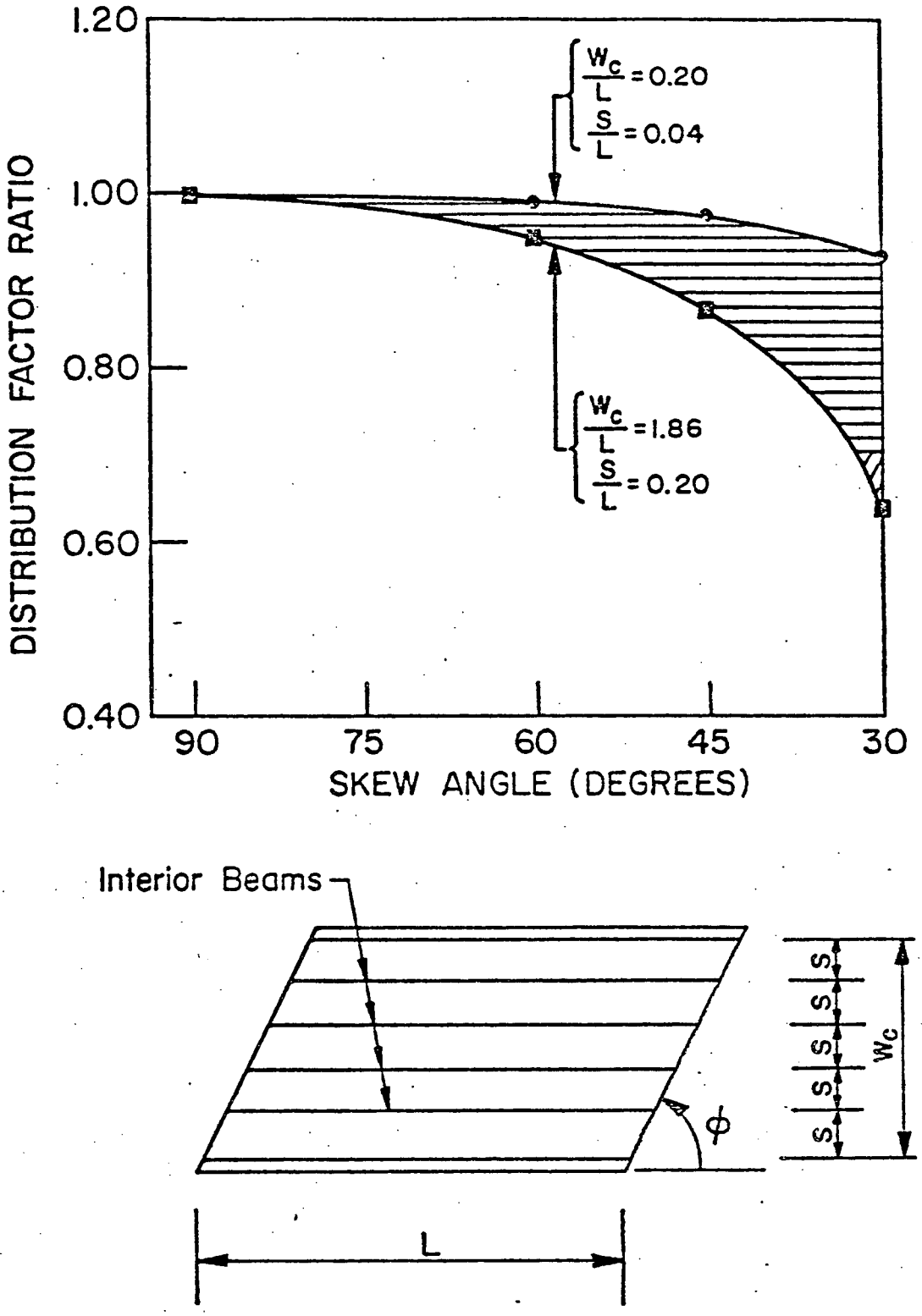

Fig. 34 Interior Beam Distribution Factor Ratio

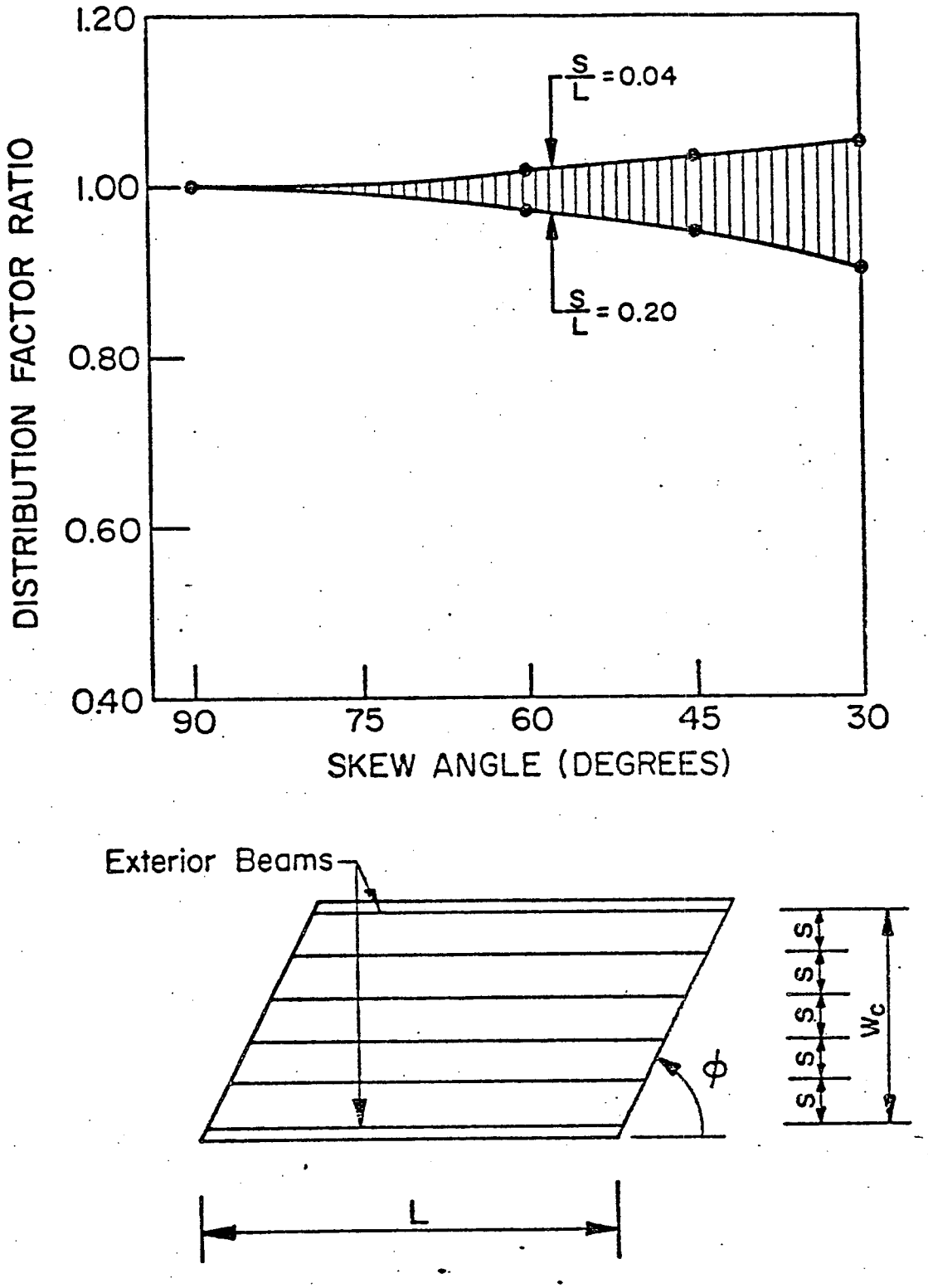

Fig. 35 Exterior Beams Distribution Factor Ratio

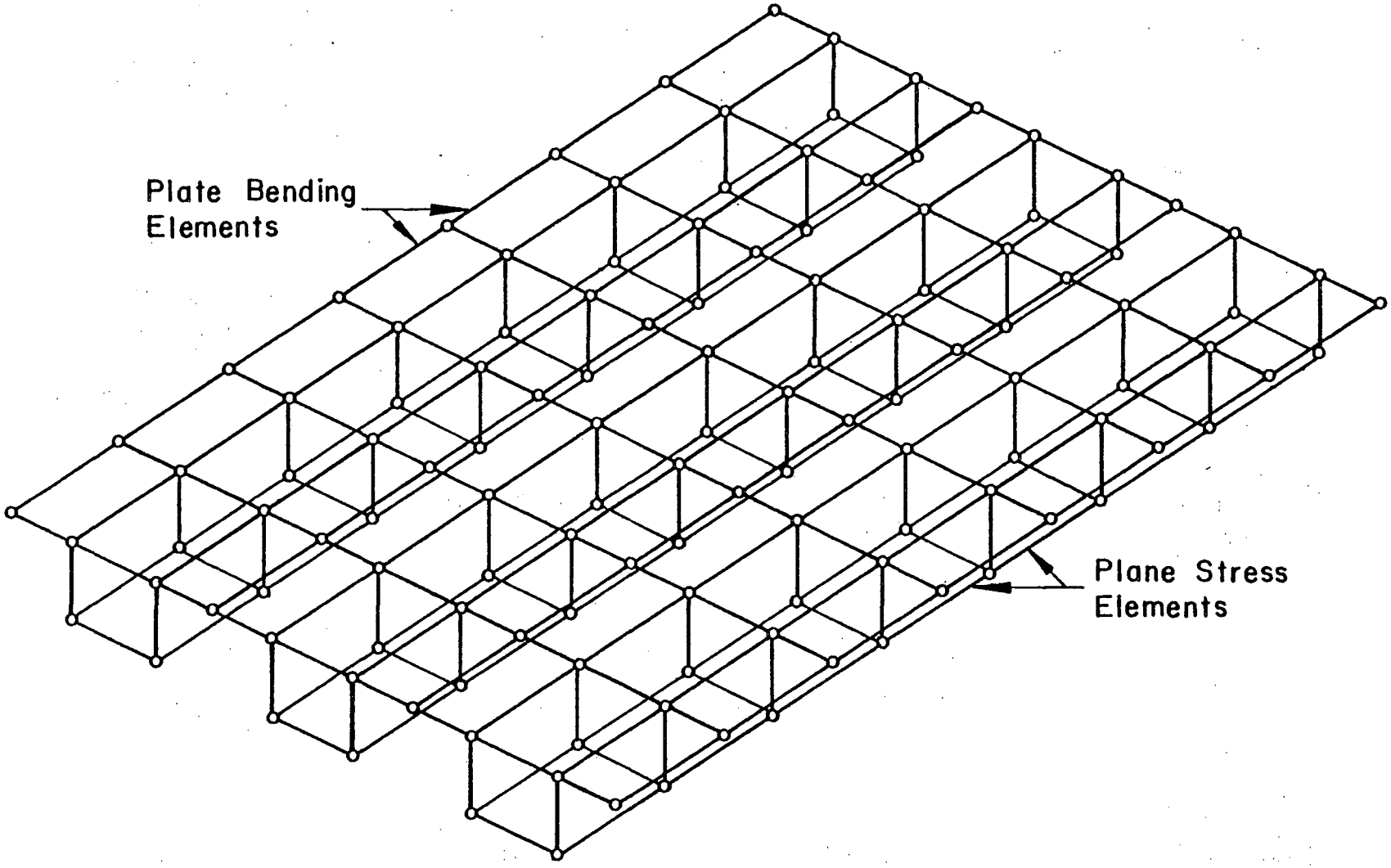

Fig. 36 Typical Skewed Spread Box-Beam Bridge Discretization

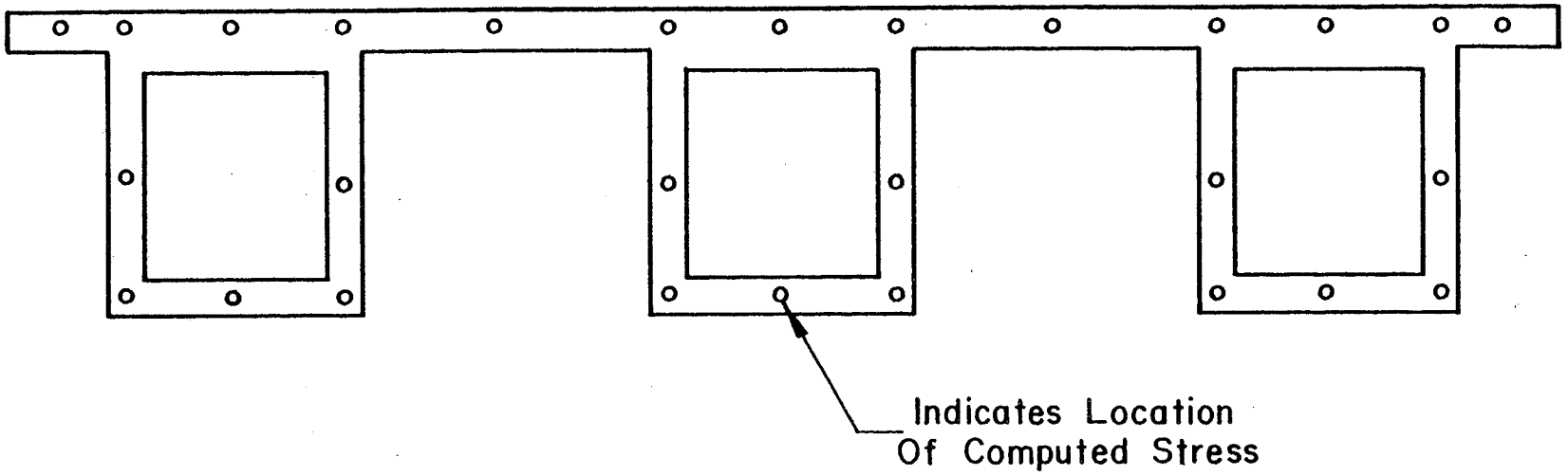

Fig. 37 Typical Locations of Computed Stresses

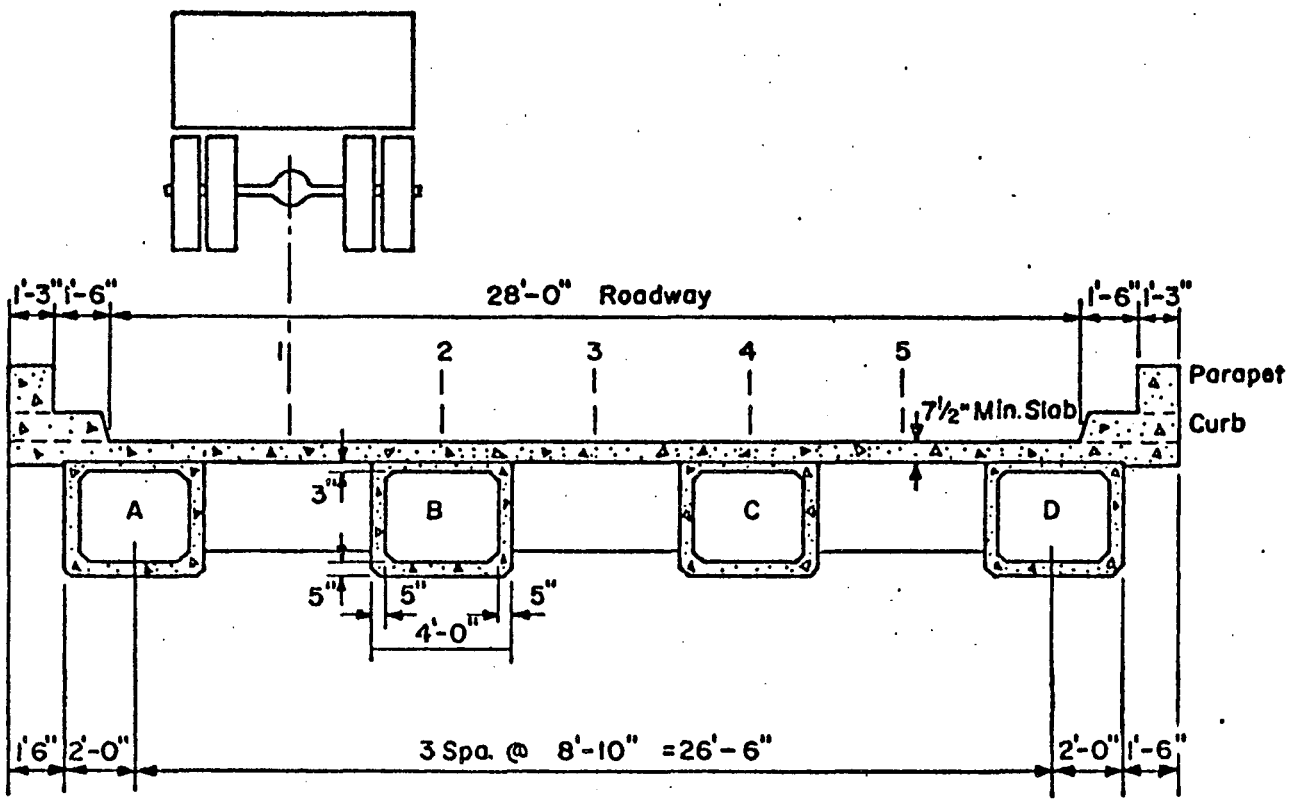

Fig. 38 Cross Section of the Brookville Bridge

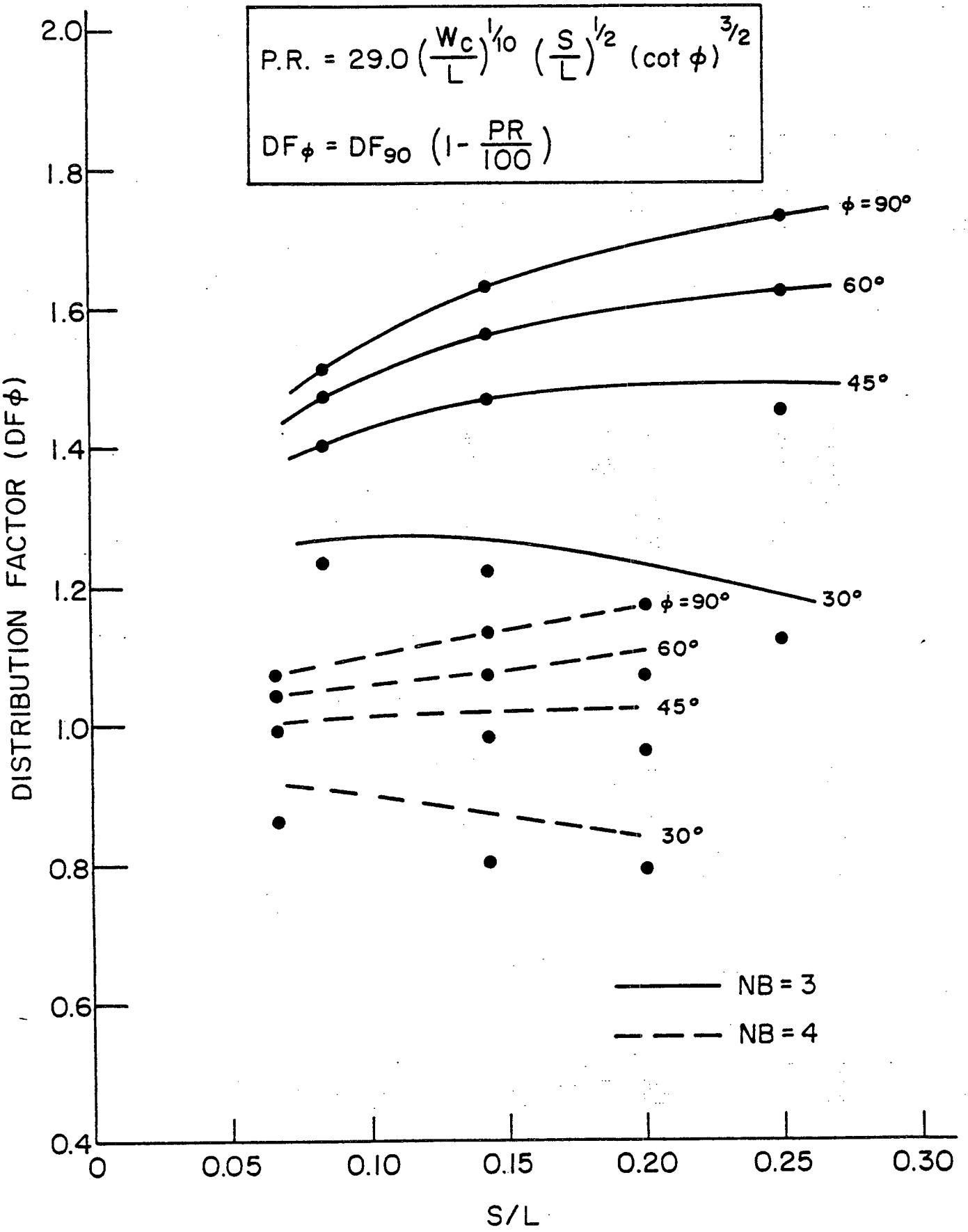

Fig. 39 Interior Box-Beam Distribution Factors, W_c = 24 ft.

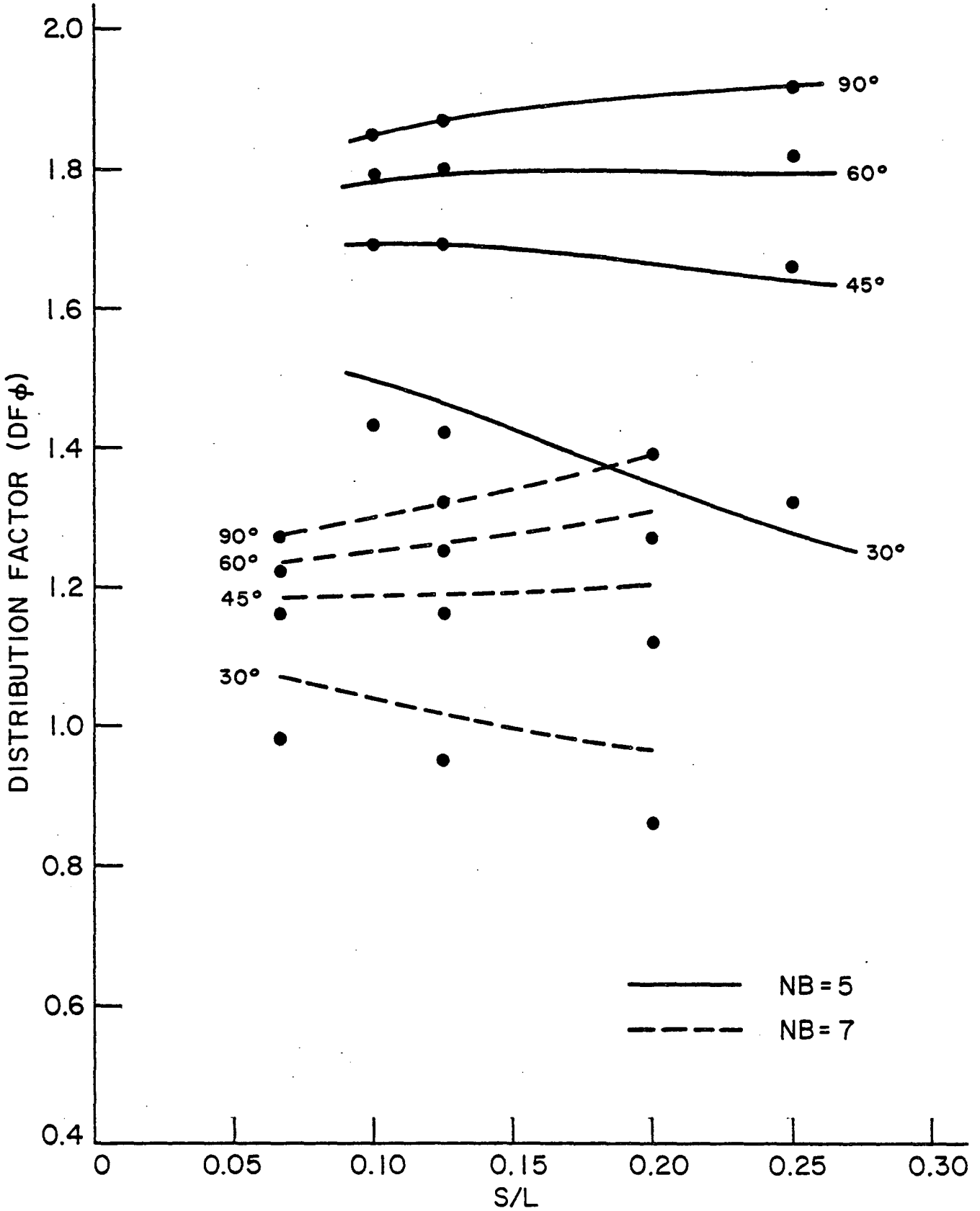

Fig. 40 Interior Box-Beam Distribution Factors, W_c = 48 ft.

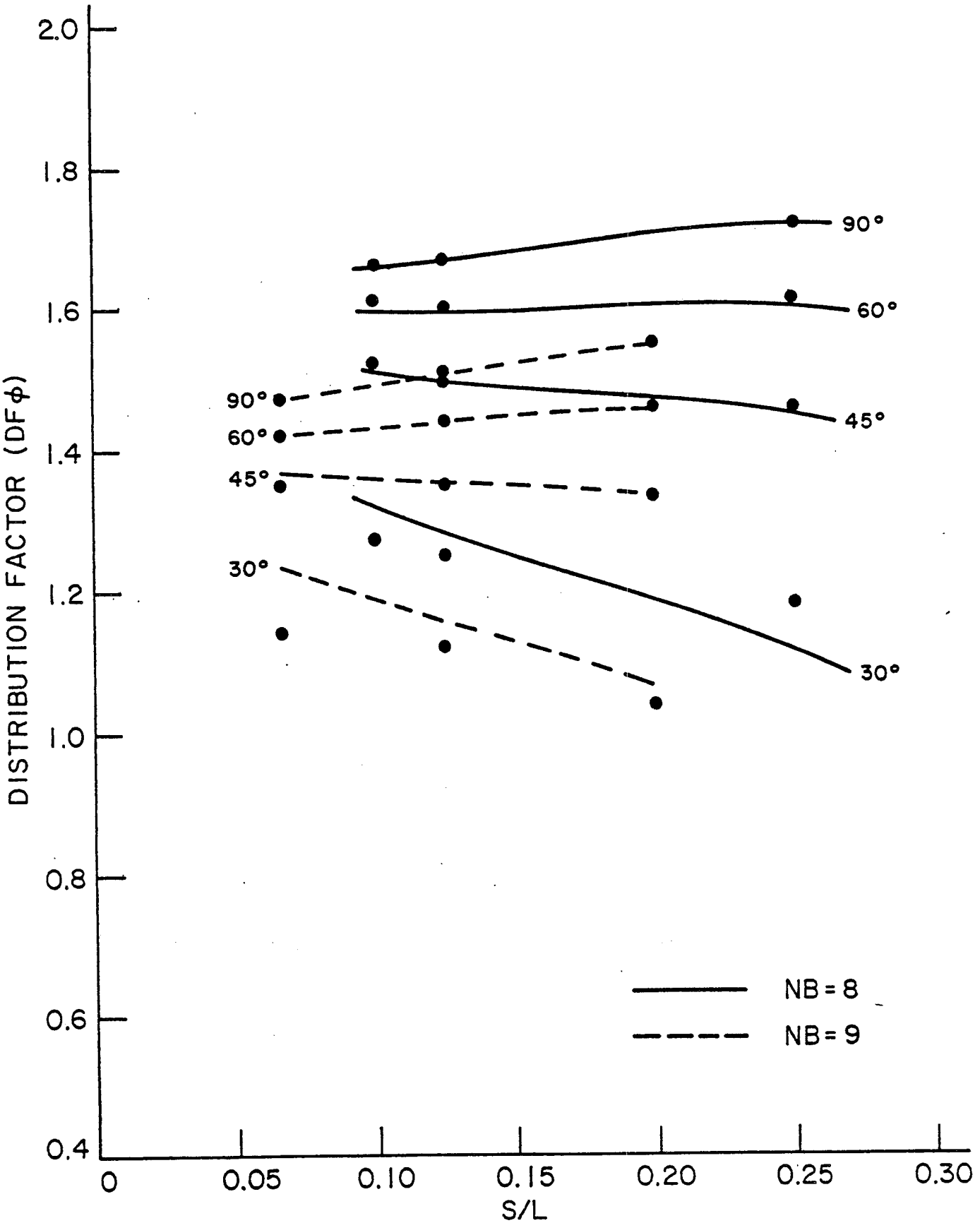

Fig. 41 Interior Box-Beam Distribution Factors, W_c = 72 ft.

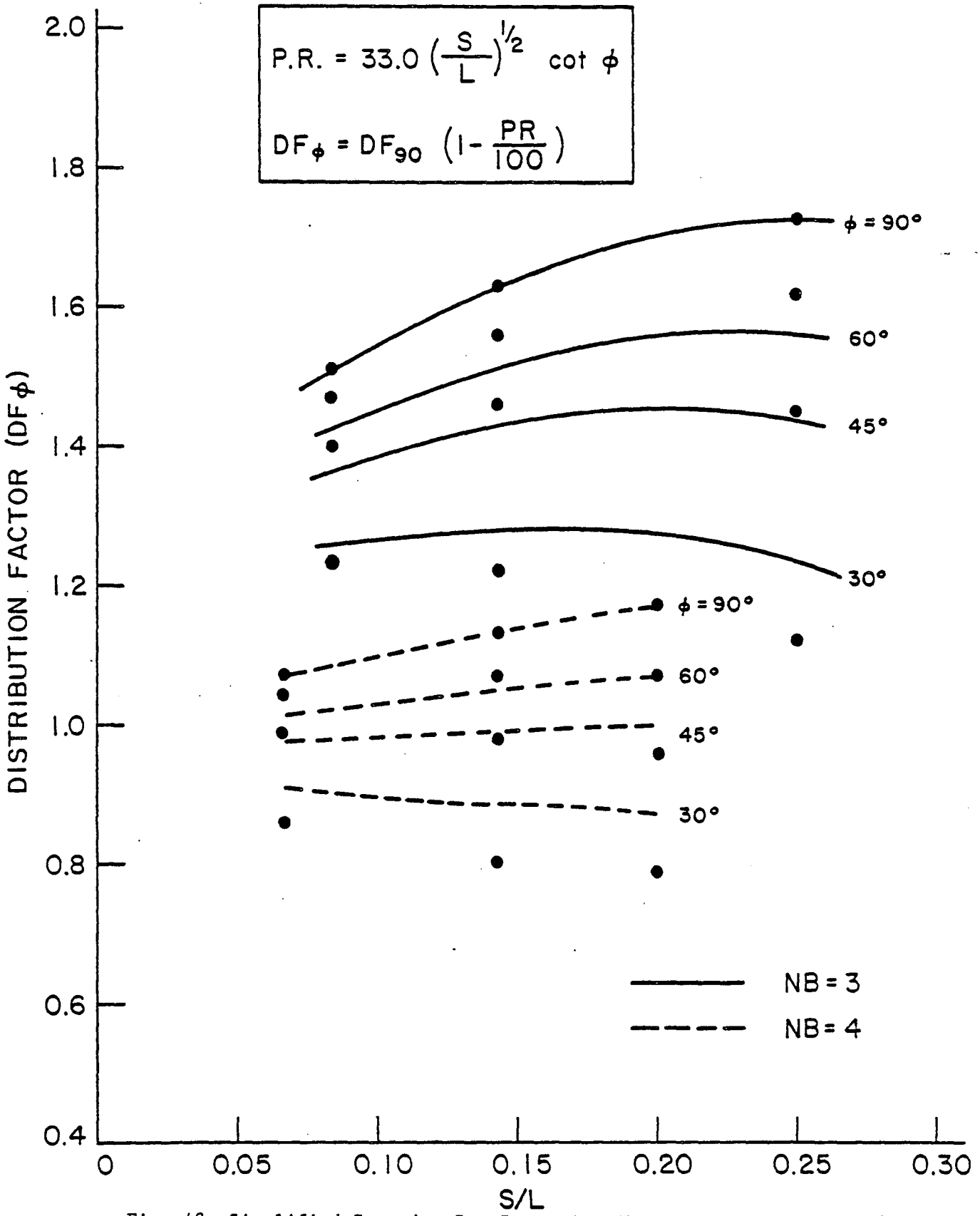

Fig. 42 Simplified Interior Box-Beam Distribution Factors, W_c = 24 ft.

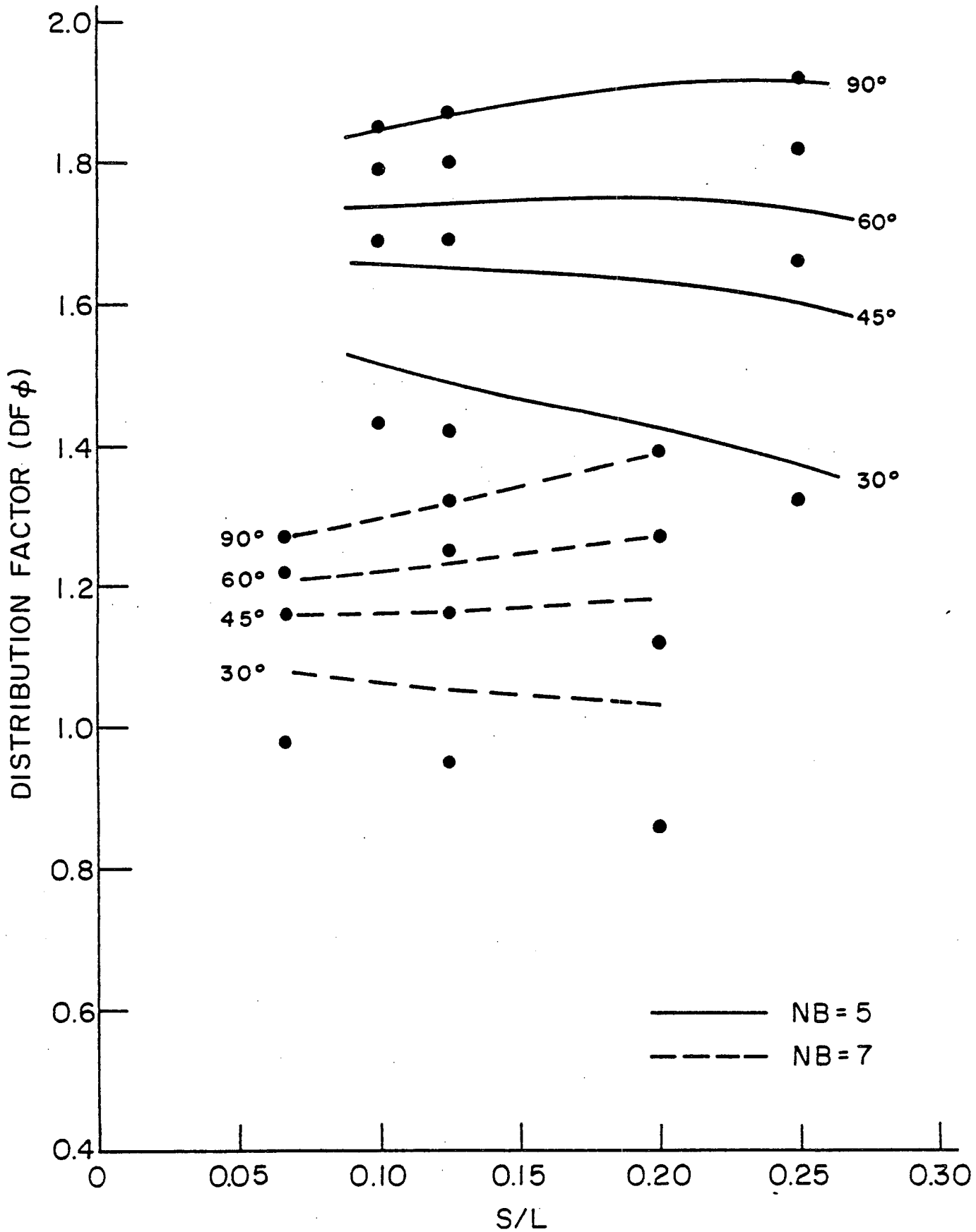

Fig. 43 Simplified Interior Box-Beam Distribution Factors, W_c = 48 ft.

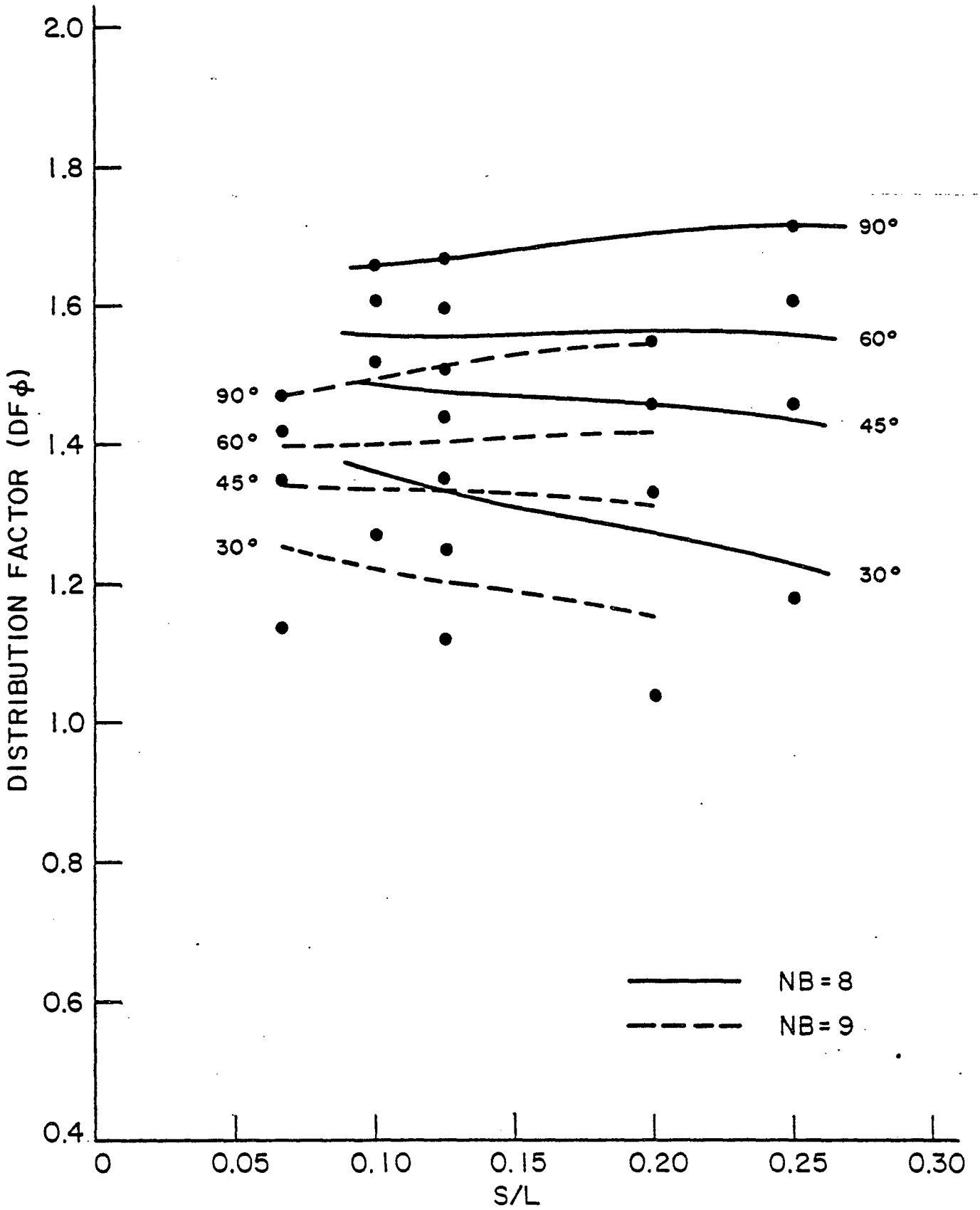

Fig. 44 Simplified Interior Box-Beam Distribution Factors, W_c = 72 ft.

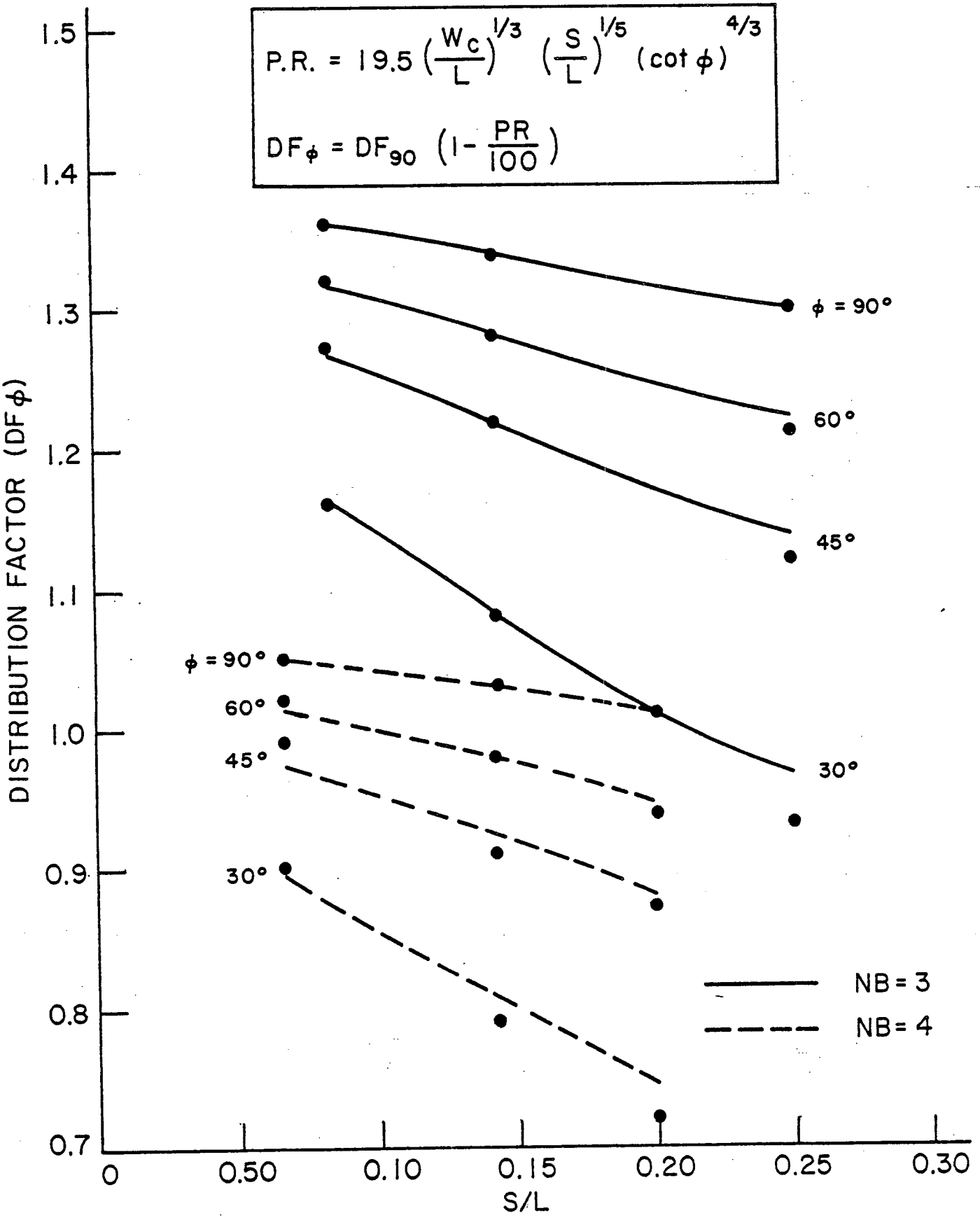

Fig. 45 Exterior Box-Beam Distribution Factors, W_c = 24 ft.

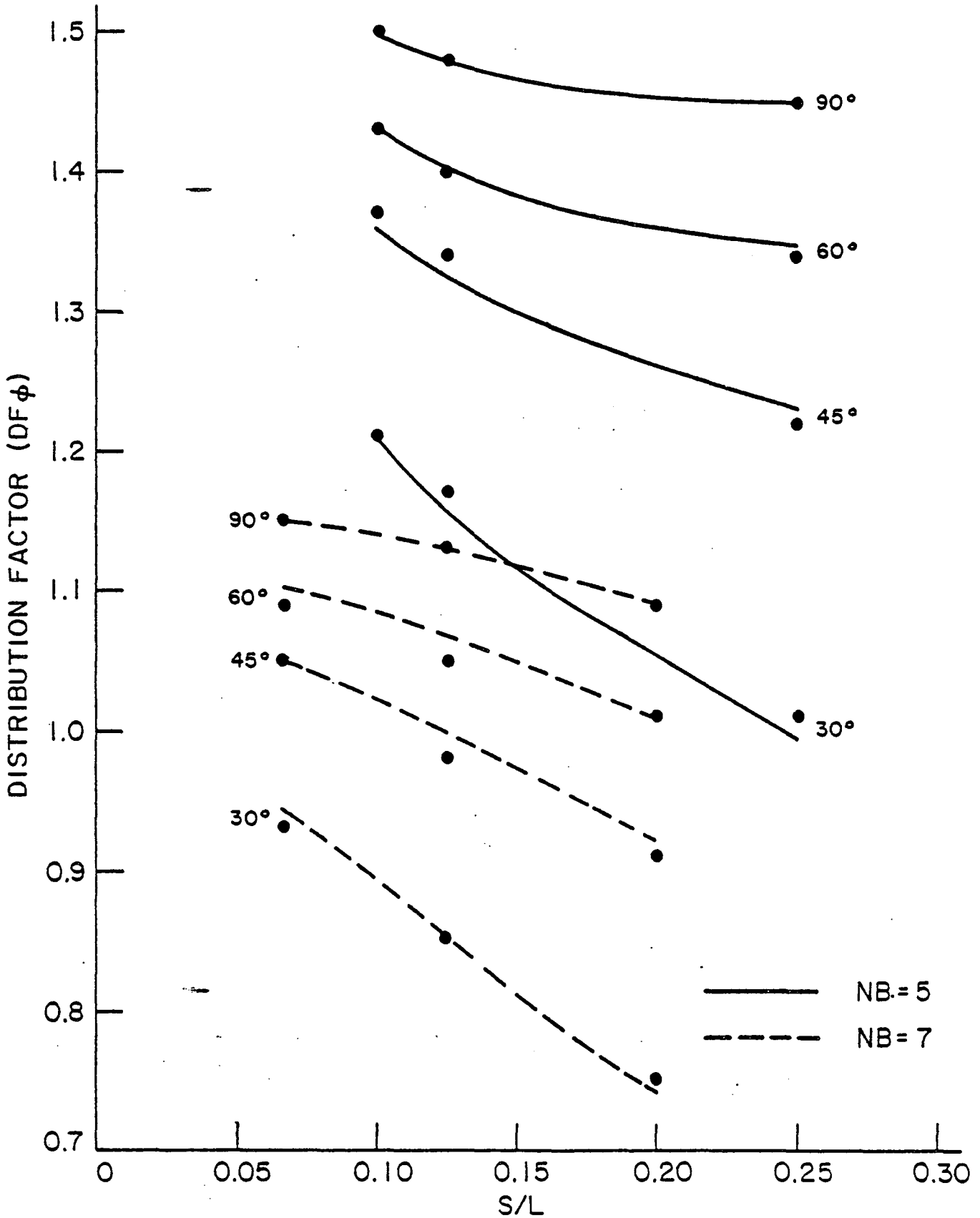

Fig. 46 Exterior Box-Beam Distribution Factors, W_c = 48 ft.

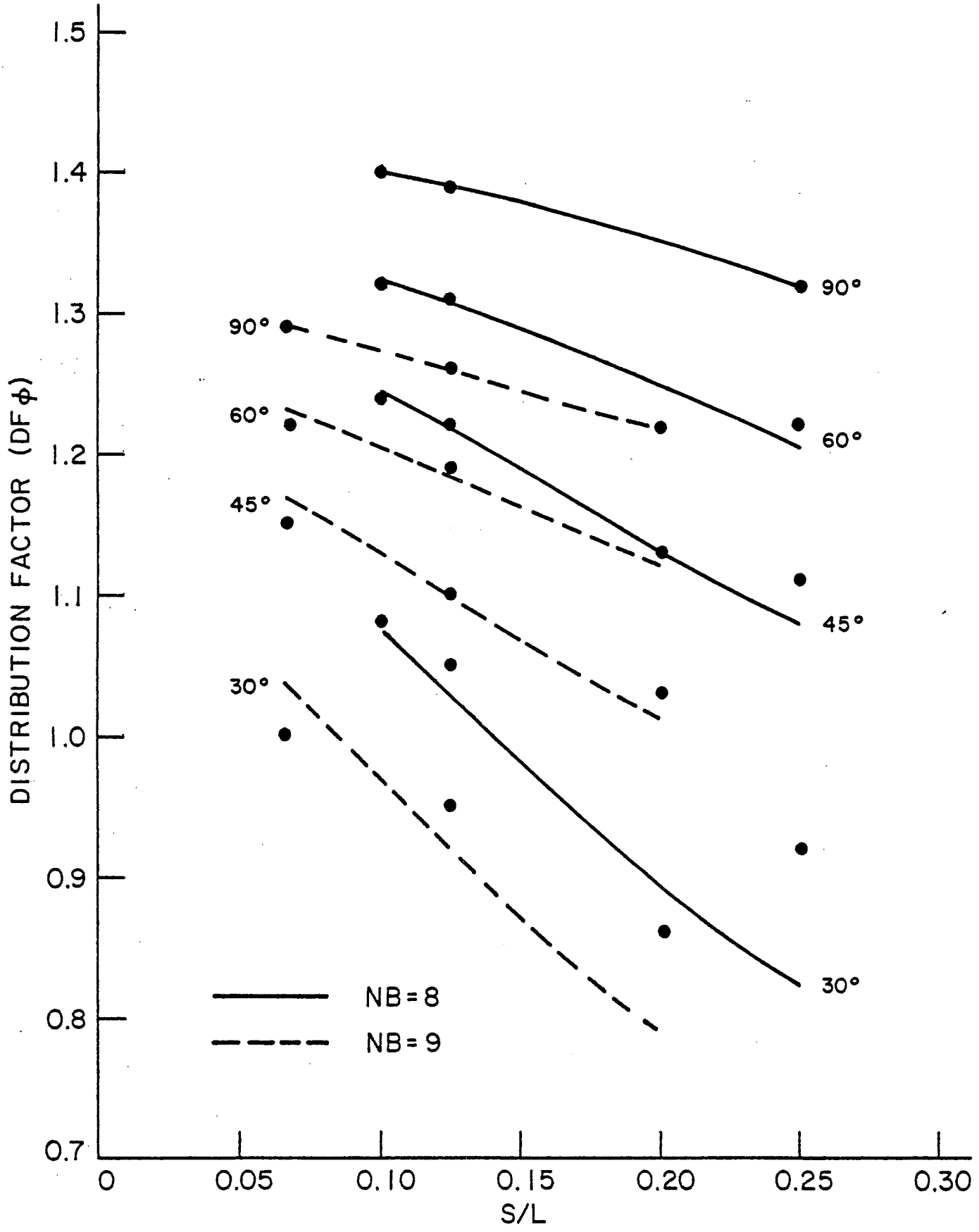

Fig. 47 Exterior Box-Beam Distribution Factors, W_c = 72 ft.

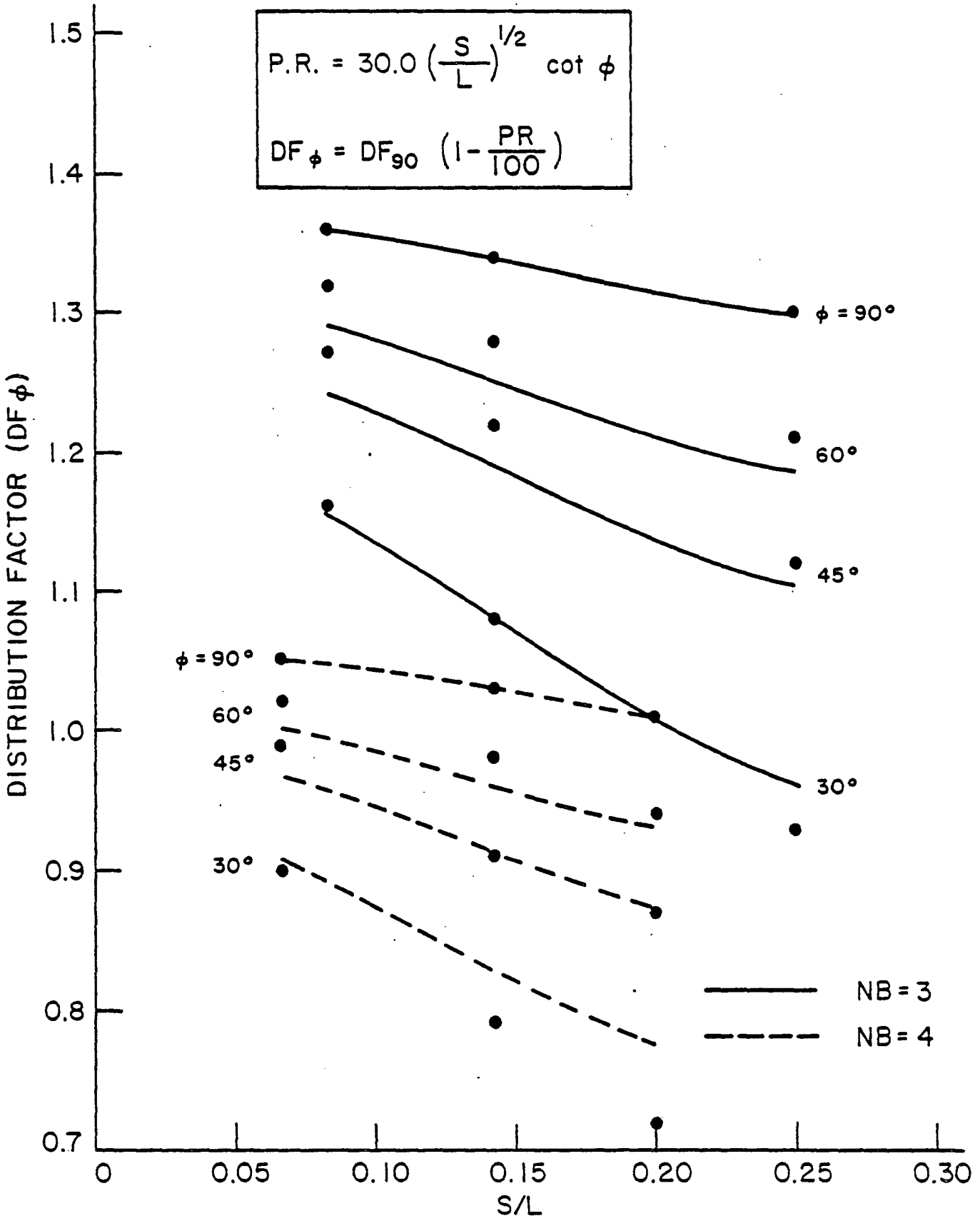

Fig. 48 Simplified Exterior Box-Beam Distribution Factor, W_c = 24 ft.

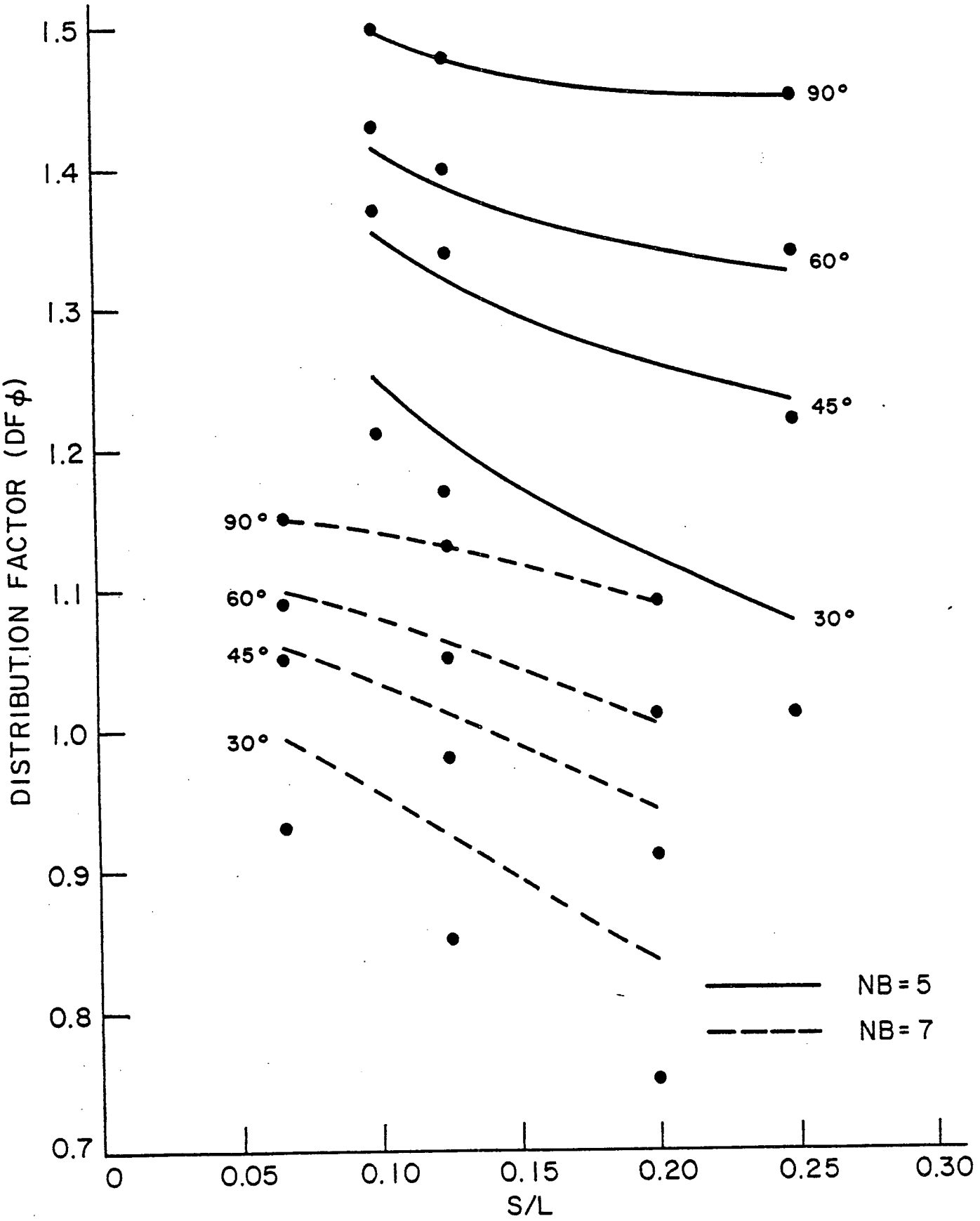

Fig. 49 Simplified Exterior Box-Beam Distribution Factors, W_c = 48 ft.

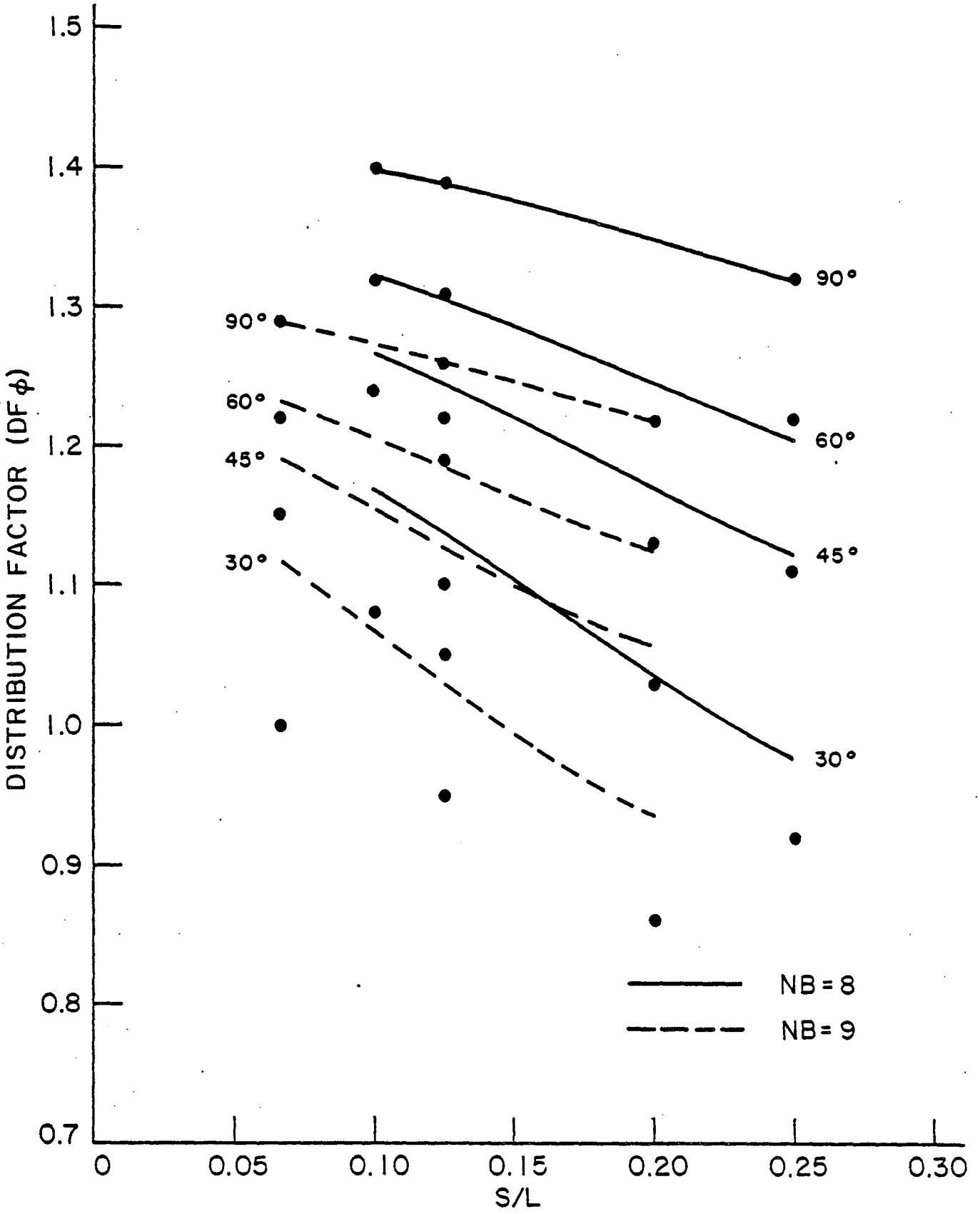

Fig. 50 Simplified Exterior Box-Beam Distribution Factors, W_c = 72 ft.

9. REFERENCES

1. American Association of State Highway Officials,
   STANDARD SPECIFICATIONS FOR HIGHWAY BRIDGES,
   10th Edition, Washington, D. C., 1969.

2. American Association of State Highway Officials,
   STANDARD SPECIFICATIONS FOR HIGHWAY BRIDGES,
   11th Edition, Washington, D. C., 1973.

3. American Association of State Highway and Transportation Officials,
   STANDARD SPECIFICATIONS FOR HIGHWAY BRIDGES,
   Interim Specifications, Washington, D. C., 1974.

4. Bathe, K., Wilson, E., and Peterson, F.
   SAP IV, A STRUCTURAL ANALYSIS PROGRAM FOR STATIC AND DYNAMIC RESPONSE OF LINEAR SYSTEMS, Earthquake Engineering Research Center Report No. EERC 73-11, University of California, Berkeley, 1974.

5. Bogner, F. K., Fox, R. L. and Schmidt, L. A.
   THE GENERATION OF INTERELEMENT COMPATIBLE STIFFNESS AND MASS MATRICES BY THE USE OF INTERPOLATION FORMULAS, Proc. Conference on Matrix Methods in Structural Mechanics, Wright Patterson Air Force Base, Dayton, Ohio, October 1965.

6. Burdette, E. G. and Goodpasture, D. W.
   FINAL REPORT ON FULL SCALE BRIDGE TESTING: AN EVALUATION OF BRIDGE DESIGN CRITERIA, Department of Civil Engineering, University of Tennessee, December 1971.

7. Chen, Chiou-Horng and VanHorn, D. A.
   STATIC AND DYNAMIC FLEXURAL BEHAVIOR OF A PRESTRESSED CONCRETE I-BEAM BRIDGE - BARTONSVILLE BRIDGE, Fritz Engineering Laboratory Report No. 349.2, January 1971.

8. Chen, Chiou-Horng and VanHorn, D. A.
   STRUCTURAL BEHAVIOR OF A PRESTRESSED CONCRETE I-BEAM BRIDGE - LEHIGHTON BRIDGE, Fritz Engineering Laboratory Report No. 349.4, October 1971.

9. Chen, T. Y., Siess, C. P. and Newmark, N. M.
   MOMENTS IN SIMPLY-SUPPORTED SKEW I-BEAM BRIDGES, Studies of Slab and Beam Highway Bridges, Part IV, University of Illinois Engineering Experiment Station Bulletin No. 439, Urbana, Illinois, 1957.

10. Clough, R. W. and Tocher, J. L.
FINITE ELEMENT STIFFNESS MATRICES FOR THE ANALYSIS OF PLATE BENDING, Proc. Conference on Matrix Methods in Structural Mechanics, Wright Patterson Air Force Base, Dayton, Ohio, October 1965.

11. Dawe, D. J.
PARALLELOGRAM ELEMENTS IN THE SOLUTION OF RHOMBIC CANTILEVER PLATE PROBLEMS, Journal of Strain Analysis, Vol. 1, No. 3, pp. 223-230, 1966.

12. DeCastro, E. S. and Kostem, C. N.
LATERAL LOAD DISTRIBUTION IN SKEWED PRESTRESSED CONCRETE I-BEAM BRIDGES, Fritz Engineering Laboratory Report No. 400.16, July 1975.

13. DeCastro, E. S. and Kostem, C. N.
USER'S MANUAL FOR PROGRAM PLATE, Fritz Engineering Laboratory Report No. 400.13, January 1975.

14. DeCastro, E. S. and Kostem, C. N.
USER'S MANUAL FOR PROGRAM INPT, Fritz Engineering Laboratory Report No. 400.18, July 1975.

15. DeCastro, E. S. and Kostem, C. N.
USER'S MANUAL FOR PROGRAM SKBRD, Fritz Engineering Laboratory Report No. 400.15, June 1975.

16. Douglas, W. J. and VanHorn, D. A.
LATERAL DISTRIBUTION OF STATIC LOADS IN A PRESTRESSED CONCRETE BOX-BEAM BRIDGE - DREHERSVILLE BRIDGE, Fritz Engineering Laboratory Report No. 315.1, August 1966.

17. Felippa, C. A.
REFINED FINITE ELEMENT ANALYSIS OF LINEAR AND NONLINEAR TWO-DIMENSIONAL STRUCTURES, SESM Report 66-22, Department of Civil Engineering, University of California, Berkeley, October 1966.

18. Felippa, C. A. and Clough, R. W.
A REFINED QUADRILATERAL ELEMENT FOR ANALYSIS OF PLATE BENDING, Second Conference on Matrix Methods in Structural Mechanics, Wright Patterson Air Force Base, Dayton, Ohio, October 1968.

19. Gaylord, H. and Gaylord, N., Editors
STRUCTURAL ENGINEERING HANDBOOK, McGraw Hill, New York, 1968.

20. Green, A. E. and Zerna, W.
THEORETICAL ELASTICITY, Clarendon Press, Oxford, 1954.

21. Guilford, A. A. and VanHorn, D. A.
LATERAL DISTRIBUTION OF VEHICULAR LOADS IN A PRESTRESSED CONCRETE BOX-BEAM BRIDGE - WHITE HAVEN BRIDGE, Fritz Engineering Laboratory Report No. 315.7, August 1968.

22. Guilford, A. A. and VanHorn, D. A.
LATERAL DISTRIBUTION OF VEHICULAR LOADS IN A PRESTRESSED CONCRETE BOX-BEAM BRIDGE - BERWICK BRIDGE, Fritz Engineering Laboratory Report No. 315.4, October 1967.

23. Gustafson, W. C. and Wright, R. N.
ANALYSIS OF SKEWED COMPOSITE GIRDER BRIDGES, Journal of the Structural Division, Proceedings of the ASCE, Vol. 94, ST4, pp. 919-941, April 1968.

24. Highway Research Board
THE AASHO ROAD TEST, Report 4, Bridge Research, Special Report 610, National Academy of Sciences, 1962.

25. Hondros, G. and Marsh, J. G.
LOAD DISTRIBUTION IN COMPOSITE GIRDER SLAB BRIDGES, Journal of the Structural Division, Proceedings of the ASCE, Vol. 86, ST11, pp. 79-109, November 1960.

26. Jensen, V. P.
ANALYSIS OF SKEW SLABS, University of Illinois Engineering Experiment Station Bulletin, No. 332, Urbana, Illinois, 1941.

27. Jumppanem, P.
BENDING OF PARALLELOGRAM PLATES, Acta Polytechnica Scandinavica, Civil Engineering and Building Construction Series No. 61, Helsinki, 1970.

28. Kennedy, J. B. and Simon, J. G.
LINEAR AND NONLINEAR ANALYSES OF SKEWED PLATES, Journal of Applied Mechanics, Vol. 34, p. 2, 1967.

29. Kostem, C. N.
ANALYTICAL MODELING OF BEAM SLAB BRIDGES, Proceedings of the International Symposium on Folded Plates and Spatial Panel Structures, Udine, Italy, September 1974.

30. Lehigh University Computing Center
THE LEAPS USER'S GUIDE AND MANUAL, Lehigh University Computing Center, Bethlehem, Pennsylvania, May 1973.

31. Lin, Chen-Shung and VanHorn, D. A.
THE EFFECT OF MIDSPAN DIAPHRAGMS ON LOAD DISTRIBUTION IN A PRESTRESSED CONCRETE BOX-BEAM BRIDGE - PHILADELPHIA BRIDGE, Fritz Engineering Laboratory Report No. 315.6, June 1968.

32. Macias-Rendon, M. A. and VanHorn, D. A.
MODEL STUDY OF BEAM SLAB BRIDGE SUPERSTRUCTURES, Journal of the Structural Division, Proceedings of the ASCE, ST9, Vol. 99, pp. 1805-1821, September 1973.

33. Meek, J. L.
MATRIX STRUCTURAL ANALYSIS, McGraw Hill, New York, 1971.

34. Melosh, R. J.
BASIS FOR THE DERIVATION OF MATRICES FOR THE DIRECT STIFFNESS METHOD, AIAA Journal, Vol. 1, No. 7, July 1963.

35. Monforton, G. R. and Schmidt, L. A.
FINITE ELEMENT ANALYSIS OF SKEW PLATES IN BENDING, AIAA Journal, Vol. 6, No. 6, pp. 1150-1152, 1968.

36. Morice, P. B. and Little, G.
ANALYSIS OF RIGHT BRIDGES SUBJECTED TO NORMAL LOADING, Cement and Concrete Association, London, D.B.11.

37. Morley, L. S. D.
SKEW PLATES AND STRUCTURES, Pergamon Press, McMillan Company, New York, 1963.

38. Motarjemi, D. and VanHorn, D. A.
THEORETICAL ANALYSIS OF LOAD DISTRIBUTION IN PRESTRESSED CONCRETE BOX-BEAM BRIDGES, Fritz Engineering Laboratory Report No. 315.9, October 1969.

39. Newmark, N. M. and Siess, C. P.
MOMENTS IN I-BEAM BRIDGES, University of Illinois Engineering Experiment Station Bulletin No. 336, Urbana, Illinois, 1942.

40. Newmark, N. M., Siess, C. P. and Pechham, W. M.
TEST OF SIMPLE SPAN RIGHT I-BEAM BRIDGES, Studies of Slab and Beam Highway Bridges: Part I, University of Illinois Engineering Experiment Station Bulletin No. 363, Vol. 43, No. 42, Urbana, Illinois, March 1946.

41. Newmark, N. M., Siess, C. P. and Pechham, W. M.
TEST OF SIMPLE SPAN SKEW I-BEAM BRIDGES, Studies of Slab and Beam Highway Bridges, Part II, University of Illinois Engineering Experiment Station Bulletin No. 375, Vol. 45, No. 31, Urbana, Illinois, January 1948.

42. Pennsylvania Department of Highways
STANDARDS FOR PRESTRESSED CONCRETE BRIDGES, ST200-ST208, Bureau of Design, Bridge Division, Commonwealth of Pennsylvania, 1960.

43. Pennsylvania Department of Transportation
STANDARDS FOR BRIDGE DESIGN, BD-201, Bureau of Design, Commonwealth of Pennsylvania, June 1973.

44. Pickett, G.
APPLICATION OF THE FOURIER METHOD TO THE SOLUTION OF CERTAIN BOUNDARY PROBLEMS IN THE THEORY OF ELASTICITY, Journal of Applied Mechanics, Vol. 11, p. 176, 1944.

45. Przemieniecki, J. S.
THEORY OF MATRIX STRUCTURAL ANALYSIS, McGraw Hill, New York, 1968.

46. Rai, S. I. and Sandhu, S. R.
FINITE ELEMENT OF AN ISOTROPIC PLATE USING Q-19 ELEMENT, PART I, THEORETICAL DEVELOPMENT, Ohio University and Air Force Flight Dynamics Laboratory, AFFDL-TR-74-120, Wright Patterson Air Force Base, Ohio, October 1974.

47. Robinson, K. E.
THE EFFECT OF SKEW ON THE BEHAVIOR OF SIMPLY SUPPORTED BRIDGE SLABS, Cement and Concrete Association, Technical Report TRB/271, July 1957.

48. Rusch, E. H. and Hergenroder, A.
EINFLUBFELDER DER MOMENTE SCHREF-WINKLIGER PLATTEN (Influence Surfaces for Moments in Skew Slabs) Werner-Verlag, Dusseldorf, 3rd Ed., 1969, Translated by C. V. Amerongen.

49. Sanders, W. W., Jr. and Elleby, H. A.
DISTRIBUTION OF WHEEL LOADS IN HIGHWAY BRIDGES, National Cooperative Highway Research Program, Report No. 83, Highway Research Board, Washington, D. C., 1970.

50. Sandhu, S. R.
FINITE ELEMENT ANALYSIS OF AN ISOTROPIC PLATE USING Q-19 ELEMENT, PART II, INSTRUCTION FOR USERS AND FORTRAN LISTING, Ohio State University and Air Force Flight Dynamics Laboratory, Wright Patterson Air Force Base, Ohio, October 1974.

51. Schaffer, T. and VanHorn, D. A.
STRUCTURAL RESPONSE OF A 45° SKEW PRESTRESSED CONCRETE BOX-GIRDER BRIDGE SUBJECTED TO VEHICULAR LOADING - BROOKVILLE BRIDGE, Fritz Engineering Laboratory Report No. 315.5, October 1967.

52. Schultchen, E. G. and Kostem, C. N.
USER'S MANUAL FOR CSTPL FINITE ELEMENT PROGRAM, Fritz Engineering Laboratory Report No. 400.2, June 1971.

53. Sisodiya, R. G. and Cheung, Y. K.
A HIGHER ORDER IN-PLANE PARALLELOGRAM ELEMENT AND ITS APPLICATION TO SKEWED CURVED BOX-GIRDER BRIDGES, Developments in Bridge Design and Constructions, Rockey et al, Editors, Crosby, Lockwood and Sons Ltd., London, 1971.

54. Timoshenko, S. P. and Goodier, V. N.
THEORY OF ELASTICITY, 3rd Edition, McGraw Hill, New York, 1970.

55. Timoshenko, S. P. and Woinoswki-Krieger, S.
THEORY OF PLATES AND SHELLS, 2nd Edition, McGraw Hill, New York, 1959.

56. Tottenham, H. and Brebbia, C. (Editors)
FINITE ELEMENT TECHNIQUES IN STRUCTURAL MECHANICS, Stress Analysis Publishers, Southampton, England, 1970.

57. VanHorn, D. A.
STRUCTURAL BEHAVIOR CHARACTERISTICS OF PRESTRESSED CONCRETE BOX-BEAM BRIDGES, Fritz Engineering Laboratory Report No. 315.8, December 1969.

58. Wegmuller, A. W. and Kostem, C. N.
FINITE ELEMENT ANALYSIS OF PLATES AND ECCENTRICALLY STIFFENED PLATES, Fritz Engineering Laboratory Report No. 378A.3, February 1973.

59. William, K. J.
FINITE ELEMENT ANALYSIS OF CELLULAR STRUCTURES, Ph.D. Dissertation, University of California, Berkeley, 1969.

60. William, K. J. and Scordelis, S. C.
COMPUTER PROGRAM FOR CELLULAR STRUCTURES OF ARBITRARY PLAN GEOMETRY, SESM Report 70-10, Department of Civil Engineering, University of California, Berkeley, 1969.

61. Yen, B. T., Chen, Y. S., et al
MODEL TESTS ON COMPOSITE BOX-BEAMS, Fritz Engineering Laboratory Report No. 380.6, October 1973.

62. Zellin, M. A., Kostem, C. N. and VanHorn, D. A.
LOAD DISTRIBUTION OF LIVE LOAD IN PRESTRESSED CONCRETE I-BEAM BRIDGES, Fritz Engineering Laboratory Report No. 387.2A, June 1975.

63. Zellin, M. A., Kostem, C. N. and VanHorn, D. A.
STRUCTURAL BEHAVIOR OF BEAM-SLAB HIGHWAY BRIDGES,
A Summary of Completed Research and Bibliography,
Fritz Engineering Laboratory Report No. 387.1,
May 1973.

64. Zienkiewicz, O. C. and Cheung, Y. K.
THE FINITE ELEMENT METHOD IN STRUCTURAL AND CONTINUUM MECHANICS, McGraw Hill, New York, 1967.

65. Zienkiewicz, O. C. and Hollister, G. S.
STRESS ANALYSIS, John Wiley and Sons, New York, 1975.

66. deCastro, E. S. and Kostem, C. N.
LOAD DISTRIBUTION IN SKEWED BEAM-SLAB HIGHWAY BRIDGES,
Fritz Engineering Laboratory Report No. 378A.7,
December 1975.

10. APPENDICES

Appendix A FINITE ELEMENT ANALYSIS OF SKEWED ELASTIC PLATES

A1. Q8S11 ELEMENT STIFFNESS MATRIX

A2. COMPATIBLE DISPLACEMENT FUNCTIONS FOR PLATE BENDING ELEMENT Q-19

Appendix B FINITE ELEMENT ANALYSIS OF SKEWED STIFFENED PLATES

APPENDIX A

FINITE ELEMENT ANALYSIS OF SKEWED ELASTIC PLATES

A.1 Skew Plate In-Plane Analysis

The skew plate also known as a parallelogram is a special case of a quadrilateral plate when opposite sides are parallel (Fig. A1). The acute angle between two adjacent sides is called the skew angle as shown in the figure. The rectangular plate is a special case of the skew plate when the skew angle is 90°.

A.1.1 Methods of Solutions

The solutions to skew in-plane problems have been arrived at by using the theory of elasticity in rectangular, oblique and polar coordinate systems (Ref. 37). As reported by Morley in Ref. 37, solutions in rectangular and oblique coordinates have been obtained by Hemp, Favre, Lardy and Theodorescu; and solutions in the polar coordinate system have been obtained by Coker and Filon, Williams, and Mansfield. Solutions in terms of the Airy stress function expressed in complex variables, trigonometric series, and infinite series have been obtained by Green and Zerna (Ref. 20) and Pickett (Ref. 44).

A.1.2 Assumptions and Basic Equations

The skew plate under any in-plane forces is assumed to be a plane stress problem. Stresses σ_x, σ_y and τ_{xy} and the generalized forces N_x, N_y and N_{xy} in an infinitesimal element are shown in Fig. A2. The components of stress and generalized forces shown in the figure indicate the assumed positive direction. The generalized forces are the stresses integrated over the thickness of the element.

The displacement at any point of the plate is defined by the components of the vector field {v}:

$$\{v\} = \begin{Bmatrix} u \\ v \end{Bmatrix} \tag{A.1}$$

where u and v are in the x and y directions respectively. The strain field at any point is defined from the displacement field by the relationship:

$$\{\varepsilon\} = \begin{Bmatrix} \varepsilon_{xx} \\ \varepsilon_{yy} \\ \gamma_{xy} \end{Bmatrix} = \begin{Bmatrix} \frac{\partial u}{\partial x} \\ \frac{\partial v}{\partial y} \\ \frac{\partial u}{\partial y} + \frac{\partial v}{\partial x} \end{Bmatrix} \tag{A.2}$$

where ε_{xx}, ε_{yy}, γ_{xy} are the well known components of strain.

The usual stress-strain relationship ($\{\sigma\} = [D]\{\varepsilon\}$) for the general orthotropic case is given by Ref. 64:

$$\begin{Bmatrix} \sigma_x \\ \sigma_y \\ \tau_{xy} \end{Bmatrix} = \frac{E_2}{(1 - n\nu_2^2)} \begin{bmatrix} n & n\nu_2 & 0 \\ n\nu_2 & 1 & 0 \\ 0 & 0 & m(1 - n\nu_2^2) \end{bmatrix} \cdot \begin{Bmatrix} \varepsilon_x \\ \varepsilon_y \\ \gamma_{xy} \end{Bmatrix} \tag{A.3}$$

where

$$n = \frac{E_1}{E_2}$$

$$m = \frac{G_2}{E_2}$$

in which E_1 and E_2 are the principal elastic moduli in the x and y direction, ν_2 is the Poisson's ratio, and G_2 is the shear modulus. For the isotropic case, $E_1 = E_2$, $\nu_2 = \nu$, and $m = \frac{1}{2(1+\nu)}$.

A.2 In-Plane Finite Element Analysis of Skew Plates

A.2.1 Geometry and Displacement Field

Consider a quadrilateral in-lane finite element as shown in Fig. A3. The local coordinate system with the origin at the centroid of the element is indicated by ζ and η. The nodes are numbered counter-clockwise with the node at the centroid being the fifth node. The edges 1-2 and 3-4 of the quadrilateral are represented by $\zeta = -1$ and $\zeta = 1$. The edges 2-3 and 4-1 are represented by $\eta = -1$ and $\eta = 1$.

The in-plane element has eight external and three internal degrees of freedom (Fig. A3). The external degrees of freedom are the displacements u_i and v_i specified at the external nodes i, i = 1 to 4. The three internal degrees of freedom are the displacements u_5 and v_5 and the strain γ_{xy}. The displacement u_5 and v_5 are specified at the fifth node while the strain γ_{xy} is assumed to be constant throughout the element. This element was originated by Doherty who designed the element based on physical concepts and was derived by Williams using concise variational formulation (Ref. 59).

The geometrical relationships between the global coordinates and the local coordinates can be expressed in matrix form by the following expressions:

$$\begin{Bmatrix} x \\ y \end{Bmatrix} = \begin{bmatrix} \Phi_x & 0 \\ 0 & \Phi_y \end{bmatrix} \begin{Bmatrix} x_i \\ y_i \end{Bmatrix} \tag{A.4}$$

where $$\Phi_x = \frac{1}{4}(1 + \zeta\zeta_i)(1 + \eta\eta_i)$$

$$\Phi_y = \frac{1}{4}(1 + \zeta\zeta_i)(1 + \eta\eta_i)$$

in which x_i and y_i are the global coordinates of node i, and η_i and ζ_i are the local coordinates of node i.

The displacement function for the element is assumed to be a linear shape function for the corner points and a quadratic interpolation function for the interior point. The internal shape function selected is the quadratic interpolation scheme with vanishing values at the boundaries (Ref. 59). Thus, the equation $\{v\} = [\Phi]\{v_i\}$, for this element, can be written as follows

$$\begin{Bmatrix} u \\ v \end{Bmatrix} = \begin{bmatrix} f_1 & 0 & f_2 & 0 & f_3 & 0 & f_4 & 0 & f_5 & 0 \\ 0 & f_1 & 0 & f_2 & 0 & f_3 & 0 & f_4 & 0 & f_5 \end{bmatrix} \begin{Bmatrix} u_i \\ v_i \end{Bmatrix} \tag{A.5}$$

where,

$$\begin{Bmatrix} u_i \\ v_i \end{Bmatrix}^T = \begin{Bmatrix} u_1 & v_1 & u_2 & v_2 & u_3 & v_3 & u_4 & v_4 & u_5 & v_5 \end{Bmatrix} \tag{A.5a}$$

and,

$$f_1 = \frac{1}{4}(1 - \zeta)(1 - \eta) \tag{A.5b}$$

$$f_2 = \frac{1}{4}(1 + \zeta)(1 - \eta) \tag{A.5c}$$

$$f_3 = \frac{1}{4}(1 + \zeta)(1 + \eta) \tag{A.5d}$$

$$f_4 = \frac{1}{4}(1 - \zeta)(1 + \eta) \tag{A.5e}$$

$$f_5 = (1 - \zeta^2)(1 - \eta^2) \tag{A.5f}$$

A.2.2 Derivation of Element Stiffness Matrix

The strain field can be derived from the standard strain displacement relationship. With the assumption of constant shear strain and with the additional strain degree of freedom, the strain components can be written (Ref. 59)

$$\begin{Bmatrix} \varepsilon_{xx} \\ \varepsilon_{yy} \\ \gamma_{xy} \end{Bmatrix} = \begin{bmatrix} U & 0 & 0 \\ 0 & V & 0 \\ 0 & 0 & 1 \end{bmatrix} \begin{Bmatrix} u_i \\ v_i \\ \alpha \end{Bmatrix} \tag{A.6}$$

where

$$U = \frac{\partial f_i}{\partial x} \tag{A.6a}$$

$$V = \frac{\partial f_i}{\partial y} \tag{A.6b}$$

and α is the generalized coordinate associated with the constant shear strain degree of freedom. The derivatives of the functions in Eqs. A.6a and A.6b can be written with the help of the chain rule (Ref. 45):

$$\frac{\partial f_i}{\partial x} = \frac{\frac{\partial f_i}{\partial \zeta} \cdot \frac{\partial y}{\partial \eta} - \frac{\partial f_i}{\partial \eta} \cdot \frac{\partial y}{\partial \zeta}}{\frac{\partial x}{\partial \zeta} \cdot \frac{\partial y}{\partial \eta} - \frac{\partial x}{\partial \eta} \cdot \frac{\partial y}{\partial \zeta}} \tag{A.7}$$

$$\frac{\partial f_i}{\partial y} = \frac{\frac{\partial f_i}{\partial \eta} \cdot \frac{\partial x}{\partial \eta} - \frac{\partial f_i}{\partial \eta} \cdot \frac{\partial x}{\partial \zeta}}{\frac{\partial x}{\partial \zeta} \cdot \frac{\partial y}{\partial \eta} - \frac{\partial x}{\partial \eta} \cdot \frac{\partial y}{\partial \zeta}} \tag{A.8}$$

The evaluation of the element stiffness for the resulting finite element model is given in Appendix A1. The final stiffness matrix is obtained by the application of the static condensation procedure on the interior node as described in Refs. 17 and 18. The element is known as Q8D11.

The explicit integration of the stiffness matrix integral is a lengthy process and difficult. The usual procedure in this case is to use the numerical integration procedure (Refs. 45,59,64).

In the procedure, the terms of the matrices are evaluated at several points call integration points. The Gaussian quadrature formulation is found to be most useful for the present problem. In the formulation, the polynomial function is integrated as the sum of the weighted values at specified points.

Thus, a function $\int_{-1}^{1} f(\zeta)d\zeta$ can be replaced by a summation

$$\int_{-1}^{1} f(\zeta)d\zeta = \sum_{j=1}^{n} W_j f(a_j) \tag{A.9}$$

where W_j are the weight coefficients and a_j are the values of the function at the n specified points.

The double integral of the form

$$I = \int_{-1}^{1} \int_{-1}^{1} f(\zeta,\eta)\, d\zeta\, dn \tag{A.10}$$

can be replaced by the following summation (Ref. 64):

$$I = \sum_{i=1}^{n} \sum_{j=1}^{n} W_j W_i f(a_j,b_i) \tag{A.11}$$

The numerical values of the coordinates at the integration points and the weight coefficients for different values of n are given by Zienkiewicz (Ref. 64). For this element, William has shown that the 2 x 2 Gaussian quadrature formula provides better results in stiffness than the improved 3 x 3 Gaussian integration scheme (Ref. 59). The coordinates of the integration points are shown in Fig. A4 and the weight coefficients are equal to 1 (Ref. 64).

The following should be noted in connection with this element. First, since a different shape function is used to describe individual displacement and strain components, the variation of displacement is not homogeneous. The stiffness property of the element is therefore directional. Secondly, monotonic convergence and boundedness is lost according to the Melosh criterion (Ref. 34). This criterion requires that interpolation function of internal nodes must be lower than the external node. However, this element has been shown to give more flexible and better results among the 8 degree of freedom family displacement models (Ref. 59).

The Q8D11 element has been tested and compared with other finite elements by William (Ref. 59). The same study showed the efficiency and accuracy of the element among the other finite elements. This element will be combined with the plate bending element in Section A.4 to make up the basic plate element used in this study. Numerical examples are provided to illustrate the accuracy of the element.

A.2.3 Numerical Examples and Comparisons

The accuracy of the finite element solution for rectangular plate problems as compared with theoretically exact answers has been reported and shown by Zienkiewicz, and Tottenham and Brebbia (Refs. 56,64). Unfortunately, very little data is available for skew plate problems except for the very simple cases.

The method of analysis must be applicable for all angles of skew. Therefore, the first test example is a rectangular plate under uniform edge loading and under pure shear loading. The plate properties and dimensions are shown in Fig. A.5. The skew angle is 90° and the exact solution can be found from the theory of elasticity. The results are tabulated in Tables A1 and A2. It can be noted that uniform strain for these loadings is accurately predicted by the element. The CST, that is, constant strain triangle (Ref. 52), finite element

solution is also shown in Tables A1 and A2 for comparison. The CST discretization in this example was with the use of 8 triangular elements formed by connecting two opposite corner nodes of the complete plate and connecting the midpoints of opposite sides.

The second example is a skew plate under uniform edge loading as shown in Fig. A6. The state of stress for this problem is uniform throughout the element and can be found directly from equilibrium. The example illustrates the applicability of the element to plate problems with a parallelogram shape. The discretization into four rhombic elements is shown in Fig. A6b. The discretization into eight triangular elements for the CST analysis follows the same procedure as the first example. The numerical results are tabulated in Table A3. Since the exact solution is that of constant strain, the analytical results verified the analytical model.

The third example is a skew plate under in-plane concentrated loads. The plate shown in Fig. A7 is fixed at the supports and subjected to two concentrated loads near midspan. This problem is chosen to illustrate the accuracy of the element under this type of loading. There is no exact solution for this problem. The solutions are provided by using linear strain equilateral -LSE (Ref. 60), constant strain triangle -CST (Ref. 52), and the reported values from Ref. 59. The results are tabulated in Table A4.

Q8D8 refers to the quadrilateral element with only four nodes and two degrees of freedom at each node. Q8D11(3) refers to the derived finite element using the 3 x 3 integration rule. The Q8D11(2)

refers to the element formulation using the 2 x 2 integration rule. The accuracy of the element using the relaxed integration rule can be seen from the table.

The final example is the problem of the beam with inclined faces under a concentrated load at midspan. The structure is shown in Fig. A8a and the two selected discretizations are shown in Figs. A8b and A8c. The analytical solution is compared to the solution by Sisodiya and Cheung (Ref. 53) who used a higher order element that gives good results for the given type of structure and loading. The results are tabulated in Table A5. The advantage of the element over the standard Q8D8 is made obvious in this example.

It should be emphasized that this example is the most severe case the element will be subjected to. In the application of this element to the beam slab problem, the element will represent the in-plane behavior of the deck slab. As such, the typical type of loading would be in-plane loads in the direction of span thus producing column behavior rather than beam behavior. The results of this example are the reasons for the choice of another element to represent the in-plane behavior of webs for box-beam bridges in Chapter 4.

A.3 Skew Plate Bending Analysis

A.3.1 Methods of Solutions

The exact solution to the differential equation of skew plates in bending is difficult to obtain if at all possible. For the

simple cases, the problem is solved by direct integration of the differential equation under associated boundary conditions, or by the application of conformal mapping (Ref. 27). Subsequently, a number of studies have been concerned with investigations of the methods of solution, the most common being the series solutions and the method of finite difference (Ref. 26). Solutions in oblique coordinates, trigonometric series, and finite difference solutions by several authors are listed and referenced by Morley in Ref. 37. Solutions by polynomials and trigonometric functions have been obtained by Jumppanem (Ref. 27) and Kennedy and Simon (Ref. 28).

Based on model tests Rusch (Ref. 48) produced design data in the form of influence surfaces for bending and torsional moments of simply-supported slabs with various angles of skew. A series of thirteen skew slab models of different side to length ratio were investigated. The slab models tested were all simple span structures and made of gypsum plaster. As in any model study, it was not possible to investigate all parameters.

One of the earliest solutions using the finite difference methods was made by Jensen (Ref. 26). This was followed by Chen et al. in 1957 and by Robinson in 1959 (Refs. 9, 47).

Within the past decade, the finite element technique has been employed successfully to analyze plates of arbitrary shape (Refs. 5,10, 18). Zienkiewicz and Cheung, and Melosh used the technique to analyze plates in bending (Refs. 34,64) using rectangular elements. Based on the same deformation pattern used in the rectangular plate element

Dawe (Ref. 11) developed the stiffness matrices for parallelogram elements. Subsequently triangular elements were introduced, the most common being those by Zienkiewicz and Cheung (Ref. 64) and by Clough and Tocher (Ref. 10). Further improvements in accuracy were subsequently obtained by Felippa and Clough (Ref. 18), and Bogner et al. (Ref. 5) with the use of refined and higher order elements.

A.3.2 Assumptions and Basic Equations

A typical element from a skew plate structure is shown in Fig. A9. The element is of differential dimensions whose sides are parallel to the orthogonal x-y system of coordinates. The reference plane is assumed to lie on the mid-plane of the plate. Forces, displacements and the adopted sign conventions are shown in the positive directions in Fig. A9. The plate is assumed to be elastic, homogeneous, orthotropic and of uniform thickness, t. The standard assumptions in small deflection theory of plates are employed:

1. Stresses normal to the plate are negligible
2. Deflections are small relative to the plate thickness
3. Deflection in the z direction is a function of x and y only
4. Shear strains γ_{xz}, γ_{yz} in the x and y faces of the element and in the direction of z are equal to zero.

The consequence of the above assumptions is that normals to the plate remain normal after deformation.

From the above assumptions, the displacement equations may be written as:

$$U(z) = u - z \frac{\partial w}{\partial x} \tag{A.12a}$$

$$V(z) = v - z \frac{\partial w}{\partial y} \tag{A.12b}$$

where U(z) and V(z) are the displacement components of the point at distance z from the reference plane; and u, v, and w are the displacement components of the point on the reference plane.

Equations A.12a and A.2b can be differentiated to obtain the relationship of the strains to displacements:

$$\begin{Bmatrix} \varepsilon_x \\ \varepsilon_y \\ \gamma_{xy} \end{Bmatrix} = \begin{Bmatrix} \frac{\partial u}{\partial x} - z \frac{\partial^2 w}{\partial x^2} \\ \frac{\partial v}{\partial y} - z \frac{\partial^2 w}{\partial z^2} \\ \frac{\partial u}{\partial y} + \frac{\partial v}{\partial x} - 2z \frac{\partial^2 w}{\partial x \partial y} \end{Bmatrix} \tag{A.13}$$

The stress-strain relationship given by Eq. A.3 in Section A.1.2 can then be rewritten explicitly by substituting the above expressions for ε_x, ε_y and γ_{xy}:

$$\sigma_x = C_{11} \left(\frac{\partial u}{\partial x} - z \frac{\partial^2 w}{\partial x^2} \right) + C_{12} \left(\frac{\partial v}{\partial y} - z \frac{\partial^2 w}{\partial y^2} \right) \tag{A.14a}$$

$$\sigma_y = C_{21} \left(\frac{\partial u}{\partial x} - z \frac{\partial^2 w}{\partial x^2} \right) + C_{22} \left(\frac{\partial v}{\partial y} - z \frac{\partial^2 w}{\partial y^2} \right) \tag{A.14b}$$

$$\gamma_{xy} = C_{33} \left(\frac{\partial u}{\partial y} + \frac{\partial v}{\partial x} - 2z \frac{\partial^2 w}{\partial x \partial y} \right) \qquad \text{(A.14c)}$$

where C_{11}, C_{12}, C_{21}, C_{33} are the material constants evaluated from Eq. A.3.

The stress resultants per unit of the plate shown in Fig. A.9b are found by integrating over the thickness.

Thus,

$$M_x = \int_{-t/2}^{t/2} \sigma_x \, z \, dz \qquad \text{(A.15a)}$$

$$M_y = \int_{-t/2}^{t/2} \sigma_y \, z \, dz \qquad \text{(A.15b)}$$

$$M_{xy} = \int_{-t/2}^{t/2} \sigma_{xy} \, z \, dz \qquad \text{(A.15c)}$$

Using Eq.A.14 and the assumption of plane sections, the above equations can be integrated easily resulting to the following equations in matrix form:

$$\begin{Bmatrix} M_x \\ M_y \\ M_{xy} \end{Bmatrix} = \begin{bmatrix} D_{11} & D_{12} & 0 \\ D_{21} & D_{22} & 0 \\ 0 & 0 & D_{33} \end{bmatrix} \begin{Bmatrix} \frac{\partial^2 w}{\partial x^2} \\ \frac{\partial^2 w}{\partial y^2} \\ -2 \frac{\partial^2 w}{\partial x \partial y} \end{Bmatrix} \qquad \text{(A.16)}$$

where

$$D_{11} = \frac{C_{11} t^3}{12}$$

$$D_{12} = D_{21} = \frac{C_{12} t^3}{12}$$

$$D_{33} = \frac{C_{33} t^3}{12}$$

Equation A.16 is the explicit form of the equation $\{\sigma\} = [D]\{\varepsilon\}$ applied to plate bending.

A.4 A Finite Element Analysis of Skew Plates in Bending

In this section, the general quadrilateral element is presented. The element is developed by Felippa and reported in Ref. 18. This element is employed in the reported investigation. The element has been tested under a variety of boundary conditions and the results compare favorably with the theory of elasticity solutions (Ref. 18).

The quadrilateral element is a conforming element formed from four triangular elements which satisfy deflection and slope continuity along the boundaries. Each one of the triangular elements is known as the LCCT-11 or the linear curvature compatible triangle with eleven fundamental degrees of freedom. The LCCT-11 is a simplified form of the triangular element LCCT-12 which has twelve degrees of freedom. The LCCT-11 is obtained from LCCT-12 by imposing the linear variation of the slope normal to one side of the triangle.

The element formulation is outlined in the following sections. Detailed derivations can be found in Refs. 17, 46 and 50.

A.4.1 Element Coordinate Systems

The geometry of a triangular element can be expressed by the projected dimensions in cartesian coordinate system (Fig. A10), by intrinsic dimensions (Fig. A11), or by dimensions in the natural coordinate system (Fig. A12).

In Fig. A12, A_1, A_2, A_3 are the three subtriangles subtended by point P such that

$$\zeta_i = \frac{A_i}{A} \tag{A.17}$$

where the index i = 1, 2, or 3 designates the number of the corner opposite to A_i and A is the total area of the complete triangle.

From Fig. A11, Eq. A.17 can also be written as

$$\zeta_i = \frac{n_i}{h_i} \tag{A.18}$$

where n_i is the normal distance of point P and h_i is the height of node i from side i. These relationships are used to simplify the expressions in the element stiffness formulations.

The relationship between cartesian and natural coordinates is expressed as follows (Ref. 33):

$$\begin{Bmatrix} 1 \\ x \\ y \end{Bmatrix} = \begin{bmatrix} 1 & 1 & 1 \\ x_1 & x_2 & x_3 \\ y_1 & y_2 & y_3 \end{bmatrix} \begin{Bmatrix} \zeta_1 \\ \zeta_2 \\ \zeta_3 \end{Bmatrix} \tag{A.19}$$

where x_i and y_i are the coordinates of the nodes i, i=1, 2, 3.

The inverse relationship can be obtained by solving for ζ_1, ζ_2, and ζ_3 from Eq. A.19:

$$\begin{Bmatrix} \zeta_1 \\ \zeta_2 \\ \zeta_3 \end{Bmatrix} = \frac{1}{2A} \begin{bmatrix} 2A_1 & b_1 & a_1 \\ 2A_2 & b_2 & a_2 \\ 2A_3 & b_3 & a_3 \end{bmatrix} \begin{Bmatrix} 1 \\ x \\ y \end{Bmatrix} \tag{A.20}$$

where a_i and b_i are the projected dimensions shown in Fig. A10.

The derivatives of a function $f(\zeta_1, \zeta_2, \zeta_3)$ with respect to the x, and y axes and a normal n_i can be obtained by the chain rule (Ref. 33):

$$\frac{\partial f}{\partial n_i} = \frac{1}{2A} \left(\frac{\partial f}{\partial \zeta_i} \ell_i + \frac{\partial f}{\partial \zeta_j} (d_i - \ell_i) - \frac{\partial f}{\partial \zeta_k} d_i \right) \tag{A.21}$$

$$\frac{\partial f}{\partial x} = \frac{1}{2A} \left(\frac{\partial f}{\partial \zeta_1} b_1 + \frac{\partial f}{\partial \zeta_2} b_2 + \frac{\partial f}{\partial \zeta_3} b_3 \right) \tag{A.22}$$

$$\frac{\partial f}{\partial y} = \frac{1}{2A} \left(\frac{\partial f}{\partial \zeta_1} a_1 + \frac{\partial f}{\partial \zeta_2} a_2 + \frac{\partial f}{\partial \zeta_3} a_3 \right) \tag{A.23}$$

where coordinates d_i and ℓ_i are shown in Fig. A11.

The above relationships are used in the formulation of the element displacement field and stiffness properties in Sections A.4.2 and A.4.3.

A.4.2 Construction of the Element Displacement Field

The twelve fundamental degrees of freedom for the LCCT-12 element at the external nodes of the triangular element are shown in Fig. A13. These can be expressed as components of the nodal displacement vector {r}:

$$\{r\}^T = \{w_1\ \theta_{x1}\ \theta_{y1}\ w_2\ \theta_{x2}\ \theta_{y2}\ w_3\ \theta_{x3}\ \theta_{y3}\ \theta_4\ \theta_5\ \theta_6\} \qquad (A.24)$$

where w_i, θ_{xi} and θ_{yi} are the transverse displacement, rotation about the x-axis, and rotation about the y-axis respectively of node i. θ_4, θ_5 and θ_6 are normal slopes at the midside nodes of the element boundaries.

As proposed by Felippa (Ref. 17) the element is subdivided into three subtriangles or subelements as shown in Fig. A13. Each subelement has three displacement components at each node and one rotation component at the midpoint of the outer side (Fig. A13). Point 0 is located at the centroid of the complete triangular element. Independent cubic displacement functions are then assumed for each subelement.

The nodal displacements for each triangle can be listed as follows:

$$\{r^{(1)}\}^T = \{w_2\ \theta_{x2}\ \theta_{y2}\ w_3\ \theta_{x3}\ \theta_{y3}\ w_0\ \theta_{x0}\ \theta_{y0}\ \theta_5\} \tag{A.25a}$$

$$\{r^{(2)}\}^T = \{w_3\ \theta_{x3}\ \theta_{y3}\ w_1\ \theta_{x1}\ \theta_{y1}\ w_0\ \theta_{x0}\ \theta_{y0}\ \theta_6\} \tag{A.25b}$$

$$\{r^{(3)}\}^T = \{w_1\ \theta_{x1}\ \theta_{y1}\ w_2\ \theta_{x2}\ \theta_{y2}\ w_0\ \theta_{x0}\ \theta_{y0}\ \theta_7\} \tag{A.25c}$$

Since each subelement has ten degrees of freedom a complete cubic polynomial expression can be used (Ref. 18). Thus for subelement i:

$$w^{(i)} = [\Phi^{(i)}]\ \{r^{(i)}\} \tag{A.26}$$

where $[\Phi^{(i)}]$ is the interpolating polynomial that relates displacements within the element to the nodal displacements by $\{v\} = [\Phi]\ \{v_i\}$. The explicit expression for $\Phi^{(i)}$ for i=1 has been derived and presented by Felippa in Ref. 18:

$$\Phi^{(1)T} = \begin{bmatrix}
\zeta_1^2\ (3 - 2\zeta_1) + 6\mu_3^{(1)}\ \zeta_1\zeta_2\zeta_3 \\
\zeta_1^2\ (b_3^{(1)}\zeta_2 - b_2^{(1)}\zeta_3) + (b_3^{(1)}\mu_3^{(1)} - b_1^{(1)})\ \zeta_1\zeta_2\zeta_3 \\
\zeta_1^2\ (a_3^{(1)}\zeta_2 - a_2^{(1)}\zeta_3) + (a_3^{(1)}\mu_3^{(1)} - a_1^{(1)})\ \zeta_1\zeta_2\zeta_3 \\
\zeta_2^2\ (3 - 2\zeta_2) + 6\lambda_3^{(1)}\ \zeta_1\zeta_2\zeta_3 \\
\zeta_2^2\ (b^{(1)}\zeta_3 - b_3^{(1)}\zeta_1) + (b_2^{(1)} - b_3^{(1)}\lambda_3^{(1)})\ \zeta_1\zeta_2\zeta_3 \\
\zeta_2^2\ (a_1^{(1)}\zeta_3 - a_3^{(1)}\zeta_1) + (a_2^{(1)} - a_3^{(1)}\lambda_3^{(1)})\ \zeta_1\zeta_2\zeta_3 \\
\zeta_3^2\ (3 - 2\zeta_3) \\
\zeta_3^2\ (b_2^{(1)}\zeta_1 - b_1^{(1)}\zeta_2) \\
\zeta_3^2\ (a_1^{(1)}\zeta_1 - a_1^{(1)}\zeta_2) \\
4h_3^{(1)}\ \zeta_1\zeta_2\zeta_3
\end{bmatrix} \tag{A.27}$$

where, $\lambda_i = \frac{d_i}{\ell_i}$

and, $\mu_i = 1 - \lambda_i$

The above interpolation function is a complete polynomial based on the choice of nodal system for n=3, i.e. cubic polynomial (Refs. 17,33).

The subscripts used in the above correspond to the renumbered node in Fig. A14; and therefore the function is the same for the other elements except for the superscript.

The vector of all the nodal displacements is expressed in the order given by Eq.A.25. The displacement w of the complete triangular element can then be expressed by:

$$\begin{Bmatrix} w^{(1)} \\ w^{(2)} \\ w^{(3)} \end{Bmatrix} = \begin{bmatrix} \Phi_e & \Phi_o \\ \Phi_e & \Phi_o \\ \Phi_e & \Phi_o \end{bmatrix} \begin{Bmatrix} r_e \\ r_o \end{Bmatrix} \qquad (A.28)$$

where the superscripts refer to the subelement number and

Φ_e refers to the interpolation polynomial associated with the displacements $\{r_e\}$ at the external nodes, and

Φ_o refers to the interpolation polynomial associated with the displacements $\{r_o\}$ at the internal node

Transverse displacement of two adjacent subelements are identical along the juncture line. However, along this line their normal slopes differ. To impose slope compatibility along the internal edges, additional nodes 7, 8 and 9 are located at midpoint of these edges (Fig. A15). The normal slopes are computed from Eq. A.21 and evaluated at nodes 7, 8 and 9. The resulting compatibility equations are then used to evaluate the displacements at the internal node $\{r_o\}$ in terms of the displacements at the external nodes $\{r_e\}$.

The final displacement field is then written only in terms of the external degrees of freedom:

$$\begin{Bmatrix} w^{(1)} \\ w^{(2)} \\ w^{(3)} \end{Bmatrix} = \begin{bmatrix} \hat{\Phi}^{(1)} \\ \hat{\Phi}^{(2)} \\ \hat{\Phi}^{(3)} \end{bmatrix} \{r\} \qquad (A.29)$$

The explicit expression for $\hat{\Phi}^{(i)}$ is given in Appendix A2 for ready reference.

A.4.3 Derivation of the Element Stiffness Matrix

The stiffness matrix for each subelement can be derived following the procedure outlined in Ref. 65 together with the displacement function given in Eq. A.28.

From Eq. A.16 $\{\varepsilon\}$ is defined to be:

$$\{\varepsilon\} = \begin{Bmatrix} \dfrac{\partial^2 w}{\partial y^2} \\ \dfrac{\partial^2 w}{\partial y^2} \\ -2\dfrac{\partial^2 w}{\partial x \partial y} \end{Bmatrix} \tag{A.30}$$

and is known as the curvature field.

For subelement i, the curvature field can be obtained by proper differentiation of the displacement function given by Eq. A.28, and the use of Eqs. A.22 and A.23

$$\{\varepsilon^{(i)}\} = \begin{bmatrix} \dfrac{\partial^2 \hat{\Phi}^{(i)}}{\partial x^2} \\ \dfrac{\partial^2 \hat{\Phi}^{(i)}}{\partial y^2} \\ -2\dfrac{\partial^2 \hat{\Phi}^{(i)}}{\partial x \partial y} \end{bmatrix} \{r\} = [T^{(i)}]\{r\} \tag{A.31}$$

The nodal values of the curvature can be obtained by evaluating Eq. A.30 at the nodes. Thus

$$\{\varepsilon_c^{(i)}\} = [\Phi_B^{(i)}]\{r\} \tag{A.32}$$

where $\{\varepsilon_c^{(i)}\}$ is the vector of nodal curvatures and $[\Phi_B^{(i)}]$ is the matrix $[T^{(i)}]$ evaluated at the node points of element i.

The linear curvature variation within the subelement can now be expressed in terms of the nodal curvatures by a linear interpolating function $[\Phi_\varepsilon]$ such that

$$\{\varepsilon^{(i)}\} = [\Phi_\varepsilon^{(i)}]\ \{\varepsilon_c^{(i)}\} \tag{A.33}$$

where

$$[\Phi_\varepsilon^{(i)}] = \begin{bmatrix} \zeta_1 & \zeta_2 & \zeta_3 & 0 & 0 & 0 & 0 & 0 & 0 \\ 0 & 0 & 0 & \zeta_1 & \zeta_2 & \zeta_3 & 0 & 0 & 0 \\ 0 & 0 & 0 & 0 & 0 & 0 & \zeta_1 & \zeta_2 & \zeta_3 \end{bmatrix}$$

With Eqs. A.16 and A.32, the stiffness matrix can be evaluated:

$$[k^{(i)}] = [\Phi_B^{(i)}]^T \int [\Phi_\varepsilon^{(i)}]^T\ [D]\ [\Phi_\varepsilon^{(i)}]\ dA\ [\Phi_B^{(i)}] \tag{A.34}$$

Since the stiffness matrix of a subelement is expressed in terms of the same set of nodal coordinates, the stiffness matrix of the complete triangular element is obtained by adding the contributions of the three subelements, thus,

$$[k] = [k^{(1)}] + [k^{(2)}] + [k^{(3)}] \tag{A.35}$$

Four of these triangular elements are assembled to form the quadrilateral. The midpoint nodes at the outermost side of the quadrilateral are however undesireable. These nodes require special programming procedures for identification in input and in the calculation of the global stiffness matrix. Moreover, these nodes increase the band

The first example is the square plate shown in Fig. A17. The dimensions of the plate are shown in Fig. A17a. Due to symmetry only a quarter of the plate is analyzed. The discretization schemes used for this problem are illustrated in Figs. A17b to A17f. The three cases considered for this problem are: (1) concentrated load at the center of the plate with completely fixed supports, (2) concentrated load at the center of the plate with simple supports, and (3) uniform load throughout the plate with simple supports. For all these cases Poisson's ratio is assumed to be equal to 0.3.

The error in percent of deflection at the center of the plate resulting from the analyses and those reported in literature are shown in Figs. A18 and A19 and Tables A6 and A7 for the first two cases. In these figures, the lines corresponding to elements developed by Wegmuller-Kostem (WK), Adini, Clough and Melosh (ACM), Melosh (M), and Pappenfuss (P) are taken from Ref. 58. The bending moments M_x and M_y for the third case are shown in Fig. A20. Shown also in this figure are the theoretical moments from Ref. 55. The above example shows the good convergence of the displacements and moments.

The second problem is a skew plate with uniform load and simply supported on all sides. The plate is ideally a rhombic plate, all sides of which are equal, and whose skew angle is varied (Fig. A21, inset). The plate is discretized into 64 equal skew elements. Rotation about the skew supports is allowed except at the corners which are completely fixed. The reduction in the deflection at the center of a skew plate due to the increase of skew is depicted in Fig. A21. The change

width of the assembled equations. In order to avoid this difficulty, without violating compatibility requirements, the midside node can be eliminated by imposing the normal slope to vary linearly along the side (Ref. 18). For example θ_4 in Fig. A13 can be expressed as the average of the corresponding slope at nodes 1 and 2. Since θ_4 is expressed now in terms of θ_x and θ_y at nodes 1 and 2, Eq. A.28 is reduced to eleven components. The resulting element is the LCCT-11.

The partially constrained elements are assembled to a quadrilateral element such that there are no midside nodes at the exterior edges (Fig. A15). The resulting general quadrilateral has nineteen degrees of freedom and more commonly known as Q-19. The seven internal degrees of freedom are eliminated by a static condensation procedure as discussed in Refs. 17 and 18. Thus the final quadrilateral is fully compatible, with linear variation of normal slopes at the edges. The element has twelve degrees of freedom: one translation and two rotations at each of the corner nodes.

A.4.4 Numerical Examples and Comparisons

Several example problems are presented to illustrate the application of the quadrilateral element to plate bending problems. Different discretization schemes are used in some of the problems to compare the accuracy and convergence of the solution with tests and other reported solutions. The different cases studied for each problem are depicted in Fig. A16.

in the principal moments M_1 as the skew angle is varied is shown in Fig. A22. For comparison, the finite difference and series solutions from Ref. 37 are also shown. The large decrease in deflection and in moment especially at skew angles beyond 60° can be observed.

The third example is a 45° skew plate which is simply supported on two sides. The plate is subjected to a concentrated load P at the center. Plate dimensions, material properties and the discretization for this problem are illustrated in Fig. A23. The theoretical results for the deflection and principal moments using finite difference, finite element and experimental values are listed in Table A8. The finite element results are comparable with the numerical values of the experiment. In most cases, the finite element results are between the experimental and the finite difference solution employing the finer mesh.

The fourth example is a skew slab model made of gypsum plaster. Two cases are studied: one with uniform load throughout the slab model and another with a concentrated load at the center. The test results are reported by Rusch in Ref. 48. The slab model is shown in Fig. A24 with the properties and dimensions indicated. Points A, B, and E are specifically selected for comparison of moments. Point A is at midspan and near the edge, point B is at the center of the slab and point E near the obtuse corner of the support (Fig. A24). Three discretizations have been tried as shown in Figs. A24 and A25. Different discretizations are used so that finer discretization could be employed near the points of interest. Table A9 shows the comparison of moments at points A, B, and E between the model test and the finite element

solutions for a uniform load of 100 psi. Table A10 lists the results for a concentrated unit load at the center of the plate. The values of the moments at points A and B are quite comparable with the experimental values. However, at point E, large discrepancies are observed. The third discretization gave only slightly improved results for point E. It is important to note here that computed values near the obtuse angle corners are questionable since they are near a region of high moment gradient.

The final example is a skew plate supported on two sides with varying angle of skew but with constant width to span ratio. The deflections and moments at the center of the plate using the finite difference solution and the finite element procedure are shown in Figs. A26 and A27. Good correlation is observed between finite difference and finite element except at the 60° skew where the available value of the width to span ratio is 0.52 instead of 0.50. A sharp decrease in the principal moment is observed for the skews beyond 60° and a much sharper decrease in deflection is obtained beyond 75°.

A.5 Summary

The analysis of skew plates under in-plane and lateral forces have been presented in this Appendix. The development of the analysis technique with the use of the finite element method of analysis was illustrated for the in-plane and the plate bending elements. Numerical examples were shown to demonstrate the application of the method of analysis to skew in-plane and plate bending problems subjected to uniform and concentrated in-plane and lateral forces.

TABLE A1

IN-PLANE DISPLACEMENTS AND STRESSES IN
A SQUARE PLATE UNDER UNIFORM EDGE LOADING (Fig. A5a)

Node	Quantity[1]	Q8D11	CST[2] (Ref. 52)	Exact
5	u	1.66667	1.66667	1.66667
	v	0.	0.	0.
	σ_x	1.0	0.99995	1.0
	σ_y	0.	0.00149	0.
	τ_{xy}	0.	0.00161	0.
9	u	3.33333	3.33333	3.33333
	v	0.25	0.25	0.25
	σ_x	1.0	0.99368	1.0
	σ_y	0.	0.00065	0.
	τ_{xy}	0.	0.00015	0.

[1] u, v displacements in inches, σ_x, σ_y, τ_{xy} stresses in ksi.

[2] .1% solution accuracy specified.

TABLE A2

IN-PLANE DISPLACEMENTS AND STRESSES IN
A SQUARE PLATE UNDER IN-PLANE SHEAR (Fig. A5b)

Quantity[1]	Q8D11	CST[2] (Ref. 52)	Exact
σ_x	0.	0.00083	0.
σ_y	0.	0.00093	0.
τ_{xy}	0.13333	0.13284	0.13333
σ_{11}, σ_{22}, σ_{12}	0.13333	0.13196	0.13333
γ_{xy}	0.1022×10^{-3}	0.1138×10^{-3}	0.1023×10^{-3}

[1] stresses in ksi.

[2] .1% solution accuracy specified.

TABLE A3

DISPLACEMENTS AND STRESSES IN A SKEW PLATE
UNDER UNIFORM EDGE LOADING (Fig. A6)

u - Displacements(in.)			v - Displacements(in.)		
Node	Q8D11	CST	Node	Q8D11	CST
1	0.	0.	1	-0.000306	-0.000308
2	0.	0.	2	0.	0.
3	0.	0.	3	0.000306	0.000301
4	0.001667	0.001657	4	0.000657	0.000647
5	0.0001667	0.001658	5	0.000962	0.000960
6	0.001667	0.001694	6	0.001268	0.001241
7	0.003333	0.003314	7	0.001619	0.001605
8	0.003333	0.003339	8	0.001924	0.001889
9	0.003333	0.003371	9	0.002230	0.002163

σ_x Stresses(ksi)			σ_y Stresses(ksi)		
Node	Q8D11	CST	Node	Q8D11	CST
1	1.0	0.995	1	0.	0.
2	1.0	0.995	2	0.	0.
3	1.0	1.005	3	0.	0.
4	1.0	0.995	4	0.	0.
5	1.0	1.002	5	0.	0.
6	1.0	1.011	6	0.	0.
7	1.0	1.002	7	0.	0.
8	1.0	1.008	8	0.	0.
9	1.0	1.007	9	0.	0.

TABLE A4

MIDSPAN DISPLACEMENT OF A SKEW PLATE
UNDER IN-PLANE CONCENTRATED LOAD (Fig. A7)

Finite Element Analysis	Displacement x 10^{-4} ft.
Q8D8[1]	11.40
CST[2]	19.58
Q8D11(3)	30.44
Q8D11(2)	51.49
LSE[1]	54.51

[1]Refs. 59, 60
[2]Ref. 52

TABLE A5

NORMAL STRESS AND DEFLECTION IN A
SIMPLY-SUPPORTED BEAM WITH INCLINED FACES (Fig. A8)

	Vertical Displacement at A x P/Et			Normal Stress at B x P/dt		
Mesh	Q8D8[1]	Q8D11	Ref. 53	Q8D8	Q8D11	Ref. 53
5 x 2	9.44	14.34	15.21	1.55	1.73	2.54
5 x 4	10.09	13.58	17.27	1.67	2.52	2.96

[1]From Ref. 53

TABLE A6

CENTER DEFLECTION OF A SQUARE PLATE WITH FIXED SUPPORTS

Multiplier PL^2/D

Source	2 x 2	4 x 4	8 x 8	10 x 10	16 x 16
ACM	.00592	.00613	.00580	--	.00568
Q19	.00521	.00515	.00546	.00551	--
EXACT	(Ref. 55)		.00560		

TABLE A7

CENTER DEFLECTION OF A SQUARE PLATE WITH SIMPLE SUPPORTS

Multiplier PL^2/D

Source	2 x 2	4 x 4	8 x 8	10 x 10	16 x 16
ACM	0.01378	0.01233	0.01133	--	0.01167
Q19	0.00975	0.01106	0.01145	0.01150	0.01159
EXACT	(Ref. 55)		0.01160		

TABLE A8

RHOMBIC PLATE UNDER CONCENTRATED LOAD
TWO SIDES SIMPLY SUPPORTED, $\varphi = 45^{o}$ (Fig. A23)

Method		w $\times Pa^2/D$	$M_{max.}$ $\times P$	$M_{min.}$ $\times P$
Finite Difference[1]	4 x 8	0.0117	0.331	0.199
Finite Difference[1]	6 x 8	0.0117	0.370	0.257
Experiment[1]		0.0099	0.354	0.254
Finite Element	8 x 8	0.0107	0.363	0.253

[1] Ref. 37

$$D = \frac{Et^3}{12(1-\nu^2)}$$

TABLE A9

MOMENTS IN A SKEW PLATE UNDER UNIFORM LOAD

Pt	Moment	Multiplier x 10^5			
			Discretization		
		Ref. 48	(1)	(2)	(3)
A	M_u [1]	0.906	0.897	0.896	
	M_{uv} [1]	0.270	0.285	0.286	
	M_I	0.980	0.975	0.981	
	M_{II}	0.068	0.058	0.056	
B	M_x	0.976	0.964	0.965	0.968
	M_y	0.019	0.010	0.010	0.012
	M_{xy}	0.188	0.205	0.207	0.206
	M_I	1.01	1.01	1.01	1.01
	M_{II}	0.027	0.032	0.032	0.030
E	M_x	0.210	0.487*	0.368	0.309
	M_y	-0.213	-0.160*	-0.245	-0.202
	M_{xy}	0.131	0.336*	0.195	0.248
	M_I	0.238	0.631*	0.425	0.410
	M_{II}	-0.238	-0.303*	-0.302	-0.302

*At center of plate element.

[1] M_u, M_{uv} are in the direction of the skew.

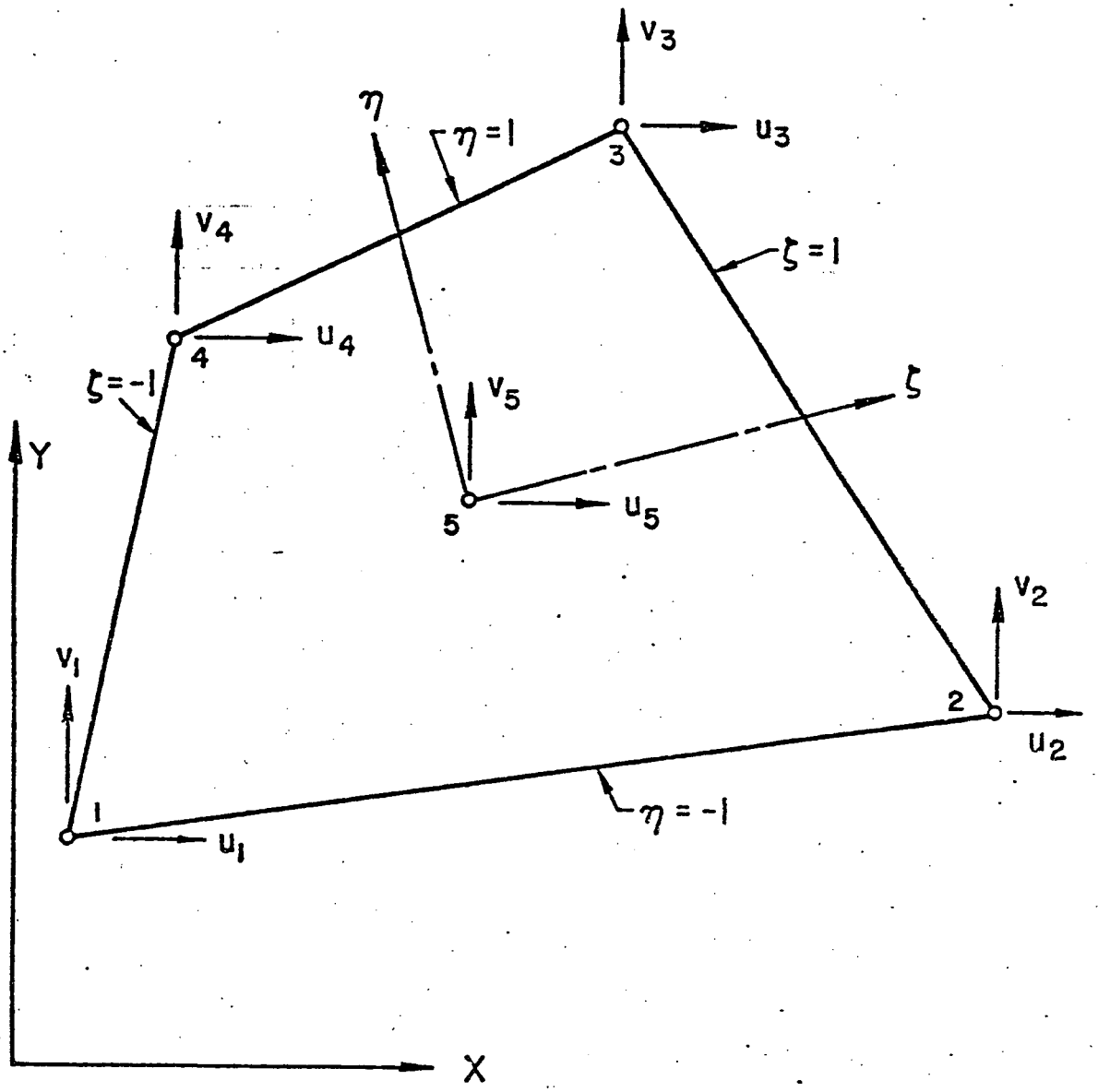

Fig. A3 A General Quadrilateral In-Plane Element, Coordinate System and Associated Degrees of Freedom

TABLE A10

MOMENTS IN A SKEW PLATE UNDER CONCENTRATED LOAD

Pt	Moment $\frac{(in\text{-}lb)}{in}$	Multiplier x 10^5			
			Discretization		
		Ref. 48	(1)	(2)	(3)
A	M_u [1]	0.453	0.461	0.457	
	M_{uv} [1]	0.134	0.125	0.125	
B	M_x	0.684	0.667	0.658	0.643
	M_y	0.262	0.240	0.231	0.221
	M_{xy}	0.122	0.106	0.108	0.104
E	M_x	0.068	0.143	0.122	0.104
	M_y	0.100	0.082	0.117	0.094
	M_{xy}	0.068	0.115	0.113	0.130

[1] M_u, M_{uv} are in the direction of the skew.

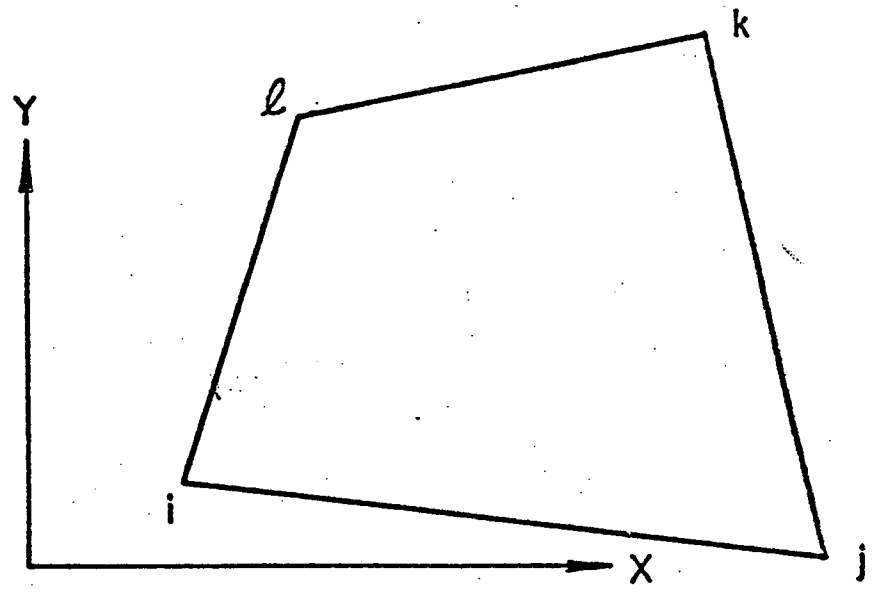

(a) Quadrilateral Plate Element

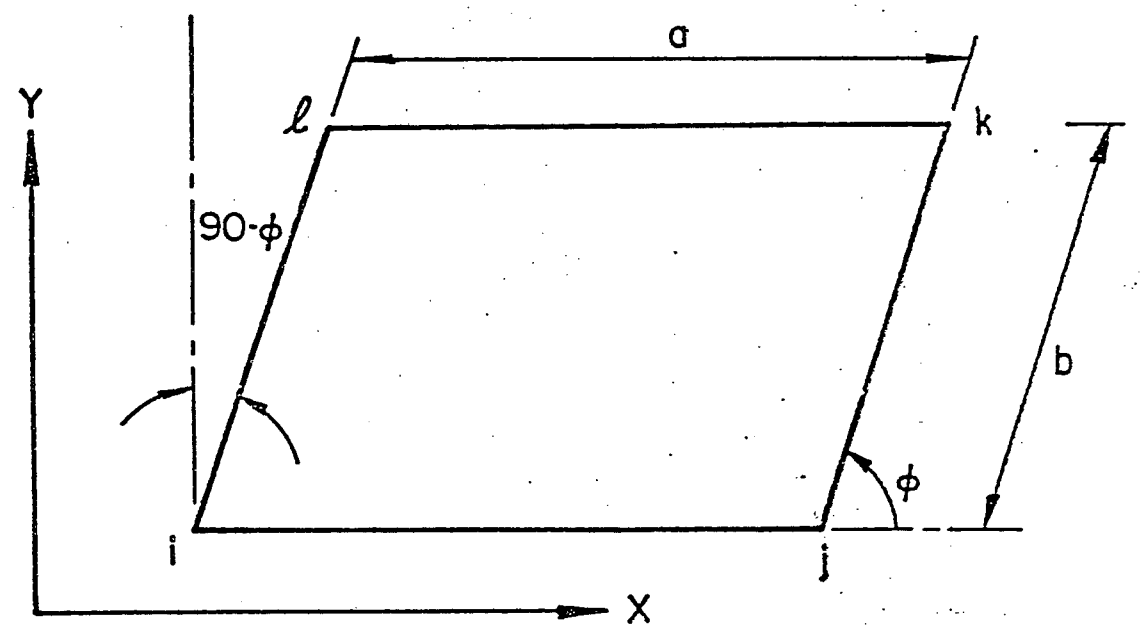

(b) Skew Plate Element

Fig. A1 Plate Finite Elements

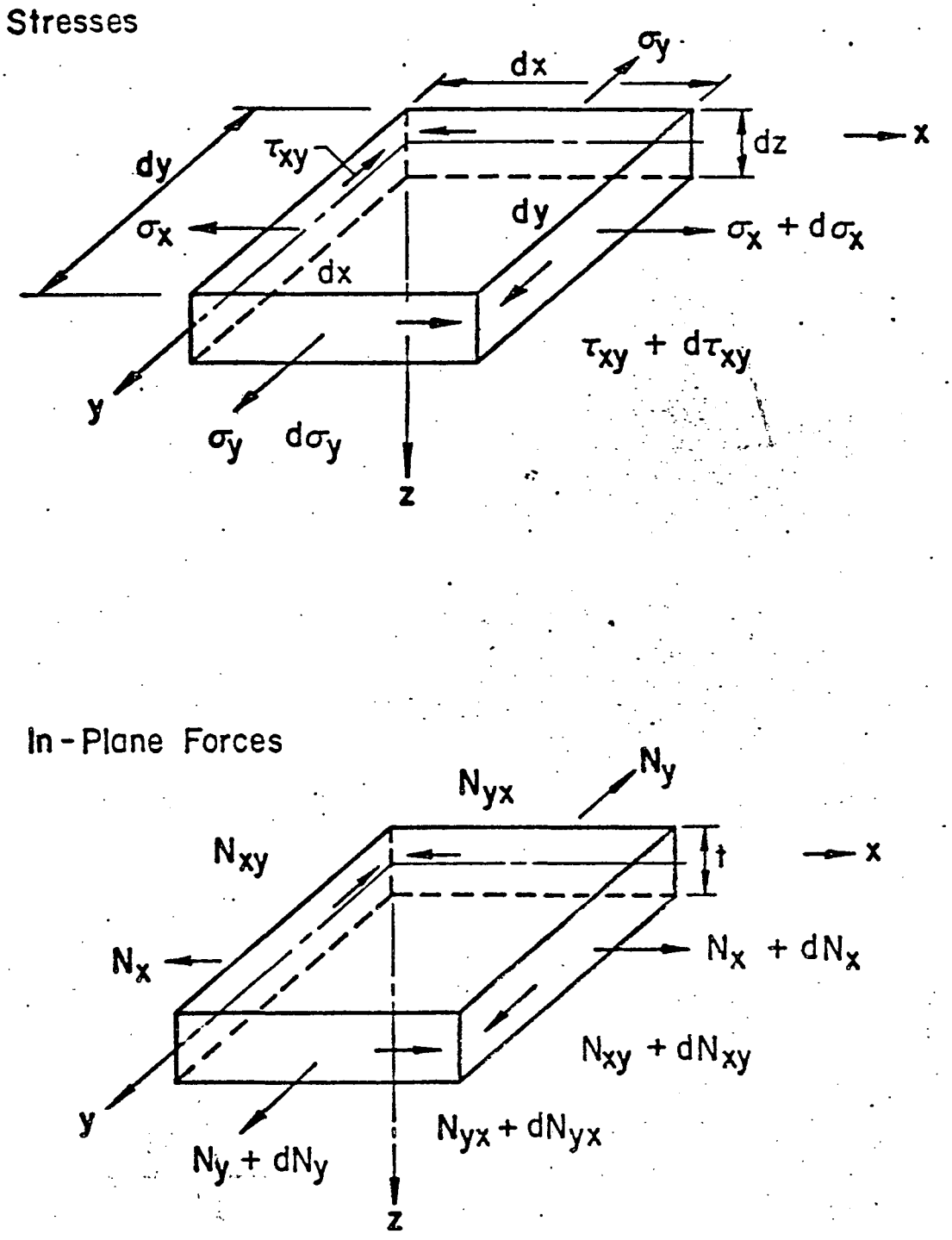

Fig. A2 In-Plane Stresses and Forces

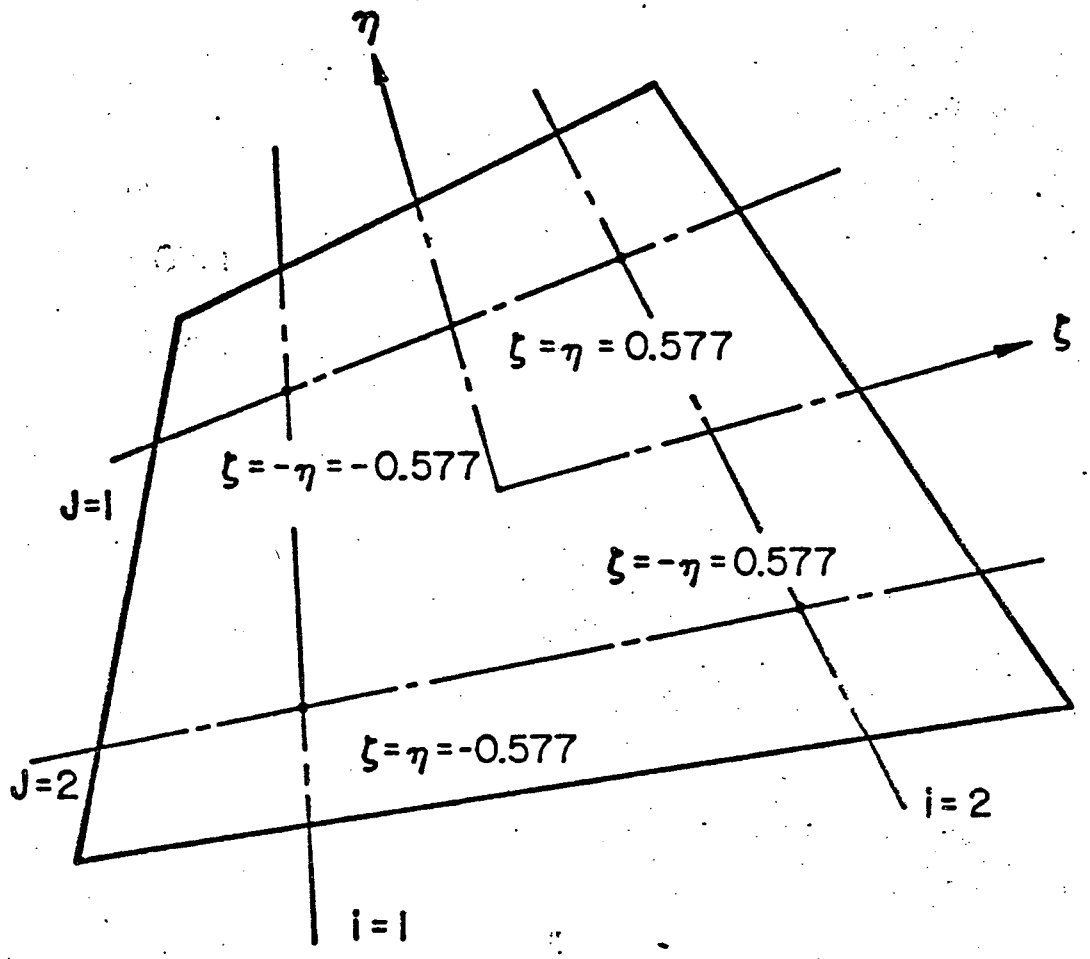

Fig. A4 2 x 2 Gaussian Quadrature for the Numerical Integration of the Quadrilateral Finite Element

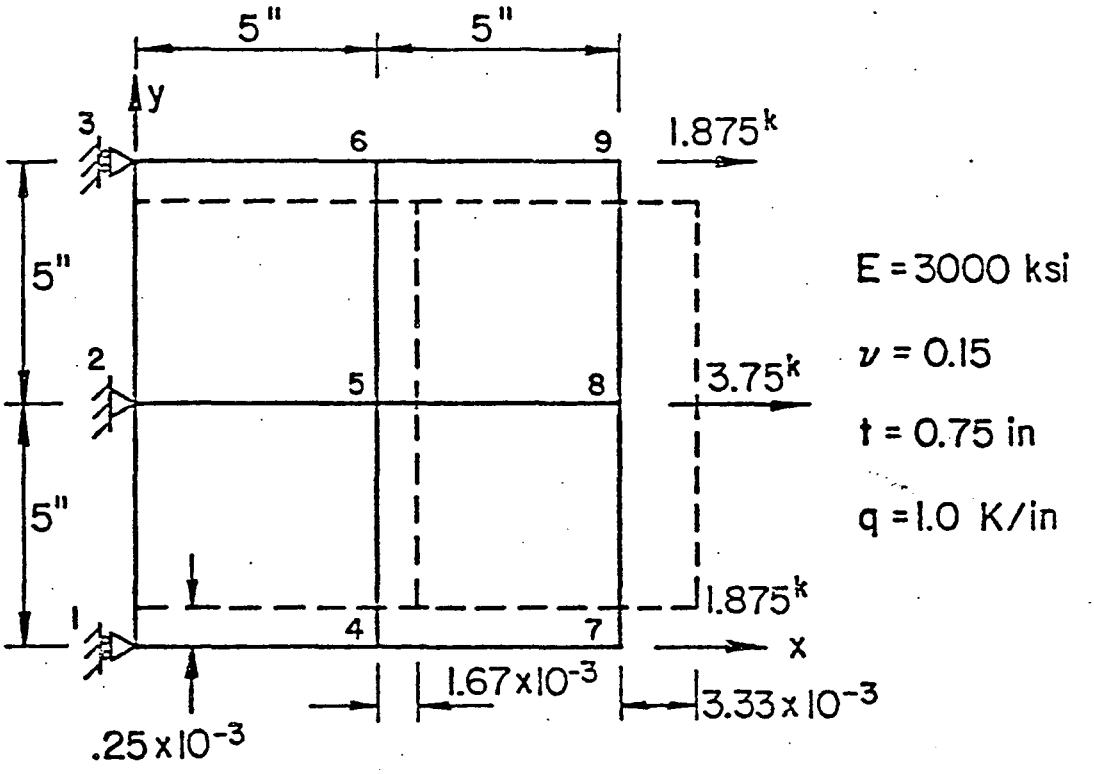

a. Normal Loads

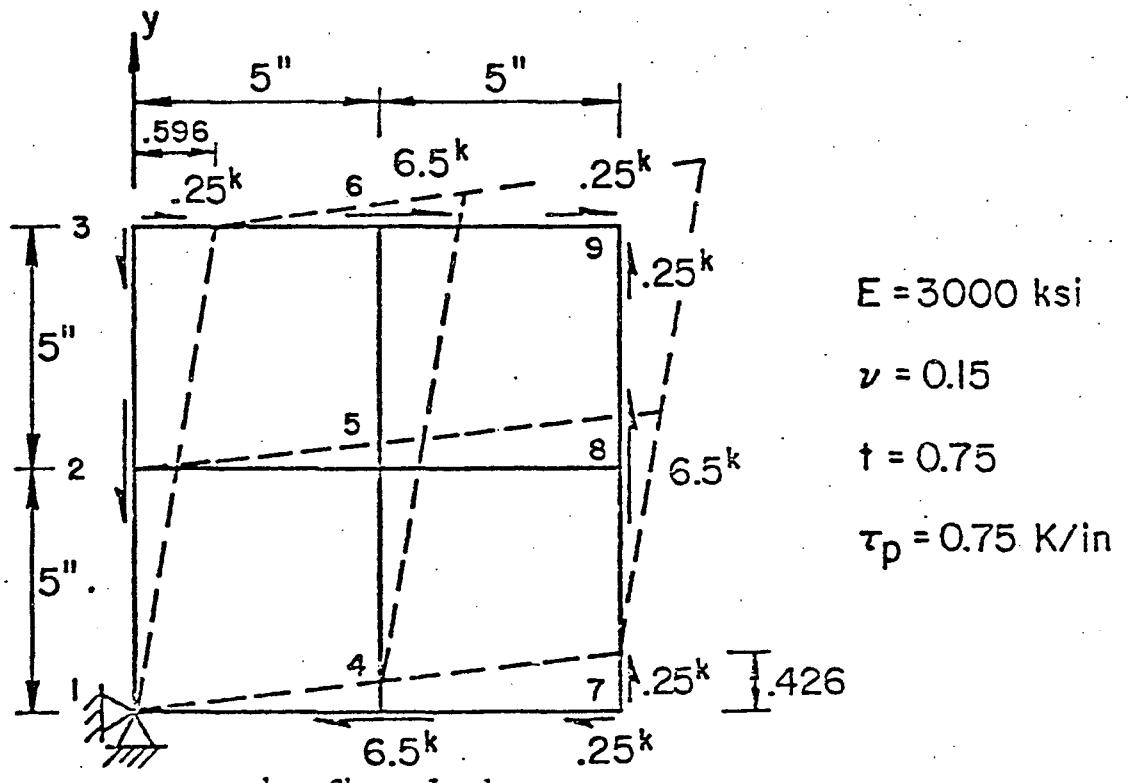

b. Shear Loads

Fig. A5 Rectangular Plate Under Uniform In-Plane Edge Loadings

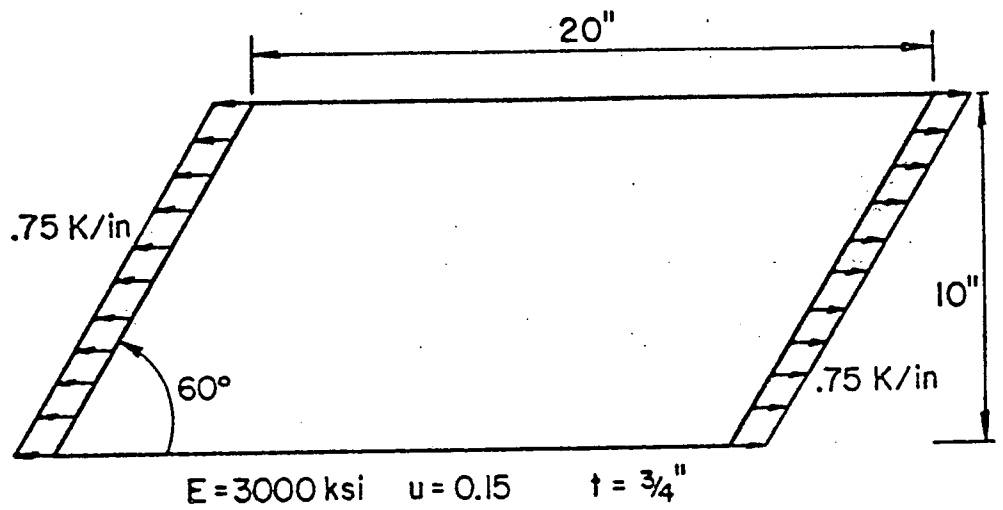

a. Plate Dimension and Properties

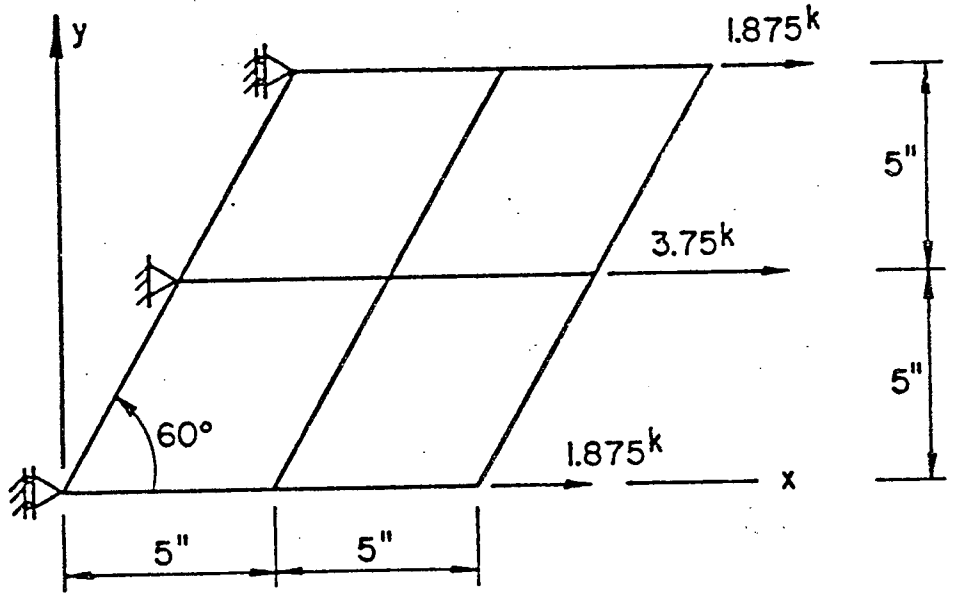

b. Idealization and Modeling

Fig. A6 Skew Plate under Uniform In-Plane Edge Loading

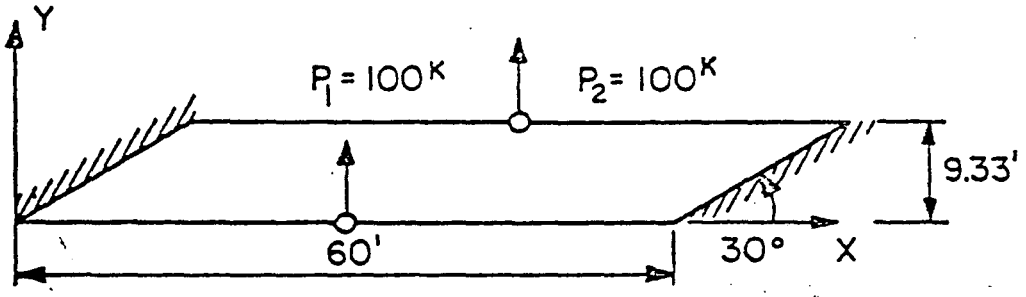

E = 432,000 KSF
ν = .15
t = 1.0

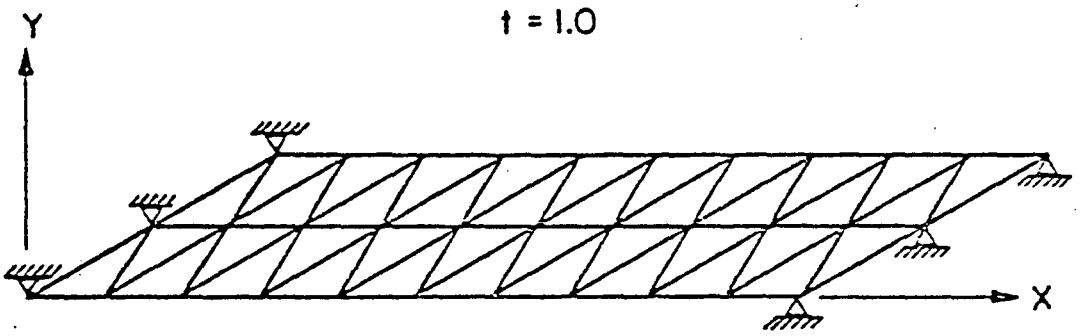

Discretization To Triangular Elements
(CST)

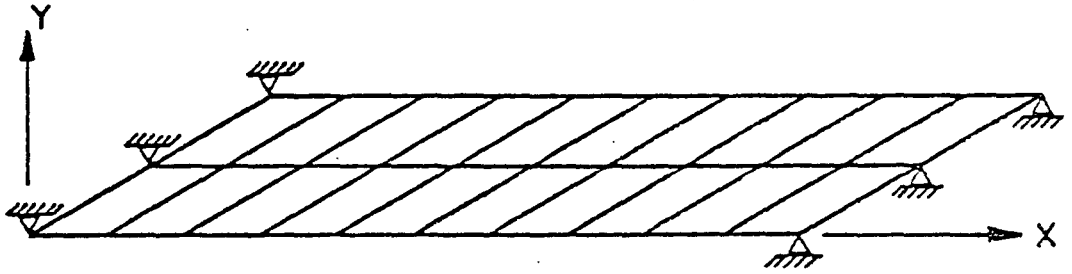

Discretization To Parallelogram Elements
(Q8D11)

Fig. A7 Skew Plate Under In-Plane Concentrated Loads

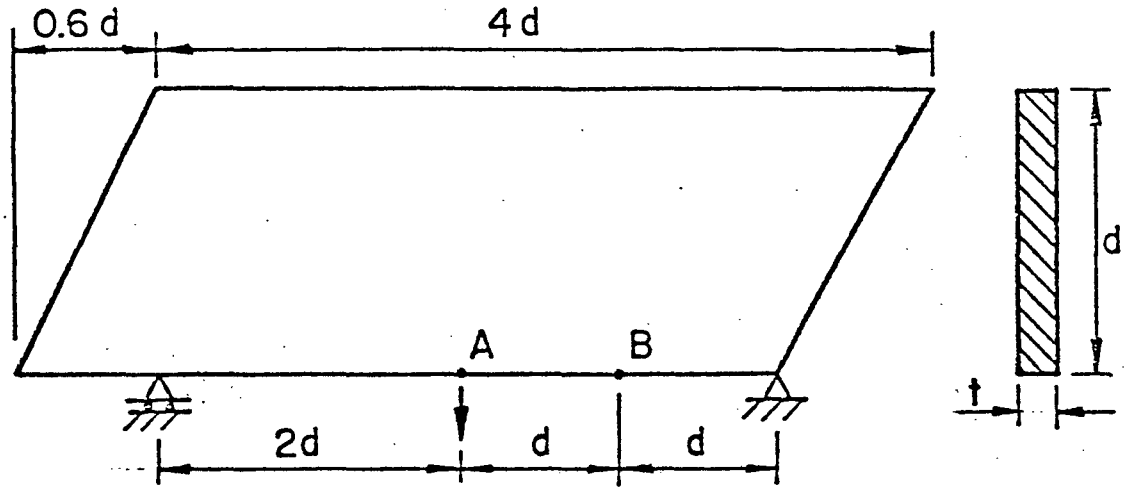

a. Structure and Loading

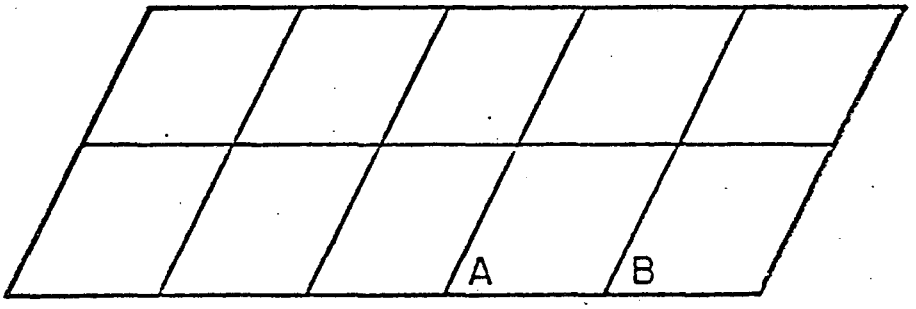

b. 2 x 5 Discretization

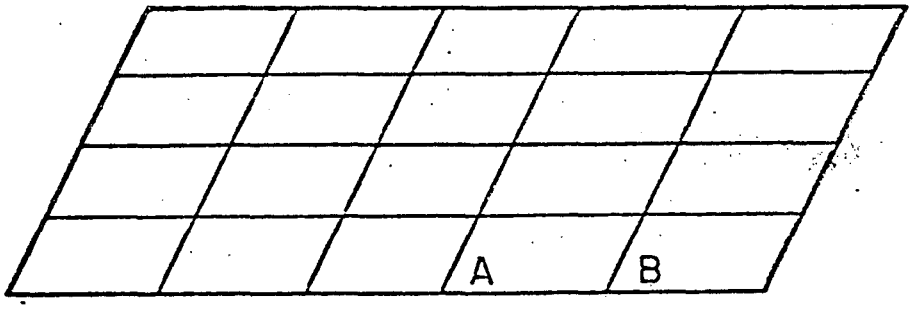

c. 4 x 5 Discretization

Fig. A8 Simply Supported Beam with Inclined Faces

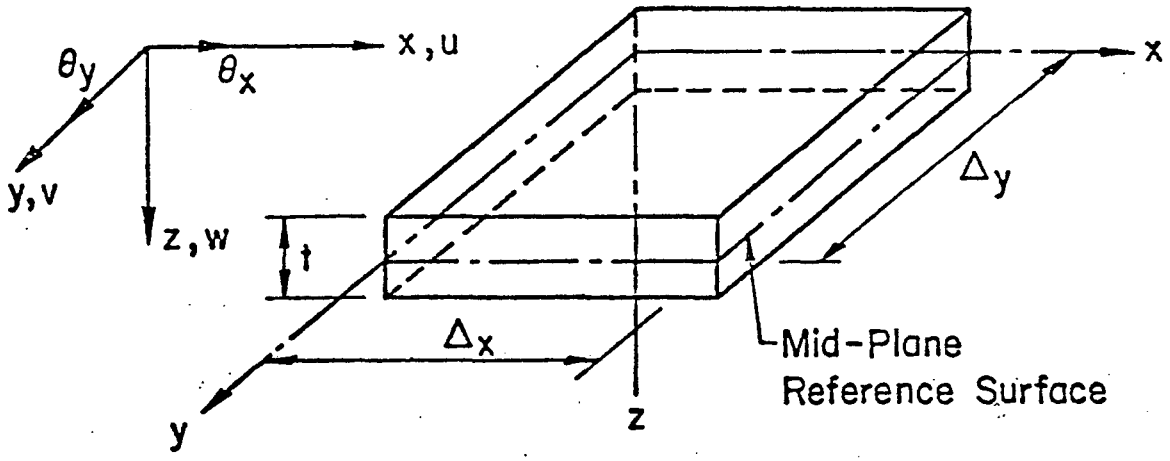

a. Displacements

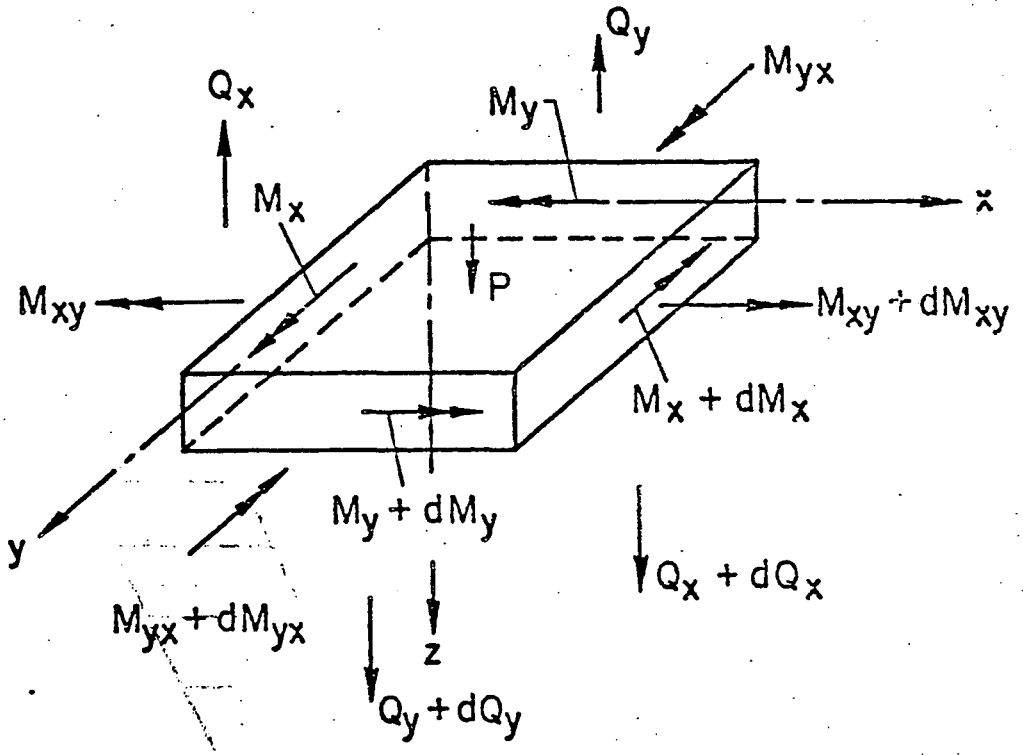

b. Stress Resultants

Fig. A9 Plate Bending Stresses and Displacements

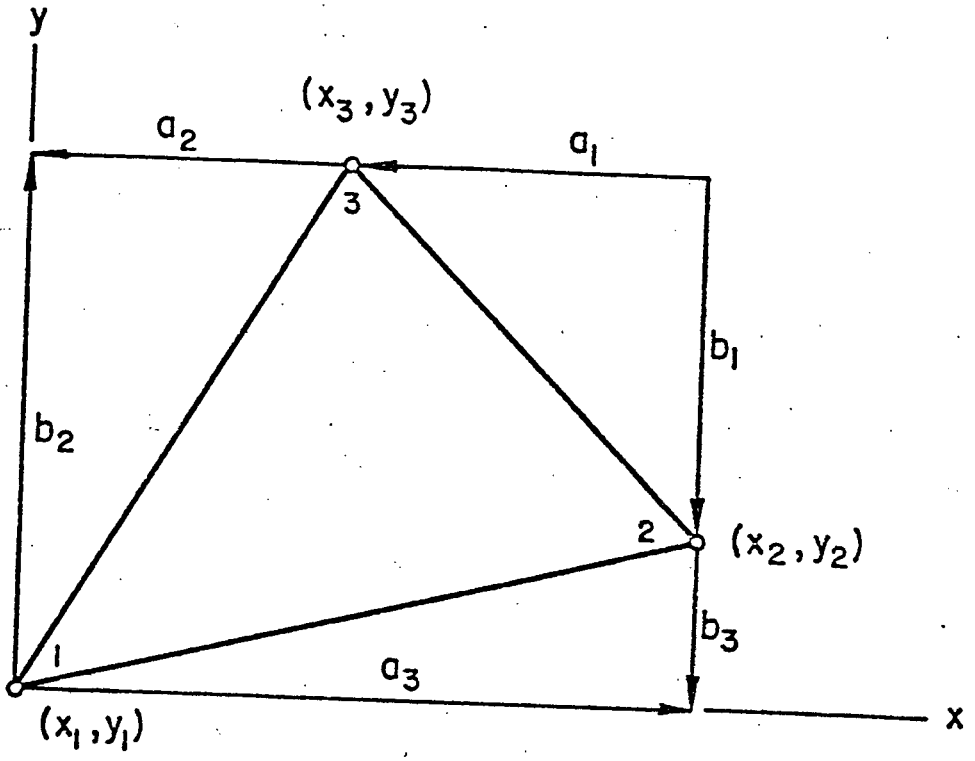

Fig. A10 Projected Dimensions

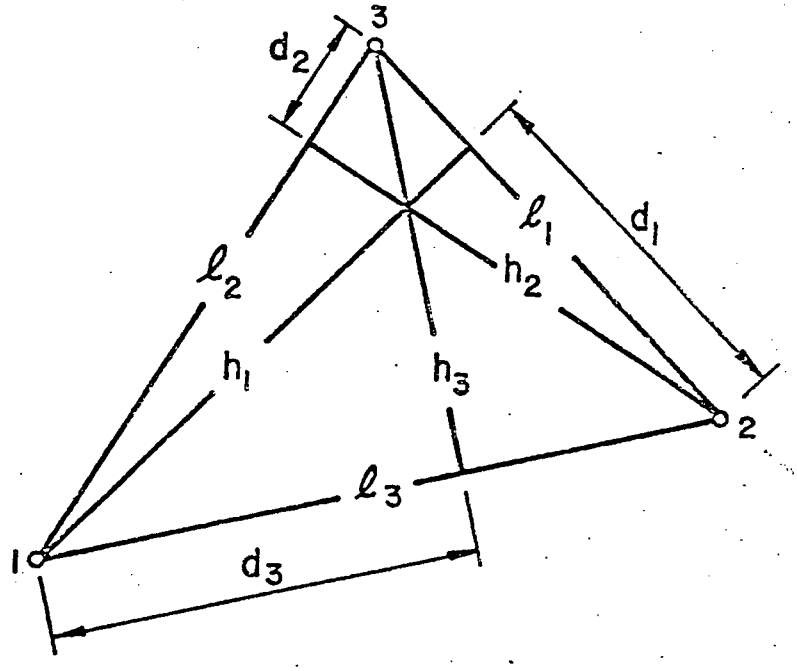

Fig. A11 Intrinsic Dimensions

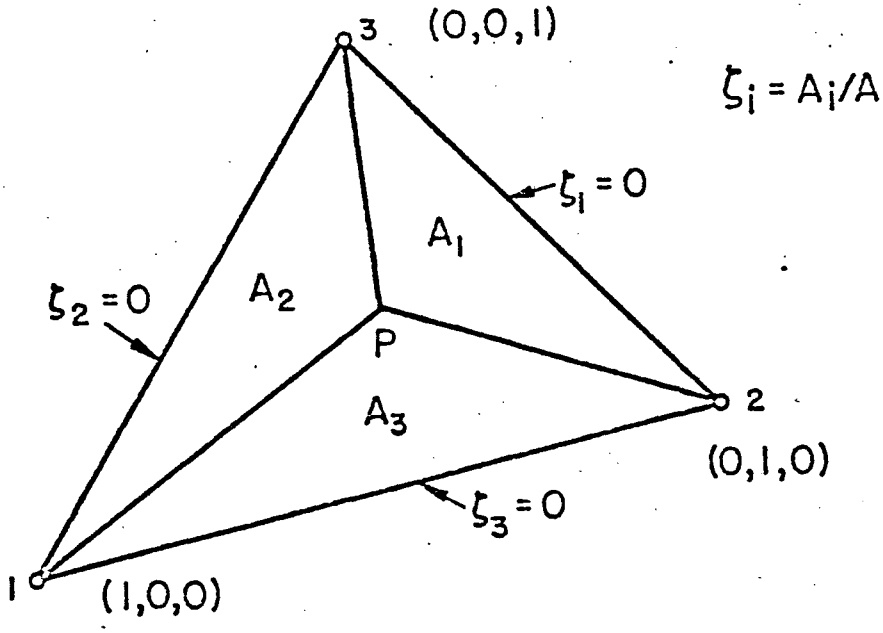

Fig. A12 Natural Coordinate System

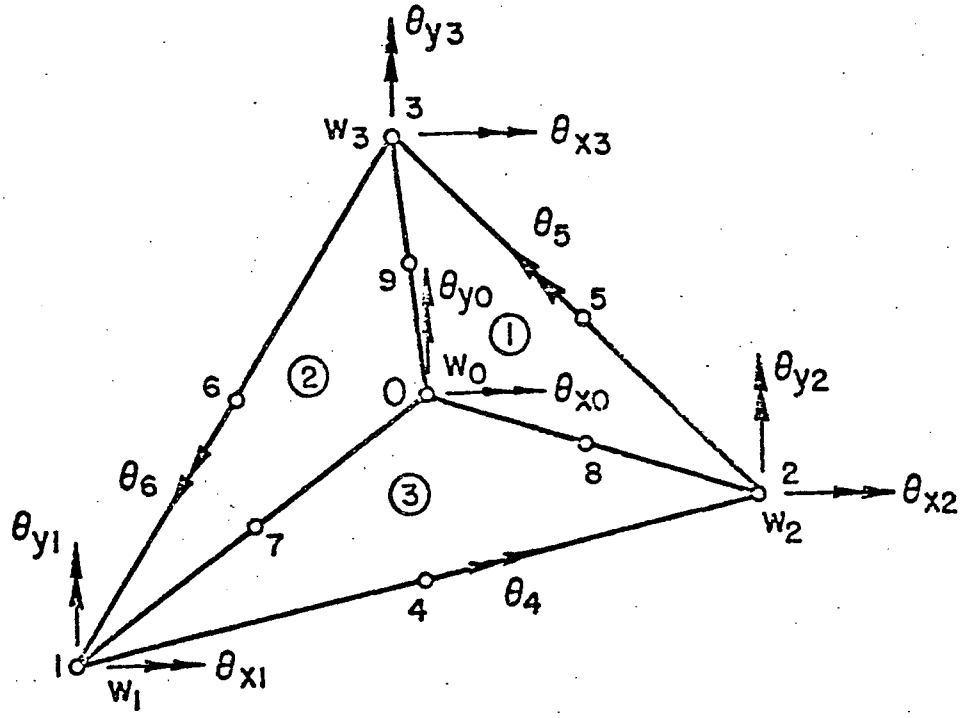

Fig. A13 Nodal Degrees of Freedom

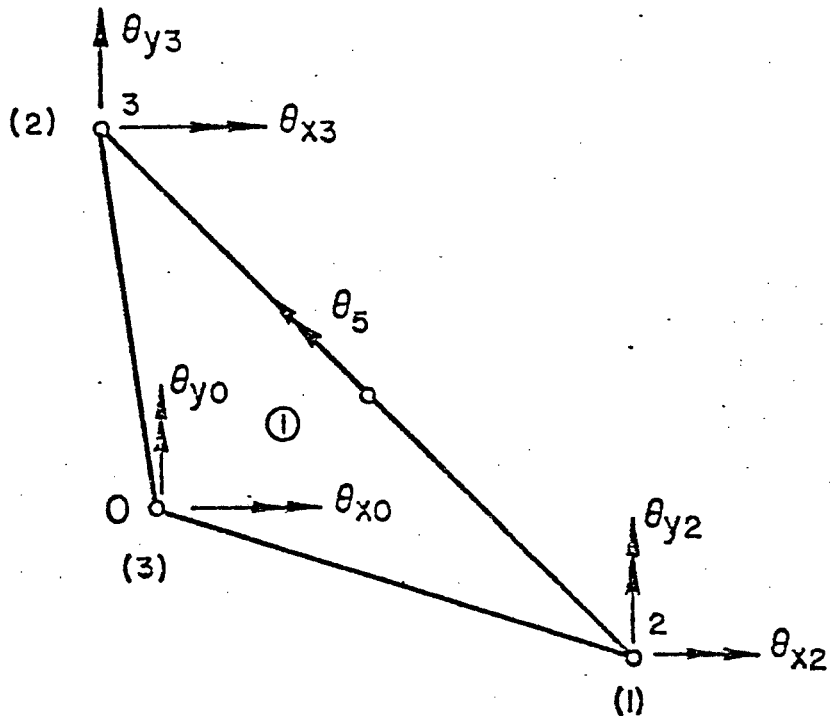

Fig. A14 Subelement Displacement Components

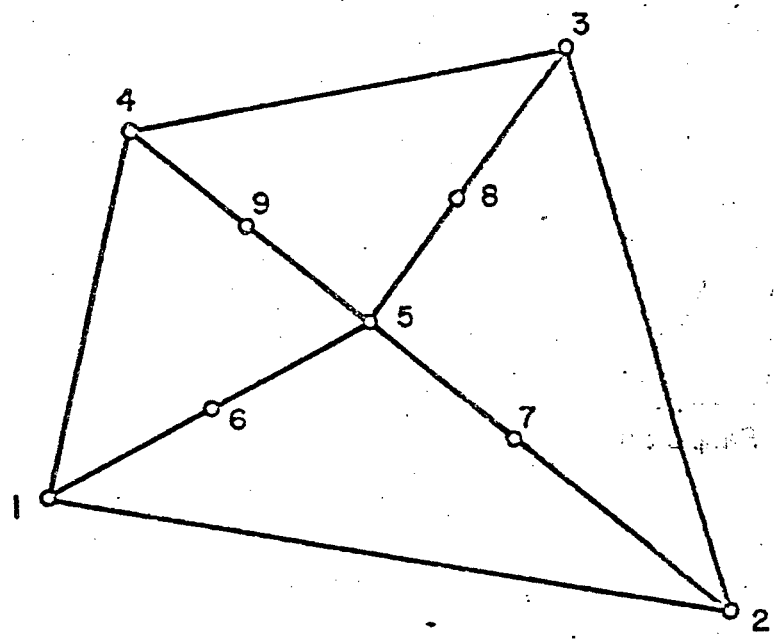

Fig. A15 Assembled Triangular Elements

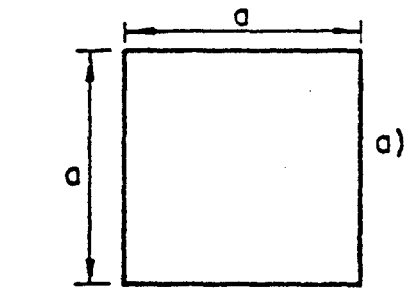

Support On All Sides

Case 1
Concentrated load at center
Fixed supports

Case 2
Concentrated load at ceter
Simply supported

Case 3
Uniform load, simply supported

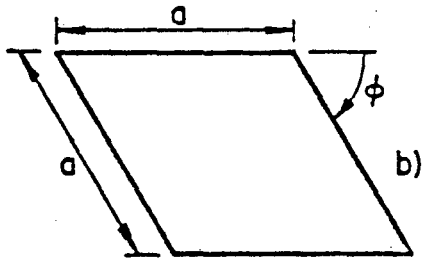

Support On 4 Sides

Uniform load
Skew angle ϕ varied

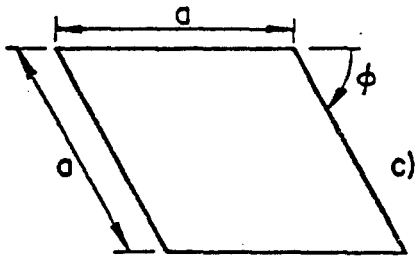

Simple Supports On 2 Sides

Case 1
Uniform load
Skew angle ϕ varied

Case 2
Concentrated load at center
$\phi = 45°$

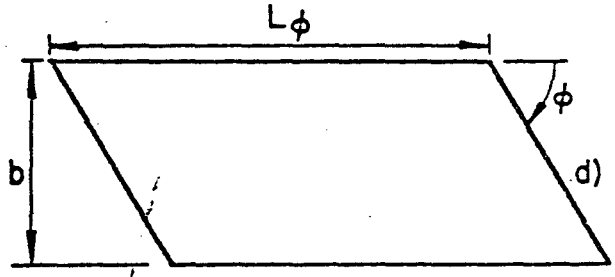

Simple Supports 2 Sides

Case 1
Uniform load
$\phi = 30°, b/L_\phi = 0.40$

Case 2
Concentrated load
$\phi = 30°, b/L\phi = 0.40$

Case 3
Uniform load
$b/L_\phi = 0.5, \phi$ varied

Fig. A16 Numerical Examples and Comparisons for Plate Loading

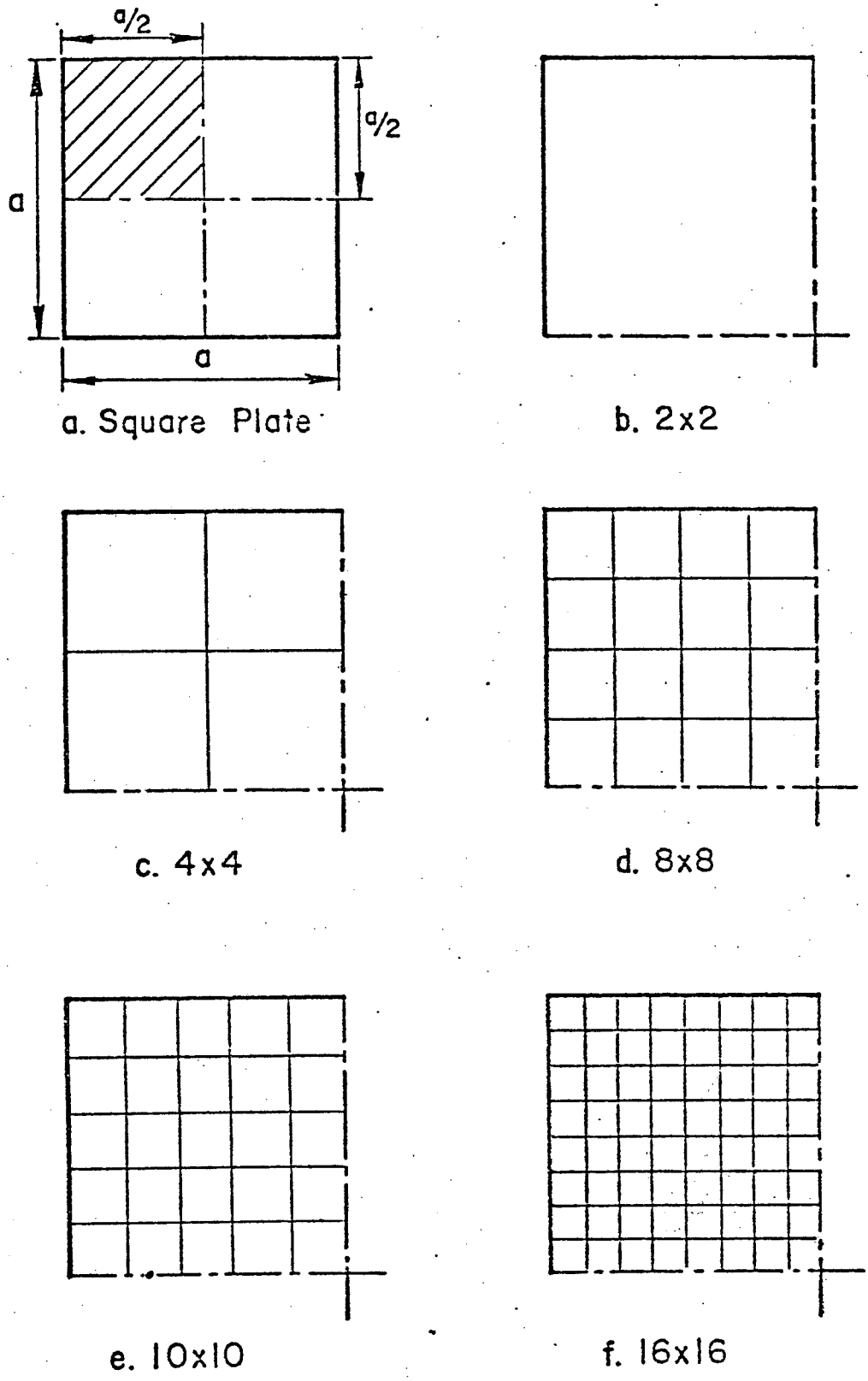

Fig. A17 Fully Supported Square Plate and Discretizations

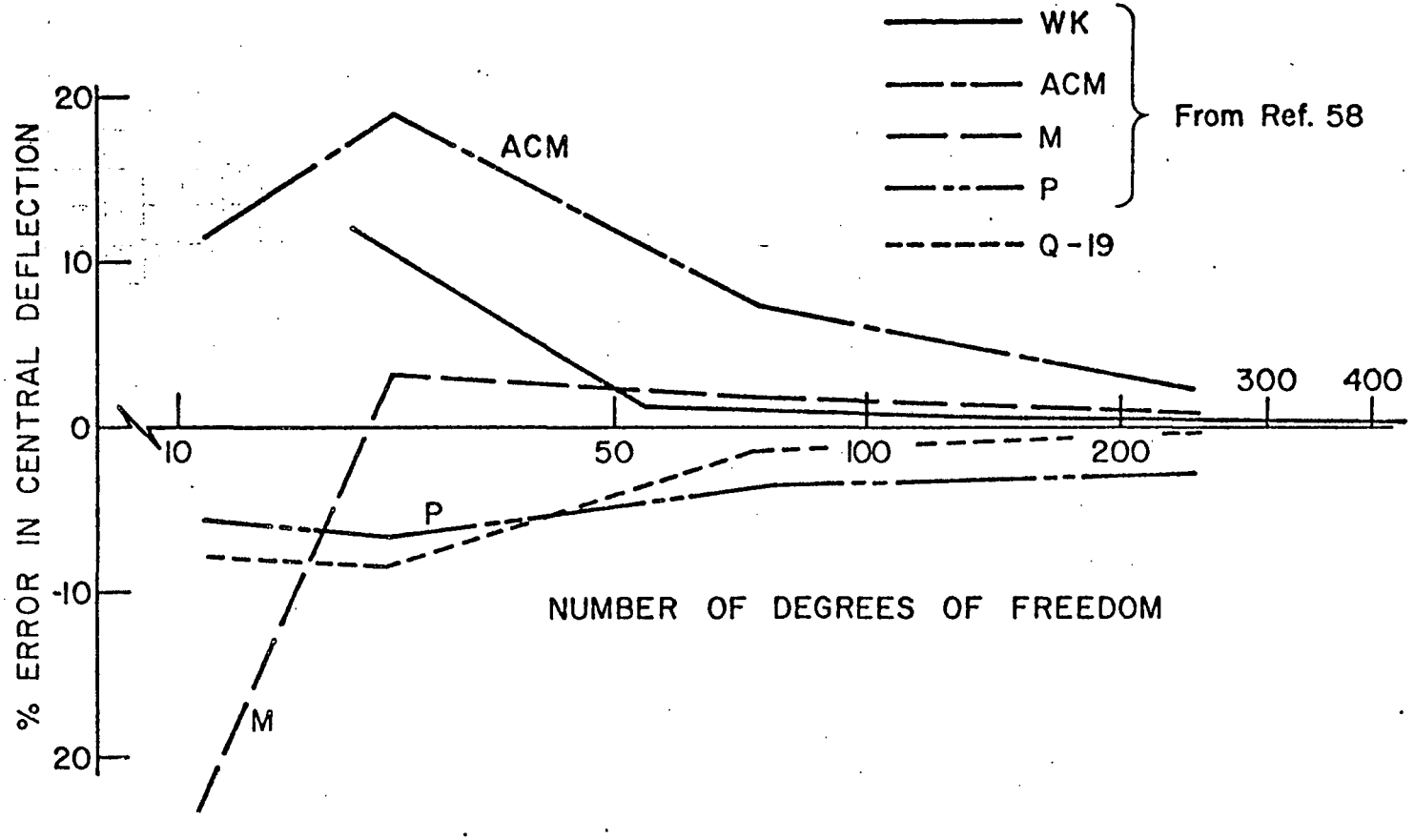

Fig. A18 Percent Error in Central Deflection Versus Number of Degrees of Freedom - Fixed Supports with Concentrated Load at Center

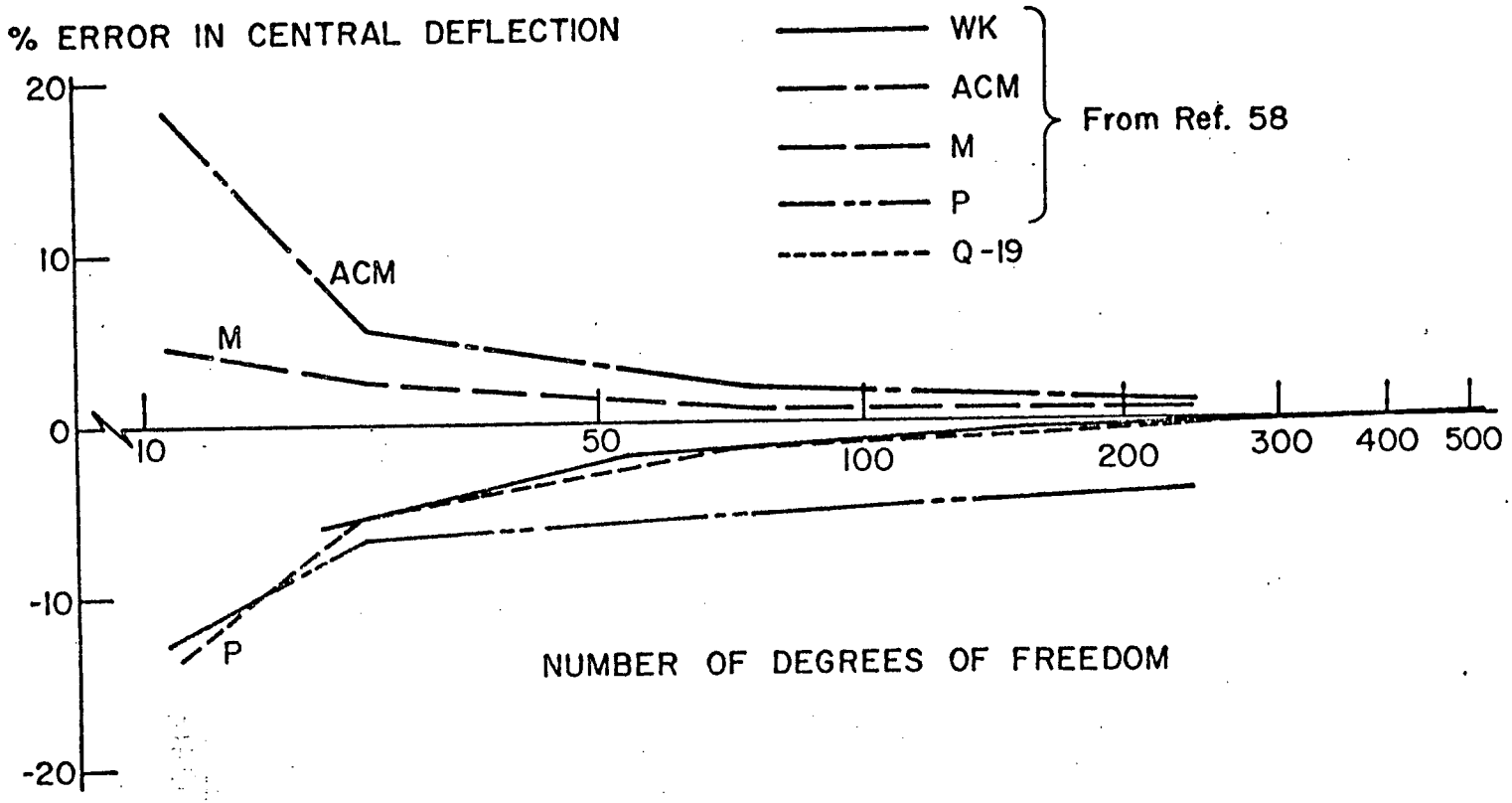

Fig. A19 Percent Error in Central Deflection Versus Number of Degrees of Freedom - Simple Supports with Concentrated Load at Center.

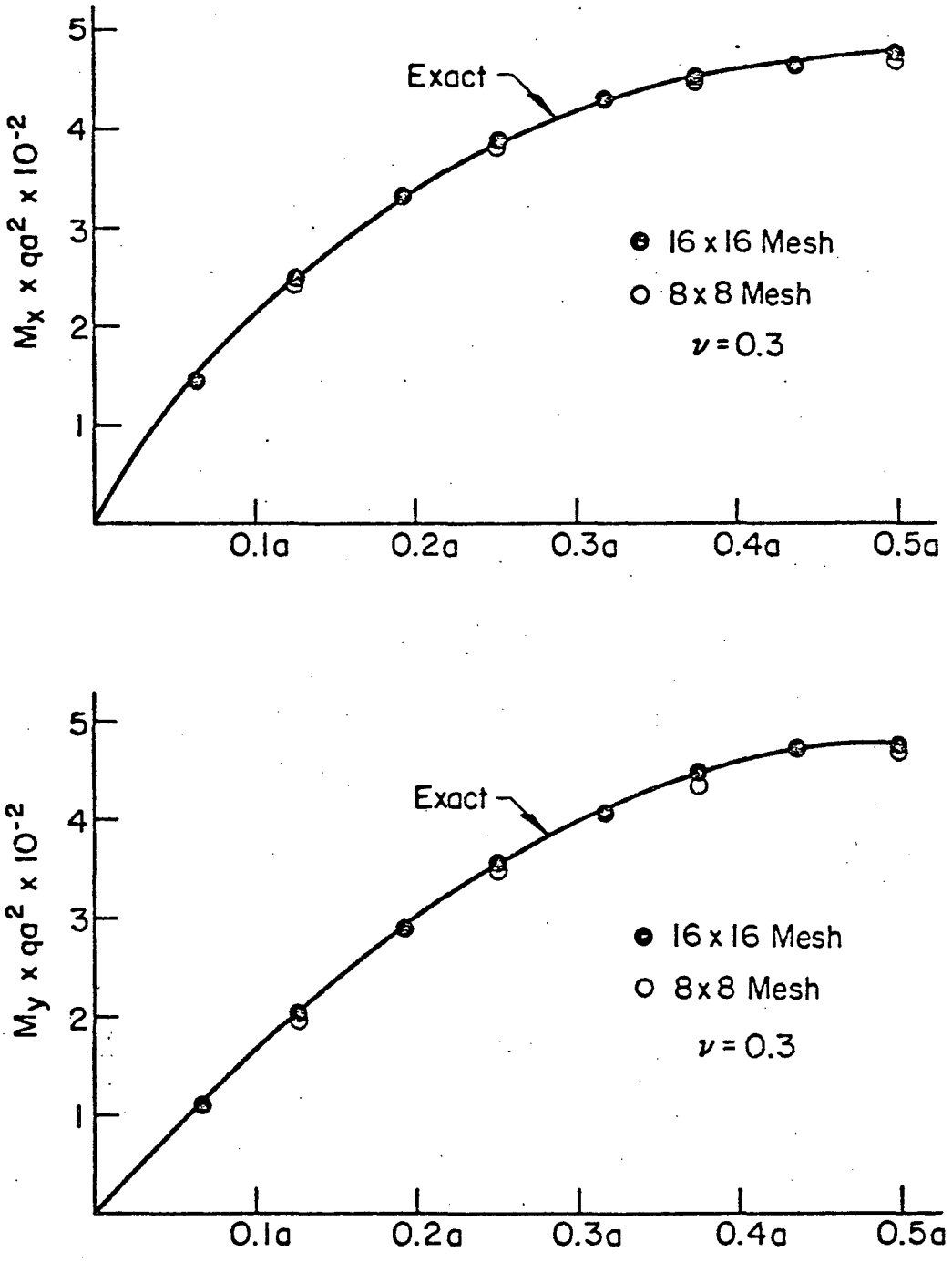

Fig. A20 Bending Moments M_x and M_y in a Simply Supported Square Plate - Uniform Load

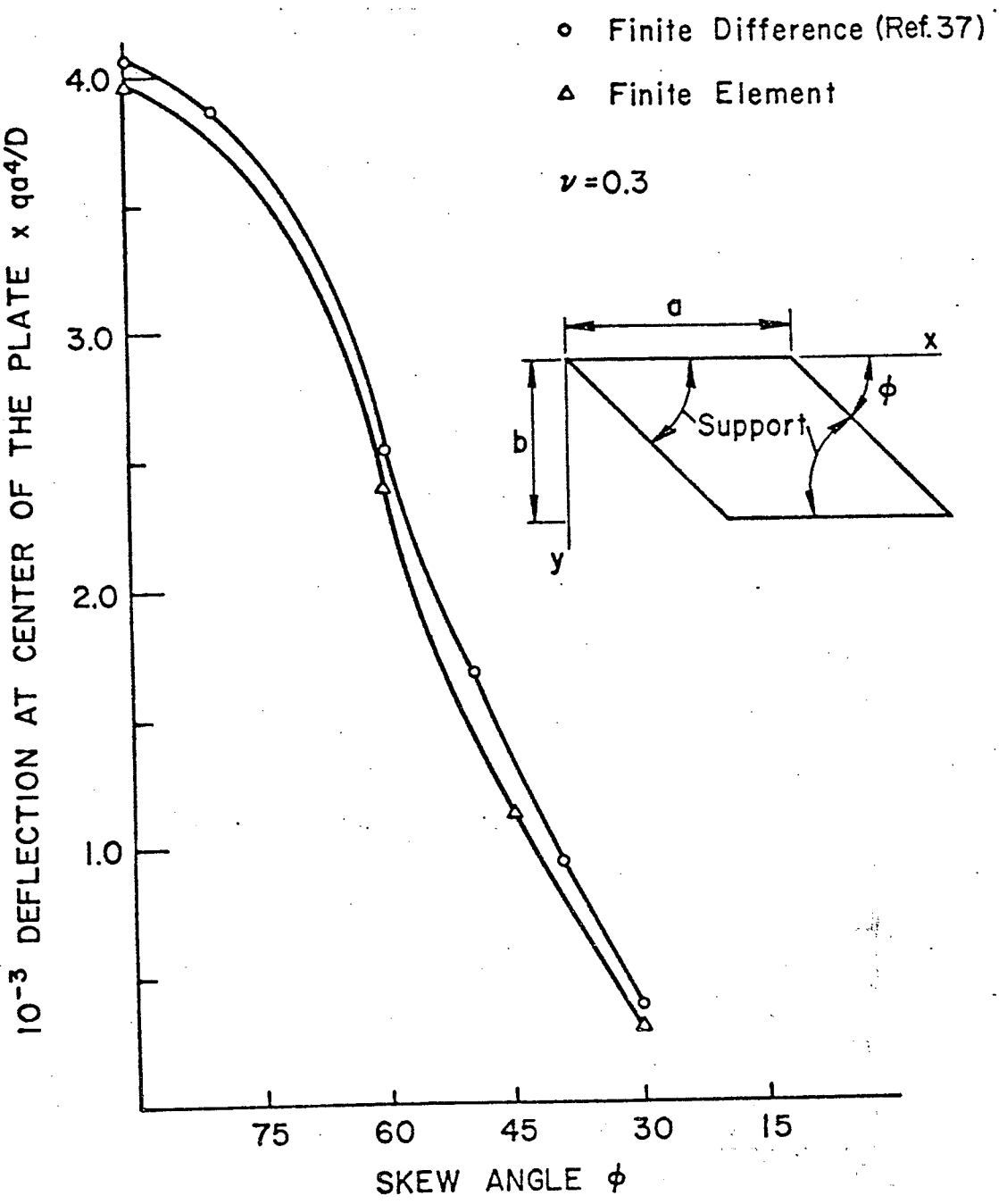

Fig. A21 Deflection at the Center of a Simply Supported Rhombic Plate - Uniform Load

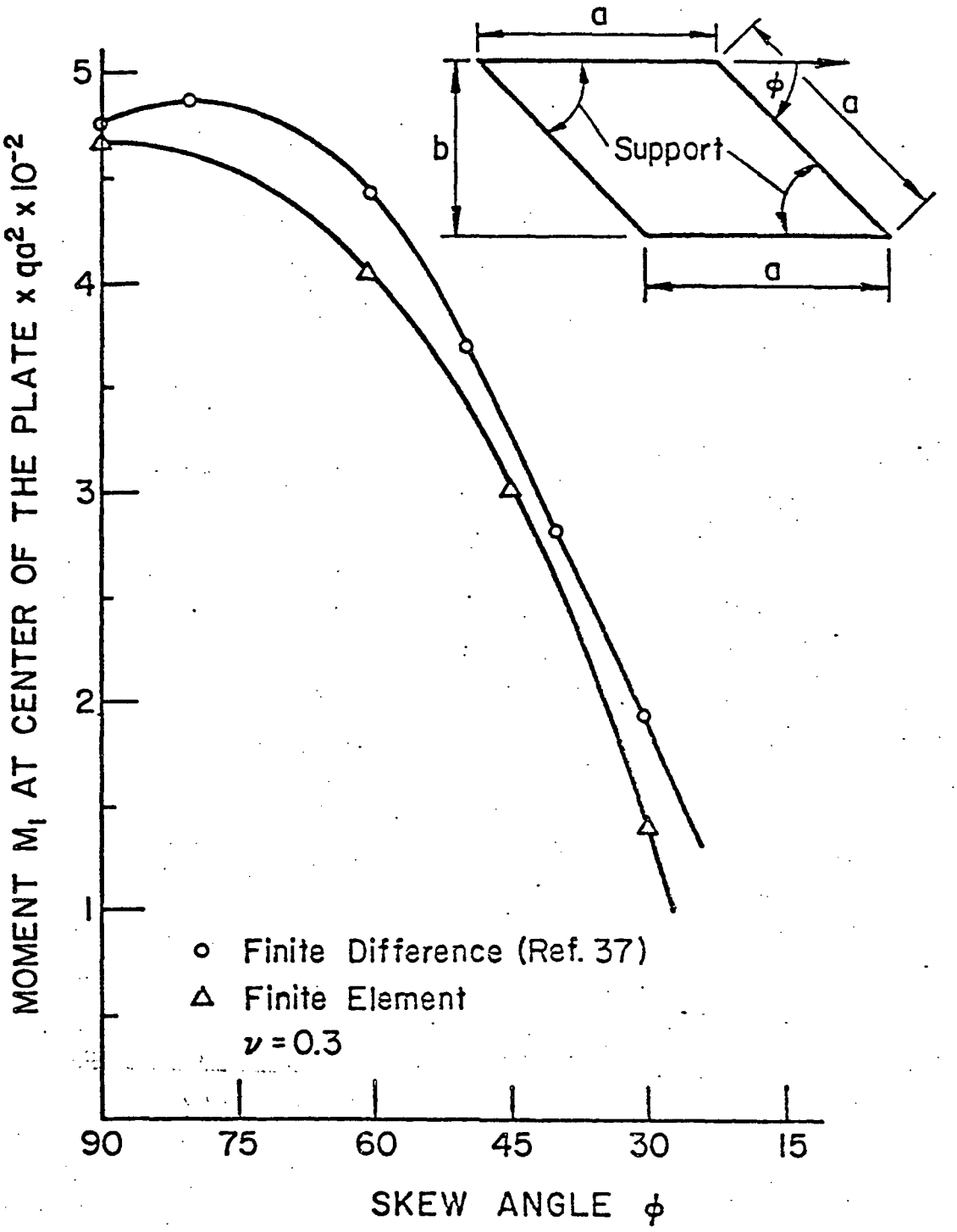

Fig. A22 Principal Moment M_1 at Center of a Simply Supported Rhombic Plate - Uniform Load

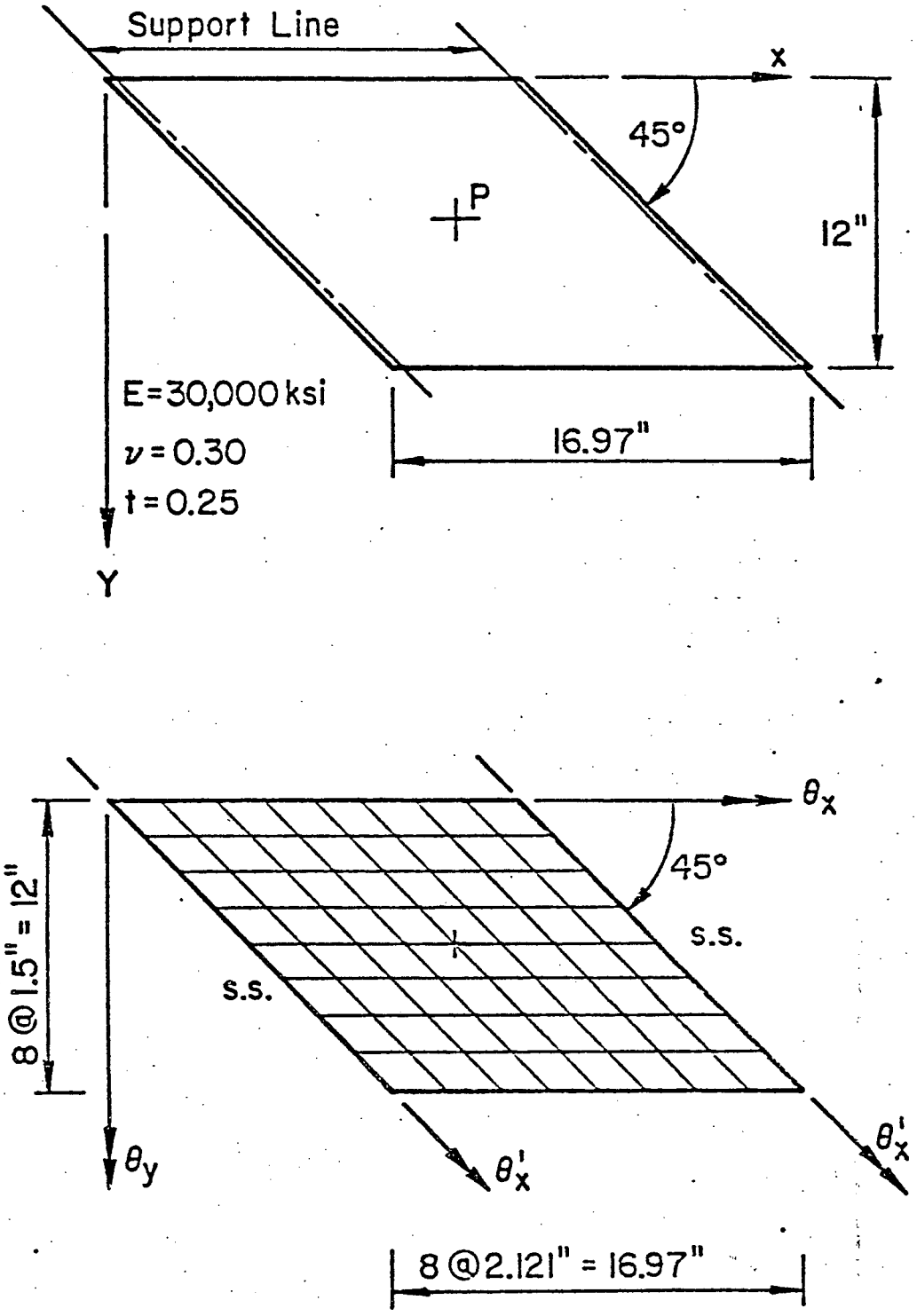

Fig. A23 Skew Steel Plate, Two Sides Simply Supported - Concentrated Load at Center

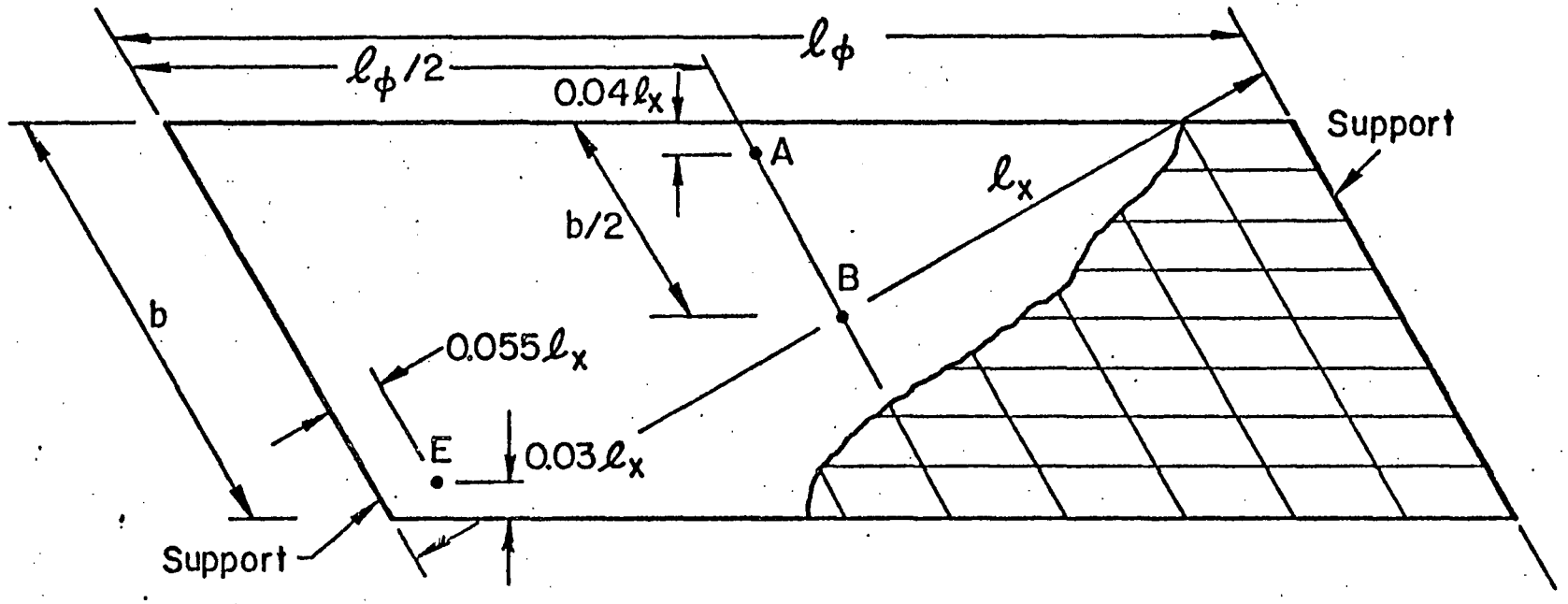

$E = 1.0665 \times 10^6$ lb/in^2

$\nu = 0.215$

$t = 3.47$

$b = 40.0$ in

$\ell_\phi = 100$ in

$\phi = 60°$

$\ell_x = 86.66$ in

Fig. A24 **Skew Slab Model (Ref. 48) and Discretization Scheme 1**

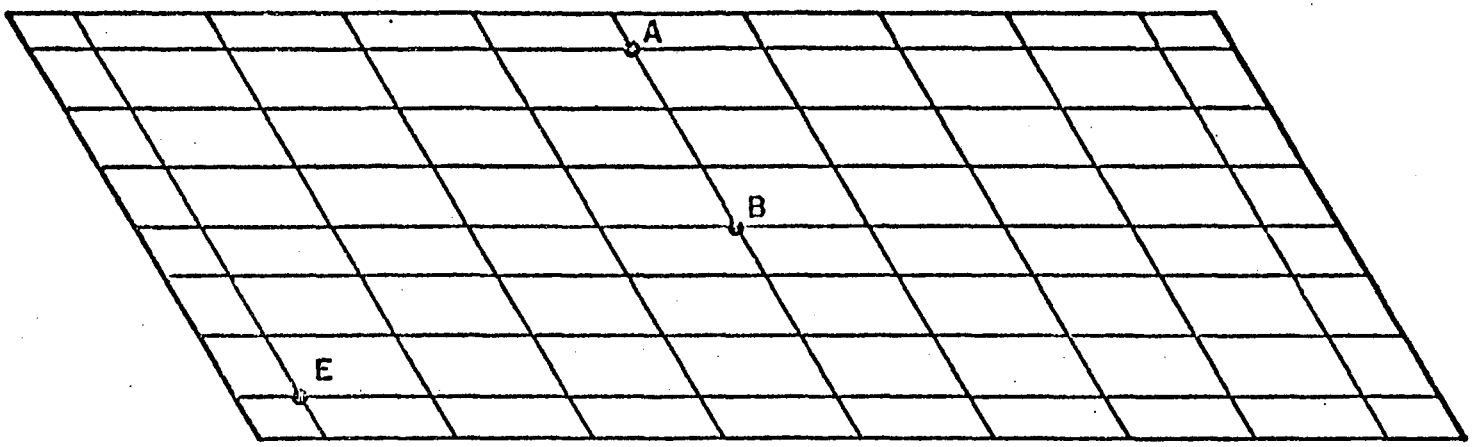

Discretization Scheme 2

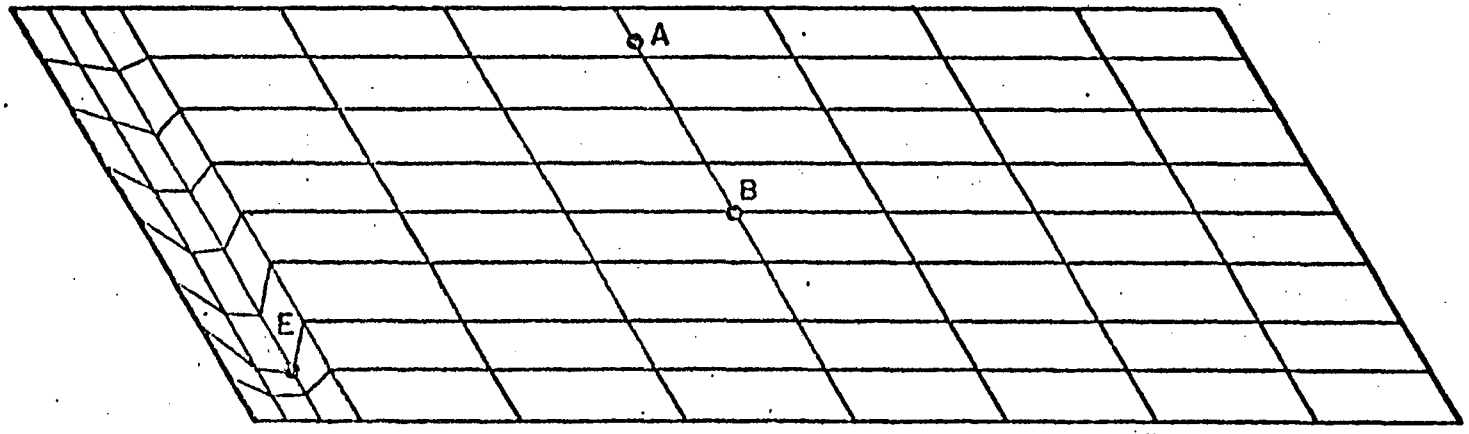

Discretization Scheme 3

Fig. A25 Skew Slab Model Discretization Schemes 2 and 3

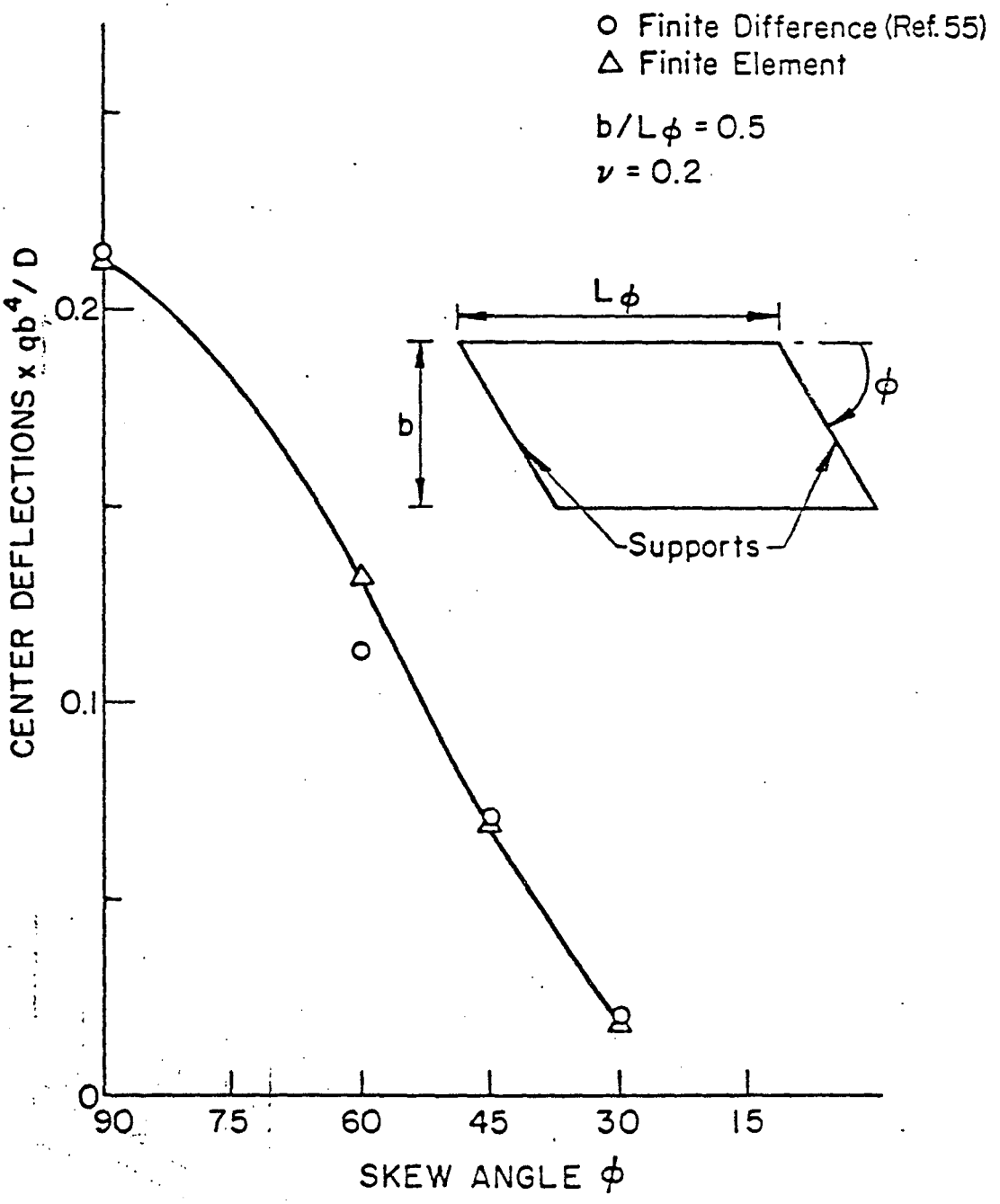

Fig. A26 Deflection of a Skew Plate, Two sides Simply Supported - Uniform Loads

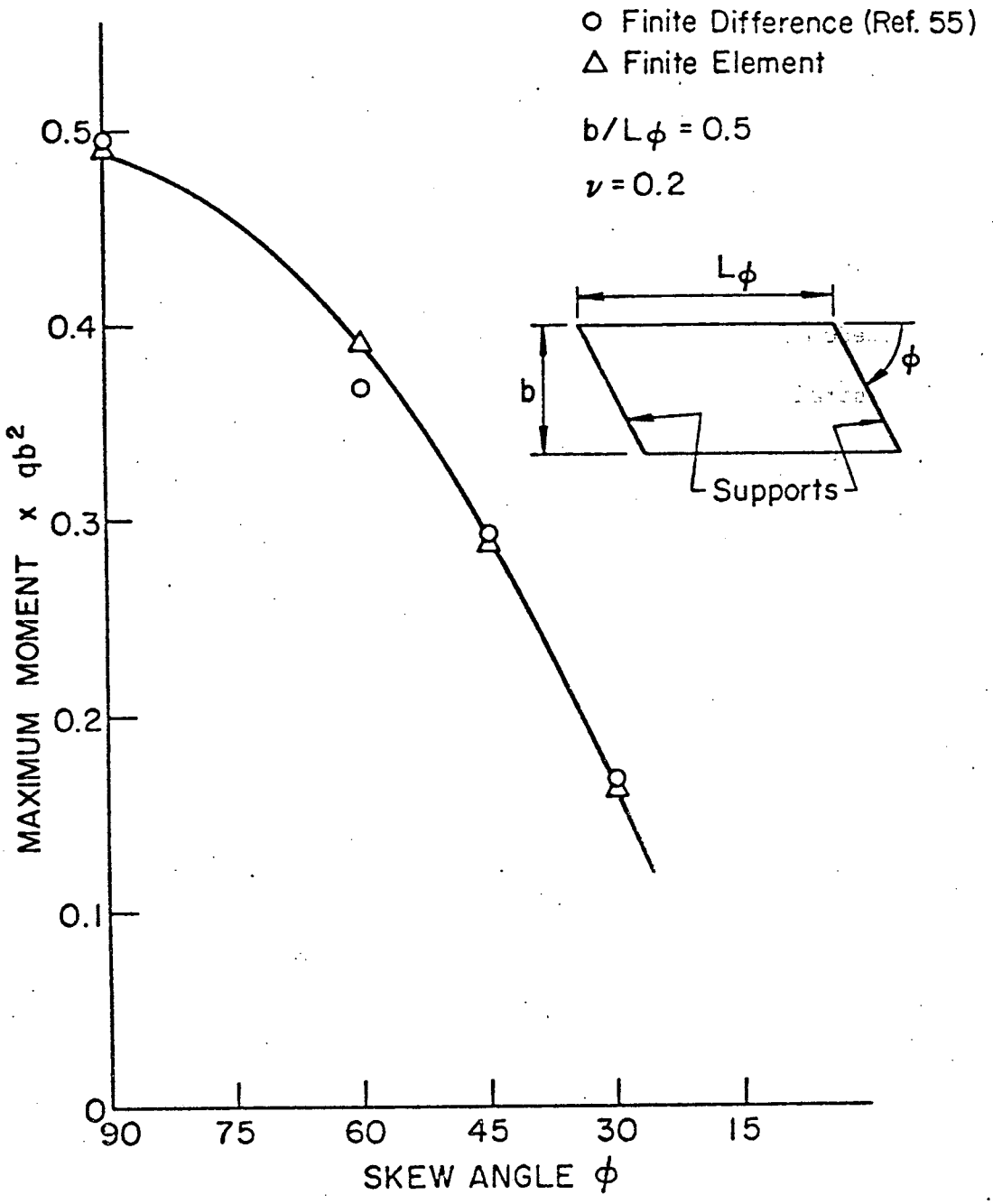

Fig. A27 Maximum Moment in a Skew Plate, Two Sides Simply Supported - Uniform Load

APPENDIX A1

Q8S11 ELEMENT STIFFNESS MATRIX

The Q8D11 element approximates the in-plane behavior of the deck slab in this study. This element has 10 fundamental degrees of freedom and one generalized coordinate α describing the constant shear strain throughout the element. The derivation follows the derivation of the element Q8D9 in Ref. 59.

The relationship between the natural system of coordinate and the global right cartesian coordinate system is expressed by:

$$\begin{Bmatrix} x \\ y \end{Bmatrix} = \begin{bmatrix} \Phi_x & 0 \\ 0 & \Phi_y \end{bmatrix} \begin{Bmatrix} x_i \\ y_i \end{Bmatrix} \tag{A.36}$$

The assumed displacement function is a linear shape function for the corner points and a quadratic function for the internal node:

$$\begin{Bmatrix} u \\ v \end{Bmatrix} = \begin{bmatrix} \Phi_1 & 0 & \Phi_2 & 0 \\ 0 & \Phi_1 & 0 & \Phi_2 \end{bmatrix} \begin{Bmatrix} u_i \\ v_i \\ u_o \\ v_o \end{Bmatrix} \tag{A.37}$$

where $\Phi_1 = \frac{1}{2}(1 + \zeta\zeta_i)(1 + \eta\eta_i)$

$\Phi_2 = (1 - \zeta^2)(1 - \eta^2)$

The displacement gradient field can be derived from Eq. A.37 by appropriate differentiation.

$$\{\nabla v\} = \begin{bmatrix} \frac{\partial \Phi_1}{\partial x} & 0 & \frac{\partial \Phi_2}{\partial x} & 0 \\ 0 & \frac{\partial \Phi_1}{\partial y} & 0 & \frac{\partial \Phi_2}{\partial y} \\ \frac{\partial \Phi_1}{\partial y} & \frac{\partial \Phi_1}{\partial x} & \frac{\partial \Phi_2}{\partial y} & \frac{\partial \Phi_2}{\partial x} \end{bmatrix} \begin{Bmatrix} u_i \\ v_i \\ u_o \\ v_o \end{Bmatrix} \qquad \text{(A.38)}$$

Equation A.38 can be rewritten in the form

$$\{\nabla v\} = [\nabla \Phi] \begin{Bmatrix} u_i \\ v_i \\ u_o \\ v_o \end{Bmatrix} \qquad \text{(A.38a)}$$

The strain field, by assuming constant strain throughout the element, can be written as:

$$\begin{Bmatrix} \epsilon x \\ \epsilon y \\ \gamma_{xy} \end{Bmatrix} = \begin{bmatrix} \frac{\partial \Phi_1}{\partial x} & 0 & \frac{\partial \Phi_2}{\partial x} & 0 & 0 \\ 0 & \frac{\partial \Phi_1}{\partial y} & 0 & \frac{\partial \Phi_2}{\partial y} & 0 \\ 0 & 0 & 0 & 0 & 1 \end{bmatrix} \begin{Bmatrix} u_i \\ v_i \\ u_o \\ v_o \\ \alpha \end{Bmatrix} \qquad \text{(A.39)}$$

Equation A.39 can be rewritten into the form

$$\begin{Bmatrix} \epsilon_x \\ \epsilon_y \\ \gamma_{xy} \end{Bmatrix} = \begin{bmatrix} \Phi_e \end{bmatrix} \begin{Bmatrix} u_i \\ v_i \\ u_o \\ v_o \\ \alpha \end{Bmatrix} \tag{A.39a}$$

With the use of the Hu-Washizu variational principle, William has shown in Ref. 59 that the stiffness relationship is of the form

$$\begin{Bmatrix} \underline{P}_v \\ \underline{0} \end{Bmatrix} = \begin{bmatrix} 0 & k_{ve} \\ k_{ev} & -k_{ee} \end{bmatrix} \begin{Bmatrix} \underline{v} \\ \underline{e} \end{Bmatrix} \tag{A.40}$$

where for this element:

$$\{\underline{P}_v\}^T = \{F_{ui} \quad F_{vi} \quad F_{uo} \quad F_{vo}\} \tag{A.40a}$$

$$\{\underline{v}\}^T = \{u_i \quad v_i \quad u_o \quad v_o\} \tag{A.40b}$$

$$\underline{e} = \gamma_{xy} \text{ strain degree of freedom} \tag{A.40c}$$

and the individual submatrices are defined as:

$$[k_{ev}] = [k_{ve}]^T = \int [\Phi_e][D][V\Phi] \, dV \tag{A.40d}$$

$$[k_{ee}] = \int [\Phi_e][D][\Phi_e] \, dV \tag{A.40e}$$

The submatrices are evaluated by numerical integration described in Section A.2.3. The strain degree of freedom is eliminated by static condensation procedure as described in Refs. 17 and 18 resulting in the following final form of the element stiffness.

$$[k] = [k_{ev}]^T [k_{ee}]^{-1} [k_{ev}] \tag{A.41}$$

APPENDIX A2

COMPATIBLE DISPLACEMENT FUNCTIONS FOR PLATE BENDING ELEMENT Q-19

This appendix contains the displacement functions for the quadrilateral element Q-19 given by Eq. A.29. The following is taken from Ref. 17 and reproduced here for completeness.

The displacement function for sub-element 3 in Eq. A.29 is expressed by

$$w^{(3)} = [\hat{\Phi}^{(3)}]\{r\} \tag{A.42}$$

where

$$\{\hat{\Phi}^{(3)}\} = \Phi_{w1}^{(3)}\Phi_{\theta x1}^{(3)}\Phi_{\theta y_1}^{(3)}\Phi_{w2}^{(3)}\Phi_{\theta x2}^{(3)}\Phi_{\theta y2}^{(3)}\Phi_{w3}^{(3)}\Phi_{\theta x3}^{(3)}\Phi_{\theta y3}^{(3)}\Phi_{\theta_4}^{(3)}\Phi_{\theta 5}^{(3)}\Phi_{\theta 6}^{(3)} \tag{A.43}$$

and the individual functions are given by the following equations in terms of the dimensions of the complete element:

$$\Phi_{w_1}^{(3)} = \zeta_1^2(3 - 2\zeta_1) + 6\mu_3\zeta_1\zeta_2\zeta_3 + \zeta_3^3[3(\lambda_2-\mu_3)\zeta_1+(2\mu_3-\lambda_2)\zeta_3-3\mu_3\zeta_2]$$

$$\Phi_{\theta x_1}^{(3)} = \zeta_1^2(b_2\zeta_3-b_3\zeta_2) + (b_1-b_3\mu_3)\zeta_1\zeta_2\zeta_3 + \frac{1}{6}\zeta_3^2[3(b_2\lambda_2 + b_3\mu_3-2b_1)\zeta_1+3(b_3\mu_3-b_1)\zeta_2+(3b_1-b_2\lambda_2-2b_3\mu_3)\zeta_3]$$

$$\Phi_{w_2}^{(3)} = \zeta_2^2(3 - 2\zeta_2) + 6\lambda_3\zeta_1\zeta_2\zeta_3 + \zeta_2^2[3(\mu_1-\lambda_3)\zeta_2 +(2\lambda_3-\mu_1)\zeta_3-3\lambda_3\zeta_1]$$

$$\Phi^{(3)}_{\theta x_3} = \zeta_2^2(b_3\zeta_1 - b_1\zeta_2) + (b_3\lambda_3 - b_2)\zeta_1\zeta_2\zeta_3 + \frac{1}{6}\zeta_3^2[3(2b_2 - b_3\lambda_3 - b_1\mu_1)\zeta_2 + 3(b_2 - b_3\lambda_3)\zeta_1 + (-3b_2 - b_1\mu_1 + 2b_3\lambda_3)\zeta_3]$$

$$\Phi^{(3)}_{w_3} = \zeta_3^2[3(1 + \mu_2)\zeta_1 + 3(1+\lambda_1)\zeta_2 + (1-\mu_2-\lambda_1)\zeta_3]$$

$$\Phi^{(3)}_{\theta x_3} = \frac{1}{6}\zeta_3^2[3(3b_1 + b_2 + b_1\lambda_1)\zeta_2 + (b_2\mu_2 - b_1\lambda_1)\zeta_3 - 3(b_1 + 3b_2 + b_2\mu_2)\zeta_1]$$

$$\Phi^{(3)}_{\theta_4} = \frac{4A}{3L_3}[6\zeta_1\zeta_2\zeta_3 + \zeta_3^2(5\zeta_3 - 3)]$$

$$\Phi^{(3)}_{\theta_5} = \frac{4A}{3L_1}[\zeta_3^2(3\zeta_2\zeta_3)]$$

$$\Phi^{(3)}_{\theta_6} = \frac{4A}{3L_2}[\zeta_3^2(3\zeta_1 - \zeta_3)]$$

For $\Phi_{\theta yi}$, all the b's in $\Phi_{\theta \hat{x} i}$ are changed to a's.

For sub-elements 1 and 2, all superscripts and subscripts permit cyclically from 1-2-3 to 2-3-1 to 3-1-2 and from 4-5-6 to 5-6-4 to 6-4-5.

APPENDIX B

FINITE ELEMENT ANALYSIS OF SKEWED STIFFENED PLATES

B.1 General

The type of structure discussed in this appendix is illustrated in Fig. 4. The plate or deck in this case can have arbitrary boundaries and the stiffeners or the beams can be eccentrically or concentrically attached to the deck.

When the stiffeners are eccentrically attached to the plate, the bending of the stiffeners causes in-plane deformations in the plate in addition to the plate bending deformations. These in-plane deformations are normally not considered in classical plate theory. In the finite element method of analysis, the in-plane and out-of-plane behavior can easily be represented with the use of in-plane and plate bending elements.

The in-plane and out-of-plane plate elements have been previously discussed. In this appendix, the stiffener element is described. Since the plane of reference for the plate elements has been defined at the midplane of the plate, the behavior of the stiffener or beam element is also defined about this plane.

Five displacement components are selected at each node in the present finite element approach. These are the displacement u, v, and w in the x, y and z directions respectively, and two slopes θ_x and θ_y about the x and y axis respectively (Fig. B1).

B.2 Derivation of the Beam Element Stiffness Matrix

The stiffener element with the plane of reference as the middle plane of the plate is shown in Fig. B1. It is assumed that the stiffener is attached to the plate along the boundary of a plate element. It is further assumed that external loads are applied only to the plate elements or directly at the nodes. Bending about the z-axis is neglected.

In order to satisfy compatibility of displacement along the juncture of the plate and the stiffener elements, the displacement functions of the plate along the juncture must be the same as for the stiffener element. Since the assumed in-plane behavior of the plate is linear and the out-of-plane behavior is cubic, a linear displacement functions is assumed for the in-plane behavior of the beam, and a cubic displacement function is assumed for the out-of-plane behavior of the beam. Furthermore, since the normal slope of the plate is assumed to vary linearly along the boundary, the twist of the beam along this boundary is assumed to be linear.

The geometry of the beam element can be described in terms of non-dimensional coordinates:

$$\zeta_1 = \frac{L - x}{L} \tag{B.1a}$$

$$\zeta_2 = \frac{X}{L} \tag{B.1b}$$

where L is in the direction of the x-axis.

The linear displacement function for u and the cubic displacement function for w can then be written as

$$u = \alpha_1 \zeta_1 \quad \zeta_2 \zeta_2 \tag{B.2}$$

$$w = \alpha_3 \zeta_1^3 \quad \alpha_4 \zeta_2^3 \quad \alpha_5 \zeta_1 \zeta_2^2 \quad \alpha_6 \zeta_1 \zeta_2^2 \tag{B.3}$$

In matrix notation:

$$\begin{Bmatrix} u \\ w \end{Bmatrix} = \begin{bmatrix} \zeta_1 & \zeta_2 & 0 & 0 & 0 & 0 \\ 0 & 0 & \zeta_1^3 & \zeta_2^3 & \zeta_1^2\zeta_2 & \zeta_1\zeta_2^2 \end{bmatrix} \{ \alpha \} \tag{B.4}$$

where $\{\alpha\}^T = \{\alpha_1 \quad \alpha_2 \quad \alpha_3 \quad \alpha_4 \quad \alpha_5 \quad \alpha_6\}$

The coefficients α_1 and α_2 can be determined from the two in-plane model displacements at the two nodes, and α_3 α_4 α_5, and α_6 can be determined from the two out-of-plane displacements and two rotations at the two nodes.

The nodal displacements can be written as,

$$\{r_s\}^T = \{u_i \quad w_i \quad \theta_{yi} \quad u_k \quad w_k \quad \theta_{yk}\} \tag{B.5}$$

where u_i and u_k are the in-plane displacements, and w_i, w_k, θ_{yi}, and 0_{yk} are the out-of-plane displacements and rotations, at nodes i and k respectively. θ_y can be expressed by definition and the use of the chain rule,

$$\theta_y = \frac{\partial w}{\partial x} = \frac{\partial w}{\partial \zeta_1} \cdot \frac{\partial \zeta_1}{\partial x} + \frac{\partial w}{\partial \zeta_2} \cdot \frac{\partial \zeta_2}{\partial x} \tag{B.6}$$

The nodal displacements can now be expressed in terms of the unknown coefficients from Eqs. B.4 and B.6.

$$\begin{Bmatrix} u_i \\ w_i \\ \theta_{YI} \\ u_k \\ w_k \\ \theta_{yk} \end{Bmatrix} = \begin{bmatrix} 1 & 0 & 0 & 0 & 0 & 0 \\ 0 & 0 & 1 & 0 & 0 & 0 \\ 0 & 0 & -3/L & 0 & 1/L & 0 \\ 0 & 1 & 0 & 0 & 0 & 0 \\ 0 & 0 & 0 & 1 & 0 & 0 \\ 0 & 0 & 0 & 3/L & 0 & -1/L \end{bmatrix} \begin{Bmatrix} \alpha_1 \\ \alpha_2 \\ \alpha_3 \\ \alpha_4 \\ \alpha_5 \\ \alpha_6 \end{Bmatrix} \qquad (B.7)$$

The vector of unknown coefficients can be expressed in terms of the nodal displacements by solving for $\{\alpha\}$ in Eq. B.7. Hence,

$$\begin{Bmatrix} \alpha_1 \\ \alpha_2 \\ \alpha_3 \\ \alpha_4 \\ \alpha_5 \\ \alpha_6 \end{Bmatrix} = \begin{bmatrix} 1 & 0 & 0 & 0 & 0 & 0 \\ 0 & 0 & 0 & 1 & 0 & 0 \\ 0 & 1 & 0 & 0 & 0 & 0 \\ 0 & 0 & 0 & 0 & 1 & 0 \\ 0 & 3 & L & 0 & 0 & 0 \\ 0 & 0 & 0 & 0 & 3 & -L \end{bmatrix} \begin{Bmatrix} u_i \\ w_i \\ \theta_{yi} \\ u_k \\ w_k \\ \theta_{yk} \end{Bmatrix} \qquad (B.8)$$

Substitution of Eq. B.8 into Eq. B.4 leads to the displacement function expression in the form of

$$\begin{Bmatrix} u \\ w \end{Bmatrix} = \begin{bmatrix} f_{s1} & 0 & 0 & f_{s2} & 0 & 0 \\ 0 & f_{s3} & f_{s4} & 0 & f_{s5} & f_{s6} \end{bmatrix} \{ r_s \} \quad \text{(B.9)}$$

where $f_{s1} = \zeta_1$ (B.9a)

$f_{s2} = \zeta_2$ (B.9b)

$f_{s3} = \zeta_1^3 + 3\,\zeta_1^2\zeta_2$ (B.9c)

$f_{s4} = \zeta_1^2\zeta_2\,L$ (B.9d)

$f_{s5} = \zeta_2^3 + 3\,\zeta_1\zeta_2^2$ (B.9e)

$f_{s6} = -\,\zeta_1\zeta_2^2\,L$ (B.9f)

It should be noted that the resulting interpolation functions are the same functions as the in-plane and plate bending elements along the boundary.

Defining $\varepsilon_x = \frac{\partial u}{\partial x}$, and $C = -\frac{\partial^2 w}{\partial x^2}$ to be the strain and the curvature respectively, at any point along the reference axis of the stiffener element, then

$$\begin{Bmatrix} \varepsilon_x \\ C \end{Bmatrix} = \begin{bmatrix} \frac{\partial f_{s1}}{\partial x} & 0 & 0 & \frac{\partial f_{s2}}{\partial x} & 0 & 0 \\ 0 & \frac{\partial^2 f_3}{\partial x^2} & \frac{\partial^2 f_4}{\partial x^2} & 0 & \frac{\partial^2 f_5}{\partial x^2} & \frac{\partial^2 f_6}{\partial x^2} \end{bmatrix} \{ r_s \} \quad \text{(B.11)}$$

The components of C can be determined with the use of the chain rule,

$$\frac{\partial}{\partial x^2} = \frac{\partial^2}{\partial \zeta_1^2}\left(\frac{\partial \zeta_1}{\partial x}\right)^2 + \frac{2\partial^2}{\partial \zeta_1 \zeta_2}\left(\frac{\partial \zeta_1}{\partial x}\cdot\frac{\partial \zeta_2}{\partial x}\right) + \frac{\partial^2}{\partial \zeta_2^2}\left(\frac{\partial \zeta_2}{\partial x}\right)^2 \quad \text{(B.12)}$$

The normal strain and curvature at the nodes can be evaluated by applying Eq. B.12 to Eq. B.11 and substituting coordinate values

$$\begin{Bmatrix} \varepsilon_x \\ C_i \\ C_k \end{Bmatrix} = \begin{bmatrix} -1/L & 0 & 0 & 1/L & 0 & 0 \\ 0 & -6/L^2 & -4/L & 0 & 6/L^2 & 2/L \\ 0 & 6/L^2 & 2/L & 0 & -6/L^2 & 4/L \end{bmatrix} \begin{Bmatrix} u_i \\ w_i \\ \theta_{yi} \\ u_k \\ w_k \\ \theta_{yk} \end{Bmatrix} \quad \text{(B.13)}$$

$$\text{or } \{\varepsilon_c\}_s = [\Phi_c]_s \{r_s\} \quad \text{(B.13a)}$$

where $\{\varepsilon_c\} = \varepsilon_x, C_i, C_k$ are the normal strain and curvatures at node i and k

$[\Phi_c]$ = Normal strain and curvature interpolating functions evaluated at the nodes.

With the assumption that plane sections remain plane before and after deformation, the displacement equation for any point on the beam at a distance of z from the reference plane can be written as:

$$U(z) = u - z \frac{\partial w}{\partial x} \tag{B.14}$$

The normal strain ε_x can be defined by differentiating Eq. B.14, from which the stress-strain relation for the beam becomes

$$\sigma_s = E_s \left(\frac{\partial u}{\partial x} - z \frac{\partial^2 w}{\partial x^2} \right) \tag{B.15}$$

where σ_s = stress on a stiffener element at distance z from the reference axis

E_s = is the modulus of elasticity of the beam

assuming only a uniaxial state of stress for the beam.

The generalized forces acting on the beam section can be evaluated by integrating Eq. B.15,

$$N_s = \int_{-t/2}^{t/2} \sigma_s \, dA \tag{B.16}$$

$$M_s = \int_{-t/2}^{t/2} \sigma_s \, z \, dA \tag{B.17}$$

These generalized forces can then be expressed in matrix form as,

$$\begin{Bmatrix} N_s \\ M_s \end{Bmatrix} = E_s \begin{bmatrix} A_s & S_s \\ S_s & I_s \end{bmatrix} \begin{Bmatrix} \frac{\partial u}{\partial x} \\ -\frac{\partial^2 w}{\partial x^2} \end{Bmatrix} \tag{B.18}$$

where A_s = cross-sectional area of the stiffener

S_s = first moment of the stiffener area with respect to the plane of reference

I_s = moment of inertia of the stiffener area with respect to the plane of reference

Given the normal strain and curvatures at the nodes as expressed by Eq. B.13, the strain and curvature expressions can be written in terms of strain interpolation functions. Thus

$$\begin{Bmatrix} \frac{\partial u}{\partial x} \\ -\frac{\partial^2 w}{\partial x^2} \end{Bmatrix} = \begin{bmatrix} 1 & 0 & 0 \\ 0 & \zeta_1 & \zeta_2 \end{bmatrix} \begin{Bmatrix} \varepsilon_x \\ C_i \\ C_k \end{Bmatrix} \tag{B.19}$$

or
$$\{\varepsilon\}_s = [\Phi_\varepsilon]_s \{\varepsilon_c\}_s \tag{B.20}$$

where $\{\varepsilon\}_s$ = normal strain and curvature $\frac{\partial u}{\partial x}$ and $-\frac{\partial^2 w}{\partial x^2}$ along the axis of the beam element about the reference plane

$[\Phi_\varepsilon]_s$ = strain interpolation functions which express a constant variation of normal strain and a linear variation of curvature

$\{\varepsilon_c\}_s$ = normal strain ε_x and curvature C at the nodes

The specific characteristics for the beam element can be expressed from Eq. B.18 to be,

$$[D]_s \quad \begin{bmatrix} A_s & S_s \\ S_s & I_s \end{bmatrix} \tag{B.21}$$

which are already integrated for the complete beam section.

The integral of the triple produce in the general expression for the stiffness matrix can be evaluated from $[\Phi_\varepsilon]_s$ from Eq. B.20, and $[D]_s$ from Eq. B.21. Thus after integration,

$$\int [\Phi_\varepsilon]_s^T [D]_s [\Phi_\varepsilon] \, dx = E_s L \begin{bmatrix} A_s & \frac{S_s}{2} & \frac{S_s}{2} \\ \frac{S_s}{2} & \frac{I_s}{3} & \frac{I_s}{6} \\ \frac{S_s}{2} & \frac{I_s}{6} & \frac{I_s}{3} \end{bmatrix} \tag{B.22}$$

The integration in Eq. B.22 is carried out only through the length because [D] is already expressed for the cross-section in Eq. B.18.

The stiffness matrix expression for the beam element can now be evaluated with Eqs. B.13 and B.22:

$$[k]_s = [\Phi_c]_s^T \int [\Phi_\varepsilon]_s^T [D]_s [\Phi_\varepsilon]_s \, dx \, [\Phi_c]_s$$

$$\begin{bmatrix} \frac{A_s}{L} & 0 & \frac{S_s}{L} & -\frac{A_s}{L} & 0 & -\frac{S_s}{L} \\ & \frac{12I_s}{L^3} & -\frac{6I_s}{L^2} & 0 & -\frac{12I_s}{L^3} & -\frac{6I_s}{L^2} \\ & & \frac{4I_s}{L} & -\frac{S_s}{L} & \frac{6I_s}{L^2} & \frac{2I_s}{L} \\ & & & \frac{A_s}{L} & 0 & \frac{S_s}{L} \\ & & & & \frac{12I_s}{L^3} & \frac{6I_s}{L^2} \\ \text{Symmetric} & & & & & \frac{4I_s}{L} \end{bmatrix} \tag{B.23}$$

It should be noted that the above expression is only for the bending stiffness of the beam. The torsional stiffness is derived separately in the following paragraphs.

For the present analysis, only St. Venant torsion is considered. It has been shown that for rectangular and stocky beam cross-sections, most of the applied twisting moment is resisted by St. Venant torsion (Ref. 58).

The twisting moment $T_{s.v.}$ in the beam element is related to the angle of twist ϕ by the relation:

$$T_{s.v.} = GK_t \phi' \tag{B.24}$$

where $\phi' = \frac{\partial}{\partial x}\left(\frac{\partial w}{\partial y}\right)$ or the rate of change of angle of twist

G = shear modulus

K_t = St. Venant torsional constant

With the assumption that the angle of twist varies linearly along the length of the element, and recognizing that the angle of twist at the nodes corresponds to the rotation about the longitudinal axis of the beam, the torsional rotation function can be written in terms of linear interpolation functions and the nodal rotations. Thus

$$\{\phi\} = [\zeta_1 \quad \zeta_2] \begin{Bmatrix} \theta_{xi} \\ \theta_{yi} \end{Bmatrix} \tag{B.25}$$

$$\{\phi'\} = \begin{bmatrix} -\frac{1}{L} & \frac{1}{L} \end{bmatrix} \begin{Bmatrix} \theta_{xi} \\ \theta_{yi} \end{Bmatrix} \tag{B.26}$$

Following the procedure for the beam bending element and using the given rotation function, the following matrices can be defined:

$$[D]_t = Gk_t \tag{B.27}$$

$$[\Phi_\varepsilon]_t = [1] \tag{B.28}$$

$$[\Phi_c]_t = \begin{bmatrix} -\frac{1}{L} & \frac{1}{L} \end{bmatrix} \tag{B.29}$$

From the general expression for the stiffness matrix, integration along the length leads to

$$[k]_t = [\Phi_c]_t^T \int [\Phi_\varepsilon]_t^T [D] [\Phi_\varepsilon]_t dx [\Phi_c]_t$$

$$= \frac{Gk_t}{L} \begin{bmatrix} -1 & -1 \\ -1 & 1 \end{bmatrix} \tag{B.30}$$

B.3 Assembly of the System Stiffness Matrix

The stiffness matrices of the individual elements are assembled to form the structural stiffness matrix of the complete system. The procedure is described in detail in Ref. 64. In the following, the assembly of the elements is illustrated in matrix form to show the

interaction of individual elements as defined by the global force and displacement vectors.

The in-plane and bending plate elements are assembled first to form a combined element with five degrees of freedom at each node. Since the in-plane plate element and out-of-plane plate element both lie on the same reference plane, there is no interaction between them. Hence, for example

$$[k_{ii}] = \left[\begin{array}{c|c} k_I & 0 \\ \hline 0 & k_{II} \end{array}\right] \tag{B.31}$$

where k_I is a 2 x 2 matrix associated with u and v displacement components and k_{II} is a 3 x 3 matrix associated with the w, θ_x, θ_x displacement and rotation components.

For the whole plate element with nodes 1, 2, 3 and 4,

$$\begin{Bmatrix} F_1 \\ F_2 \\ F_3 \\ F_4 \end{Bmatrix} = [k_{ij}] \begin{Bmatrix} r_1 \\ r_2 \\ r_3 \\ r_4 \end{Bmatrix} \tag{B.32}$$

where the submatrices of $[k_{ij}]$ are in the form of Eq. B.31, and

$$\{F_i\}^T = \{F_{xi} \quad F_{yi} \quad F_{zi} \quad M_{xi} \quad M_{yi}\} \tag{B.33}$$

$$\{r_i\}^T = \{u_i \quad v_i \quad w_i \quad \theta_{xi} \quad \theta_{yi}\} \tag{B.34}$$

for i = 1, 2, 3, or 4.

The bending and torsional stiffness matrices of the beam element are assembled in a similar manner. The stiffness terms associated with the neglected displacement component are taken as zero in forming the complete five degrees of freedom system at the node. Hence, from Eq. B.23 and Eq. B.30 at beam nodes i and k,

$$\begin{Bmatrix} F_{xi} \\ F_{yi} \\ F_{zi} \\ M_{xi} \\ M_{yi} \\ F_{xk} \\ F_{yk} \\ F_{zk} \\ M_{xk} \\ M_{yk} \end{Bmatrix} = \begin{bmatrix} A_s L^2 & 0 & 0 & 0 & S_s L^2 & -A_s L^2 & 0 & 0 & 0 & -S_s L^2 \\ & 0 & 0 & 0 & 0 & 0 & 0 & 0 & 0 & 0 \\ & & 12I_s & 0 & -6I_s L & 0 & 0 & -12I_s & 0 & -6I_s L \\ & & & \frac{Gk_t}{E_s} L^2 & 0 & 0 & 0 & 0 & -\frac{Gk_t}{E_s} L^2 & 0 \\ & & & & 4I_s L^2 & -S_s L^2 & 0 & 6I_s L & 0 & 2I_s L^2 \\ & & & & & A_s L^2 & 0 & 0 & 0 & S_s L^2 \\ & & & & & & 0 & 0 & 0 & 0 \\ & & \text{Symmetric} & & & & & 12I_s & 0 & 6I_s L \\ & & & & & & & & \frac{Gk_t}{E_s} L^2 & 0 \\ & & & & & & & & & 4I_s L^2 \end{bmatrix} \begin{Bmatrix} u_i \\ v_i \\ w_i \\ \theta_{xi} \\ \theta_{yi} \\ u_k \\ u_k \\ w_k \\ \theta_{xk} \\ \theta_{yk} \end{Bmatrix} \tag{B.35}$$

The stiffness matrix expression for the beam element in Eq. B.35 can be modified to include the additional deflection due to shear (Ref. 45). Defining

$$\Gamma = \frac{12\, E_s I_s}{G_s A_s L^2} \tag{B.36}$$

The beam stiffness matrix can be rewritten to include the shear deformation (Ref. 45).

$$[k]_s = \frac{E_s}{L^3}\begin{bmatrix}
A_s L^2 & 0 & 0 & 0 & S_s L^2 & -A_s L^2 & 0 & 0 & 0 & -S_s L^2 \\
 & 0 & 0 & 0 & 0 & 0 & 0 & 0 & 0 & 0 \\
 & & \frac{12 I_s}{(1+\Gamma)} & 0 & \frac{-6 I_s L}{(1+\Gamma)} & 0 & 0 & \frac{-12 I_s}{(1+\Gamma)} & 0 & \frac{-6 I_s L}{(1+\Gamma)} \\
 & & & \frac{G k_t}{E_s} L^2 & 0 & 0 & 0 & 0 & -\frac{G k_t}{E_s} L^2 & 0 \\
 & & & & \frac{(4+\Gamma) I_s L^2}{(1+\Gamma)} & -S_s L^2 & 0 & \frac{6 I_s L}{(1+\Gamma)} & 0 & \frac{(2-\Gamma) I_s L^2}{(1+\Gamma)} \\
 & & & & & A_s L^2 & 0 & 0 & 0 & S_s L^2 \\
 & & & & & & 0 & 0 & 0 & 0 \\
 & & & & & & & \frac{12 I_s}{(1+\Gamma)} & 0 & \frac{6 I_s L}{(1+\Gamma)} \\
 & & & & \text{Symmetric} & & & & \frac{G k_t}{E_s} L^2 & 0 \\
 & & & & & & & & & \frac{(4+\Gamma) I_s L^2}{(1+\Gamma)}
\end{bmatrix} \tag{B.37}$$

The beam stiffness matrix is given for the beam element whose longitudinal axis is parallel to the x-axis. When the beam elements are not parallel to the x-axis, standard tensor transformation must be applied to the beam stiffness matrix before assembly into the structural system (Ref. 64).

The displacements of the plate and beam elements at common nodes are expressed by Eq. B.32 and Eq. B.35 in terms of the global degrees of freedom. The elements have equal number of degrees of freedom at the nodes and therefore can be assembled directly to the system stiffness matrix following the procedure specified in Ref. 64.

B.4 Application of Boundary Conditions

One of the advantages of the finite element method of analysis is its adaptability to solutions of problems with various boundary conditions. If a degree of freedom at the boundary is fixed, the corresponding row and column of the stiffness matrix is easily eliminated from the solution procedure. If the support at the boundary is flexible, the stiffness of the support is simply added to the stiffness of the element at that boundary (Ref. 65).

In certain cases, the nodes are constrained to displace in a specified direction, and to rotate at a specified angle. For example, the u displacement of a node may be specified to displace in the direction of a line at an angle ω from the x-axis and the θ_x rotation may be specified to rotate about a line at an angle β from the x-axis. For

these cases, the stiffness matrix must be transformed accordingly. It is shown in Ref. 64 that the required transformation is of the form

$$[k'] = [T]^T [k] [T] \tag{B.38}$$

where $[k']$ = the transformed stiffness matrix

$[k]$ = the original stiffness matrix

$[T]$ = the transformation matrix

It should be noted that the transformation can be carried out in the element stiffness level [k] or at the assembled system stiffness matrix [K]. It should be noted further that the applied nodal forces and the resulting deformations are in the direction specified by the constraint.

For the five degree of freedom system in this study, the transformation matrix for a given node is

$$[T] = \begin{bmatrix} \cos\omega & \sin\omega & 0 & 0 & 0 \\ -\sin\omega & \cos\omega & 0 & 0 & 0 \\ 0 & 0 & 1 & 0 & 0 \\ 0 & 0 & 0 & \cos\beta & \sin\beta \\ 0 & 0 & 0 & -\sin\beta & \cos\beta \end{bmatrix} \tag{B.39}$$

where ω = the angle from the global x-axis along which u displaces, measured clockwise; and

β = the angle from the global x-axis about which θ_x rotates, measured clockwise.

B.5 Application of Loads

The components of the force vector as defined by Eq. B.33 are applied at the nodes in the direction of the associated displacements. For uniformly distributed loads, the force vector can be computed from (Ref. 17).

$$\{F_e\} = - \int [\Phi]^T p\ (x,y)\ dV \qquad (B.40)$$

The uniform load is conveniently equated to a set of concentrated forces and moments applied at the nodes. For concentrated loads, the discretization can be made such that the load will be directly on a node; and hence the loads can be applied directly to the global force vector. However, the procedure of changing the discretization to accommodate concentrated loads is obviously inefficient especially for the analysis of one structure under different types of loading. For this reason, the concept of a statically equivalent force vector for a concentrated load is introduced. In this concept, the element with a concentrated load is analyzed as a substructure, and the reaction forces at the nodes are computed. The negative of these reaction forces at the nodes become the applied nodal forces for the assembled structure. In this study only the concentrated load normal to the plate element is considered.

The stiffness equation for the Q-19 element gives the force displacement relationships of a quadrilateral element with the fifth node at the center of the element. If the fifth node is located at the point where the concentrated load is applied, the resulting structure

is a quadrilateral plate of four triangles with a concentrated load at the interior node (Fig. B2). The stiffness of the four triangles can be recomputed and reassembled in the form:

$$\begin{Bmatrix} F_E \\ F_I \end{Bmatrix} = \begin{bmatrix} k_{EE} & k_{EI} \\ k_{IE} & k_{II} \end{bmatrix} \begin{Bmatrix} 0 \\ r_I \end{Bmatrix} \tag{B.41}$$

where 0 refers to the supported nodes and, where the subscripts E and I refer to the external nodes and the internal node respectively. The external nodes in this case are completely fixed in displacements and rotations. $\{F_E\}$ can therefore be easily found to be

$$\{F_E\} = [k_{EI}]\ [k_{II}]^{-1}\ \{F_I\} \tag{B.42}$$

Since Eq. B.41 is an equilibrium equation, $\{F_E\}$ is a statically equivalent force vector. In cases however when the concentrated load is very near to a corner node of the quadrilateral, the stiffness formulation may get into numerical difficulty because of the resulting shape of one or more of the triangular elements. In such cases, the concentrated load is applied directly to the nearest node. When the concentrated load is on the boundary of the element but not on the node, the load is proportioned to the two nodes of that boundary. The components of the equivalent force vector due to a concentrated load normal to a quadrilateral element are illustrated in Fig. B2.

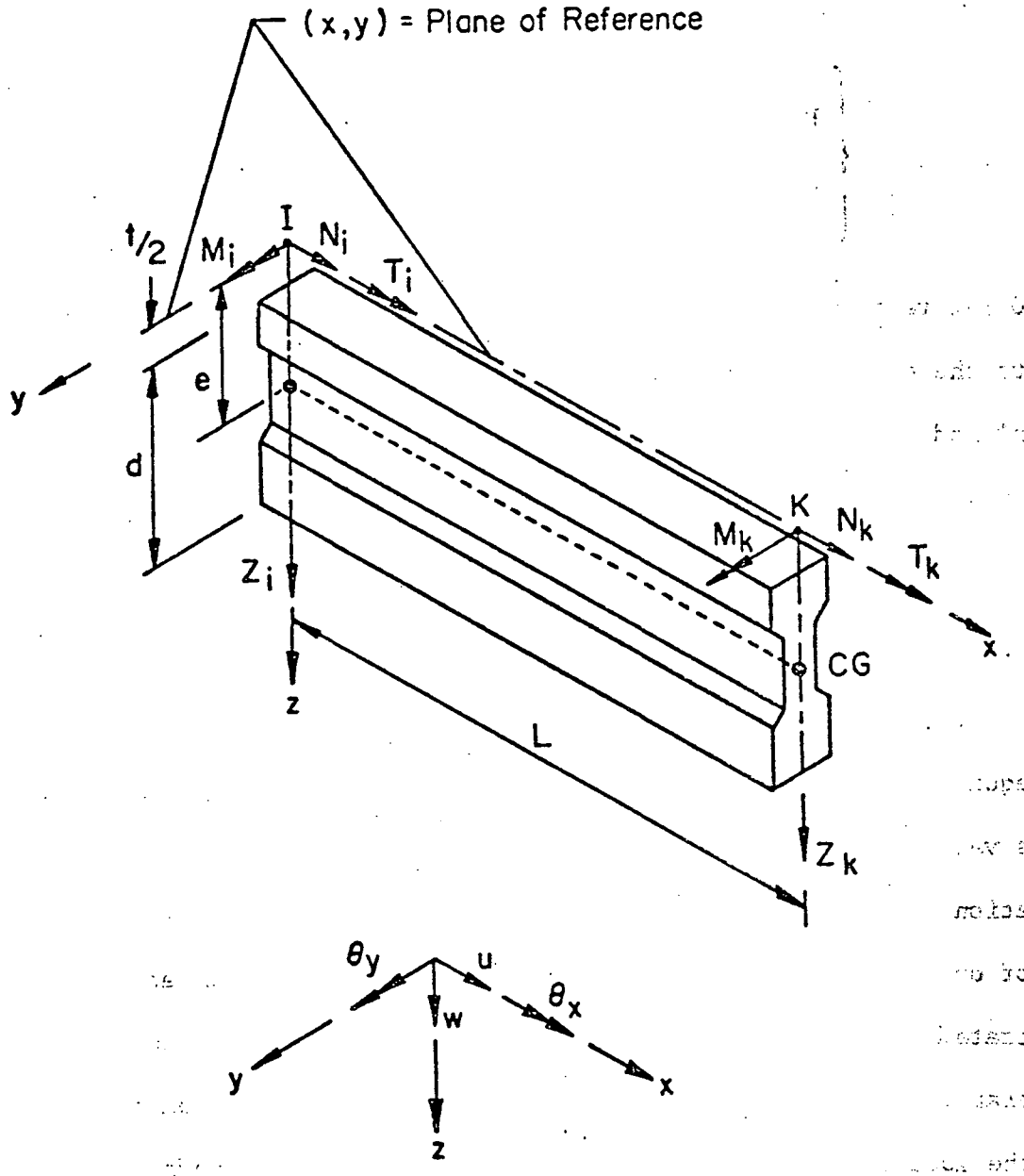

Fig. B1 A Stiffener Finite Element with Associated Degrees of Freedom and Nodal Forces

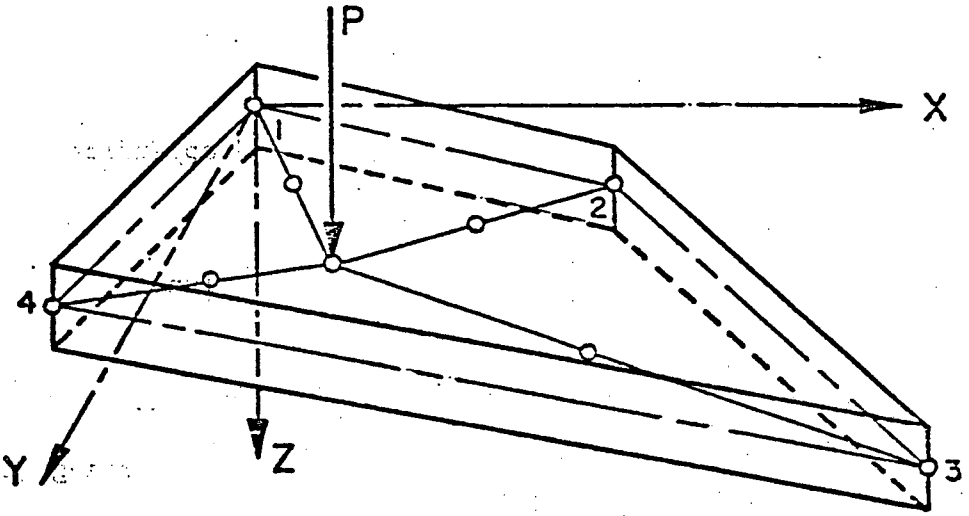

$$\{F_I\}^T = \{P\ 0\ 0\ 0\ 0\ 0\}$$

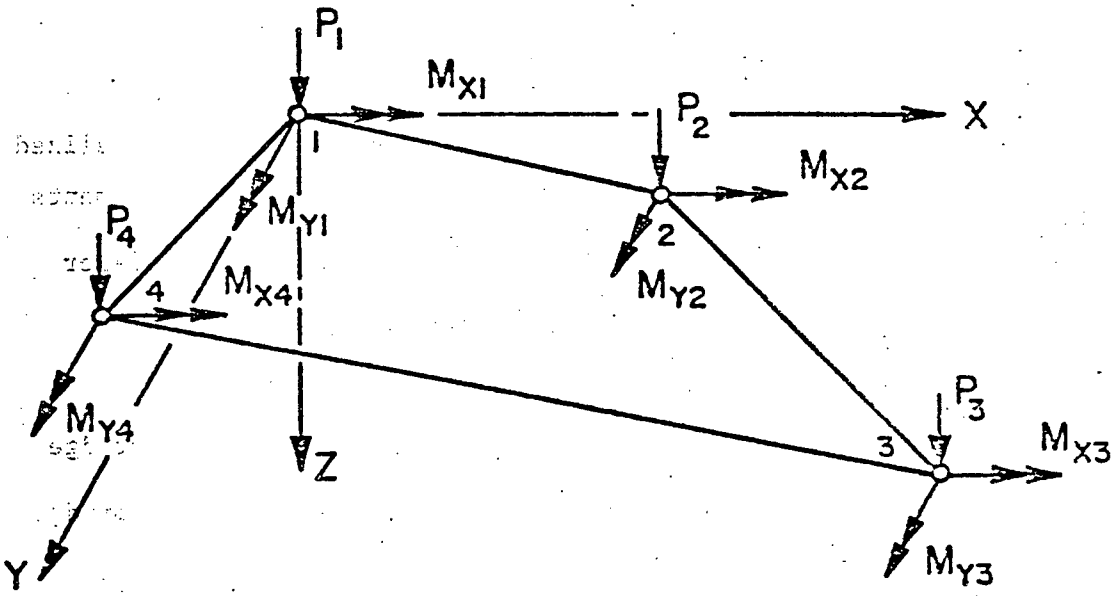

$$\{F_E\}^T = \{P_1 M_{X1} M_{Y1}\ P_2 M_{X2} M_{Y2}\ P_3 M_{X3} M_{Y3}\ P_4 M_{X4} M_{Y4}\}$$

Fig. B2 Equivalent Force Vector $\{F_E\}$ Due to Concentrated Load P Normal to the Element

10. NOMENCLATURE

The following symbols were used in the text and appendices:

A. Capital Latin Letters (matrices and scalars)

$[A]$	= Matrix of displacement functions evaluated at the nodes
A	= Area of a triangular element
A_i	= Area of sub element i in a triangular element
A_s	= Cross section area of stiffener element
$[B]$	= Matrix of differentiated displacement functions
C	= Curvature in a stiffener element
$C_{11}, C_{12}, C_{21}, C_{33}$	= Material constants
$[D]$	= Elasticity matrix relating generalized stresses to generalized displacements
$[D]_s$	= Elasticity matrix for the stiffener element
D.F.	= Distribution factor
DF_Φ	= Distribution factor in a skew bridge
DF_{90}	= Distribution factor in a right bridge
E, E_1, E_2	= General and principal modulus of elasticity
E_s	= Stiffener element modulus of elasticity
$\{F_e\}$	= Statically equivalent force vector due to distributed loads

$\{F_i\}$ = Vector of element nodal forces

$\{F_E\}$ = Applied force vector associated with external nodes

$\{F_I\}$ = Applied force vector associated with internal nodes

$\{F'\}$ = Statically equivalent force vector due to concentrated load

$F_{xi}, F_{yi}, F_{zi}, M_{xi}, M_{yi}$ = Components of element nodal forces $\{F_i\}$

G, G_2 = General and second principal shear moduli

G_s = Stiffener element shear modulus

H = Stiffener to slab stiffness ratio, $(EI)_{stiffener}/(EI)_{slab}$

I = Integrand expression

I_s = Moment of inertia of stiffener element about reference plane

$J_{11}, J_{12}, J_{21}, J_{22}$ = Components of Jacobian matrix

$[K]$ = Global stiffness matrix

L = Bridge span length, stiffener element dimension

$[M]$ = Matrix of displacement functions

M_s, N_s = Generalized forces in stiffener element

$M_x, M_y, M_{xy}, M_1, M_2$ = Cartesian and principal plate moments

$N_x, N_y, N_{xy}, N_1, N_2$ = Cartesian and principal in-plane

M_u, M_{uv} = Moment resultants in the direction of skew

PCTR = Percent reduction in the distribution factor for interior I-beams

$PCTR_{(EXT)}$ = Percent reduction in the distribution factor for exterior I-beams

$PCTR_{(BOX)}$ = Percent reduction in the distribution factor for interior box-beams

[R] = Global force vector

S = Beam spacing

S_s = First moment of the stiffener area with respect to the reference plane

[T] = Transformation matrix

U, V = In-plane strain function

$U_{(z)}, V_{(z)}$ = In-plane displacement at distance z from the reference plane

W_c = Bridge curb to curb width

W_i, W_j = Weight coefficients

B. Small Latin Letters (matrices and scalars)

a, b = Web element dimensions

a_i, b_i = Projected dimensions on x and y axes

d = Stiffener element depth; distance from the centroid of a truck wheel load to the drive wheels

d_i = $2A/\ell_i$

e = Eccentricity of the centroid of the stiffener element cross section to the plane of reference

f_i = In-plane displacement function

f_{si} = Stiffener element displacement function

h_i = normal distance of node i to side ℓ_i

i,j,k,ℓ = Node or sub element number

$[k]$ = Element stiffness matrix

$k_{EE}, k_{EI}, k_{IE}, k_{II}$ = Partitioned matrices of the element stiffness matrix associated with external and internal nodes

k_{ev}, k_{ve}, k_{ee} = Submatrices of the element stiffness matrix associated with displacement and strain formulations

$[k_I], [k_{II}]$ = Submatrices associated with in-plane and out-of-plane behavior

$[k]_s$ = Stiffener element stiffness matrix

$[k]_t$ = Stiffener element stiffness matrix for torsional behavior

$[k']$ = Transformed element stiffness matrix

ℓ_i = Length of side i in a triangular element

m = Ratio of shear modulus G_2 to elastic modulus E_2

n = Order of interpolation function; principal modulus of elasticity ratio, E_1/E_2

n_i = Normal distance of a point i to side ℓ_i in a triangular element

$P(x,y)$, q = Distributed load intensity

$\{p_v\}$ = Consistent force vector associated with the displacement formulation

$\{r\}$ = Global displacement vector

$\{r_i\}$ = Element nodal displacements

$\{r^{(i)}\}$ = Sub element nodal displacements

$\{r_s\}$ = Stiffener element nodal displacements

$\{r_e\}$ = External node displacements for plate element

$\{r_o\}$ = Internal node displacements for plate element

u,v,w = Displacement components

u_i,v_i,w_i = Components of the element nodal displacements

$\{v_E\}$ = Nodal displacements at exterior nodes

$\{v_I\}$ = Nodal displacements at interior nodes

x,y,z = Cartesian coordinates

x_i,y_i = Cartesian coordinates of node i

C. Capital Greek Letters (matrices and scalars)

Γ = Shear deformation parameters

$[\Phi]$ = Matrix of interpolation or shape functions

$[\hat{\Phi}]$ = Interpolation functions for a triangular element in terms of the external degrees of freedom

$[\Phi^{(i)}]$ = Sub element i interpolation function

$[\Phi_c]$ = Strain interpolation functions evaluated at the nodes

$[\Phi_c]_s$ = Strain interpolation function for the stiffener element evaluated at the nodes

$[\Phi]_t$ = Twist interpolation function for the stiffener element evaluated at the nodes

$[\Phi_e]$ = Interpolation functions associated with the external nodes

$[\Phi_o]$ = Interpolation functions associated with the internal nodes

$[\Phi_B^{(i)}]$ = Curvature interpolation functions $[\Phi^{(i)}]$ evaluated at the nodes

$\Phi_{Ti}, \bar{\Phi}_{Ti}$ = Shape functions associated with the global nodal derivatives

$\Phi_{Ri}, \bar{\Phi}_{Ri}$ = Shape functions associated with the local nodal derivatives

$[\Phi_\epsilon]$ = Strain shape functions describing the variation of strains

$[\Phi_\epsilon^{(i)}]$ = Triangular sub element strain interpolation functions describing the variation of curvature

$[\Phi_\epsilon]_t$ = Stiffener strain interpolation function describing the variation of twist

$[\Phi_x], [\Phi_y]$ = Geometric shape functions

Φ_1 = Linear shape function

Φ_2 = Quadratic shape function

$[\Phi_{1i}]$ = Linear shape functions associated with nodes i

$[\ ^{(i)}]$ = Matrix relating curvature components to nodal degrees of freedom

D. Small Greek Letters (matrices and scalars)

$\{\alpha\}$ = Generalized coordinates

β = Angle measured from the global x-axis in the direction of which u displaces

γ_{xy} = Shear strain

$\{\epsilon\}$ = Strain field

$\{\epsilon_c\}$ = Vector of nodal strains

$\epsilon_{xx}, \epsilon_{yy}$ = Normal strains

ζ, η = Local coordinates

ζ_i, η_i = Non-dimensional nodal coordinates

θ_x, θ_y = Rotations about the global x and y axes

$\theta_{xi}, \theta_{yi}, \theta_i$ = Nodal rotations

λ_i = d_i/ℓ_i

μ_i = $1 - \lambda_i$

ν, ν_2 = Poisson's ratio

$\{\sigma\}$ = Stress field

σ_{xx}, σ_{yy} = Normal stresses

τ_{xy} = Shear stresses

ϕ = Skew angle, angle of twist

$\hat{\phi}_{wi}, \hat{\phi}_{\theta xi}, \hat{\phi}_{\theta ii}, \hat{\phi}_{\theta i}$ = Interpolation functions in terms of the nodal out-of-plane displacements

ω = Angle from the global x-axis about which θ_x rotates

$\omega_{\zeta i}$ = Local derivative at node i

E. Element Designation

ACM = Adini, Clough and Melosh plate bending element

CST = Constant strain triangle in-plane element

LCCT-12 = Linear curvature compatible triangle with 12 degrees of freedom

LCCT-11 = Linear curvature compatible triangle with 11 degrees of freedom

LSE = Linear strain equilateral

M = Melosh plate bending element

P = Pappenfuss plate bending element

Q-19 = Quadrilateral plate bending element with 19 degrees of freedom

Q8D11 = Basic 8 degree of freedom in-plane element with 3 additional internal degrees of freedom

Q8SP12 = Basic 8 degree of freedom in-plane element with 4 additional nodal rotations

WK = Wegmuller and Kostem plate bending element